AD-766 642

STOL TACTICAL AIRCRAFT INVESTIGATION. VOLUME V. PART I. FLIGHT CONTROL TECHNOLOGY: SYSTEM ANALYSIS AND TRADE STUDIES FOR A MEDIUM STOL TRANSPORT WITH VECTORED THRUST/MECHANICAL FLAPS

Kenneth J. Crandall, et al

Boeing Aerospace Company

Prepared for:

Air Force Flight Dynamics Laboratory

January 1973

AFFDL-TR-73-19
Volume V, Part I

STOL TACTICAL AIRCRAFT INVESTIGATION

Volume V, Part I

Flight Control Technology: System Analysis and Trade Studies for a Medium STOL Transport with Vectored Thrust/Mechanical Flaps

Kenneth J. Crandall
David J. Maund
William E. Gerken
James H. Vincent
the BOEING company

Technical Report AFFDL-TR-73-19 – Volume V, Part I

May, 1973

Air Force Flight Dynamics Laboratory
Air Force Systems Command
Wright-Patterson Air Force Base, Ohio 45433

Notice

When Government drawings, specifications, or other data are used for any purpose other than in connection with a definitely related Government procurement operation, the United States Government thereby incurs no responsibility nor any obligation whatsoever; and the fact that the Government may have formulated, furnished, or in any way supplied the said drawings, specifications, or other data, is not to be regarded by implication or otherwise as in any manner licensing the holder or any other person or corporation, or conveying any rights or permission to manufacture, use or sell any patented invention that may in any way be related thereto.

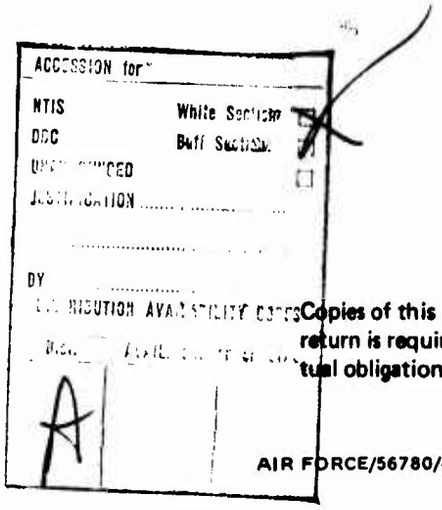

Copies of this report should not be returned unless return is required by security considerations, contractual obligations, or notice on a specific document.

AIR FORCE/56780/4 September 1973 —150

Security Classification

DOCUMENT CONTROL DATA - R & D

(Security classification of title, body of abstract and indexing annotation must be entered when the overall report is classified)

1 ORIGINATING ACTIVITY (Corporate author) The Boeing Company , Aerospace Group Seattle, Washington 98124	2a. REPORT SECURITY CLASSIFICATION Unclassified 2b GROUP

3 REPORT TITLE

Flight Control Technology: System Analysis and Trade Studies for a Medium STOL Transport with Vectored Thrust and Mechanical Flaps.

4 DESCRIPTIVE NOTES (Type of report and inclusive dates)

Final Technical Report June 1971 through December 1972

5 AUTHOR(S) (First name, middle initial, last name)

Kenneth J. Crandall, David J. Maund, William E. Gerken, and James H. Vincent

6 REPORT DATE January 1973	7a TOTAL NO OF PAGES 257	7b NO OF REFS 22
8a CONTRACT OR GRANT NO F33615-71-C-1757 b PROJECT NO 643A c d	9a ORIGINATOR'S REPORT NUMBER(S) AFFDL-TR-73-~~HK~~ 19 9b OTHER REPORT NO(S) (Any other numbers that may be assigned this report) D180-14412-1	

10 DISTRIBUTION STATEMENT

11 SUPPLEMENTARY NOTES	12 SPONSORING MILITARY ACTIVITY Air Force Flight Dynamics Laboratory, Wright-Patterson Air Force Base, Ohio.

13 ABSTRACT

A program of flight control technology applicable to an Advance Medium STOL Transport (AMST) airplane equipped with a vectored-thrust powered lift system has been conducted. Low "q" moment producers were evaluated. Mathematical models (control laws) of control systems suitable for the STOL landing approach were defined. The effect of control system mechanization complexity on performance, weight, cost, safety, design risk, and vulnerability to small arms fire was evaluated. A candidate control system was selected and its performance was validated using a piloted moving base simulation.

While this study specifically concerned control technology for airplanes equipped with the vectored thrust form of powered lift, the results are considered to have direct application to airplanes with other forms of powered lift, such as internally blown jet flaps and upper surface blown flaps.

DD FORM 1 NOV 65 1473

Security Classification

14 KEY WORDS	LINK A		LINK B		LINK C	
	ROLE	WT	ROLE	WT	ROLE	WT
Control Law						
Moment Producer Trade Study (Low q)						
Stability Augmentation Systems						
Control Augmentation System						
Fly - by - Wire System						
Vectored Thrust						
Flight Control Trade Study						

☆U.S.Government Printing Office: 1973 — 758-425/35

STOL TACTICAL AIRCRAFT INVESTIGATION

Volume V, Part I

Flight Control Technology: System Analysis and Trade Studies for a Medium STOL Transport with Vectored Thrust/Mechanical Flaps

Kenneth J. Crandall
David J. Maund
William E. Gerken
James H. Vincent

FOREWORD

This report was prepared for the United States Air Force by The Boeing Company, Seattle, Washington in partial fulfillment of Contract F33615-71-C-1757, Project No. 643A. It is one of eight related documents covering the results of investigations of vectored-thrust and jet-flap powered lift technology, under the STOL Tactical Aircraft Investigation (STAI) Program sponsored by the Air Force Systems Command, Wright-Patterson Air Force Base, Ohio. The relation of this report to the others of this series is indicated below:

AFFDL TR-73-19	STOL TACTICAL AIRCRAFT INVESTIGATION	
Vol I	Configuration Definition: Medium STOL Transport with Vectored Thrust/Mechanical Flaps	
Vol II Part I	Aerodynamic Technology: Design Compendium, Vectored Thrust/Mechanical Flaps	
Vol II Part II	A Lifting Line Analysis Method for Jet-Flapped Wings	
Vol III	Takeoff and Landing Performance Ground Rules for Powered Lift STOL Transport Aircraft	
Vol IV	Analysis of Wind Tunnel Data: Vectored Thrust/Mechanical Flaps and Internally Blown Jet Flaps	
Vol V Part I	Flight Control Technology: System Analysis and Trade Studies for a Medium STOL Transport with Vectored Thrust and Mechanical Flaps	THIS REPORT
Vol V Part II	Flight Control Technology: Piloted Simulation of a Medium STOL Transport with Vectored Thrust/Mechanical Flaps	
Vol VI	Air Cushion Landing System Study	

The work reported here was performed in the period 8 June 1971 through 8 December 1972 by the Sensors, Guidance, and Control Staff of the Research and Engineering Division and by the Tactical Airlift Program, Aeronautical and Information Systems Division, both of the Aerospace Group, The Boeing Company. Mr. Franklyn J. Davenport served as Program Manager.

Mr. Kenneth J. Crandall was principal investigator. The control law development and analysis was done by W.E. Gerken, D.J. Maund, and J.H. Vincent. The moment producer and control mechanization analysis were accomplished with the support of Harold S. Lewis, Myles L. Holmdahl, and William C. Brockway.

The Air Force Project Engineer for this investigation was Mr. Garland S. Oates, Air Force Flight Dynamics Laboratory (PTA), Wright-Patterson Air Force Base, Ohio.

The main body of this report was released within The Boeing Company as Document D180-14412-1, and submitted to the USAF in December 1972.

This technical report has been reviewed and approved.

E. J. Cross Jr., Lt. Col., USAF
Chief, Prototype Division
Air Force Flight Dynamics Laboratory

ABSTRACT

A program of flight control technology applicable to an Advance Medium STOL Transport (AMST) airplane equipped with a vectored-thrust powered lift system has been conducted. Low "q" moment producers were evaluated. Mathematical models (control laws) of control systems suitable for the STOL landing approach were defined. The affect of control system mechanization complexity on performance, weight, cost, safety, design risk, and vulnerability to small arms fire was evaluated. A candidate control system was selected and its performance was validated using a piloted moving base simulation.

While this study specifically concerned control technology for airplanes equipped with the vectored thrust form of powered lift, the results are considered to have direct application to airplanes with other forms of powered lift, such as internally blown jet flaps and upper surface blown flaps.

(vi blank)

Preceding page blank

TABLE OF CONTENTS

TABLE OF CONTENTS (Continued)

LIST OF ILLUSTRATIONS

LIST OF ILLUSTRATIONS (continued)

LIST OF ILLUSTRATIONS (continued)

LIST OF ILLUSTRATIONS (continued)

LIST OF ILLUSTRATIONS (continued)

LIST OF TABLES

LIST OF TABLES (continued)

LIST OF TABLES (continued)

LIST OF ABBREVIATIONS

AMST	Advanced Medium STOL Transport
APU	Auxillary Power Unit
CAS	Control Augmentation System
CTOL	Conventional Takeoff and Landing
DLC	Direct Lift Control
EAS	Equivalent Airspeed
FBW	Fly-by-Wire
FBW + Rev.	Fly-by-Wire with Mechanical Reversion
FPS	Feet Per Second
IFR	Instrument Flight Rules
INS	Inertial Navigation System
kn	Knots
MCS	Mechanical Control System
RMS	Root Mean Square
SAS	Stability Augmentation System
STAI	STOL Tactical Aircraft Investigation
STOL	Short Takeoff and Landing
TAT-ADP	Tactical Airlift Technology Advanced Development Program
VFR	Visual Flight Rules

LIST OF SYMBOLS

A/P	Autopilot
$A_{Y_{CG}}$	Lateral Acceleration at the Center of Gravity ∿ Ft./Sec.^{2}
$A_{Y_{PS}}$	Lateral Acceleration at the Pilot Station ∿ Ft./Sec.^{2}
$\dot{A}/_{ft.}$	Moment Producer Control Power Data Obtained in Phase I
$\dot{A}_{2D}$	(Å/Ft.) (Span Available)
a_n	Normal Acceleration ∿ g s
$\dot{B}$	Coupled Axis Response
b	Mechanical System Lost Motion Deadzone ∿ Deg. or Wing Span ∿ Ft.
$C_{D_{MAX}}$	Maximum Drag Coefficient
C_L	Lift Coefficient
C_ℓ	Rolling Moment Coefficient About cg
$C_{\ell_{()}}$	Partial Derivative of C_ℓ with Respect to the Subscripted Variable
C_n	Yawing Moment Coefficient about cg
$C_{n_{()}}$	Partial Derivative of C_n with Respect to the Subscripted Variable
C_R	Wing Root Chord ∿ Ft.
C_T	Wing Tip Chord ∿ Ft.
C_V	Nozzle Velocity Coefficient
C_x	Computed Value for Complexity or Total Complexity Value
C_Y	Side Force Coefficient
$C_{Y_{()}}$	Partial Derivative of C_Y with Respect to the Subscripted Variable
C_μ	Boundary Layer Momentum Coefficient

LIST OF SYMBOLS (continued)

$\bar{C}$	Wing Mean Aerodynamic Chord ∿ Ft.
c.g.	Center of Gravity
F	Force of Thrust ∿ Lbs.
FC	Force Conversion Complexity Rating
F_{col}	Column Push or Pull Force ∿ Lbs.
F_G	Gross Thrust Magnitude ∿ Lbs.
F_m	Figure-of-Merit
F_{PED}	Rudder Pedal Force ∿ Lbs.
F_S	Stick Force ∿ Lbs.
F_W	Wheel Force ∿ Lbs.
F_{11}	Airspeed Due to δ_1 Control Transfer Function
F_{22}	Flight Path Due to δ_2 Control Transfer Function
$G_{CF}(s)$	Wheel to Rudder Crossfeed Transfer Function
g	Earth Gravitational Attraction ∿ Ft./Sec.^{2}
H	Altitude ∿ Ft.
$\dot{h}$	Altitude Rate - Ft./Sec.
$\dot{h}_{baro}$	Barometric Altitude Rate ∿ Ft./Sec.
Ixx	Body Axis Roll Inertia ∿ Slug-Ft.^{2}
I_{XZ}	Body Axis Product of Inertia ∿ Slug-Ft.^{2}
Iyy	Body Axis Pitch Inertia ∿ Slug-Ft.^{2}
I_{zz}	Body Axis Yaw Inertia ∿ Slug-Ft.^{2}
$K_{(a)(b)}$	Represents a Feedback Gain where the (a) Subscript is the Sensed Variable and the (b) Subscript is the Appropriate Moment Producer
$K_{P()}$	Represents a Pilot Feed Forward Gain where the Subscript Represents the Controlled Variable

LIST OF SYMBOLS (continued)

$K_{()}$	Represents a Feedback Gain Where the Subscript is the Sensed Variable
K_3	Lateral Control Power Coefficient
$L_{()}$	Turbulence Characteristic Length of Subscripted Variable ∿ Ft.
M_1	Mechanical Signal Path Including Feel System
M	Pitching Moment ∿ Ft.-Lbs. or Mach Number
$M_{()}$	Partial Derivative of M with Respect to the Subscripted Variable
m	Mass ∿ Slugs or Nozzle Air Mass Flow Rate ∿ Slugs/Sec.
N_{LC}	Number of Points Where a 9 mm Round can Cause Loss of Control
N_{L_2}	Number of Points Where a 9 mm Round can Cause Level 2 Operation
N_{L_3}	Number of Points Where a 9 mm Round can Cause Level 3 Operation
Δn	Incremental Load Factor ∿ gs
P_D	Power Distribution Complexity Rating
P_E	Electric Mode Hydraulic Pressure ∿ Lbs./In.^{2}
P_{EW}	Figure of Merit for the Probability of Excessive Pilot Workload
P_F	Failure Effects Cooper-Harper Pilot Rating
P_G	Power Generation Complexity Rating
$P_{H.Q.}$	Handling Quality Cooper-Harper Pilot Rating
P_{LC}	Figure of Merit for the Probability of Loss of Control
P_R	Overall Performance Rating
P_{S_D}	Figure of Merit for the Probability of Structural Damage
P_T	Tracking Task Performance Data or Total Pressure ∿ Lbs./Ft.^{2}

LIST OF SYMBOLS (continued)

$\dot{P}$	Roll Acceleration (Body Axis Unless Noted Otherwise) ∿ Deg./Sec.^{2}
p_s	Roll Rate (Stability Axis) ∿ Deg./Sec.
psia	Lbs./In.^{2} (Absolute)
ϕ P/β	Phase Angle Between Roll Rate and Sideslip for Dutch Roll Oscillations ∿ Deg.
Q	Body Axis Pitch Rate ∿ Deg.
P_B	Roll Rate (Body Axis) ∿ Deg./Sec.
$Q_{()}$	Failure Probability for the Subscripted Variable
Q_{EW}	Computed Failure Probability for Excessive Pilot Workload
Q_{LC}	Computed Failure Probability for Loss of Control
Q_{SD}	Computed Failure Probability for Structural Damage
Q_{f_m}	Probability of Failure Mode
$\dot{Q}$	Pitch Acceleration (Body Axis) ∿ Deg./Sec.^{2}
q	Dynamic pressure ∿ Lbs./Ft.^{2}
q_c	Impact Pressure ∿ Lbs/Ft.^{2}
R_F	Relative Rating Factor
R_V	Vulnerability Factor
$\dot{R}$	Yaw Acceleration (Body Axis Unless Noted Otherwise) ∿ Deg./Sec.^{2}
r_s	Yaw Rate (Stability Axis) ∿ Deg./Sec.
S_A	Surface Actuator
S_{ik}	Surface Area Influenced by the Control Element between Semi-Spans i and k
S_R	Safety Rating
S_W	Wing Area ∿ Ft.^{2}
s	Laplace Operator

LIST OF SYMBOLS (continued)

T_G	Gross Thrust ∿ Lbs.
T_L	Lead Time Constant ∿ Sec.
r_B	Yaw Rate (Body Axis) ∿ Deg./Sec.
$T_{90\%\alpha_{n_{ss}}}$	Time to Reach 90 Percent of Steady State Normal Acceleration Following a Column Step ∿ Sec.
$T_{90\%\dot{\theta}_{ss}}$	Time to Reach 90 Percent of Steady State Pitch Attitude Rate Following a Column Step ∿ Sec.
u	Airspeed Pertubation ∿ Ft./Sec.
u_{air}	Relative Velocity Component Along the x Axis ∿ Ft./Sec.
u_g	Gust Velocity Component Along the x Axis ∿ Ft./Sec.
$\dot{u}$	Acceleration along x Axis ∿ Ft./Sec.^{2}
V_E	Airspeed Error ∿ Ft./Sec.
V_G	Ground Speed - Ft./Sec.
V_{ID}	Nozzle Ideal Air Flow Velocity ∿ Ft./Sec.
V_{REF}	Landing Approach Reference Airspeed ∿ Ft./Sec.
V_S	Stall Airspeed ∿ Knots
V_T	True Airspeed ∿ Ft./Sec.
V_{12}	Roll Rate from Sideslip Coupling Transfer Function or Airspeed to Flight Path Coupling Transfer Function
V_{21}	Sideslip from Roll Rate Coupling Transfer Function or Flight Path to Airspeed Coupling Transfer Function
v_g	Gust Velocity Component Along the y Axis ∿ Ft./Sec.
w	Vertical Speed Perturbation ∿ Ft./Sec.
$\dot{w}$	Acceleration along z Axis ∿ Ft./Sec.^{2}
W_g	Gust Velocity Component Along the z Axis ∿ Ft./Sec.

LIST OF SYMBOLS (continued)

X	External Force Component Along x Axis ∿ Lbs.
$X_{()}$	Partial Derivative of X with Respect to the Subscripted Parameter
$\ddot{x}$	Acceleration Along the x Axis ∿ Ft./Sec.^{2}
Y_{P_θ}	Pilot Pitch Attitude Describing Function
$\ddot{y}$	Acceleration Along the y Axis ∿ Ft./Sec.^{2}
Z	External Force Component Along z Axis ∿ Lbs.
$Z_{()}$	Partial Derivative of z with Respect to the Subscripted Parameter
$\ddot{z}$	Acceleration Along the z Axis ∿ Ft./Sec.^{2}
α	Angle of Attack Relative to x Axis ∿ Radians
β	Sideslip Angle
β_G	Gust Sideslip Component Deg.
β_{MAX}	Maximum Excursion of Sideslip Following a Rudder Step ∿ Deg.
$\dot{\beta}$	Sideslip Rate ∿ Deg./Sec.
$\dot{\beta}_{SAS}$	Computed Sideslip Rate ∿ Deg./Sec.
γ	Flight Path Angle Perturbation ∼ Deg.
$\dot{\gamma}$	Flight Path Angle Rate ∿ Deg./Sec.
δ_A	Aileron Deflection ∿ Deg.
δ_c	Elevator and DLC Input ∿ Deg.
δ_{col}	Column Deflection ∿ Inches
δ_{DLC}	Direct Lift Control Deflection ∿ Deg.
δ_e	Elevator Deflection ∿ Deg.
δ_{σ}	Vector Angle Deflection ∿ Deg.
$\hat{c}_{\sigma_P}$	Vector Lever Angle ∿ Deg.

δ_{PED}	Rudder Pedal Deflection ∿ Inches
δ_R	Rudder Deflection ∿ Deg.
δ_{SP}	Spoiler Deflection ∿ Deg.
δ_{TH}	Throttle Lever Deflection ∿ Deg.
δ_W	Aileron and Spoiler Input ∿ Deg.
δ_{W_P}	Wheel Displacement ∿ Deg.
$\Delta\beta$	The Maximum Change in Sideslip Following an Abrupt Roll Control Pulse ∿ Deg.
ΔC_ℓ	Incremental Rolling Moment Coefficient
$\Delta\gamma_{MAX}$	Maximum Excursion of Flight Path Following a Vector Step ∿ Deg.
$\Delta\gamma_{SS}$	Steady State Flight Path Change Following a Column Pulse ∿ Deg.
ΔF_D	Incremental Drag Force ∿ Lbs.
ΔF_L	Incremental Lift Force ∿ Lbs.
ΔL	Incremental Lift Force ∿ Lbs.
ΔM	Resonant Peak ∿ Decibels
$\Delta\Theta_{MAX}$	Maximum Excursion of Pitch Attitude Following a Vector Step ∿ Deg.
$\Delta\Theta_{SS}$	Steady State Pitch Attitude Change Following a Column Pulse ∿ Deg.
ΔS_x	Longitudinal Touchdown Dispersion ∿ Ft.
ΔSy	Lateral Touchdown Dispersion ∿ Ft.
ΔV_{MAX}	Maximum Excursion of Airspeed Following a Column Pulse ∿ Ft./Sec.
ΔV_{SS}	Steady State Excursion of Airspeed Following a Vector Step ∿ Ft./Sec.
ΔW	Total Incremental Weight ∿ Lbs.

LIST OF SYMBOLS (continued)

$\epsilon_{G.S.}$	Glideslope error ~ dots [= .35° of $\epsilon_{G.S.}$]
ϵ_{LOC}	Locolizer error ~ dots [= .5° of ϵ_{LOC}]
ϵ_{VT}	Airspeed error ~ ft./sec.
ζ	Damping ratio of subscripted variable
θ	Pitch attitude perturbation ~ deg.
θ_C	Pitch attitude command ~ deg.
θ_{REF}	Reference pitch ~ deg.
$\dot{\theta}$	Pitch attitude rate ~ deg./sec.
$\dot{\theta}_{SS}$	Steady state pitch attitude rate excursion following a column step ~ deg./sec.
$\dot{\theta}_{MAX}$	Maximum pitch attitude rate excursion following a column step ~ deg./sec.
λ	Wing taper ratio
σ	Thrust vector angle ~ deg.
$\sigma_{( )}$	RMS value of subscripted variable
$\tau_{( )}$	Time constant of subscripted variable ~ sec.
τ_S	Spiral mode time constant ~ sec.
$\Phi_{( )}(\Omega)$	Turbulence power spectral density of subscripted variable ~ ft.^{2}/sec.
ϕ	Bank angle ~ deg.
ϕ_1	Bank angle at the first peak following an abrupt roll control pulse ~ deg.
$\lvert\phi/\beta\rvert_d$	Ratio of the magnitude of $\phi(s)$ to the magnitude of $\beta(s)$ evaluated at the Dutch roll pole location.
$\phi/\beta_{T=3 \text{ secs.}}$	Ratio of bank angle to sideslip three seconds after the initiation of a rudder pedal step.
ϕ_{SS}	Steady state value of bank angle rate resulting from a wheel step ~ deg./sec.
ψ	Airplane heading ~ deg.

LIST OF SYMBOLS (continued)

ψ_β	Phase angle of the Dutch roll oscillation in sideslip. $\sim$ deg.
Ω	Spatial frequency $\sim$ radians/ft.
$\omega_{(\ )}$	Undamped natural frequency of subscripted variable $\sim$ radians/sec.

SUBSCRIPTS

BW	Bandwidth
D	Dutch roll mode
PH	Phugoid mode
R	Roll subsidence mode
SP	Short period mode or spoiler
SPIR	Spiral mode

SECTION I

INTRODUCTION

1.1 Background

The U.S. Air Force has determined the requirement to modernize its Tactical Airlift capability. The Tactical Airlift Technology Advanced Development Program (TAT-ADP) was established as a first step in meeting this requirement, contributing to the technology base for development of an Advanced Medium STOL Transport (AMST).

The AMST must be capable of handling substantial payloads and using airfields considerably shorter than those required by large tactical transports now in the Air Force inventory. If this short-field requirement is to be met without unduly compromising aircraft speed, economy, and ride quality, an advanced-technology powered-lift concept will be required.

The STOL Tactical Aircraft Investigation (STAI) is a major part of the TAT-ADP, and comprises studies of the aerodynamics and flight control technology of powered lift systems under consideration for use on the AMST. Under the STAI, The Boeing Company was awarded Contract No. F33615-71-C-1757 by the USAF Flight Dynamics Laboratory to conduct investigations of the technology of the vectored-thrust powered lift concept. These investigations included:

(1) Aerodynamic analysis and wind tunnel testing.

(2) Configuration studies.

(3) Control system design, analysis, and simulation.

The control system technology work was of as much importance as the first two items because powered lift STOL flight introduces several problems absent (or not severe) in conventional (CTOL) aircraft and operations.

1.2 The STOL Control Problem

Short landings demand low speed approaches. Low speed implies a low dynamic pressure (q), so the effectiveness of ordinary aerodynamic control surfaces is reduced. Yet the moments of inertia of the airplane are similar in magnitude to the CTOL case. Furthermore, the relatively large engines typical of STOL designs imply larger engine-out control forces than for CTOL. The economical solution to the problem of more moment at less q, by providing the right combination of high-lift technology control surfaces and increased control surface areas, properly integrated into the overall airplane design, requires careful analysis.

Low speed also implies that gusts, wind shears, and cross winds will be a larger fraction of total airplane velocity than for the CTOL case. Consequently, the perturbations in angle of attack or sideslip due to turbulence, as well as the crab angle in a cross wind approach, will also be greater.

Moreover, at the high lift coefficients of STOL flight, aerodynamic cross coupling between axes is usually more severe, tending to degrade the flying qualities of the unaugmented airplane.

Nevertheless, short field landing performance demands minimum dispersion of the touchdown point, implying that better flying qualities than those acceptable for CTOL will be required, permitting more precise control despite the more severe design conditions. The need was clear, therefore, to investigate the design of control laws and mechanization concepts that would provide stability and control augmentation to a new degree of capability.

1.3 Technical Approach

Three closely related programs were therefore undertaken to deal with the problems stated above:

(1) A moment producer tradeoff study. Candidate moment producers were compared by a numerical scoring system accounting for effectiveness, weight, complexity, and cost.

(2) A study of control laws and control system mechanization. Control laws were developed and compared analytically and in piloted simulation. The mechanization of the selected control law was then actually designed.

(3) Development and operation of a piloted simulation of a vectored thrust STOL transport. Both fixed base and moving base simulations were used in selecting control laws and validating the mechanization of the one selected.

1.4 Document Organization

This document (Volume V, Part I) covers the first two of the programs discussed above. The third program, development and operation of a piloted simulation, is treated in Volume V, Part 2.

Section II summarizes the analysis and results presented more completely later. Section III states in detail the analysis procedures used in the moment producer study and in the control law and mechanization studies. Section IV describes the specific control laws and control mechanizations. Section V presents and compares the results of the evaluations of the various candidate moment producers and control laws. Section VI presents the conclusions and recommendations. Appendix I tabulates the complete moment producer analysis data. Appendix II defines the linear vehicle derivatives used in the control law analysis. Appendix III presents the complete control mechanization analysis data.

SECTION II

SUMMARY

2.1 Scope

A study of the control technology for a vectored thrust STOL transport has been made. Moment producers suitable for flight at low dynamic pressure were evaluated, control laws suitable for precision STOL approach and landing were developed, and several techniques of control system mechanization were investigated.

The major emphasis was placed on the landing approach task using a reference approach speed of 75 knots. However, the mechanized control system studies provide for operation over the full flight envelope.

2.2 Control System Development

The STOL control system must incorporate moment producing devices capable of controlling the vehicle at low speeds and these devices must receive the proper intelligence to produce precise flight path control. Once the proper intelligence (control law) is defined, the means of physically realizing the system can be determined.

The control system development determined the characteristics of the candidate moment producers and defined several control laws compatible with the following mechanization concepts:

- Mechanical Control Systems
- Stability Augmentation Systems
- Control Augmentation Systems
- Fly-by-Wire with Mechanical Reversion Systems
- Fly-by-Wire Systems

The systems were synthesized and analyzed using off-line digital analysis techniques and real time piloted simulation.

2.3 Results

Several moment producers, for each axis of control, satisfied the control power criteria. In general, the aerodynamic controls provided better performance than the propulsive candidates. This was especially true with regard to control capability with an engine failed. Best performance in the lateral and directional axes was obtained with either a double hinged surface or blown surface using engine bleed as the air source. The use of a double slotted elevator rated best for the pitch axis, being slightly better than a blown elevator.

Control laws were developed that provided good performance (i.e., Cooper-Harper ratings of 2 to 3) for STOL landing tasks that included IFR glideslope and localizer tracking using "raw" glideslope and localizer data. This performance was achieved by providing a longitudinal system that approximately decoupled speed response from flight path response. This reduced the pilot work load even though portions of the approach were flown on the "back side" of the thrust required curve. The lateral/directional control systems corrected for an inherent spiral divergence and provided good turn coordination. Although all the proposed lateral stability augmentation systems satisfied the military specification lateral handling quality response criteria, only those systems exhibiting excellent turn coordination characteristics were acceptable to the pilots. (See Volume V, Part II, Section 4.2.3.)

The comparative ratings of the control augmented, the fly-by-wire with reversion, and the fly-by-wire mechanized systems were very close. The control augmented system had a slight edge and was selected for validation on the moving base piloted simulation.

A major ingredient for the successful development of control systems for this STOL vehicle was the ability to separate flight path and speed control functions in the longitudinal axis. This required modulation of the propulsive lift vector to control speed while flight path was controlled by DLC and elevator control. Similarly, the lateral/direction l system must exhibit a high degree of turn coordination to be acceptable. The "decoupled" control analysis technique discussed herein provides a superior method for defining control systems with acceptable turn coordination.

2.4 Applicable to Other Powered Lift Concepts

The control technology developed in this program is applicable, with obvious minor adaptations, to the other powered lift concepts which have been considered for the AMST airplane.

In particular, this work has contributed directly to The Boeing Company's progress to date on the AMST prototype. That airplane uses the upper surface blowing (USB) form of the jet flap for powered lift. The longitudinal control scheme for STOL flight with USB employs the USB flap angle to control speed and the elevator to control flight path angle. The USB flap angle control is, in that application, precisely analogous to the thrust vector angle control for the vectored thrust/mechanical flap airplane studied in this report.

SECTION III

CONTROL SYSTEM SYNTHESIS TECHNIQUES

GENERAL

The control technology study for the STAI program was divided into three separate areas. These were:

(1) Comparative evaluation of moment producers suitable for low dynamic pressure (q) operations.

(2) Definition of control laws to provide precise flight path control in the landing approach modes.

(3) Mechanization of these control laws, recognizing the limitations of mechanical and electronic hardware.

The analysis techniques used in these studies, the constraints used in the analyses, and the scope of each study are defined below.

3.1 Moment Producer Study

The purpose of the moment producer study was to evaluate candidate moment producers for their ability to provide adequate low q control power while simultaneously considering the impact on weight, complexity, and cost. The moment producers considered were those applicable to an airplane equipped with mechanical flaps plus powered lift in the form of vectored thrust.

3.1.1 Candidate Moment Producers

The moment producer candidates considered in this study are enumerated in Table I. They include conventional aerodynamic, high lift aerodynamic, blown aerodynamic, and thrust reaction control devices.

The aerodynamic moment producer candidates are shown schematically in Figures 1 through 4 and the thrust vector modulation and reaction devices are shown in Figure 5. The aerodynamic characteristics are shown in detail in Tables XXI through XXV of Appendix I and are summarized in Table II. The thrust reaction devices used the bleed air available from the engines for thrust generation. Also, thrust modulation and thrust vector angle modulation of the main engines were considered. The engine bleed mass flow rate allowed approximately 1110 pounds of thrust to be generated in a bleed-air type reaction control. The comparative performance of the final candidates is discussed in the Moment Producer Trade Study, Section 5.1. The analysis procedure and techniques used to provide a measure of comparative performance, are described in the following sections.

TABLE I - SUMMARY OF MOMENT PRODUCER CANDIDATES

Moment Producer Type	Moment Producer Candidates
Conventional Aerodynamic	Single hinge trailing edge surface
	Double hinge trailing edge surface
	Panel spoilers
	Drooped trailing edge surface
	Slab horizontal tail
	Slab horizontal tail plus geared elevator
Blown Aerodynamic	Chordwise blown trailing edge surface
	Spanwise blown trailing edge surface
High Lift Aerodynamic	Double slotted elevator
	Double and triple slotted flaperons
	Vented Spoilers
	Slot deflector spoilers
Thrust Reaction Devices	Main engine differential modulation
	Main Engine differential vector angle modulation
	Reaction nozzles using engine bleed air
	"Bleed and burn" reaction nozzles

3.1.2 Moment Producer Analysis Procedure

The analysis of the moment producers was done in two phases. In the first phase the general group of candidates was defined. Their relative performance was evaluated using two dimensional (section) aerodynamic lift and drag data (aerodynamic candidates) or by estimating the reaction thrust capabilities (propulsive elements). The penalties associated with the implementation of these candidates as a part of an aircraft control system were also identified and compared. These initial implementation penalties included "cross-axis" induced acceleration coupling, reduction of engine thrust efficiency, incremental weight penalty, and projected complexity.

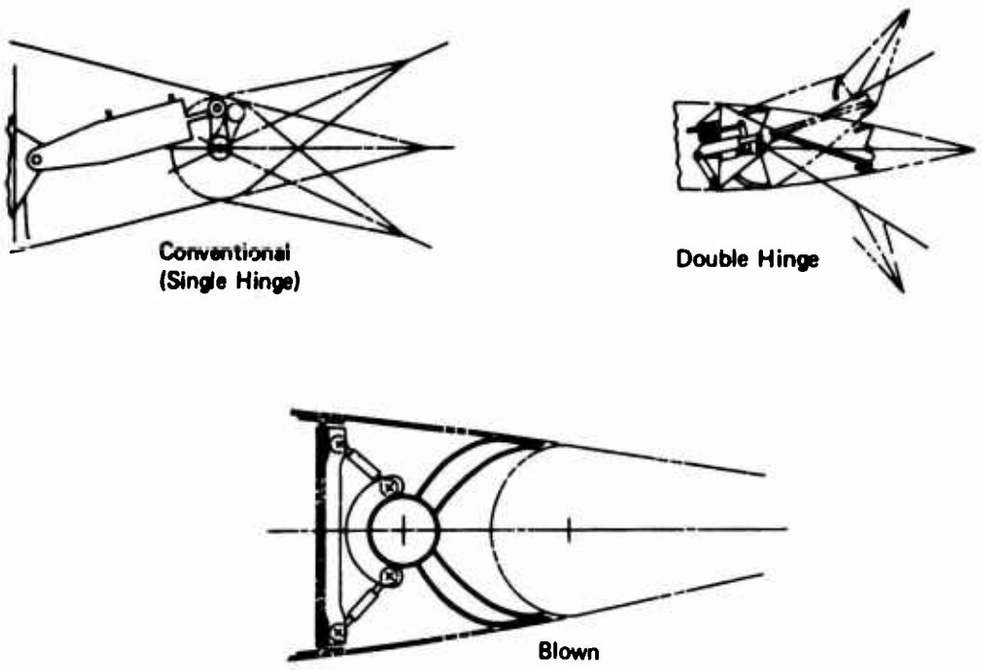

Figure 1: Trailing Edge Moment Producers – Used for Ailerons, Rudder, and Elevators

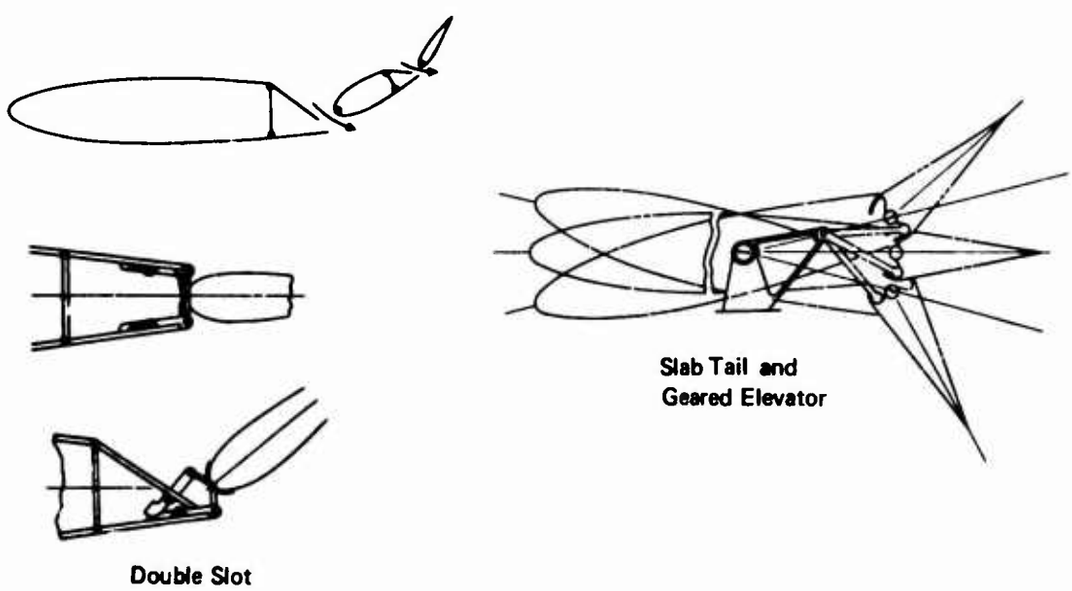

Figure 2: Special Trailing Edge Surface Moment Producers

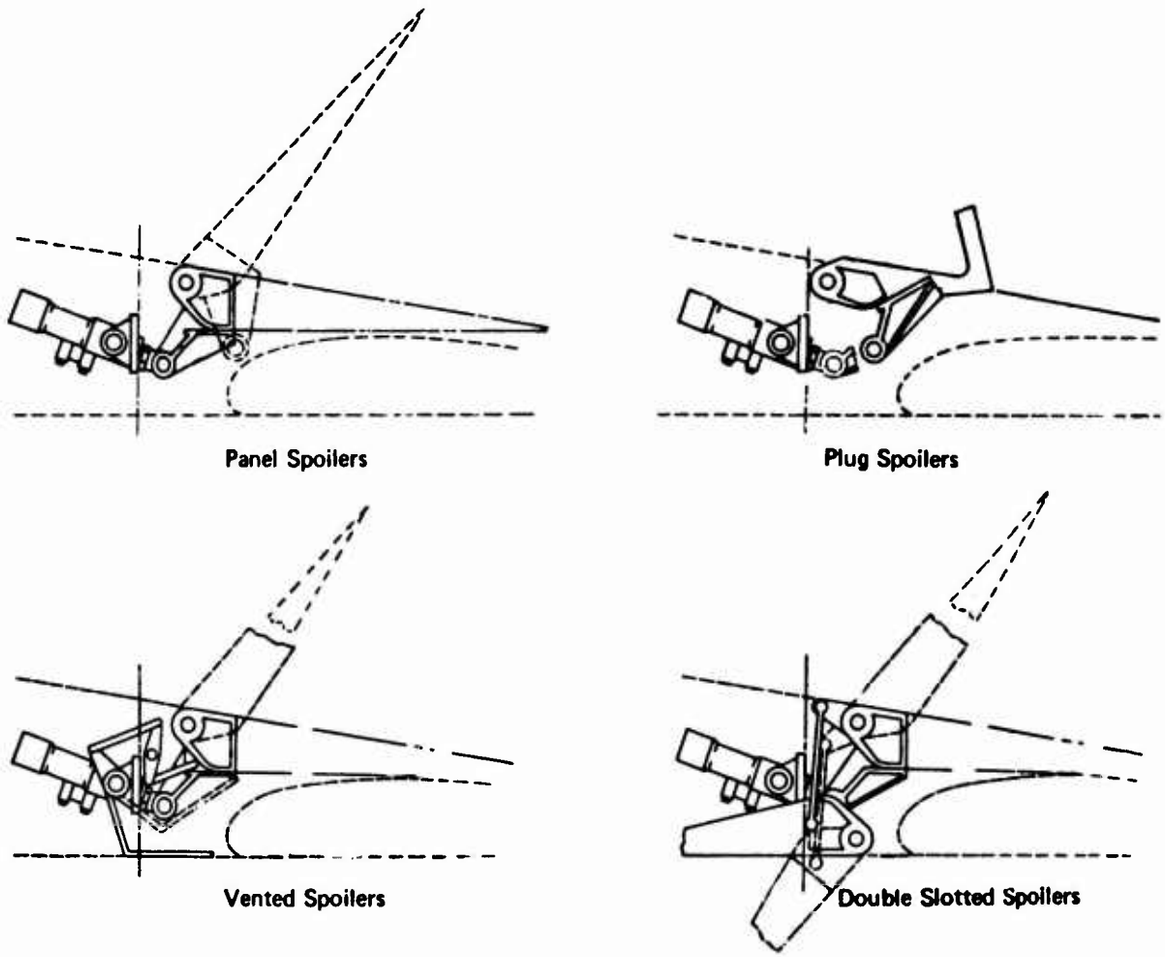

Figure 3 : Lift-Destructive Lateral Control Moment Producers

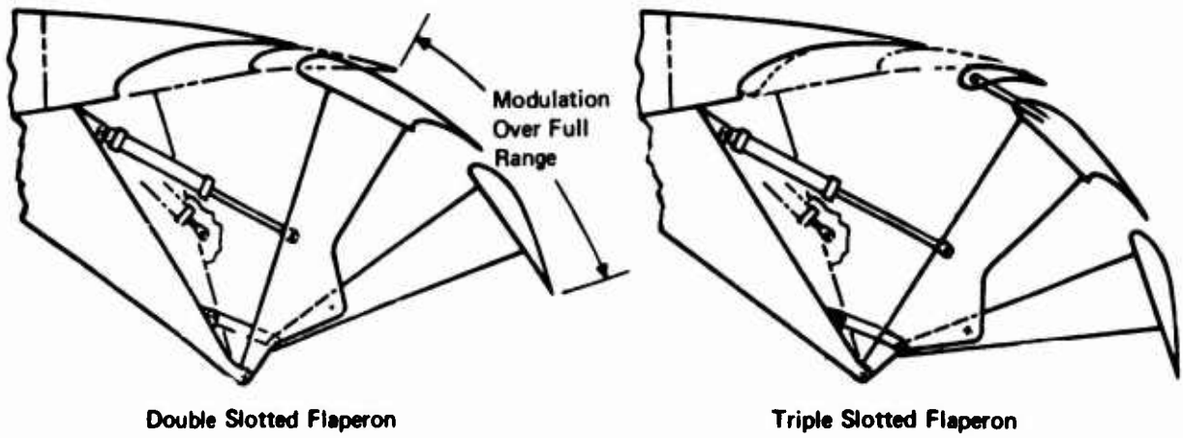

Figure 4 : Special Lateral Control Moment Producers

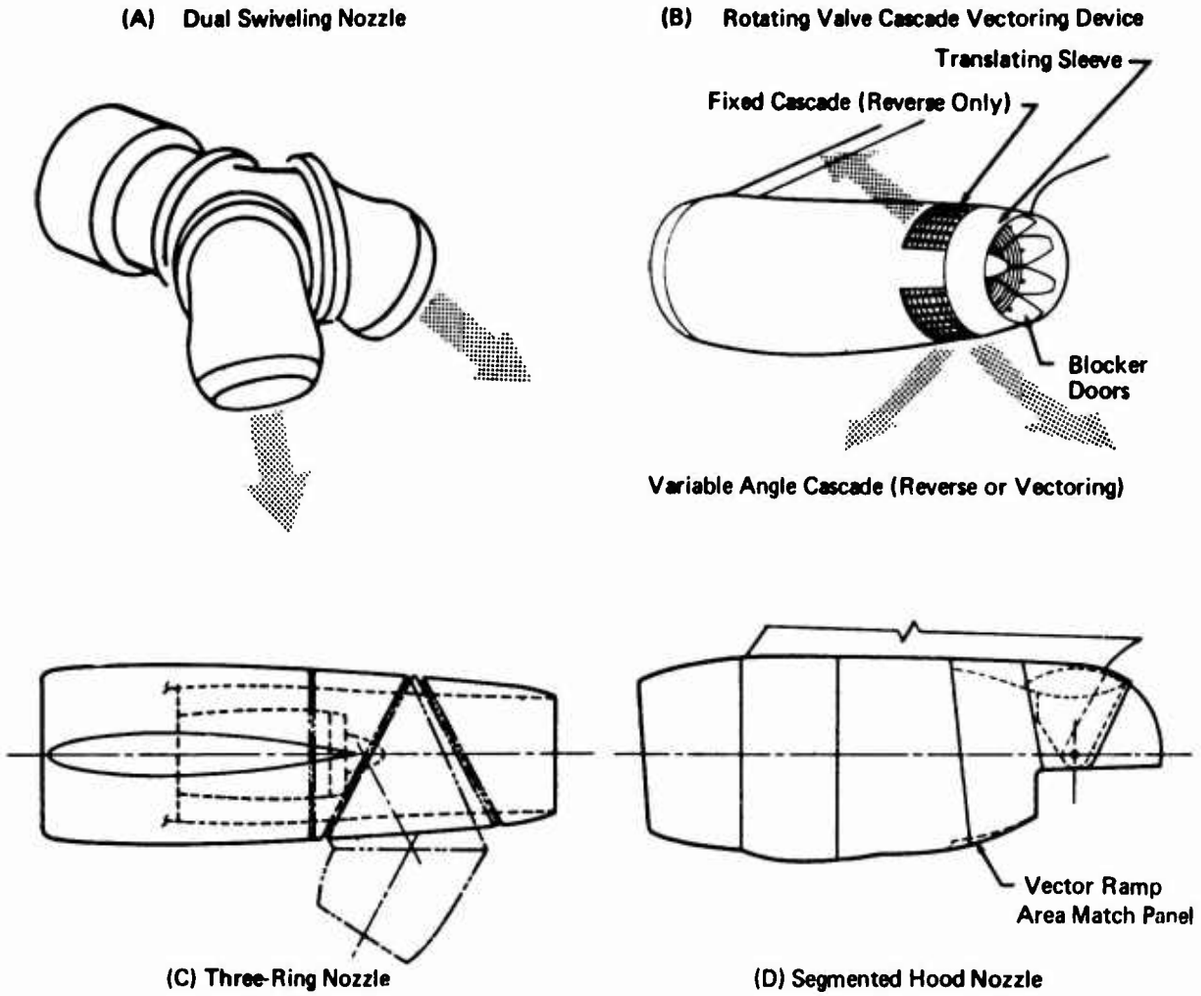

Thrust Vector Angle Modulation Devices

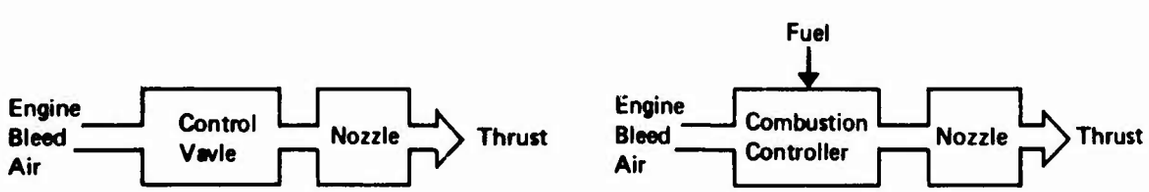

(A) Engine Bleed Reaction Controller

(B) Engine Bleed and Burn Reaction Controller

Reaction Control Candidate

Figure 5: Thrust Vector Modulation Devices and Reaction Control Candidates

TABLE II
SUMMARY DEFINITION OF AERODYNAMIC MOMENT PRODUCER CANDIDATES

Control Axis	Candidate Description (1)			Section Properties			
	Type	% Chord	Seg. RAT	$C_{\mu_{MAX}}$	Surface Deflect	$C_{L_{MAX}}$	$C_{D_{MAX}}$
DIRECTIONAL	Single Hinge Rudder	35	0	0	30	1.54	.107
	Double Hinge Rudder	35	50%	0	30/30	2.45	.142
	Blown Single Hinge	35	0	.059	60	3.26	.293
LATERAL	Single Hinge Aileron	25	0	0	30	1.17	.060
	Double Hinge Aileron	25	50%	0	30/30	1.85	.080
	Drooped Single Hinge	25	0	0	30	.895	.077
	Chordwise Blown Aileron	25	0	.070	60	2.80	.140
	Chordwise Blown 50 deg Drooped Aileron	25	0	.097	30	1.21	-.023
	Double Slotted Flaperon	30	50%	0	40/20, 10/10	.785	.019
	Triple Slotted Flaperon	30	50%	0	40/20, 10/10	.900	.007
	Panel Spoiler (2)	15	0	0	60	.891	.103
	Vented Spoiler (2)	15	0	0	60	1.004	.130
	Spoiler Slot Deflector (2)	15	0	0	60	1.33	.201
LONGITUDINAL	Single Hinge Elevator	35	0	0	30	1.47	.107
	Double Hinge Elevator	35	50%	0	30/30	2.35	.142
	Double Slotted Elevator	35	50%	0	40/30	3.43	.143
	Blown Single Hinge	35	0	.0665	60	3.10	.34
	Slab Tail	100	0	0	16	1.23	.04
	Slab + Geared Elevator	100	35%	0	13/30	1.98	.157

(1) See Appendix I for detailed description of chord ratios and surface deflection.

(2) Detailed aerodynamic characteristics interpolated from Table XXIII data.

In the second phase the most promising candidates identified in phase one were examined considering the impact of projected control power criteria, the effect of limited spanwise extent, and the relative cost of each candidate. Those candidates incapable of providing adequate control power for "engine-out" operation were excluded.

The moment producers were analyzed in the context of a "study" airplane. This was the STAI "Baseline Configuration" designed early in the program, and described in detail in the appendix to Ref. 1. The applicable mass and geometric properties are given in Tables III and IV.

3.1.2.1 Analysis of Moment Producer Control Power and Control Coupling

The maximum rotational acceleration, in the controlled axis, was used as the measure of control power. Rotational and translational accelerations, in axes other than the desired axis, were used as a measure of the "control coupling" or "cross-axis" coupling.

The control capability of aerodynamic elements was computed by determining the change of force on the surface area associated with the control elements (see Figure 6). These force variations were based on the following assumptions:

(1) The surface involved was at zero angle of attack.

(2) The aerodynamic surfaces were deflected to maximum displacement.

(3) The applicable control force area was computed in accordance with Figure 8.

(4) Section lift and drag coefficients were used in the initial evaluation of control capability (see Table II).

(5) The control capability per foot of span, computed during Phase I, used a dynamic pressure of 27.4 lbs/sq ft (90 knots EAS). Later performance studies indicated that a lower approach speed was appropriate; therefore, the control power for candidate systems was computed at 21.6 lbs/sq ft (80 knots EAS).

The lift and drag forces were used to compute angular accelerations in each degree of freedom by the following equations:

$$F_L = C_{L_{2D}} \, q \, S_{ik} = 27.4 \, C_{L_{2D}} \, S_{ik} \qquad (1)$$

$$F_D = C_{D_{2D}} \, q \, S_{ik} = 27.4 \, C_{D_{2D}} \, S_{ik} \qquad (2)$$

where i and k define the semi-span boundaries of the effective area S_{ik}

$$F_L = -F_Z \quad \text{(longitudinal and lateral axis)} \qquad (3)$$

or

$$F_L = F_Y \quad \text{(directional axis)} \qquad (4)$$

$$F_D = -F_X \quad \text{(all axes)} \qquad (5)$$

TABLE III

GEOMETRIC AND MASS PROPERTIES - STUDY AIRPLANE

Geometric Properties			Mass Properties	
WING				
Span	105.83	ft	Ixx	1.19×10^6 slug-ft^2
Area	1400.0	ft^2	Iyy	1.44×10^6 slug-ft^2
Aspect Ratio	8.0		Izz	2.58×10^6 slug-ft^2
VERTICAL TAIL				
Span	16.05	ft	M	4068.32 slugs
Area	260.0	ft^2		
Aspect Ratio	1.0			
			Engine Properties	
HORIZONTAL TAIL			Gross Thrust (Sea Level)	21,400 lbs.
Span	36.5	ft	Net Thrust (Sea Level)	19,200 lbs.
Area	332.6	ft^2	Bleed Air - (3 Engines)	36.4 lbs/sec
Aspect Ratio	4.0		@ 980° and 29 psia.	

TABLE IV

MOMENT PRODUCER EFFECTIVE LEVER ARMS - STUDY AIRPLANE

Surface or Moment Producer	LEVER ARM (FEET FROM C.G.)		
	x	y	z
All Vertical Tail Surfaces	-55.4	0	15.8
All Horizontal Tail Surfaces	51.7 (Low) 62.4 (Tee)	0 0	7.7 (Low) 24.2 (Tee)
All Wing Mounted Elements	Varies with location on wing	Varies with location on wing	6.0
Engines			
Inboard	5.2	15.8	- 1.5
Outboard	2.6	26.8	- 1.5
Reaction Jets			
Longitudinal	60.0	0	0
Lateral	0	51.4	0
Directional	60.0	0	0

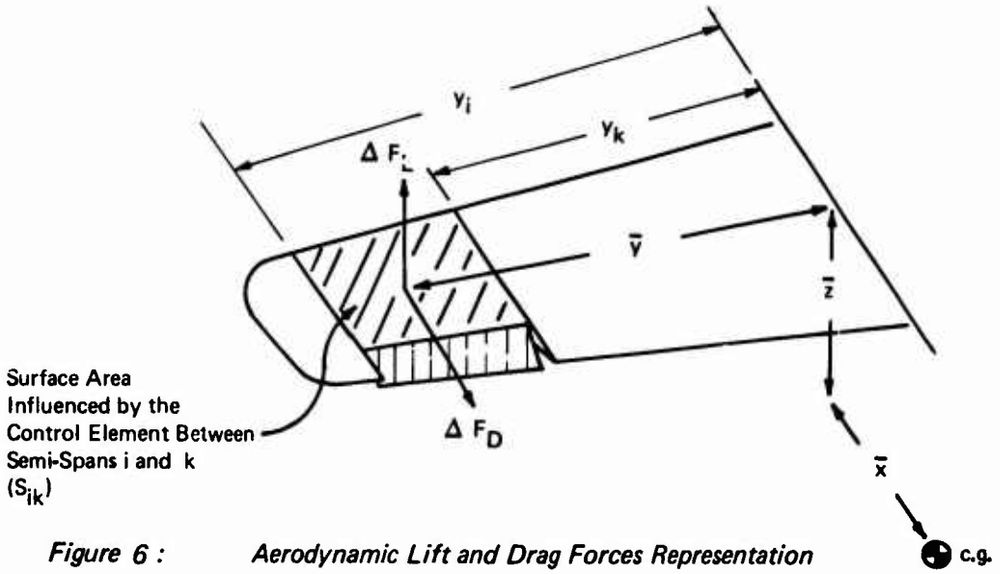

Figure 6 : Aerodynamic Lift and Drag Forces Representation

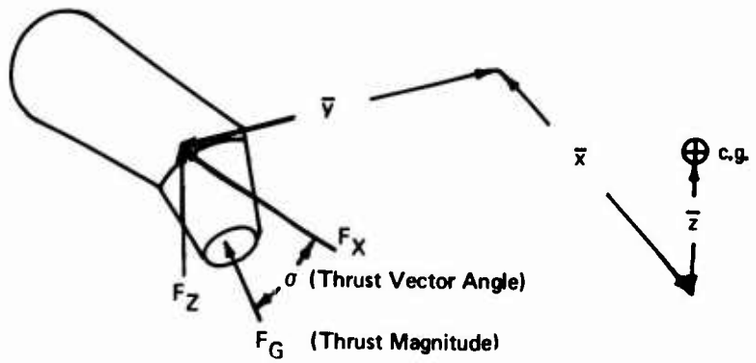

Figure 7 : Engine Thrust and Force Representation

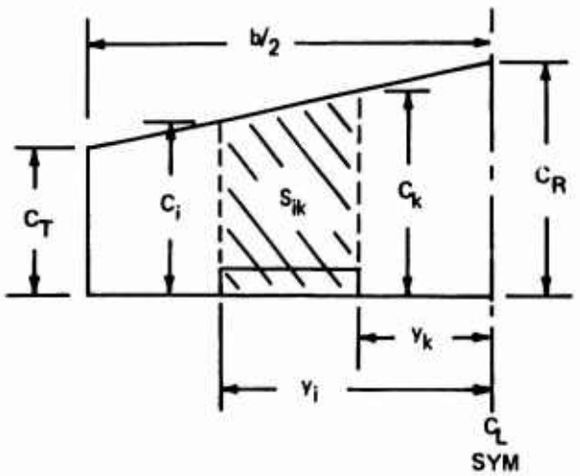

Where :

$$S_{ik} = \frac{2\,Sw}{(1+\lambda)}\left[1+\frac{(\lambda-1)}{b}(y_i+y_k)\right](y_i-y_k)$$

See Appendix I for Derivation

Figure 8 : Control Influenced Surface Area

The rotational accelerations are then:

$$\dot{P} = \frac{\Sigma F_z \cdot y - \Sigma F_y \cdot z}{I_{xx}} \tag{6}$$

$$\dot{R} = \frac{\Sigma F_y \cdot x - \Sigma F_x \cdot y}{I_{zz}} \tag{7}$$

$$\dot{Q} = \frac{\Sigma F_x \cdot z - \Sigma F_z \cdot x}{I_{yy}} \tag{8}$$

Since the effective lever arms and control influenced surface area is a function of wing location for wing mounted control elements, data was obtained for several locations with each candidate. The effect of wing location is thoroughly examined in Appendix I.

In addition to the rotational accelerations the impact of lift and drag on the translation accelerations were computed using the following equations:

$$\dot{W} = \frac{-\Sigma F_z}{m} \tag{9}$$

$$\dot{U} = \frac{\Sigma F_x}{m} \tag{10}$$

When a rotational acceleration demand results in axial acceleration ($\dot{U}$) or a normal acceleration ($\dot{W}$), this "coupled" response was assumed undesirable since it would require pilot compensation. The evaluation of acceleration capability of thrust modulation and thrust vector techniques utilized the force versus vector angle plots of Figure 9 to compute applicable F_z and F_x force components.

The general nozzle equation below was used to compute the reaction thrust of the reaction thrust candidates.

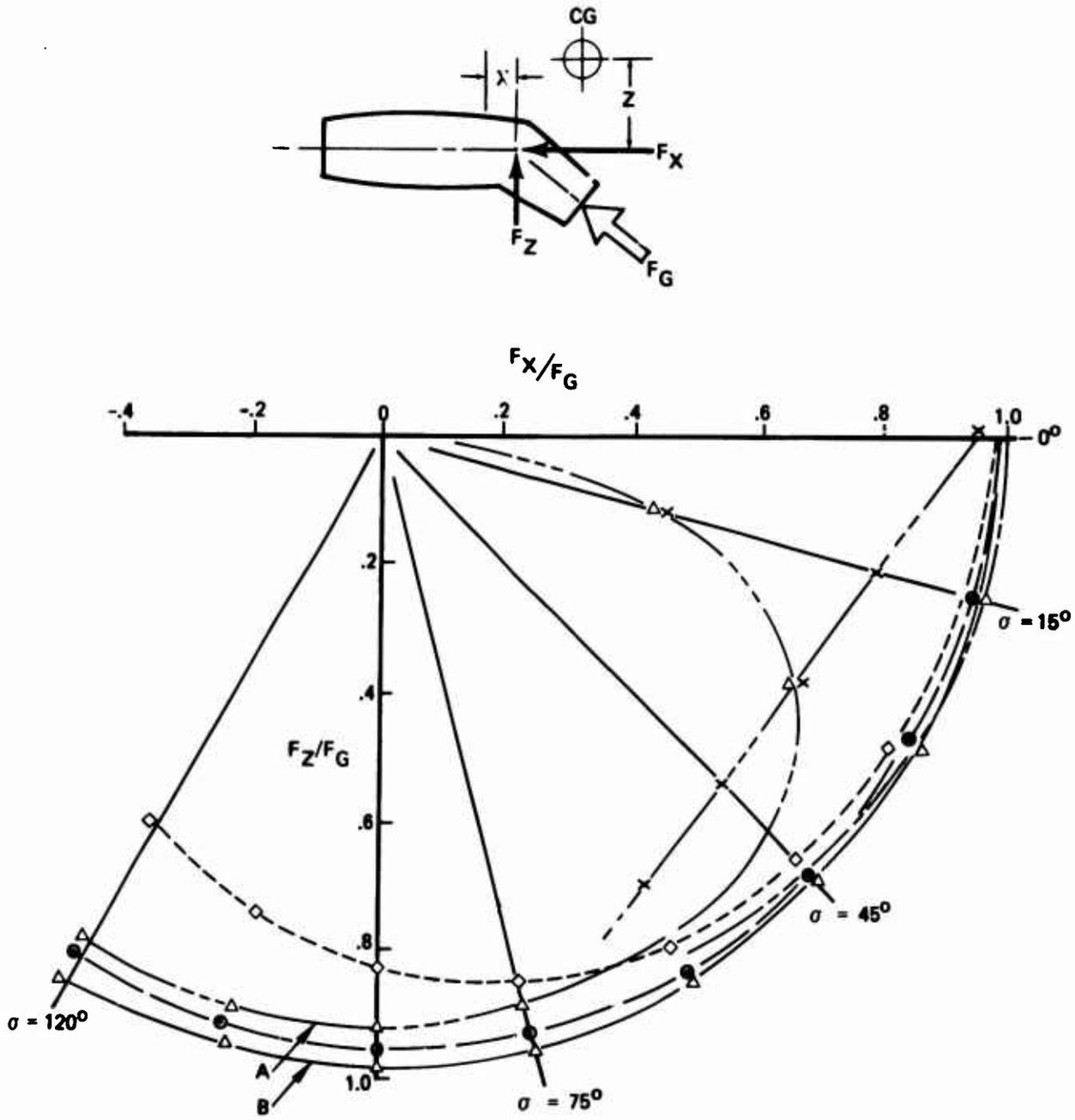

- □ Eyeball
- ● Three Bearing
- △ Rotating Cascade, (A, α = 45°, ϕ = 45°), (B, α = 0° - ϕ = 90°)
- ◇ Dual Swivel
- X Rotating Valve
- σ Effective Vector Angle
- α Nozzle Angle
- ϕ Blade Angle

Figure 9: Thrust Vector Functions

$$F = C_V \, m \, V_{ID} \tag{11}$$

where:

F = Reaction force

C_V = Velocity coefficient

m = Nozzle air mass flow

V_{ID} = Nozzle air flow velocity

The reaction elements were installed to obtain maximum rotational acceleration about a specific axis. The reaction force, which was aligned with either the x, y, or z axis, was substituted into appropriate equations to obtain the rotational or translation accelerations.

Phase 1

The control power, control coupling, and accelerations were computed for each candidate element. The accelerations were then normalized by dividing by the control element span or the reaction thrust. This normalized magnitude was used to compare the relative performance of alternate candidates installed at identical locations or to compare the relative performance of a common element located at alternate positions. The complete data computed during this phase of the study are recorded in Tables XXVI through XXIX of Appendix I.

Phase 2

All candidates appeared to have the ability to provide adequate control power to overcome the engine-out moment and satisfy Level 3 control requirements except for those systems using differential thrust modulation or differential thrust vector modulation. Since the loss of an engine on landing approach requires that the remaining engines be advanced to full thrust to maintain a constant level of powered lift, the resultant moment increases the magnitude of aircraft upset. Powered lift would have to be reduced significantly to simply achieve a moment balance. This excessive loss of powered lift was not considered satisfactory for a vectored thrust high lift flap airplane. Therefore, these candidates were not considered during the second phase of the moment producer study.

The second phase of the moment producer study considered the integration of potential candidates into an airplane control system. Since the mechanical flap/vectored thrust airplane requires a large portion of the trailing edge surface for high lift devices, the following rules were established governing the integration of lateral control elements of the wing:

(1) All trailing edge control surfaces would be located outboard of 80% of the wing semi-span.

(2) Aileron and spoiler control elements would not overlap.

(3) No control surface was located in the outboard 3% of the wing span because of insufficient structural support.

The ideal "two-dimensional" control power capabilities of aerodynamic candidates are not realized because of the finite span. The three dimensional factors applicable to the study airplane were developed using Datcom methods and are given in Table V.

TABLE V

THREE DIMENSIONAL AERODYNAMIC FACTORS - STUDY AIRPLANE

Control Surface	Three Dimensional Factors	
	$K_{CL_{3D}}$	$K_{CD_{3D}}$
Vertical Tail	.40	$.14\ (\Delta C_{L_{2D_{max.}}})^2$
Horizontal Tail		
elevators	.668	1.0
slab surface	.860	1.3
slab plus gear elevator	1.0	1.5
Ailerons/Flaperons	.80	1.0
Spoilers	.755	.755

Denoting a generalized two-dimensional control acceleration by $(\dot{A}_{2D})$, the generalized three-dimensional control capability can be represented as:

$$\dot{A}_{3D} = (K_{C_{L_{3D}}}) \cdot (\dot{A}_{2D}) \text{ for terms derived using } C_L \quad (12)$$

$$\dot{A}_{3D} = (K_{C_{D_{3D}}}) \cdot (\dot{A}_{2D}) \text{ for terms derived using } C_D \quad (13)$$

where $\dot{A}_{2D} = (\dot{A}/_{ft}) \cdot$ (available span)

and $\dot{A}/_{ft}$ was the control power data obtained in phase 1.

The candidate system control power is computed using this equation. Control coupling is similarly computed. This three-dimensional correction completes the evaluation of control power and control coupling.

3.1.2.2 Analysis of Moment Producer Weight

The control system weight was computed by comparing the proposed moment producer system to those on existing aircraft using statistical analysis methods. Included in the incremental weight for each candidate was the structural weight associated with the surface or reaction nozzle, the weight of its control system, (i.e., actuation plus mechanical reaction linkages), and the incremental weight of the pneumatic system when applicable. It was assumed that double hinge surfaces other than flaperons would have both segments mass balanced.

A consistent statistical method was used throughout a class of moment producers in order to avoid introducing differences due to method. A cross check with an alternate statistical method for each class was employed frequently. For example, the weight of the surface control system for a conventional rudder was established by a statistical equation using the area of the rudder as the correlation parameter. This weight was confirmed by another method using gross weight, body length, wing span and tail arm as the correlation parameters. Since statistical data did not exist for weighing the thrust modulation systems, they were weighed by estimating the weight of individual elements.

During the phase one moment producer analyses, the incremental weight was normalized per foot of span or per thousand pounds of thrust in the same manner as the element control power. This provided a common basis for comparing the relative merits of like systems.

During phase two, the incremental weight for the available span was computed and divided by the available control power to determine the weight required to obtain a specific acceleration capability (i.e., pounds/rad/sec^2). Thus;

$$\frac{\Delta W}{\text{rad/sec}^2} = \frac{\Delta W \text{ candidate}}{\dot{A} \text{ candidate}} \qquad (14)$$

Where: ΔW is total incremental weight and $\dot{A}$ is applicable control power

3.1.2.3 Analysis of Moment Producer Complexity

To provide a rational basis for the analysis of moment producer complexity, three major areas associated with moment producer systems were identified. These three areas are power generation, power distribution, and force conversion. These three items were assigned maximum numerical values of three, two, and five respectively. The computed value for complexity was then:

$$C_x' = PG + PD + FC \qquad (15)$$

where PG is a power generation complexity rating (value 0-3)

PD is a power distribution complexity rating (value 0-2)

FC is a force conversion complexity rating (value 0-5)

To provide a uniform method of evaluating these three major areas, they were divided into equally weighted "sub-items". These were:

(1) Power generation

(a) Quantity and type of components required for conversion of prime mover force to a power source compatible with moment generator elements. Are conversion units standard or new design?

(b) Special power source controls (speed regulation, pressure regulation, pneumatic pressure controls)

(c) Spatial integration with prime mover

(d) Ease of maintenance

(2) Power distribution

(a) Quantity and type of components required for power transmission. Has design been proven in operation?

(b) Flexibility of transmission routing

(c) Ease of completing interface with actuation system

(d) Spatial integration with structure and other systems

(e) Ease of maintenance.

(3) Force conversion

(a) Quantity and type of actuation (or force generation) units. Are there requirements for special functions (eg; force limiting, displacement limiting, or is retention of the moment producer required if power is lost) ?

(b) Ease of integrating various actuation units with signal path

(c) Spatial integration with structure and other systems

(d) Complexity of structure to complete load path (hinge and reaction links, flap tracks, or inter-element gearing)

(e) Ease of maintenance.

To provide consistency in the evaluation, a standard for comparison was defined with median rank. This standard was an aileron powered by a single hydraulic actuator mounted at the aileron. The rating for this unit was:

Power Generation	1.6
Power Distribution	.8
Force Conversion	2.4
Total	4.8

The second phase moment producer analysis used complexity numbers divided by control power to compare relative performance. Thus, the normalized complexity was

$$\frac{C_x}{\text{rad/sec}^2} = \frac{C_{x\ \text{candidate}}}{\dot{A}\ \text{candidate}} \tag{16}$$

The complexity for blended lateral systems, where a portion of the total span employed some elements more complex than others, was computed by pro-rating the combined complexity to reflect the proportions contributed by each element:

$$C_{x\ \text{system}} = \frac{\dot{A}_1 C_{x_1} + \dot{A}_2 C_{x_2} + \cdots \dot{A}_n C_{x_n}}{\dot{A}_1 + \dot{A}_2 + \cdots + \dot{A}_n} \tag{17}$$

3.1.2.4 Analysis of Moment Producer Cost

The cost of control candidates was analyzed in a manner similar to that used for weights. The elements of the proposed mechanizations were broken down and compared to similar elements in existing airplanes. This analysis included cost per pound for structure, incremental cost for element control actuation, incremental costs for the pneumatic system when applicable, and incremental costs for APU's when used as a pneumatic air source. Where statistical data did not exist, as in the case of the thrust vectoring systems, proposed mechanizations were defined and incremental costs were estimated element by element.

The cost data was generated only in the second phase of the moment producer study. As in the case with weight and complexity, the cost was normalized for a given control power capability as follows:

$$\frac{\text{Cost}}{\text{rad/sec}^2} = \frac{\text{Cost system}}{\dot{A}\ \text{system}} \tag{18}$$

3.1.2.5 Comparative Analysis of Moment Producer Parameters

A "figure-of-merit" was established to compare the dissimilar parameters used in the trade study. This figure-of-merit established a value of 1 for "most" merit and 10 for "least" merit in a specific category. Weighting factors were assigned by the evaluator to reflect the relative importance of each parameter. Control power and coupling between axes, being the most significant factors, were assigned weighting factors (W's) of one. The weighting factors for the remaining parameters were incremental weight (.6), complexity (.4), and cost (.3).

Some parameters, such as cost, weight, or complexity, must have a low rating to reflect "merit". For these quantities the following equation was used to compute the figure-of-merit:

$$F_m = \frac{9P + P_{max} - 10\,P_{min}}{P_{max} - P_{min}} \tag{19}$$

When a large value represented "merit", as in control power, the following equation was used in the computation of merit.

$$F_m = \frac{10\,P_{max} - P_{min} - 9P}{P_{max} - P_{min}} \tag{20}$$

where P is the parameter being evaluated and $P_{max} - P_{min}$ reflect the range of the variable being considered.

The computation of the merit figure for control coupling required special consideration. The coupling of some axes was so large that the total control capability of the coupled axis was required to balance the induced moment. In other cases, the coupling was nearly insignificant. A formula was devised to assign a value of ten when the cancellation of induced moment required the full capability of the coupled axis, as follows:

$$F_m = 10\left[\frac{\dot{B}\text{ candidate}}{\dot{A}\text{ candidate}}\right]\left[\frac{\dot{A}\text{ maximum demand}}{\dot{B}\text{ maximum capability}}\right] \tag{21}$$

Finally, overall rating factors for each candidate were computed by

$$R_F = \Sigma W F_m \tag{22}$$

3.2 Control Law Synthesis

Both "classical" root locus and frequency response methods, and "modern" decoupling techniques were used to develop control laws providing good handling qualities in the critical landing approach flight condition. The development process was necessarily an iterative one, in which concepts designed by the various techniques were further tested by piloted simulation, modified, and retested.

In the sections to follow, analysis procedures are defined in detail and illustrated by examples drawn from the actual design and analysis effort.

3.2.1 Synthesis of Multiloop Control Systems by Root Locus Method

The discussion that follows is organized in two parts: (1) a general outline of the root locus technique, and (2) a detailed application of the root locus method to the development of a lateral-directional augmentation control law.

Each output variable of an interacting multi-variable plant responds in general to all system inputs or disturbances. It is possible to relate each output to each input or disturbance by a transfer function (a ratio of two polynominals of the Laplace operators common denominator exists for all such transfer functions, and is called the system characteristic equation. The loci of roots of the characteristic equation determine stability. The form of the individual transfer functions defines the response of each output to each input or disturbance. These concepts were applied as follows:

(1) A quantity was selected for feedback for which a sensor is available and which has potential for modifying an undesirable system characteristic, and the characteristic equation derived.

(2) A root locus plot was made. The trajectory of the characteristic roots enabled the selection of a trial gain setting.

(3) Using a gain setting obtained from Step (2), time histories were computed for significant output-input pairs to determine the interaction effects. These time histories and their associated transfer functions showed whether this feedback closure is aiding convergence of the control system design toward the desired overall performance specifications.

(4) If the closure looked promising, the system was considered a candidate for further loop closures.

An acceptable final closed-loop control system generally required iteration of the feedback closures and gains to reach the desired specifications.

The details of application of this synthesis technique to a multivariable control system depends on the specific form of the system and the nature of the specifications. The remainder of this section gives an example of the derivation of a control law for the lateral-directional axes to illustrate those details.

In the unaugmented airplane, the pilot controlled aileron and spoiler deflections with the wheel and the rudder by the rudder pedals. This example of control law derivation made use of the following feedback quantities: (1) yaw rate, (2) roll rate, and (3) computed sideslip rate. The computed sideslip rate used yaw rate, roll attitude, and airspeed.

Several feedback closures were sequentially made to improve the excessive spiral divergence and poor turn coordination characteristics of the unaugmented airplane. First, yaw rate was fed back to ailerons and spoilers to neutralize the spiral mode. Next, computed sideslip rate was fed back in an attempt to improve turn coordination. This closure improved turn coordination but exceeded the dutch roll mode damping in terms of the a priori design objective. By lagging the computed sideslip rate, turn coordination was improved while keeping the dutch roll damping at the desired value. Then roll rate was fed back to ailerons and spoilers to correct the sluggish roll rate response that resulted from

the previous closure. The control law development ended with a derivation of a wheel-to-rudder cross-feed compensation to further improve turn coordination. The detailed control law development follows.

Consider the unaugmented bank angle to wheel transfer function, which generally takes the form of:

$$\frac{\phi}{\delta_{W_p}}(s) = K \frac{(s^2/\omega 2_\phi + 2\zeta_\phi/\omega_\phi s + 1)}{(\tau_s s \pm 1)(\tau_R s+1)(s^2/\omega_D^2 + 2\zeta_D/\omega_D s+1)} \qquad (23)$$

where

τ_S = spiral mode time constant (sec.),

τ_R = roll subsidence mode time constant (sec.),

ζ_D = dutch roll damping ratio

ω_D = dutch roll undamped natural frequency (radians/sec.)

ζ_ϕ = roll zeros damping ratio

ω_ϕ = roll zeros undamped natural frequency (radians/sec.)

In order that the augmented airplane satisfy the flying quality requirements of military specifications MIL-F-83300 and MIL-F-8785B, the following design objectives were established:

(1) The spiral mode should be neutralized (τ_S>30 seconds)

(2) The roll time constant should be less than 1.4 seconds (τ_R<1.4 seconds)

(3) The roll zeros should be near the dutch roll poles ($\zeta_\phi \cong \zeta_D$ and $\omega_\phi \cong \omega_D$)

(4) The dutch roll poles should be fairly well damped ($\zeta_D \geq .4$)

(5) The dutch roll undamped natural frequency should be larger than one radian per second ($\omega_D > 1$)

(6) Turn coordination should be acceptable ($|\Delta\beta/\phi_1| < .3$ ...$\Delta\beta$ and ϕ_1 are defined in MIL-F-83300)

(7) The roll rate to wheel ratio should be approximately .3 degree per second per degree.

For the unaugmented AMST in its landing configuration, the spiral mode is excessively divergent (τ_S = 7.5 secs.); the dutch roll mode has low damping (ζ_D = .184); and the turn coordination is poor ($|\Delta\beta/\phi_1| \cong .58$). Figure 10 illustrates these characteristics in detail in terms of the bank angle to wheel transfer function and the transient responses to wheel and pedal inputs.

The initial loop closure was yaw rate fed back to the ailerons and spoilers, in an attempt to move the spiral pole closer to the origin of the complex plane. (See Figure 11). For a gain of 1.35 deg/(deg./sec.), the spiral root is very nearly neutralized ($\tau_S = 1.4 \times 10^3$ seconds). The resultant system has low dutch roll damping (ζ_D = .139) and exhibits poor turn coordination ($|\Delta\beta/\phi_1| \cong .57$). Figure 12 shows the effect of feeding back a computed sideslip rate to the rudder in addition to the yaw rate feedback. From the root locus, it is seen that the $\dot{\beta}_{SAS} \rightarrow \delta_R$ feedback damps the dutch roll mode substantially. With the $\dot{\beta}$ gain set at 1.5 deg./(deg/sec.), the wheel input time responses exhibit better turn coordination than was seen for the $r \rightarrow \delta_A$, δ_{SP} gain = -1.35 system. At this point of the synthesis, the design goal of $\omega_D > 1$ radian/sec. is still not met. Increasing the $\dot{\beta}$ gain would increase ω_D but would over damp the dutch roll mode. The Figure 12 root locus shows the angle of departure for the dutch roll pole trajectory to be approximately 180 degrees. Figure 13 shows that if the computed sideslip rate is fed back through a 0.8 second first order lag filter the angle of departure is changed to 145 degrees. This leads to a larger ω_D but does not change dutch roll damping significantly. Roll rate can now be fed back to the ailerons and spoilers to increase roll rate response (decrease the roll subsidence time constant). Figure 14 shows the effect of closing the roll rate feedback loop when $r \rightarrow \delta_A$, δ_{SP} gain = 1.35, $\dot{\beta} \rightarrow \delta_R$ gain = -3.0, and $\tau_{\dot{\beta}}$ = 0.8 second. Most design goals have now been satisfied, but the last design iteration has produced a system that still lacks turn coordination ($|\Delta\beta/\phi_1| \cong .41$). A wheel to rudder crossfeed was next implemented. (The method used for implementation is described in Ref. 2 , but is repeated in this section for completeness.) Assuming linear equations of motion in still air, total sideslip produced in a turn is, by super-position, equal to the sum of sideslip resulting from both wheel and pedal inputs. Expressed in equation form:

$$\text{i.e., } \beta(s)_{total} = \beta/\delta_W(s) \cdot \delta_W(s) + \beta/\delta_{PED}(s) \cdot \delta_{PED}(s) \qquad (24)$$

By definition, when the turn is coordinated, $\beta_{total} = 0$. Hence the required pedal input for a coordinated turn commanded through the wheel is:

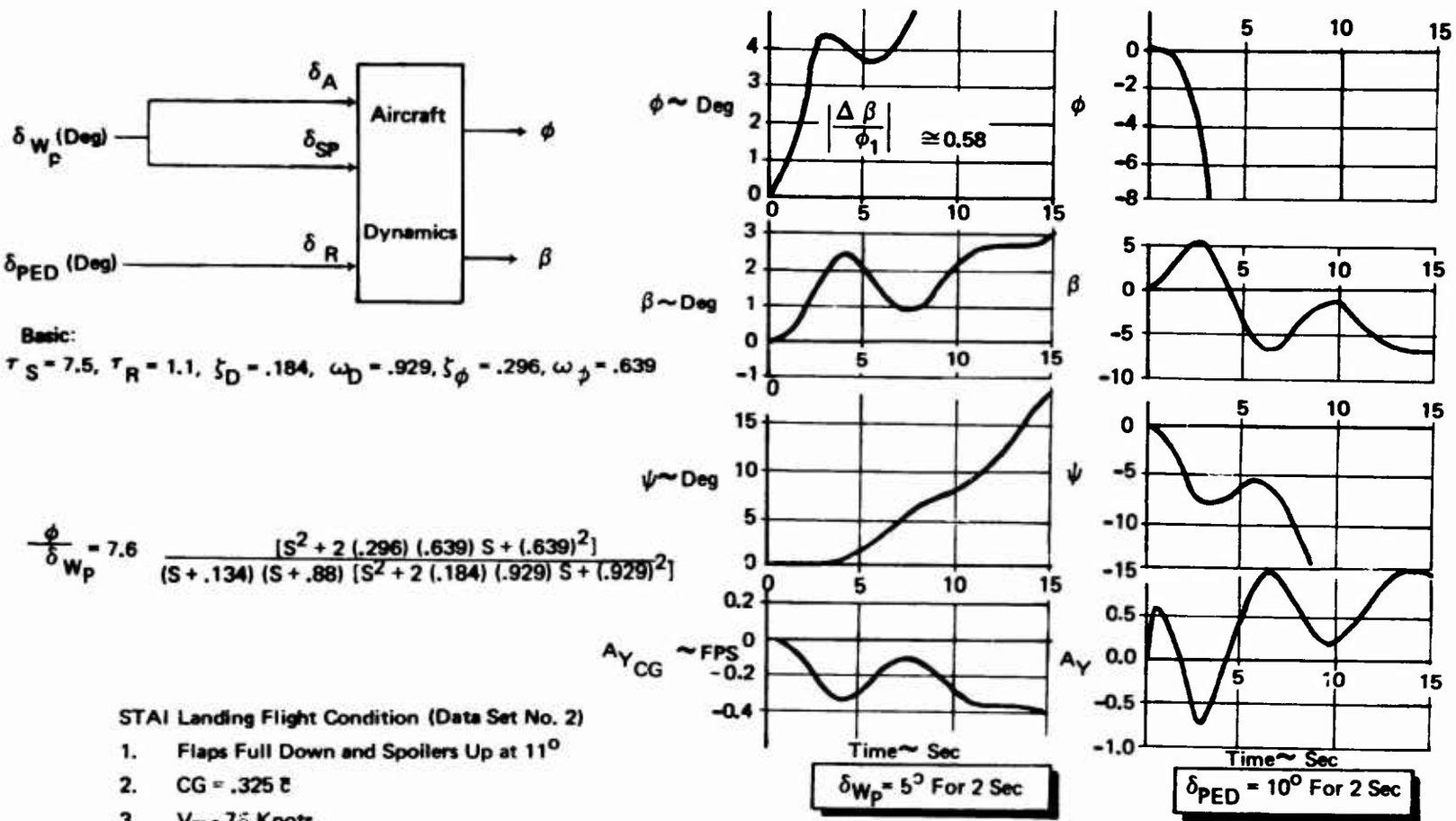

Figure 10: Lateral/Directional Dynamics for the Unaugmented Airplane

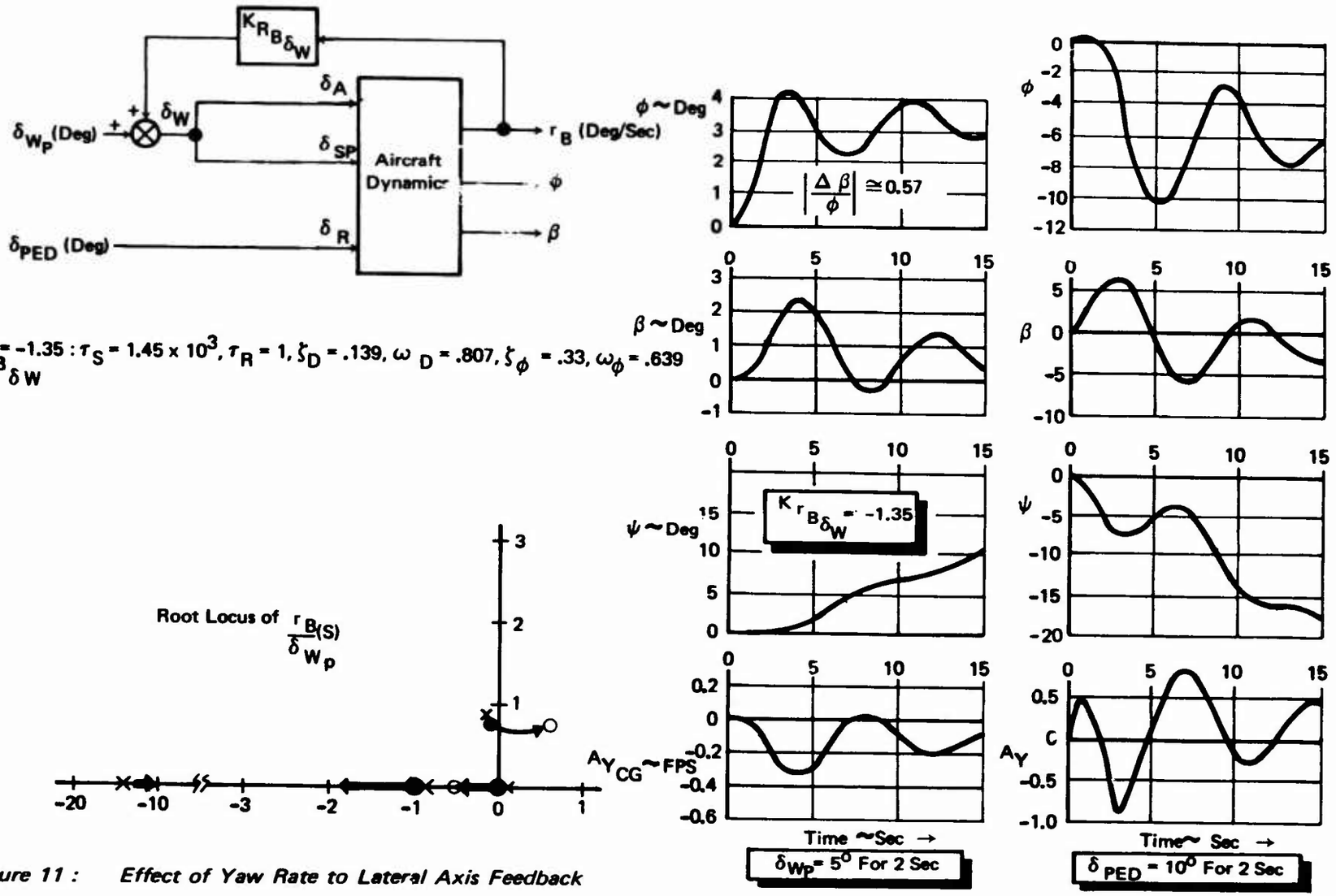

Figure 11 : Effect of Yaw Rate to Lateral Axis Feedback

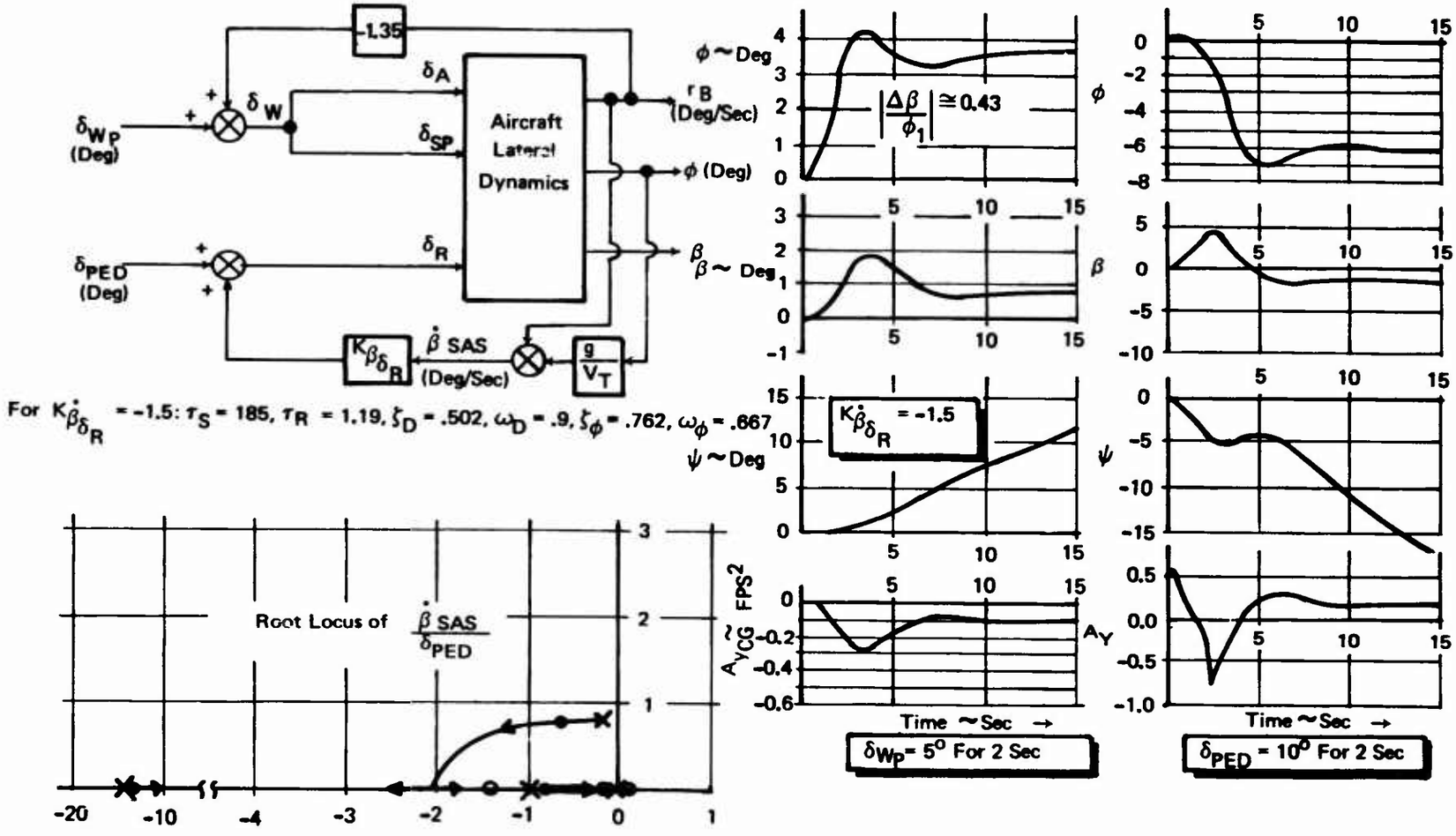

Figure 12 : Effect of Sideslip Rate to Rudder Feedback

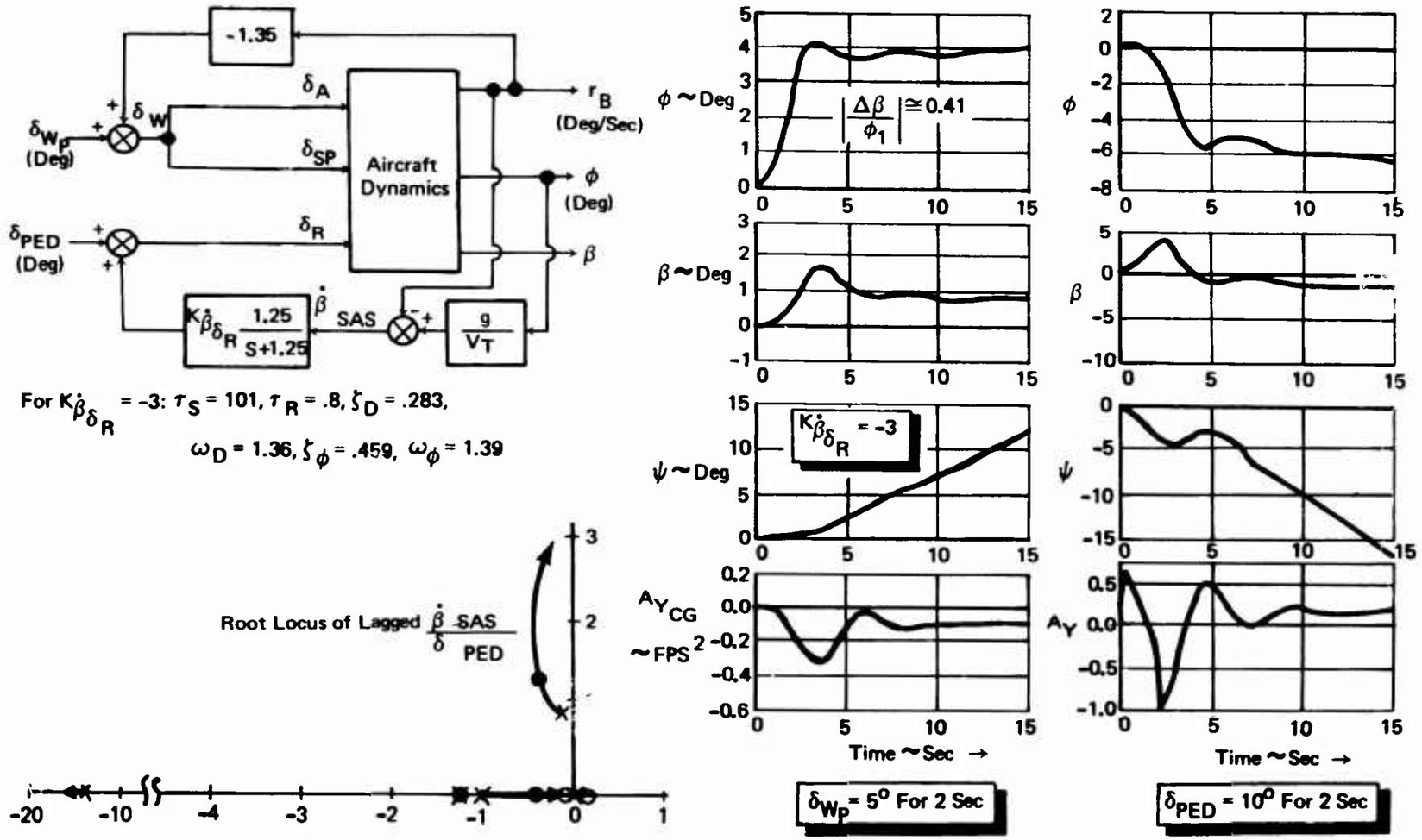

Figure 13 : Effect of the Lagged Sideslip Rate to Rudder Feedback

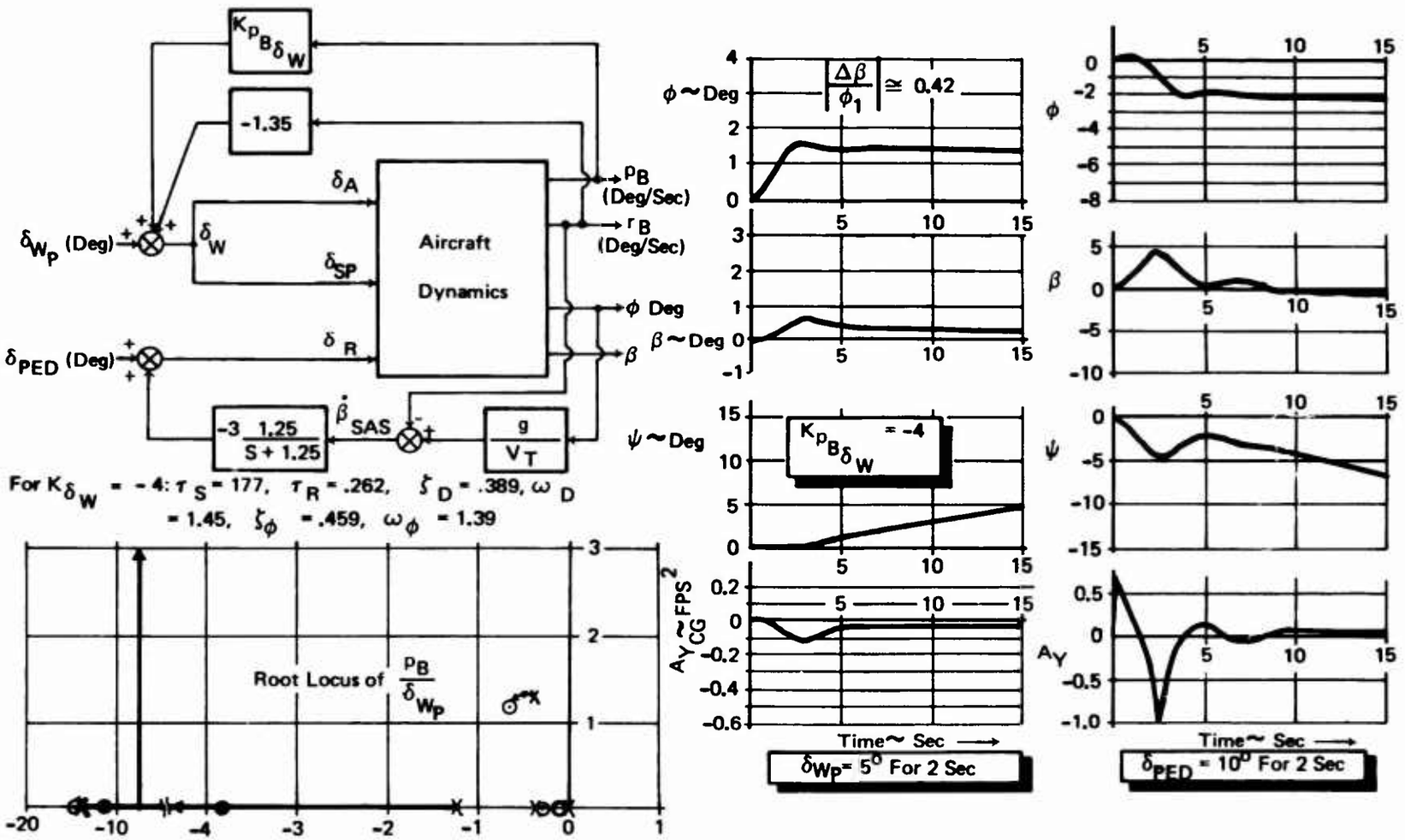

Figure 14 : Effect of the Roll Rate to Lateral Axis Feedback

$$\delta_{PED}(s) = - \left[{}^{\beta}/_{\delta_W}(s)\right] \cdot \left[{}^{\beta}/_{\delta_{PED}}(s)\right]^{-1} \cdot \delta_W(s) \qquad (25)$$

or

$$\delta_{PED}(s) = G_{CF}(s) \cdot \delta_W(\beta) \qquad (26)$$

where

$$G_{CF}(s) = - \left[{}^{\beta}/_{\delta_W}(s)\right] \cdot \left[{}^{\beta}/_{\delta_{PED}}(s)\right]^{-1} \qquad (27)$$

A straight line Bode plot is shown in Figure 15 for $G_{CF}(\omega)$. Also shown in the plot is a first order lag approximation to $G_{CF}(\omega)$. Using this lag, the turn coordination is brought within the bounds of the design objective ($\left|{}^{\Delta\beta}/_{\phi_1}\right| \cong .17$). The desired roll rate to wheel input sensitivity is now set by adding a feedforward gain of 1.5 deg./deg. from the wheel to the roll command which completes the design. Responses and a block diagram of the final control law are shown in Figure 15.

3.2.2 Multiloop Synthesis by the Frequency Response Method

This section describes an application of the frequency response analysis technique using a pilot describing function in the synthesis of a longitudinal control system. Therefore, the first task of this synthesis was determination of the pilot loop closures and control compensation required for precise control of the unaugmented airplane. The control law structure was then formed by substituting augmentation loops for those parts of the "pilot" loop closure dealing with suppression of unwanted motion. Rate feedback paths were mechanized to eliminate any requirement on the pilot's part for lead compensation. This substitution is based on the assumption that pilot ratings are best when a pilot can achieve good closed loop dynamics with pure gain control (i.e., $\delta_{Col} \propto \theta_{error}$). The primary advantage to this design technique is that it allows an integrated analysis of the pilot/augmented airframe combination as a closed loop control system. Tradeoffs between control system gains and control sensitivity, closed loop stability and bandwidth were easily assessed by using this approach.

System analysis techniques which use pilot describing functions have been widely used (e.g., Refs. 3 through 6) for the synthesis and evaluation of pilot-airframe control systems. The pilot describing function, its details, and the validity of its application have been discussed at great length in the literature (i.e., Refs. 3 and 7). Only the basic concept is repeated here.

The application example given in this section is the synthesis of a control law for the longitudinal modes. The describing

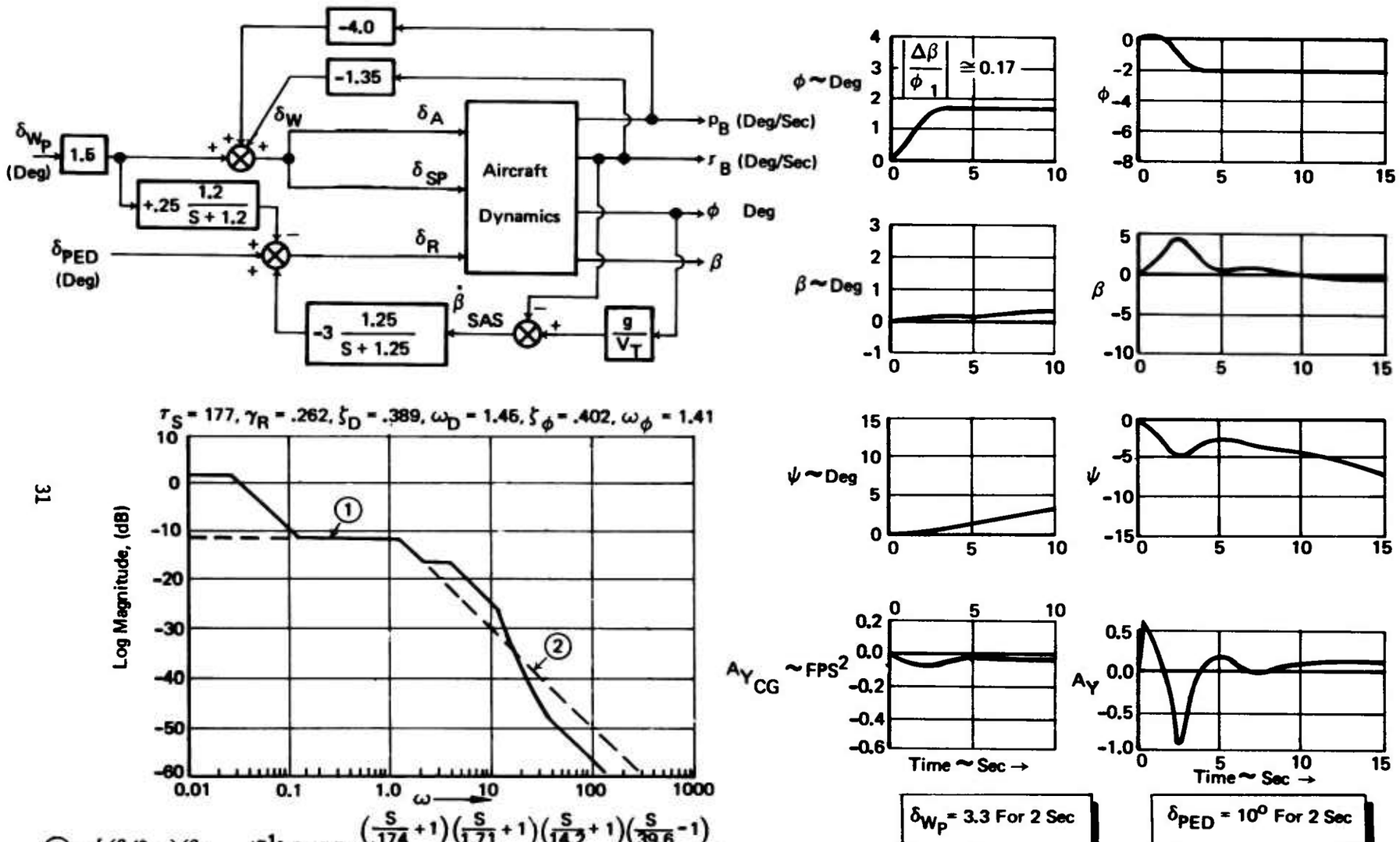

① $-[(\beta/\delta_{W_P})(\beta/\delta_{PE_D})^{-1}] \cong 1.5 \dfrac{\left(\frac{S}{.174}+1\right)\left(\frac{S}{1.71}+1\right)\left(\frac{S}{14.2}+1\right)\left(\frac{S}{39.6}-1\right)}{\left(\frac{S}{.0288}+1\right)\left(\frac{S}{1.25}+1\right)\left(\frac{S}{4.2}+1\right)\left(\frac{S}{10.4}+1\right)\left(\frac{S}{12.4}+1\right)}$

② – Lag Approximation of $-[(\beta/\delta_{W_P})(\beta/\delta_{PED})^{-1}] = .25 \dfrac{1}{S/1.2+1}$

Figure 15 : ***Design of the Feed Forward Compensation From Wheel to Rudder***

function for the pilot's "inner control loop" for the pitch axis is

$$Y_{P_\theta} = K_{P_\theta} e^{-\tau s}(T_L s + 1) \tag{28}$$

Where

Y_{P_θ} = pilot pitch attitude describing function

K_{P_θ} = pilot gain

τ = effective transport lag (used .2 sec.)

T_L = lead time constant

For the linear analysis, the effective transport lag ($e^{-\tau s}$) is approximated by a second order Pade' approximation of the form:

$$e^{-\tau s} \doteq \frac{\tau^2 s^2 - 4\tau s + 8}{\tau^2 s^2 + 4\tau s + 8} \tag{29}$$

The variation in closed loop attitude dynamics due to "pilot" gain and lead compensation is presented in Figure 16. The closed loop dynamics are described in terms of frequency response parameters (bandwidth and resonant peak) and time responses. The bandwidth, ω_{BW}, is significant because it is a measure of the speed of response of a given system and its ability to follow the input signal. An increase in bandwidth implies an improvement in system response. A system should be responsive and reach the desired steady-state value rapidly, but it should not be oscillatory. The damping characteristics of a system may be evaluated by the height of the resonant peak, ΔM. The effects of ω_{BW} and ΔM on the attitude response are illustrated by the time responses. These data show that increasing pilot gain produces a faster response and that lead compensation is required to stabilize the faster response. Satisfactory attitude control dynamics (i.e., ω_{BW}>1.5 rad/sec. ΔM<2db) are obtained by setting K_{P_θ} = .4 in/deg and T_L = .5 sec. Thus, the pilot-describing function used for the inner loop is $Y_{P_\theta} = .4e^{-.2s}(.5s + 1)$.

Single path control of pitch attitude does not provide satisfactory control of flight path angle because of excessive coupling between airspeed and pitch attitude. Figure 17 shows the effect of having the pilot control airspeed error in addition to pitch attitude error. Frequency and time responses, which relate flight path angle and airspeed to commanded pitch attitude, θ_c, are used to illustrate the influence of the velocity error vector deflection ($V_E \rightarrow \delta\sigma_p$) closure.

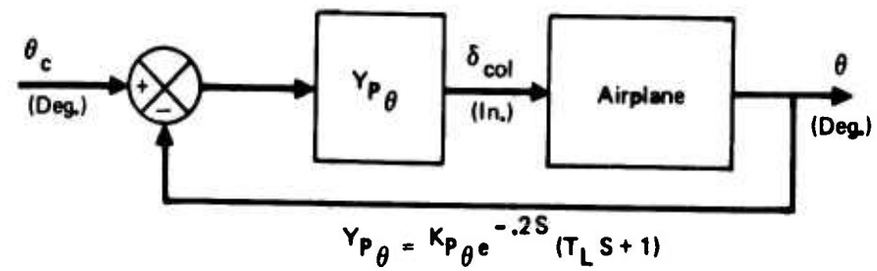

$$Y_{P_\theta} = K_{P_\theta} e^{-.2S} (T_L S + 1)$$

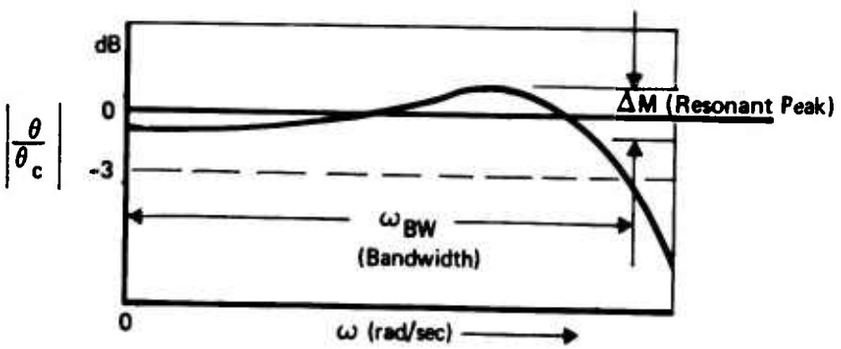

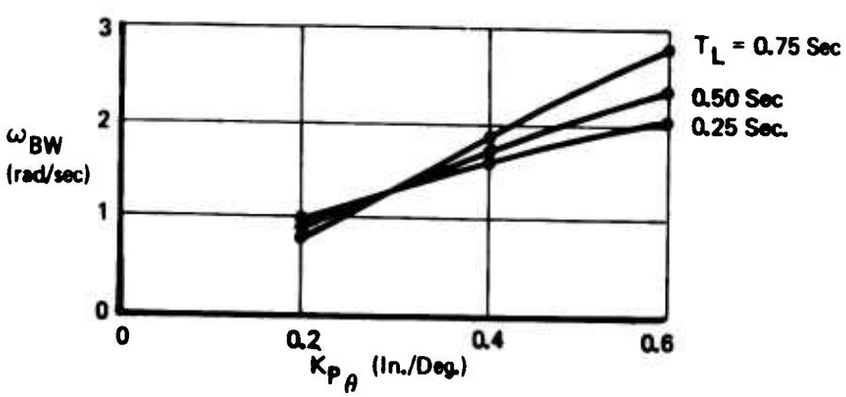

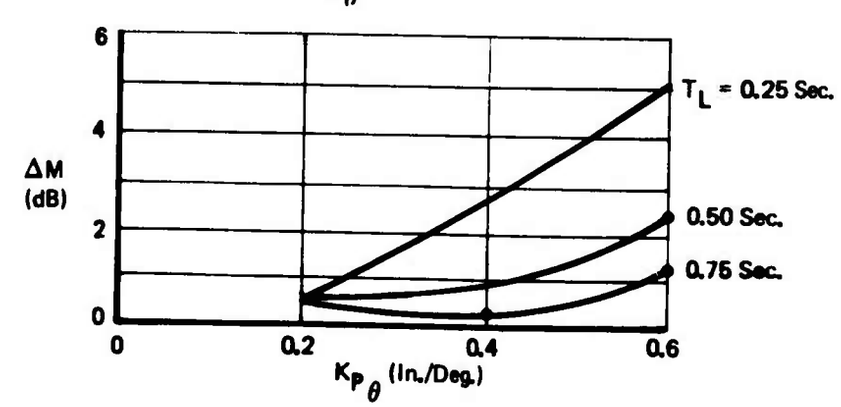

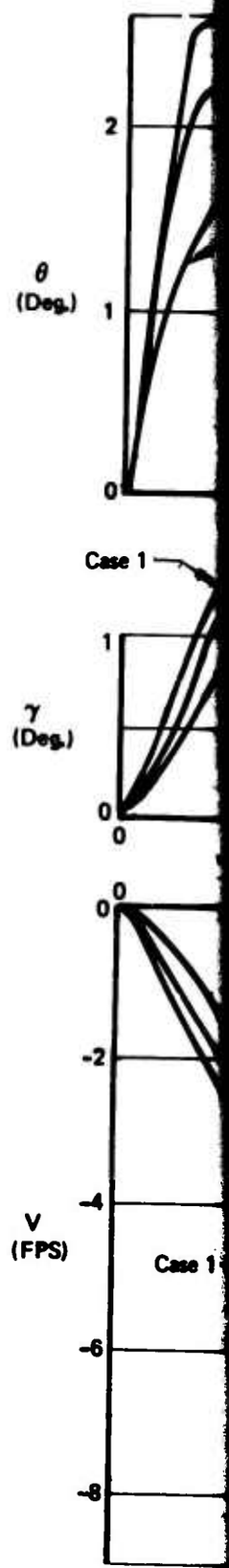

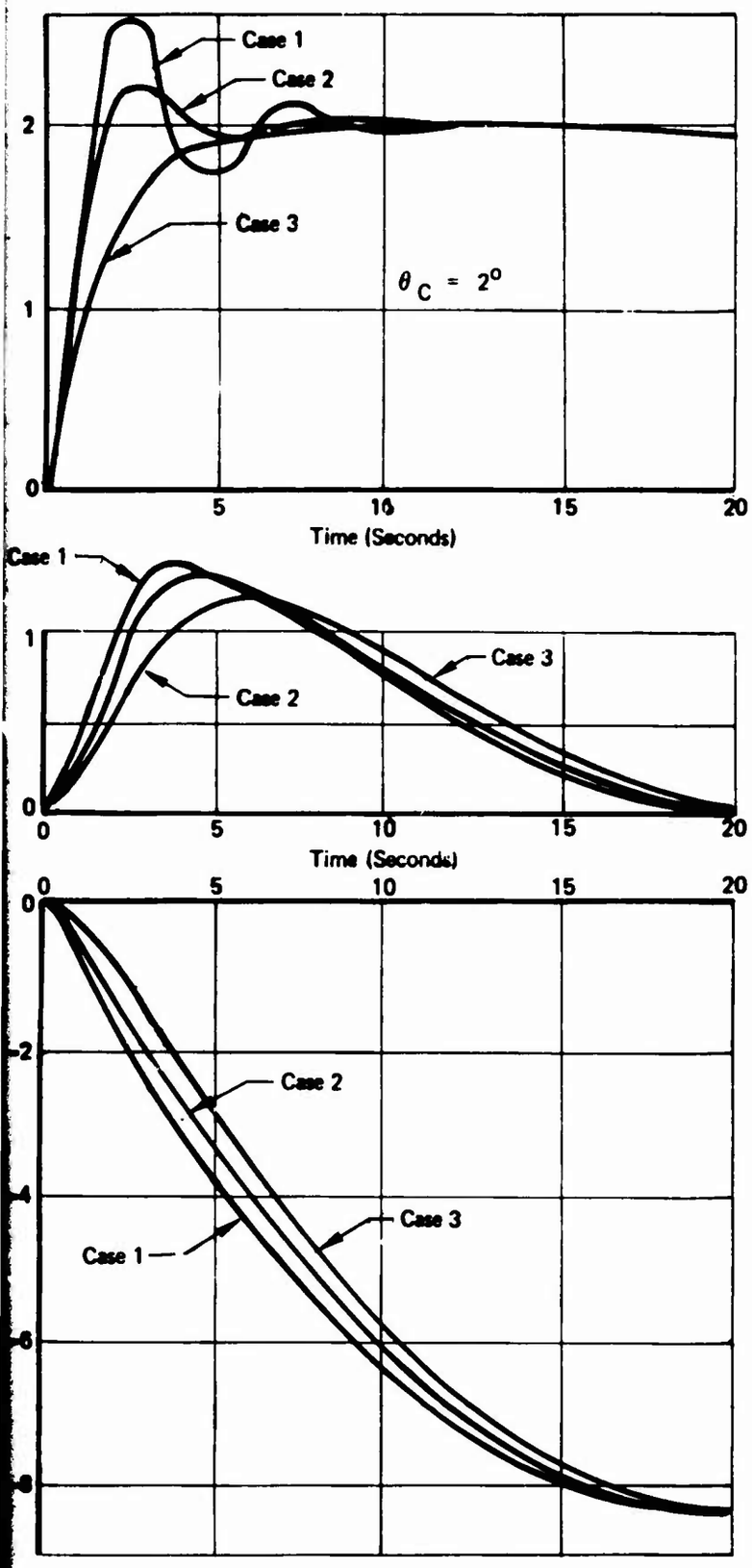

Case	K_{P_θ}	T_L	θ_c
1	0.6	0.25	2^o
2	0.4	0.5	2^o
3	0.2	0.75	2^o

Figure 16: Pilot Control of Attitude θ Inner Loop

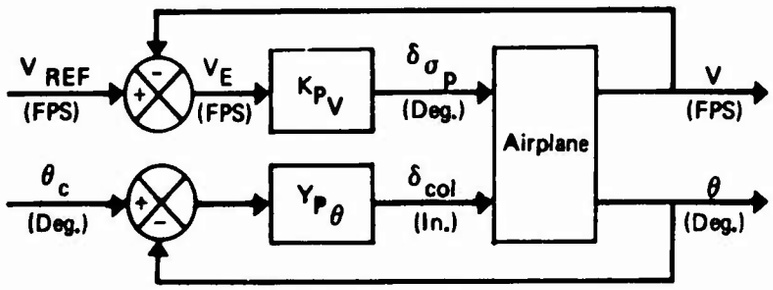

$$Y_{P_\theta} = 0.4\, e^{.2S}\ (0.5S + 1)$$

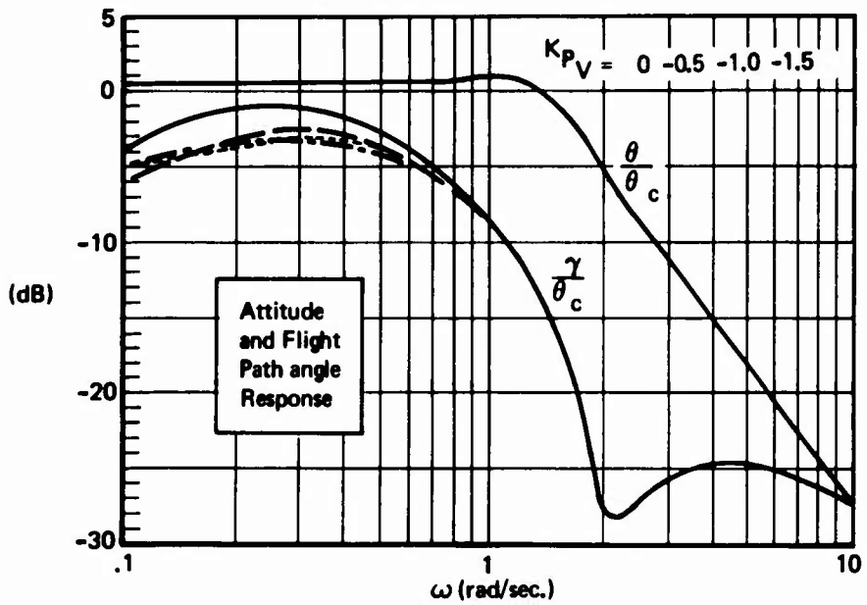

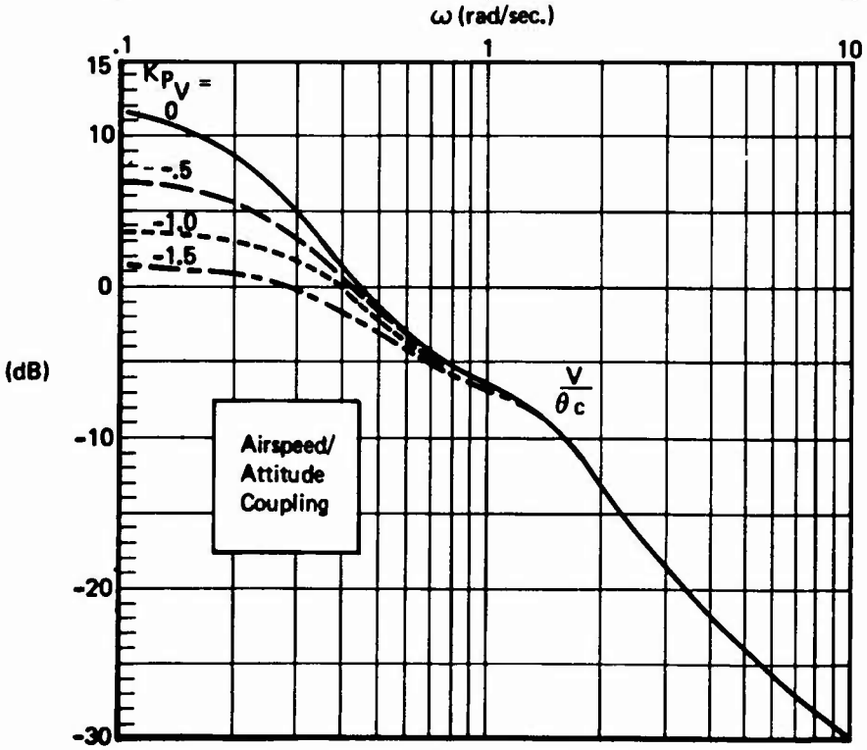

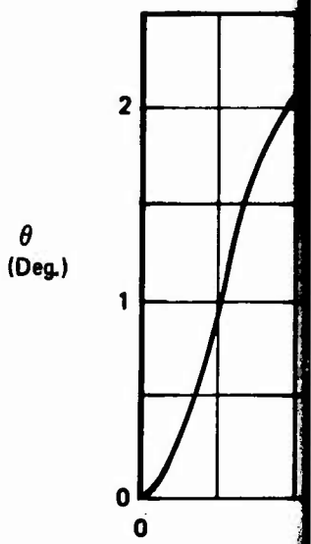

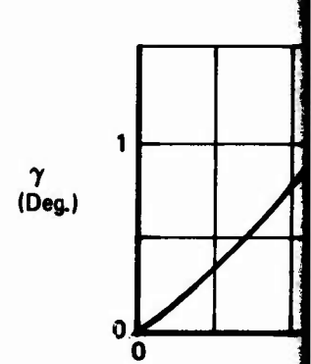

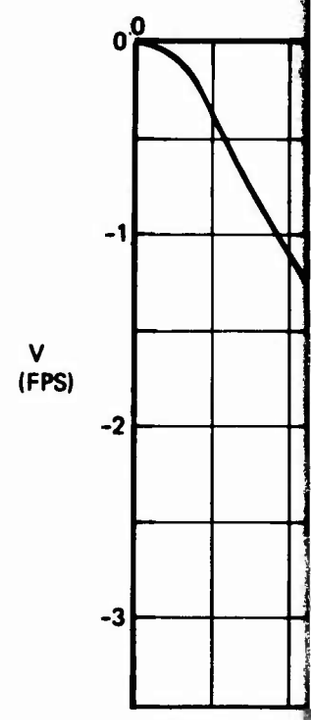

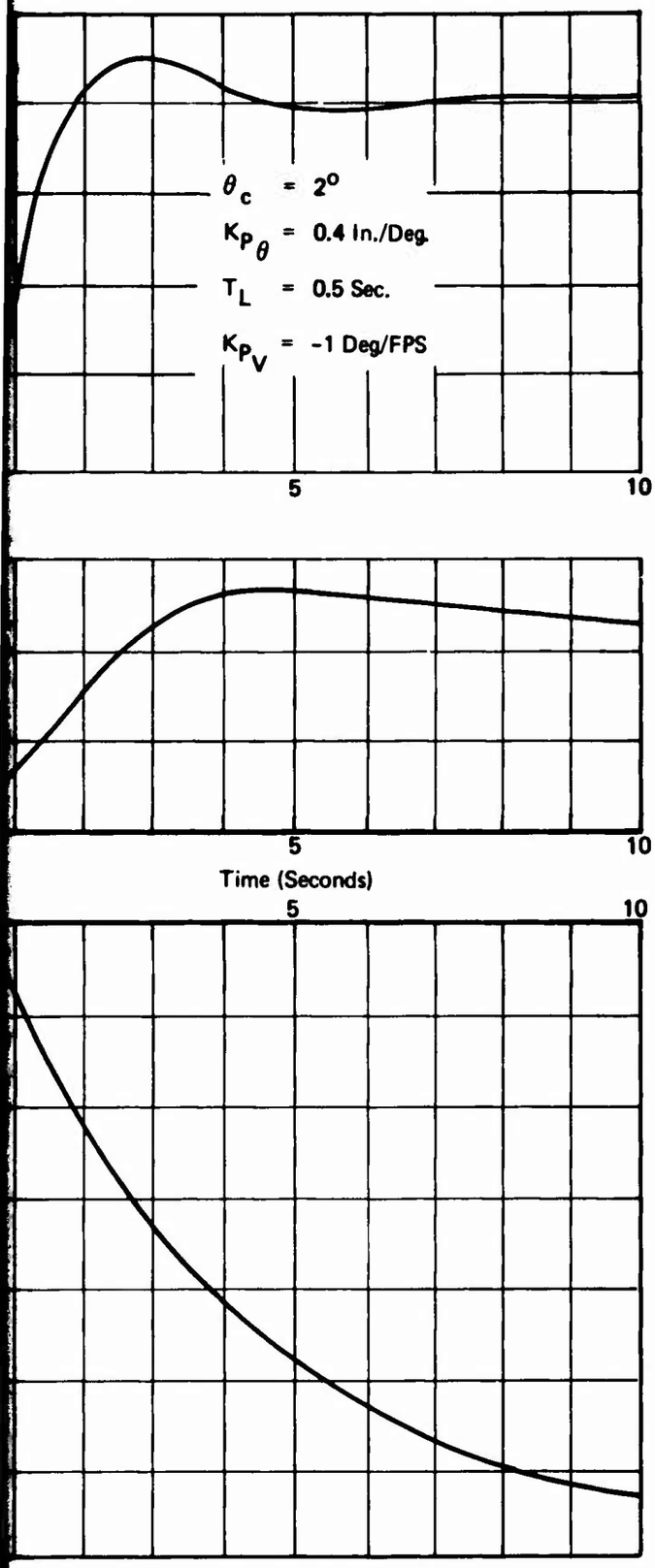

Figure 17: Effect of Speed Error Loop Closure on Longitudinal Control

The reduction in low frequency coupling between V and Θ_c due to this control loop is apparent. The γ/Θ_c frequency and time responses show the improvement in flight path control resulting from controlling airspeed.

These control loops do not completely eliminate the coupling between airspeed and pitch attitude. A retrimming loop, which has the "pilot" commanding vector angle in proportion to commanded changes in pitch attitude, is required in addition to the speed error ($V_\epsilon \rightarrow \delta\sigma_p$) loop to decouple airspeed from pitch attitude and flight path angle. Figure 18 shows the benefits of this retrimming loop. The flight path to pitch attitude response (γ/Θ_c) remains satisfactory while the undesired speed response (V/Θ_c) is reduced significantly. These characteristics are evident in the frequency response, where the speed to pitch attitude low frequency coupling has been reduced by approximately 10 db, and in the time response.

Figure 19 depicts the dynamic properties of a longitudinal control system which has been synthesized from the pilot loop closures just described. The decoupling gains for this control system (K_{V_1} and K_{V_2}) are identical to those (Kp_V and Kp_{V_Θ}) used by the "paper pilot." The pitch rate feedback replaces his lead compensation. Thus, the pilot closure is reduced to $Y_{P_\Theta} = .4e^{-.2s}$. Because this control system reduces the pilot's loop closures to a single, straight gain loop, a sizeable reduction in pilot workload can be expected.

3.2.3 Decoupled Control Synthesis

The "decoupling" approach to control system synthesis combines the classical methods with the more modern state variable techniques. Prior to defining the feedback loops from root-loci, the system is transformed into "V-Canonical form." This transformation explicitly determines internal coupling between outputs and shows how they may be cancelled. "Classical" design procedures may then be applied to optimize the response of the various outputs one at a time. The following advantages result:

(1) Equivalent performance to a classical system is usually possible with reduced feedback gains.

(2) The interaction of sequential feedback closures prevalent in classical multiloop feedback design is eliminated.

(3) Only one pass through the design process is needed to obtain predetermined augmented characteristics, if the system is linear.

3.2.3.1 Longitudinal Modes

The response of the unaugmented airplane to longitudinal control inputs shows that in the landing/approach condition there is strong coupling between airspeed, attitude, and flight path changes (Figure 20). Therefore, if the pilot wishes to control either airspeed or pitch attitude alone he is required to manipulate at least two control inputs. The decoupled approach to control system design isolates selected responses from particular pilot inputs thereby reducing pilot workload, and, ideally, increasing control accuracy.

As an initial application of the decoupling technique to the TAI longitudinal axis, it was postulated that the pilot would prefer his primary control inputs to provide independent control of airspeed and flight path angle. Having selected the airplane responses to be decoupled, the next problem was to determine the most appropriate blend of force/moment producers. The available controls were elevator, thrust magnitude, thrust angle, and direct lift control (DLC) through symmetric spoiler operation. If each control input provided non-zero pitching moment and lift and drag forces, it would be possible theoretically to use any three control inputs to give the desired result. However, a simpler and lower gain configuration results if the controls are chosen so that each controller provides a maximum of force or moment in the favorable axis and a minimum of coupling in the unfavorable axis. For example, the elevator provides considerable lift by changing angle-of-attack, and relatively little drag. Similarly, if the thrust vector is at 72 degrees to the body axis in trimmed flight (nominal landing/approach condition), then small changes in thrust vector angle provide large axial force changes and relatively small normal force changes.

To determine the decoupling transfer functions for a given configuration, the system is first put in a V-Canonical form as shown in Figure 21. In this form, airspeed perturbations (u) affect flight path angle (γ) through the transfer functions:

$$\gamma = (V_{21})(F_{22})(u) \tag{30}$$

and the coupling from γ to u is:

$$u = (V_{12})(F_{11})(\gamma) \tag{31}$$

Thus one method to provide control of airspeed without affecting γ is to cancel the internal coupling ($V_{21}.F_{22}$) by the feedback of u to δ_2 through the transfer function ($-V_{21}$). Similarly, $\delta_2 \rightarrow$ u coupling can theoretically be removed by feedback of γ through ($-V_{12}$).

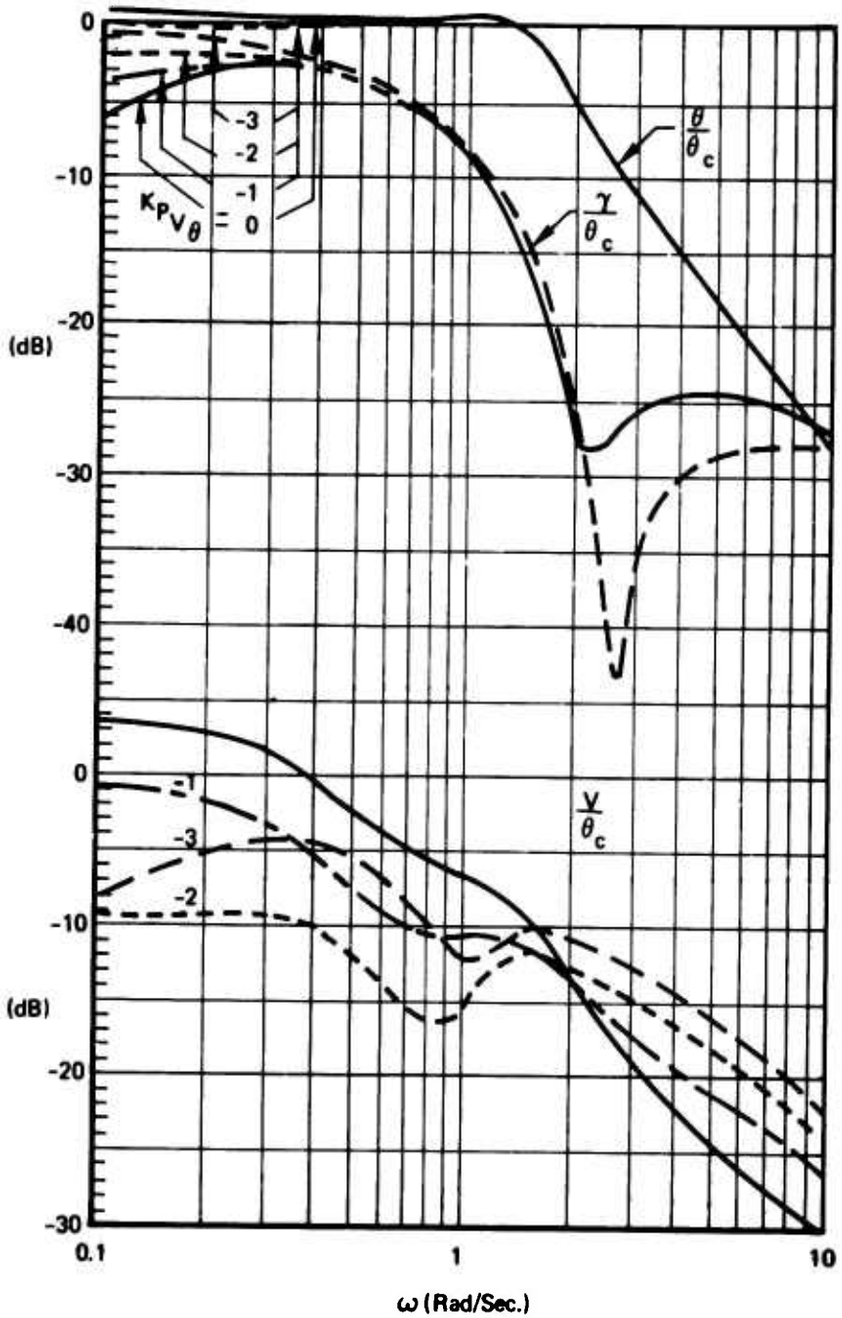

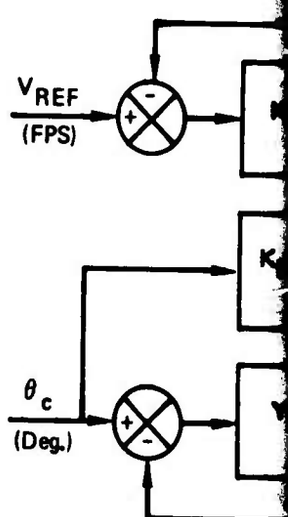

Attitude, Flight Path/Attitude Coupling, and
Airspeed/Attitude Coupling

A

θ_c = 2°

K_{P_θ} = 0.4 In./Deg.

T_L = 0.5 Sec.

K_{P_V} = -1.0 Deg./FPS

$K_{P_{V_\theta}}$ = -2.0 Deg./Deg.

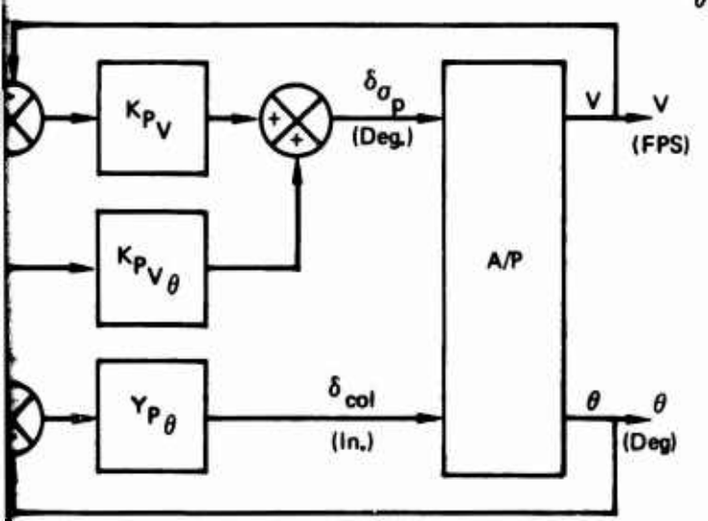

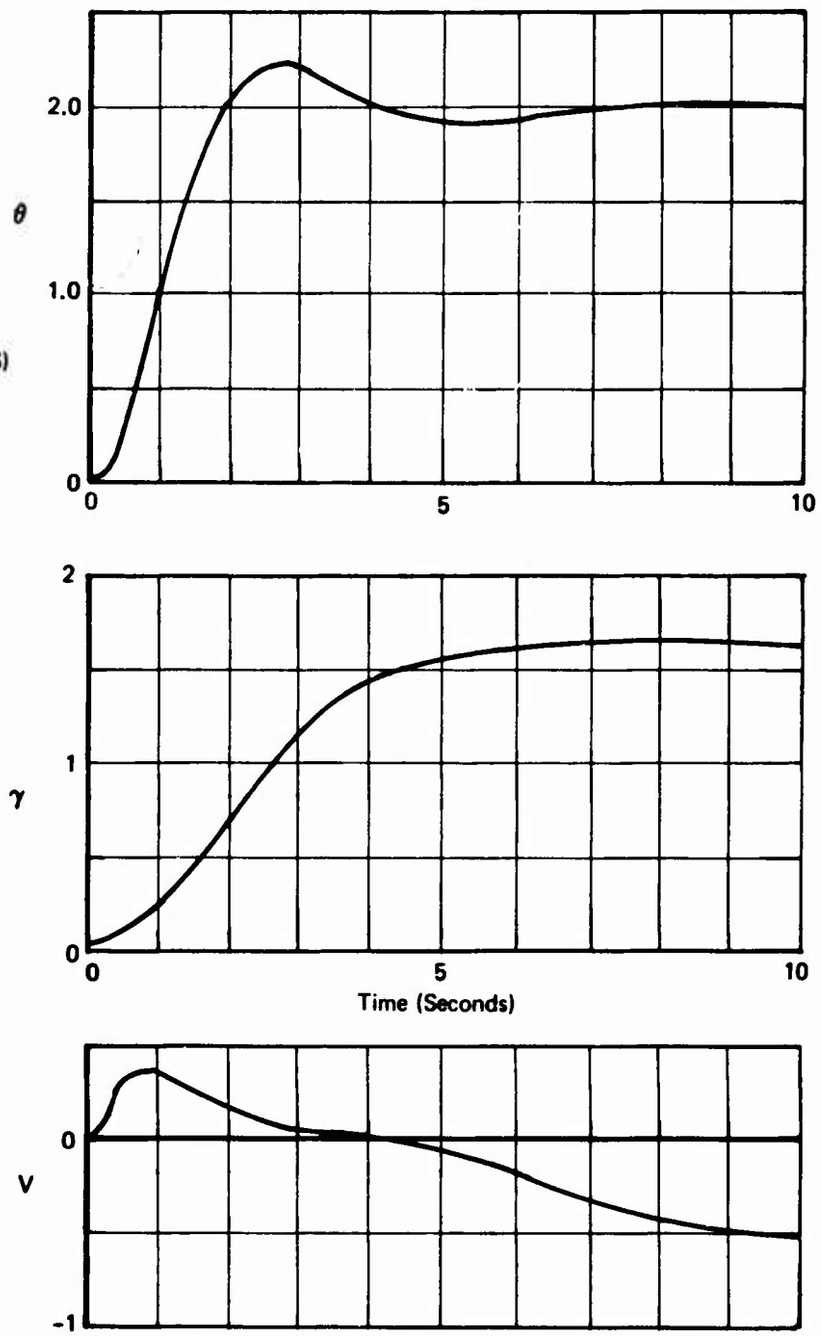

Figure 18: Effect on Longitudinal System of Speed Error Plus Pitch Attitude Feedback to Velocity Control

(Page 40 Blank)

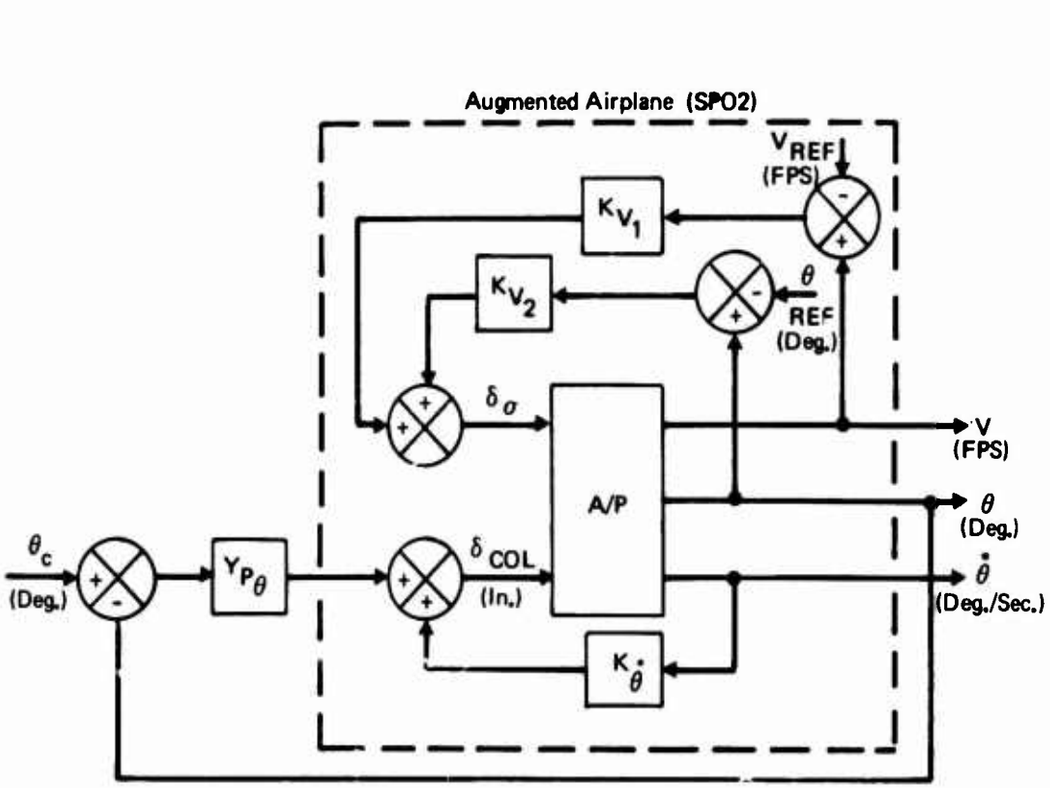
Augmented Airplane (SPO2)
V_{REF} (FPS)
K_{V_1}
K_{V_2}
θ REF (Deg.)
δ_σ
A/P
V (FPS)
θ (Deg.)
$\dot{\theta}$ (Deg./Sec.)
θ_c (Deg.)
Y_{P_θ}
δ COL (In.)
$K_{\dot{\theta}}$

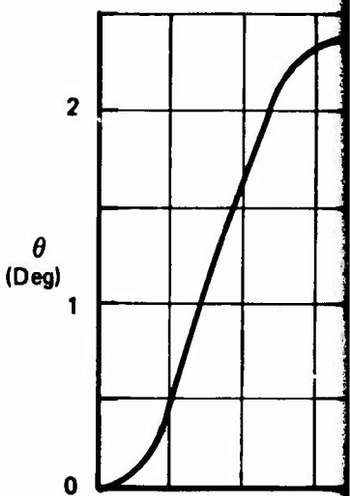
2
θ (Deg)
1
0

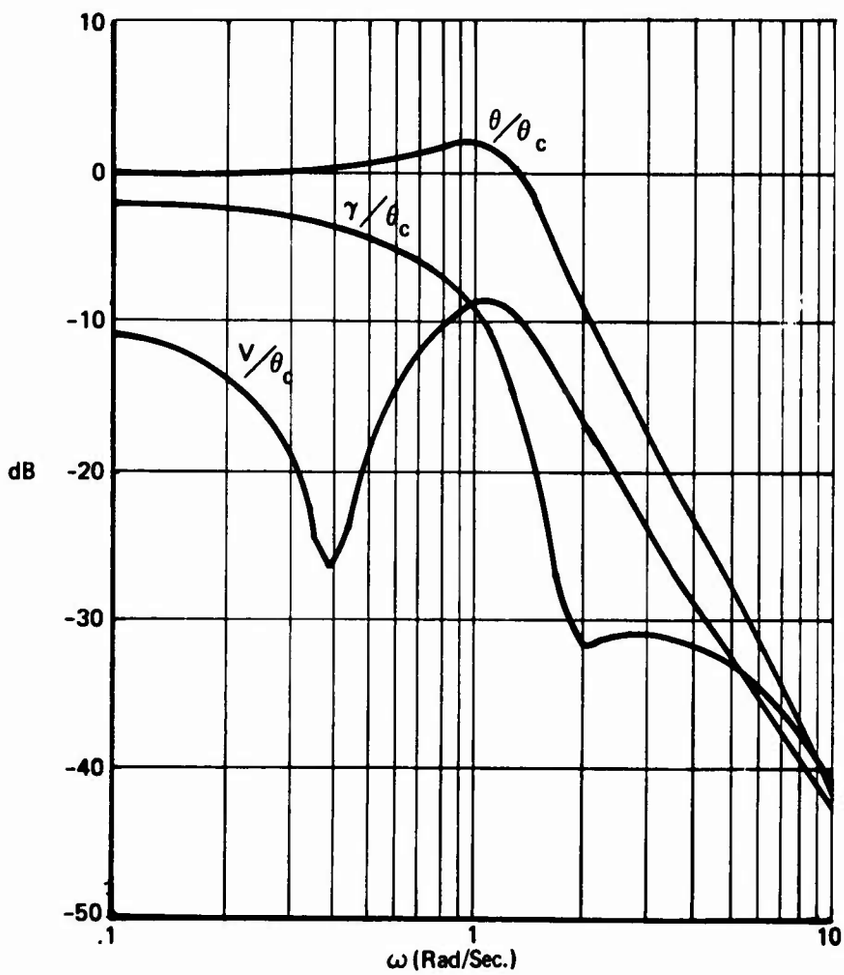
10
0
-10
dB
-20
-30
-40
-50
.1
1
10
ω (Rad/Sec.)
θ/θ_c
γ/θ_c
V/θ_c

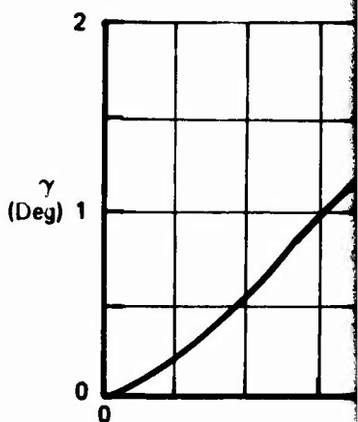
2
γ (Deg)
1
0
0

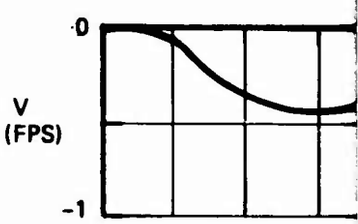
0
V (FPS)
-1

A

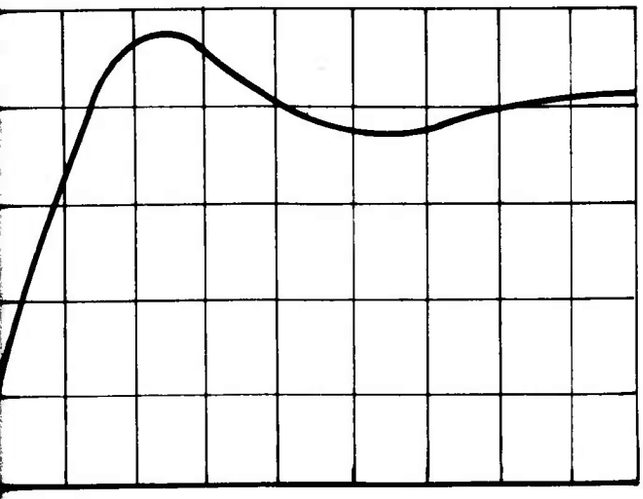

$Q_c = 2^o$

$K_{P_\theta} = .4_e^{.25}$

$K_{\dot{\theta}} = -.12$ In/Deg/Sec.

$K_{V_1} = 1.0$ Deg/FPS

$K_{V_2} = -2.0$ Deg/Deg

} Control System Gains

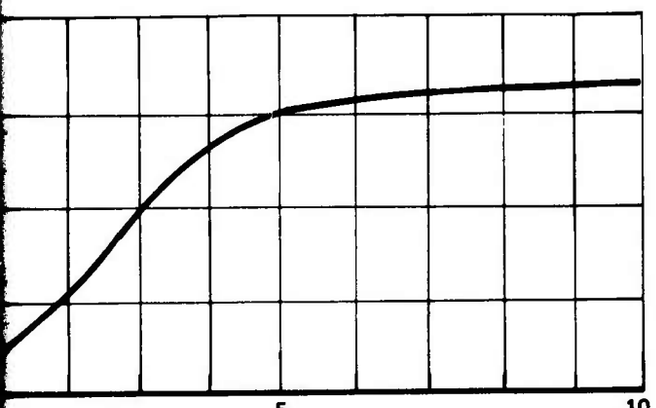

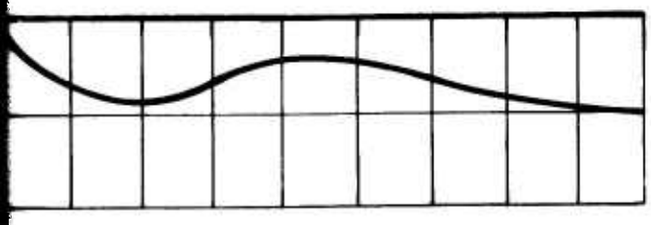

Figure 19: Longitudinal Control with Pitch Rate and Speed Augmentation

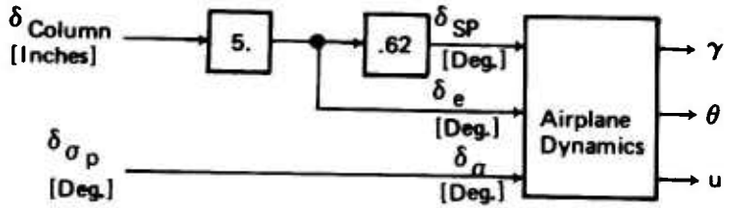

$$\frac{\gamma}{\delta_{Column}} = \frac{-.32\,[S-.051]\,[S^2+2\,(.23)\,(2.0)\,S+(2.0)^2]}{[S^2+2\,(.84)\,(.75)\,S+(.75)^2]\,[S^2+2\,(.58)\,(.051)\,S+(.051)^2]}$$

$$= \frac{[N_\gamma/\delta_c]\ \text{[Deg./Inch]}}{\text{[C.E.]}}$$

$$\frac{\theta}{\delta_{Column}} = \frac{-2.9\,[S+.35]\,[S+.18]}{[\text{ C.E. }]}\ \text{[Deg./Inch]}$$

$$\frac{u}{\delta_{\sigma_c}} = \frac{-2.1\,[S^2+2\,(.88)\,(.72)\,S+(.72)^2]}{[\text{ C.E. }]}\quad \frac{\text{[Ft/Sec.]}}{\text{[Deg.]}}$$

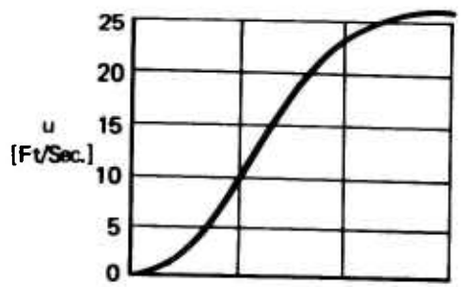

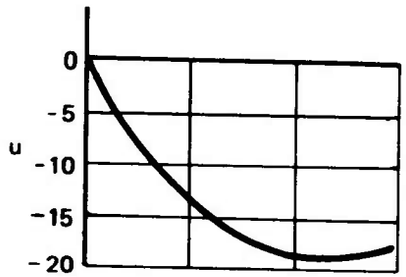

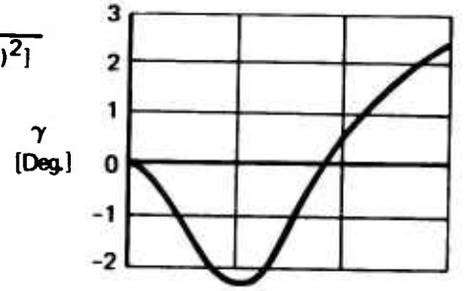

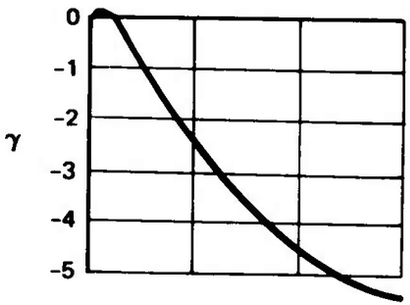

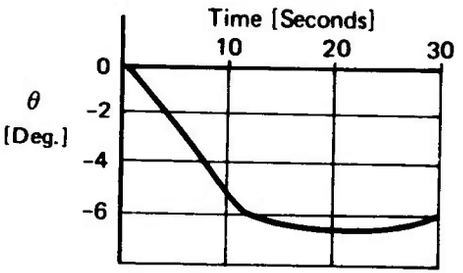

Response to 0.2" δ_{Column} Pulse for 10 Seconds

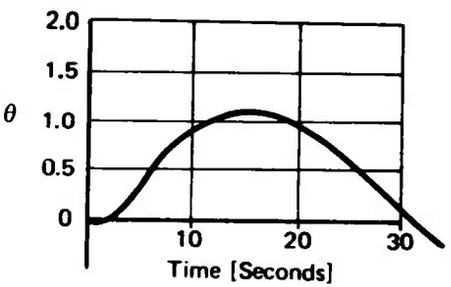

Response to 10° δ_σ Step

Figure 20 : Unaugmented Longitudinal Response to Column Pulse and Thrust Vector Angle Step

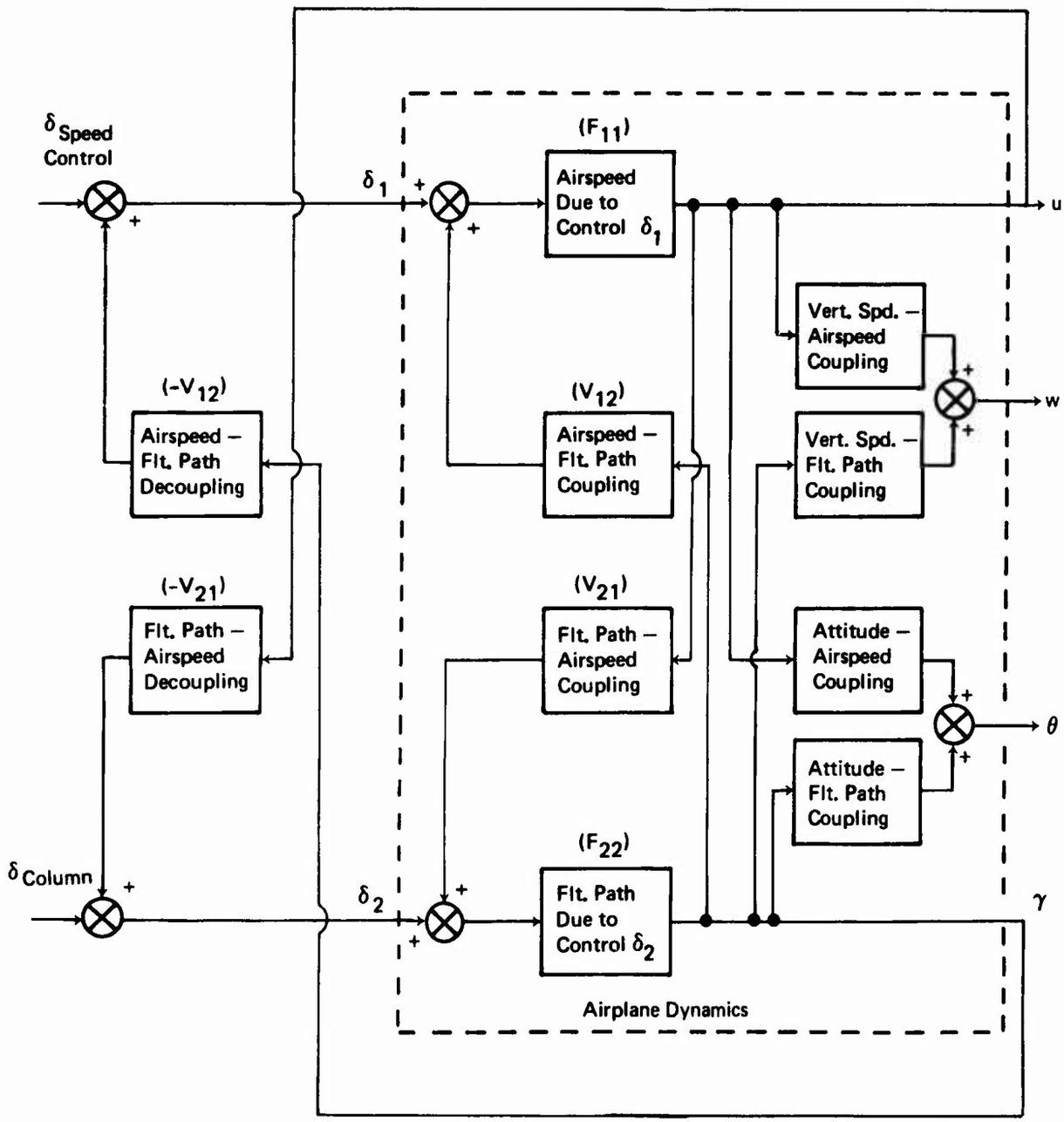

Figure 21 : V-Canonical Form for the Longitudinal Equations of Motion

Consider the following Laplace-transformed, small-perturbation, stability-axis, longitudinal equations of motion:

$$\begin{bmatrix} s-X_u & 0 & -X_w & \frac{g}{57.3} & -X_{\delta_1} & -X_{\delta_2} \\ 0 & 1 & \frac{57.3}{U_o} & -1 & 0 & 0 \\ -Z_u & 0 & s(1-Z_{\dot{w}}) - Z_w & \frac{-U_o s}{57.3} - Z_q s & -Z_{\delta_1} & -Z_{\delta_2} \\ -M_u & 0 & -M_{\dot{w}} s - M_w & \frac{s^2}{57.3} - M_q s & -M_{\delta_1} & -M_{\delta_2} \\ 0 & 0 & 0 & 0 & 1 & 0 \\ 0 & 0 & 0 & 0 & 0 & 1 \end{bmatrix} \begin{bmatrix} u \\ \gamma \\ w \\ \theta \\ \delta_1 \\ \delta_2 \end{bmatrix} = \begin{bmatrix} 0 \end{bmatrix} \quad (32)$$

where u = airspeed (ft/sec)
γ = flight path angle (degs)
w = vertical velocity (normal to X-Y stability axis plane) (ft/sec)
Θ = pitch attitude (degs)
δ_1, δ_2 = control inputs (to be determined)

These equation may be written as:

$$\left[\begin{array}{c|c} A & B \end{array}\right] \left[\begin{array}{c} \bar{p} \\ \hline \bar{x} \end{array}\right] = \left[0 \right] \quad (33)$$

where A and B are matrices, $\bar{p}$ is a 4-dimensional output vector, and $\bar{x}$ is a 2-dimensional input vector.

i.e.,

$$A = \begin{bmatrix} s-X_u & 0 & -X_w & \frac{g}{57.3} \\ 0 & 1 & \frac{57.3}{U_o} & -1 \\ -Z_u & 0 & s(1-Z_{\dot{w}}) - Z_w & \frac{-U_o s}{57.3} - Z_q s \\ -M_u & 0 & -M_{\dot{w}} s - M_w & \frac{s^2}{57.3} - M_q s \end{bmatrix} ; \quad B = \begin{bmatrix} -X_{\delta_1} & -X_{\delta_2} \\ 0 & 0 \\ -Z_{\delta_1} & -Z_{\delta_2} \\ -M_{\delta_1} & -M_{\delta_2} \end{bmatrix} \quad (34)$$

Consider the following Laplace-transformed, small-perturbation, stability-axis, longitudinal equations of motion:

$$\begin{bmatrix} s-X_u & 0 & -X_w & \frac{g}{57.3} & -X_{\delta_1} & -X_{\delta_2} \\ 0 & 1 & \frac{57.3}{U_o} & -1 & 0 & 0 \\ -Z_u & 0 & \frac{s(1-Z_{\dot{w}})-Z_w}{U_o} & \frac{-U_o s/57.3-Z_q s}{} & -Z_{\delta_1} & -Z_{\delta_2} \\ -M_u & 0 & \frac{-M_{\dot{w}} s-M_w}{} & \frac{s^2/57.3-M_q s}{} & -M_{\delta_1} & -M_{\delta_2} \\ 0 & 0 & 0 & 0 & 1 & 0 \\ 0 & 0 & 0 & 0 & 0 & 1 \end{bmatrix} \begin{bmatrix} u \\ \gamma \\ w \\ \theta \\ \delta_1 \\ \delta_2 \end{bmatrix} = \begin{bmatrix} 0 \end{bmatrix} \qquad (32)$$

where u = airspeed (ft/sec)
γ = flight path angle (degs)
w = vertical velocity (normal to X-Y stability axis plane) (ft/sec)
Θ = pitch attitude (degs)
δ_1, δ_2 = control inputs (to be determined)

These equation may be written as:

$$\left[\begin{array}{c|c} A & B \end{array}\right] \left[\begin{array}{c} \bar{p} \\ \hline \bar{x} \end{array}\right] = \left[0 \right] \qquad (33)$$

where A and B are matrices, $\bar{p}$ is a 4-dimensional output vector, and $\bar{x}$ is a 2-dimensional input vector.

i.e.,

$$A = \begin{bmatrix} s-X_u & 0 & -X_w & \frac{g}{57.3} \\ 0 & 1 & \frac{57.3}{U_o} & -1 \\ -Z_u & 0 & \frac{s(1-Z_{\dot{w}})-Z_w}{U_o} & \frac{-U_o s/57.3-Z_q s}{} \\ -M_u & 0 & \frac{-M_{\dot{w}} s-M_w}{} & \frac{s^2/57.3-M_q s}{} \end{bmatrix} ; \quad B = \begin{bmatrix} -X_{\delta_1} & -X_{\delta_2} \\ 0 & 0 \\ -Z_{\delta_1} & -Z_{\delta_2} \\ -M_{\delta_1} & -M_{\delta_2} \end{bmatrix} \qquad (34)$$

$$\bar{P} = \begin{bmatrix} u \\ \hline \gamma \\ \hline w \\ \hline \theta \end{bmatrix} \quad ; \quad \bar{X} = \begin{bmatrix} \delta_1 \\ \hline \delta_2 \end{bmatrix} \tag{35}$$

Equation (33) is now partitioned to separate the decoupled output variables (u, γ) from the remaining outputs:

$$\left[\begin{array}{c|cc} A_1 & A_2 & B \end{array}\right] \left[\begin{array}{c} \bar{Y} \\ \hline \bar{Z} \\ \bar{X} \end{array}\right] = \left[\begin{array}{c} 0 \end{array}\right] \tag{36}$$

where,

$$A_1 = \left[\begin{array}{c|c} s - X_u & 0 \\ \hline 0 & 1 \\ \hline -Z_u & 0 \\ \hline -M_u & 0 \end{array}\right] \quad ; \quad A_2 B = \left[\begin{array}{c|c|c|c} -X_w & \frac{g}{57.3} & -X_{\delta_1} & -X_{\delta_2} \\ \hline \frac{57.3}{U_o} & -1 & 0 & 0 \\ \hline s(1-Z_{\dot{w}}) & \frac{-U_o s}{57.3} & -Z_{\delta_1} & -Z_{\delta_2} \\ \hline -Z_w - M_{\dot{w}} s & -Z_q s \frac{s^2}{57.3} & -M_{\delta_1} & -M_{\delta_2} \\ -M_w & -M_q s & & \end{array}\right] \tag{37}$$

$$\bar{Y} = \begin{bmatrix} u \\ \gamma \end{bmatrix} \quad ; \begin{bmatrix} \bar{Z} \\ \bar{X} \end{bmatrix} = \begin{bmatrix} w \\ \theta \\ \delta_1 \\ \delta_2 \end{bmatrix} \tag{38}$$

The required decoupling tranfer functions ($-V_{12}$, $-V_{21}$) may now be written as the ratio of polynominals in "s" (Laplace transform variable)

$$-V_{12} = \frac{-N_{12}(s)}{\Delta(s)} \quad ; \quad -V_{21} = \frac{-N_{21}(s)}{\Delta(s)}$$

If $-V_{12}$, $-V_{21}$ are to be stable and realizable, the roots of Δ must be in the "left-half-plane" and the order of N_{12} and N_{21} must not be greater than the order of Δ. Considering first the problem of stability, Reference 8 shows that,

$$\Delta = \det\left[A_2 B\right] = \begin{vmatrix} -X_w & \frac{g}{57.3} & -X_{\delta_1} & -X_{\delta_2} \\ \frac{57.3}{U_o} & -1 & 0 & 0 \\ \frac{}{s(1-Z_{\dot{w}})} & \frac{-U_o s}{57.3} & -Z_{\delta_1} & -Z_{\delta_2} \\ -Z_w & -Z_q s & & \\ \frac{}{-M_{\dot{w}} s} & \frac{}{s^2} & -M_{\delta_1} & -M_{\delta_2} \\ -M_w & \frac{57.3}{-Z_q s} & & \end{vmatrix} \qquad (39)$$

Rewriting Δ as a polynomial in s gives:

$$\Delta = \frac{s^2}{U_o}\left[X_{\delta_2} Z_{\delta_1} - Z_{\delta_2} X_{\delta_1}\right] + s\left[-\left(M_{\dot{w}} + \frac{57.3}{U_o} M_q\right)\left(X_{\delta_2} Z_{\delta_1} - Z_{\delta_2} X_{\delta_1}\right)\right.$$

$$\left. + \frac{57.3}{U_o} Z_q \left(X_{\delta_2} M_{\delta_1} - M_{\delta_2} X_{\delta_1}\right)\right] + \left[-M_w \left(X_{\delta_2} Z_{\delta_1} - Z_{\delta_2} X_{\delta_1}\right)\right. \qquad (40)$$

$$\left. + Z_w \left(X_{\delta_2} M_{\delta_1} - M_{\delta_2} X_{\delta_1}\right) + \left(\frac{g}{U_o} - X_w\right)\left(Z_{\delta_2} M_{\delta_1} - M_{\delta_2} Z_{\delta_1}\right)\right]$$

The stability of Δ as a function of various control inputs can be computed after introducing numerical values for the aerodynamic derivatives at the landing/approach condition. Thus:

$$\Delta = 0.00787\, s^2 \left[X_{\delta_2} Z_{\delta_1} - Z_{\delta_2} X_{\delta_1} \right] + s \left[.00641 \left(X_{\delta_2} Z_{\delta_1} - Z_{\delta_2} X_{\delta_1} \right) \right.$$

$$\left. -.0279 \left(X_{\delta_2} M_{\delta_1} - M_{\delta_2} X_{\delta_1} \right) \right] + \left[.0029 \left(X_{\delta_2} Z_{\delta_1} - Z_{\delta_2} X_{\delta_1} \right) \right. \quad (41)$$

$$\left. -.432 \left(X_{\delta_2} M_{\delta_1} - M_{\delta_2} X_{\delta_1} \right) + .112 \left(Z_{\delta_2} M_{\delta_1} - M_{\delta_2} Z_{\delta_1} \right) \right]$$

Table VI shows the roots of Δ for several possible control configurations. It can be seen that of the controls considered, only thrust angle plus a blend of DLC (δ_{DLC}) and elevator show stable poles in the feedback transfer function. Note that the poles are unchanged when the same two controllers are used to control either of the decoupled outputs. A comparison of the Δ polynomial for $\delta\sigma$ with high and low gain DLC plus elevator inputs, (δ_{DLC_L} or δ_{DLC_H}) shows that the poles are complex in both cases but with a larger damping ratio when high gain DLC is used. Therefore, the initial computation of the transfer functions ($-V_{12}$, $-V_{21}$) was done for control inputs $\delta\sigma$, δ_{DLC_H}.

TABLE VI
POLES OF DECOUPLING TRANSFER FUNCTIONS FOR VARIOUS CONTROL INPUTS

Speed Controller (δ_1)	Flight Path Controller (δ_2)	Decoupling Feedback Denominator (Δ)
δ_{TH}	Elevator (δ_e)	$5.41\times10^{-6}(s+82)(s-85.1)$
δ_σ	δ_e	$-9.92\times10^{-5}(s+3.46)(s-2.63)$
δ_{TH}	δ_{DLC_L} [$K\delta_{DLC}/\delta_e$=0.31 degs/deg]	$4.28\times10^{-5}(s+75)(s-9.61)$
δ_σ	δ_{DLC_L}	$6.15\times10^{-5}(s+33\pm i3.76)$
δ_{DLC_L}	δ_{TH}	$-4.28\times10^{-5}(s+75)(s-9.61)$
δ_{DLC_L}	δ_σ	$-6.15\times10^{-5}(s+33\pm i3.76)$
δ_σ	δ_{DLC_H} [$K\delta_{DLC}/\delta_e$=.62 deg/deg]	$2.23\times10^{-4}(s+36+i1.91)$

The general form obtained for $(-V_{12}, -V_{21})$ when inputs $\delta\sigma$ and δ_{DLC_H} are assumed is:

$$-V_{ij} = \frac{N_{ij}}{\Delta} = \frac{a_{ij}s^3 + b_{ij}s^2 + c_{ij}s + d_{ij}}{s^2 + e_{ij}s + f_{ij}} \; ; \; (ij) = (12) \text{ or } (21) \tag{42}$$

Since the numerator is of higher order than the denominator, these transfer functions are unrealizable. The assumption was therefore made that the low frequency characteristics of the decoupling would be most beneficial to the pilot, and the transfer functions were simplified by equating coefficients as follows:

$$-V_{ij} = \frac{a_{ij}s^3 + b_{ij}s^2 + c_{ij}s + d_{ij}}{s^2 + e_{ij}s + f_{ij}} \cong A_{ij} + B_{ij}s \tag{43}$$

$$\text{i.e.,} \quad A_{ij} = \frac{d_{ij}}{f_{ij}} \quad \text{and} \quad B_{ij} = \frac{1}{f_{ij}}\left[c_{ij} - A_{ij} \cdot e_{ij}\right] \tag{44}$$

For example, if $\delta\sigma$ is used to control airspeed, and δ_{DLC_H} to control γ, the values obtained for Aij, Bij are:

$$\frac{\delta\sigma}{\gamma} = A_{12} + B_{12}s = (-3.0 - 4.4s) \text{ Deg./Deg.} \tag{45}$$

$$\frac{\delta_{DLC_N}}{u} = A_{21} + B_{21}s = (.04 + .34s) \text{ Deg./FPS} \tag{46}$$

After computing the feedback gains to provide low frequency decoupling, the closed-loop stability was next evaluated. If thrust vector angle were used to control flight path, with elevator and DLC controlling airspeed, the closed-loop stability would have been unacceptable. Decoupling was obtained by cancellation of a right-half-plane pole and zero in which the instability implied by the pole was unacceptable. Small variations in system parameters would move the unstable pole away from the zero, thereby requiring additional stabilization from the pilot. With $\delta\sigma$ controlling airspeed and δ_{DLC_H} controlling flight path, pole-zero cancellation again occurs in the right-half-plane, but sufficiently close to the origin to be only a minor problem.

$$\frac{\gamma}{\delta DLC_H} = \frac{-.057\left[s^2+2(.23)(2.0)s+(2.0)^2\right]\left[s-.029\right]}{\left[s-.0016\right]\left[s^2+2(.83)(.77)s+(.77)^2\right]\left[s-.023\right]} \text{ Deg./Deg.} \quad (47)$$

$$\frac{u}{\delta\sigma} = \frac{-.185\left[s^2+2(.81)(.79)s+(.79)^2\right]\left[s+.0035\right]}{\left[s-.0016\right]\left[s^2+2(.83)(.77)s+(.77)^2\right]\left[s-.023\right]} \text{ FPS/Deg.} \quad (48)$$

After decoupling, functions of γ may be fed back to δ_{DLC_H} and functions of u fed back to $\delta\sigma$ without adversely affecting the decoupling. Thus as the final stage of the decoupling synthesis, $\dot{\gamma}$ is fed back to δ_{DLC_H} and u fed back to $\delta\sigma$ to provide pilot control commands proportional to flight path rate and airspeed. After feedback of $\dot{\gamma}$ and u the closed-loop transfer functions are approximately:

$$\frac{\dot{\gamma}}{\delta DLC_H} = \frac{-.04\left[s+2.5\right]\left[s^2+2(.23)(2.0)s+(2.0)^2\right]}{\left[s+.8\right]\left[s^2+2(.81)(1.4)s+(1.4)^2\right]} \frac{\text{degs./sec.}}{\text{deg}} \quad (49)$$

$$\frac{u}{\delta\sigma} = \frac{-0.2}{s+.24} \frac{\text{ft./sec.}}{\text{deg.}}; \quad \frac{K_{\delta\sigma}}{u} = 1.3 \; ; \quad \frac{F_{K_{\delta DLC_H}}}{\dot{\gamma}} = \frac{7(s+.5)}{s+2.5} \quad (50)$$

Since the computed feedback gains from airspeed to δ_{DLC_H} appeared sufficiently low to be insignificant (See Equation 46), the system was further simplified by setting $A_{21} = B_{21} = 0$. The block diagram and transient responses for this system, with and without A_{21}, B_{21}, are shown in Figure 22.

Decoupled systems which provide independent control of airspeed and pitch attitude were developed using the method previously outlined for the (γ, u) systems. The most significant difference between the (γ, u) and the (Θ, u) synthesis was that a stable Δ polynominal was obtainable in the latter case when thrust angle ($\delta\sigma$) and elevator (δe) were assumed as control inputs; i.e., direct lift was necessary for Δ stability in the case of the (γ, u) systems but not for the (Θ, u) systems. Block diagrams and transient responses for (Θ, u) decoupled systems with and without DLC are shown in Figures 23 and 24.

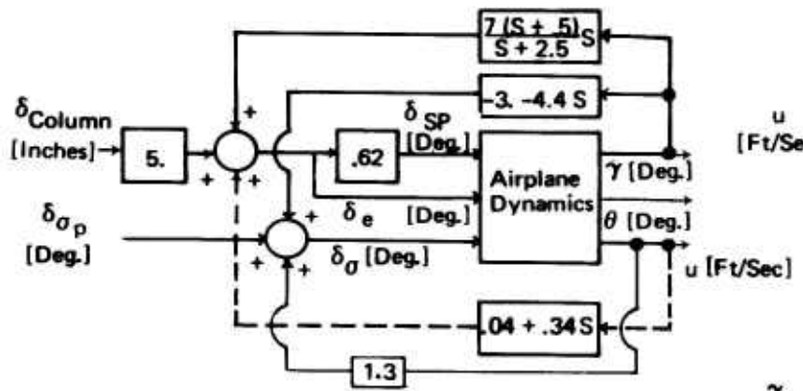

With u, $\dot{u}$ Feedback to δ_e, δ_{sp}

$$\frac{\gamma}{\delta_{Column}} = \frac{-0.2\,[S+2.5]\,[S^2+2]\,(.23)\,(2.0)\,S+(2.0)^2]}{S\,[S+.8]\,[S^2+2\,(.81)\,(1.4)\,S+(1.4)^2]} \quad \frac{\text{Deg.}}{\text{Inch}}$$

$$\frac{\theta}{\delta_{Column}} = \frac{-2.1\,[S+2.5]\,[S+.45]}{S\,[S+.8]\,[S^2+2\,(.81)\,(1.4)\,S+(1.4)^2} \quad \frac{\text{Deg.}}{\text{Inch}}$$

$$\frac{u}{\delta_{\sigma_p}} = \frac{-0.20}{(S+.24)} \quad \frac{\text{Ft/Sec.}}{\text{Deg.}}$$

* F/B = Feedback

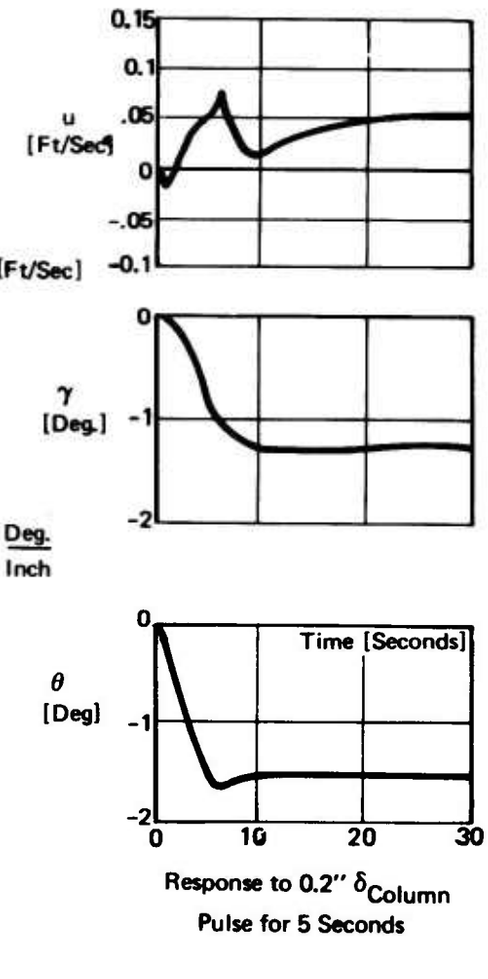

Response to 0.2" δ_{Column} Pulse for 5 Seconds

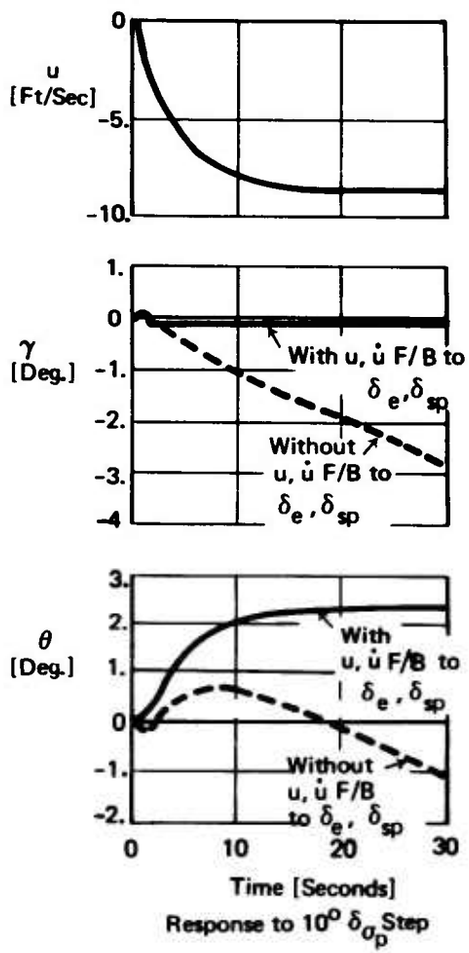

Response to 10° δ_{σ_p} Step

Figure 22 : Longitudinal System DPO5 Response to Column Pulse and Thrust Vector Angle Step

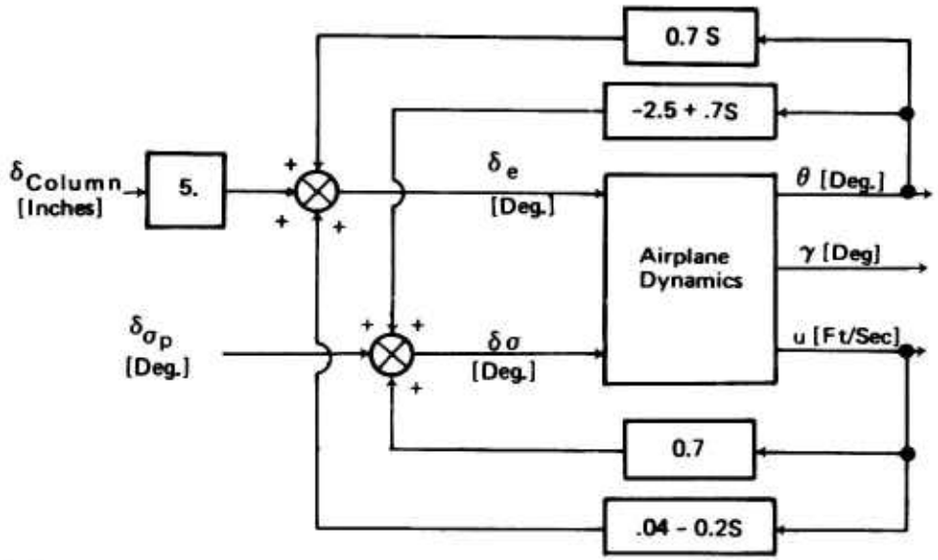

$$\frac{\gamma}{\delta_{Column}} = \frac{0.17\,[S + .35]\,[S + 2.5]\,[S - 2.5]}{S\,[S + 1.3]\,[S^2 + 2\,(.91)\,(.42)\,S + (.42)^2]} \quad \frac{\text{Deg.}}{\text{Inch}}$$

$$\frac{\theta}{\delta_{Column}} = \frac{-3.4\,[S^2 + 2\,(.91)\,(.36)\,S + (.36)^2]}{S\,[S + 1.3]\,[S^2 + 2\,(.91)\,(.42)\,S + (.42)^2]} \quad \frac{\text{Deg.}}{\text{Inch}}$$

$$\frac{u}{\delta_{\sigma_p}} = \frac{-0.21\,[S^2 + 2\,(.96)\,(.94)\,S + (.94)^2]}{[S + 1.3]\,[S^2 + 2\,(.91)\,(.42)\,S + (.42)^2]} \quad \frac{\text{Ft/Sec}}{\text{Deg.}}$$

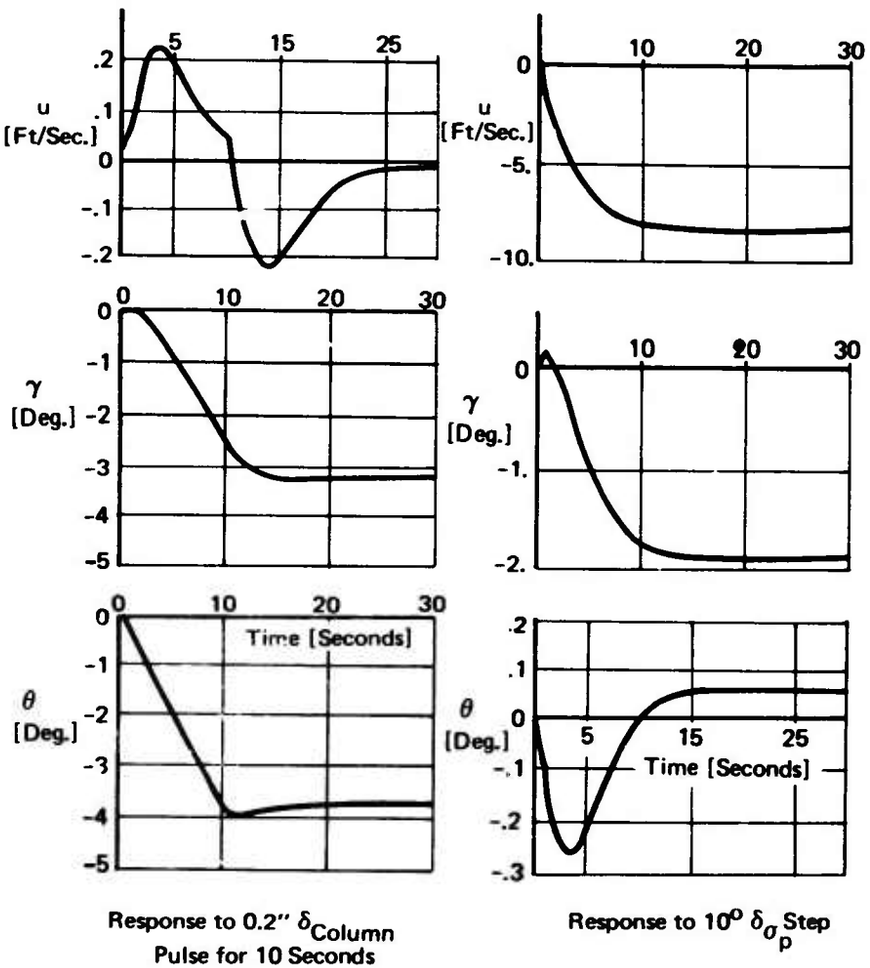

Figure 23 : Longitudinal System DP03 Response to Column Pulse and Thrust Vector Angle Step

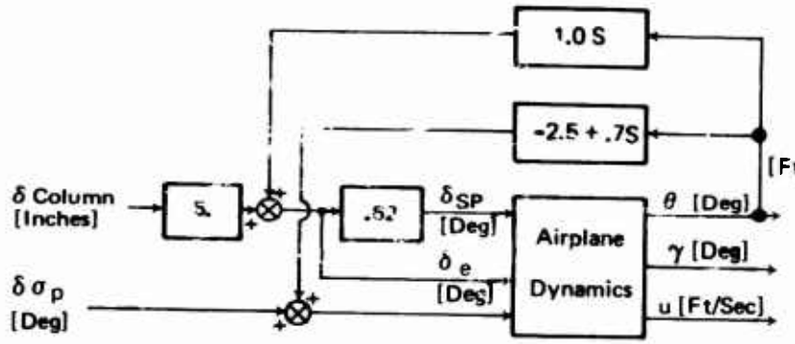

$$\frac{\gamma}{\delta\ \text{Column}} = \frac{-.33\,[S^2 + 2\,(.30)\,(1.8)\,S + (1.8)^2]}{S\,[S + .52]\,[S + 1.4]} \quad \frac{\text{Deg}}{\text{Inch}}$$

$$\frac{\theta}{\text{Column}} = \frac{-3.0\,[S + .38]}{S\,[S + .52]\,[S + 1.4]} \quad \frac{\text{Deg}}{\text{Inch}}$$

$$\frac{u}{\delta\sigma_c} = \frac{-0.21\,[S^2 + 2\,(.97)\,(.99)\,S + (.99)^2}{[S + .15]\,[S + .52]\,[S + 1.4]} \quad \frac{\text{Ft/Sec}}{\text{Deg}}$$

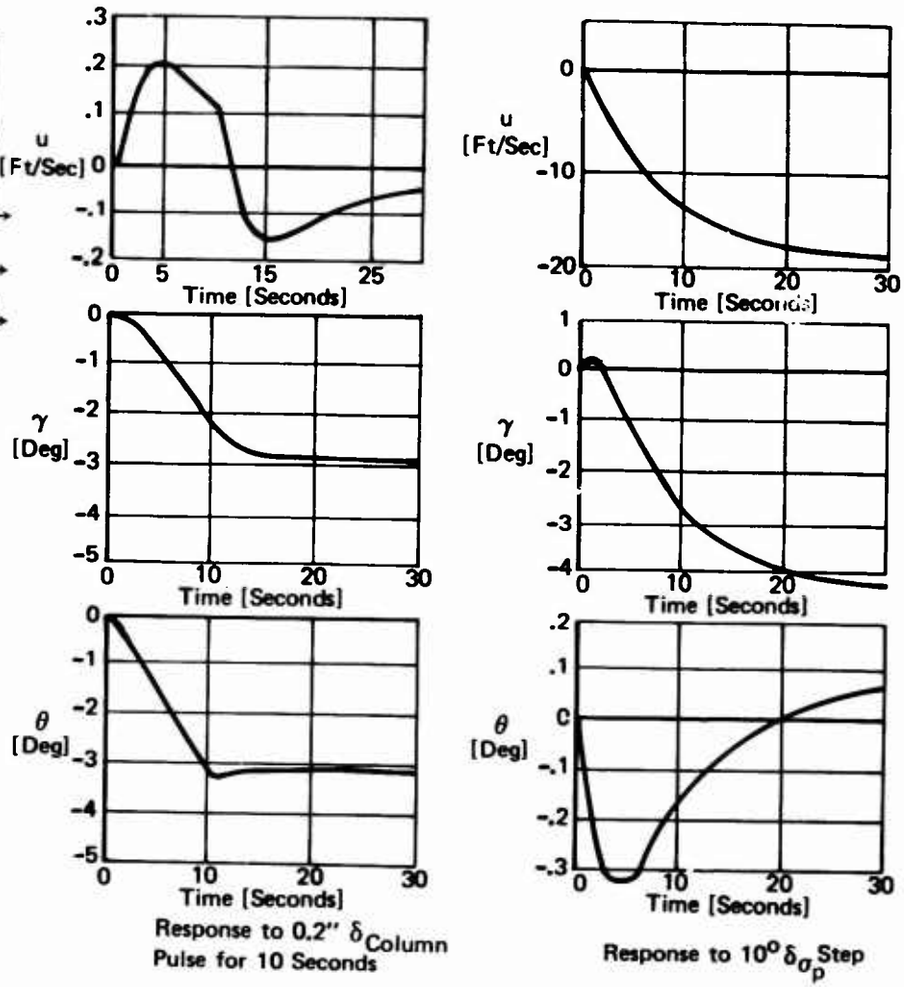

Figure 24 : Longitudinal System SPO3 Response to Column Pulse and Thrust Vector Angle Step

3.2.3.2 Lateral Directional Modes

As discussed in Section 3.2.1, the unaugmented airplane had poor lateral/directional handling qualities. Since the unaugmented dutch roll and roll time constant characteristics were considered adequate the initial lateral/directional decoupling studies concentrated on improving turn coordination and spiral stability. A "coordinated turn" implies the ability to roll the airplane without sideslipping. This is achieved in a decoupled system by providing roll attitude (ϕ) from the wheel without sideslip (β) and conversely, sideslip from the rudder pedals without roll attitude. Although the airplane response to wheel commands is conventional, the response to rudder pedal commands is contrary to most pilot's experience. This pedal response permits large decrab maneuvers with minimum roll coupling which is desirable for the landing case. Both Reference 9 and Reference 23 indicate that the lack of bank angle response to pedal input is not objectionable and the hypothesis assumed for the initial decoupling development was that once the pilots became used to the lack of dihedral effect they would find the response preferable.

Development of the lateral/directional decoupling systems used the same general method discussed for the longitudinal decoupling, as follows:

(1) The equations of motion were transformed to the principle axes to eliminate the product of inertia term (I_{xz}). "Cross-coupling" inter-ties were introduced between the rudder and the lateral control surfaces to balance the aerodynamic control coupling (C_ℓ/δ_R). Similar inter-ties between the lateral controls and the rudder serve to balance the lateral to directional coupling (C_ℓ/δ_A and C_ℓ/δ_{SP}).

(2) Yaw rate (r) was fed back to the lateral controls and the rudder to give neutral spiral stability and the required dutch roll damping.

(3) The system was put into V-Canonical form (Figure 25) and the feedback decoupling transfer functions $-V_{12}$. and $-V_{21}$ calculated.

(4) Sideslip was fed back to the rudder to give the required dutch roll frequency, and roll rate fed back to the lateral controls to establish the roll time constant. Note that since the system was decoupled to give roll from wheel and sideslip from pedals, feeding back roll rate to lateral controls and yaw rate to the rudder did not reintroduce coupling.

(5) Since sideslip is not commonly available as a feedback variable, the sideslip feedbacks were replaced by equivalent side acceleration (A_y) feedbacks.

(6) The control surface "cross-coupling" inter-ties introduced mathematically in step (1) were redefined physically in terms of inter-ties from wheel to rudder and from pedal to ailerons and spoilers.

A system was thus synthesized, having neutral spiral stability, turn coordination, and with specified dutch roll characteristics and

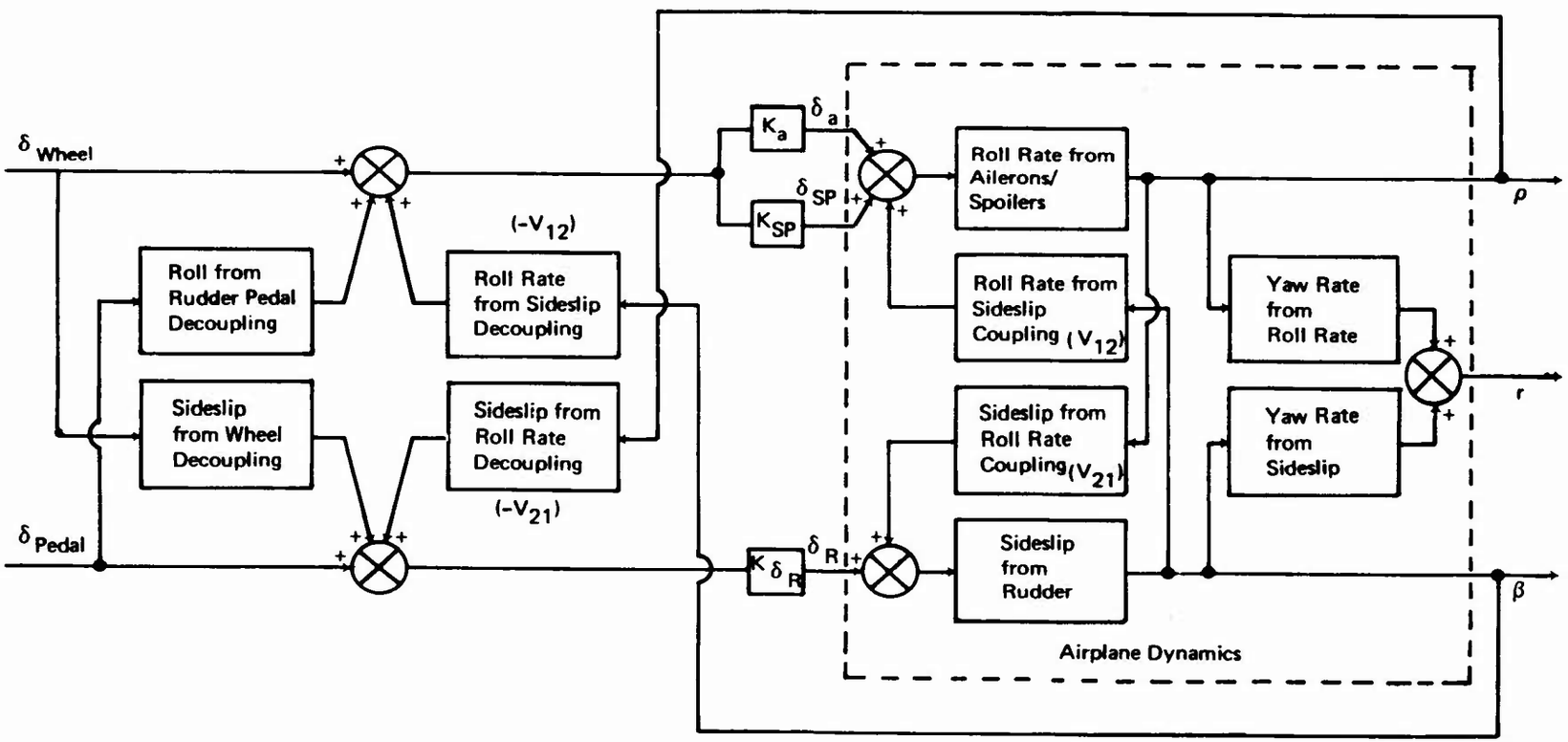

Figure 25 : V-Canonical Form for the Lateral/Directional System

roll time constant, without the iterative process common to classical multiloop design techniques. Figure 26 depicts the characteristics of a typical control law developed by this technique.

3.3 Analysis of Mechanized Control Laws

Once the control mechanization characteristics were established, the trade study parameters (i.e., safety, performance, complexity, weight, cost, design risk, and vulnerability) were numerically represented using the techniques discussed in this section.

3.3.1 Safety Analysis

This section will deal with the analysis methods used in the determination of control system safety. The complete safety computation results are given in Appendix III.

The system safety was computed separately for longitudinal and lateral/directional systems. This is consistent with major separation of axes throughout the control law design, and reduced the number of systems that had to be considered since the best longitudinal and lateral/directional systems were combined after the individual analysis of each major axis.

There were three major issues of concern:

(1) The probability of loss of control capability. (i.e., the inability to accomplish a safe CTOL landing.)

(2) The probability of control system failures inducing aircraft structural damage.

(3) The probability of encountering excessive pilot workload, considered in this study to be Level 3 operation during the STOL landing approach.

The Q method of reliability calculation of Reference 10 was used. In this computational method the probability of failure of a system is the sum of the probabilities of all major failure modes. This method is shown graphically in Figure 27. The failure modes are separated into two major classes. Failure modes where failure of any one of a series of components will cause system failure, comprise the first class. The probability of this failure mode is the sum of the probability of failure of each component. When multiple components must fail to cause system failure (i.e., components are used in a parallel fashion where any path provides success), the probability of the failure modes is the product of the component failures probabilities. This shows how the use of redundancy (i.e., parallel success paths) improves system safety.

This Q analysis method is applied to other evaluations beside system failure by replacing the failure modes causing system failure with failure modes appropriate to the specific evaluation(i.e.,the probability

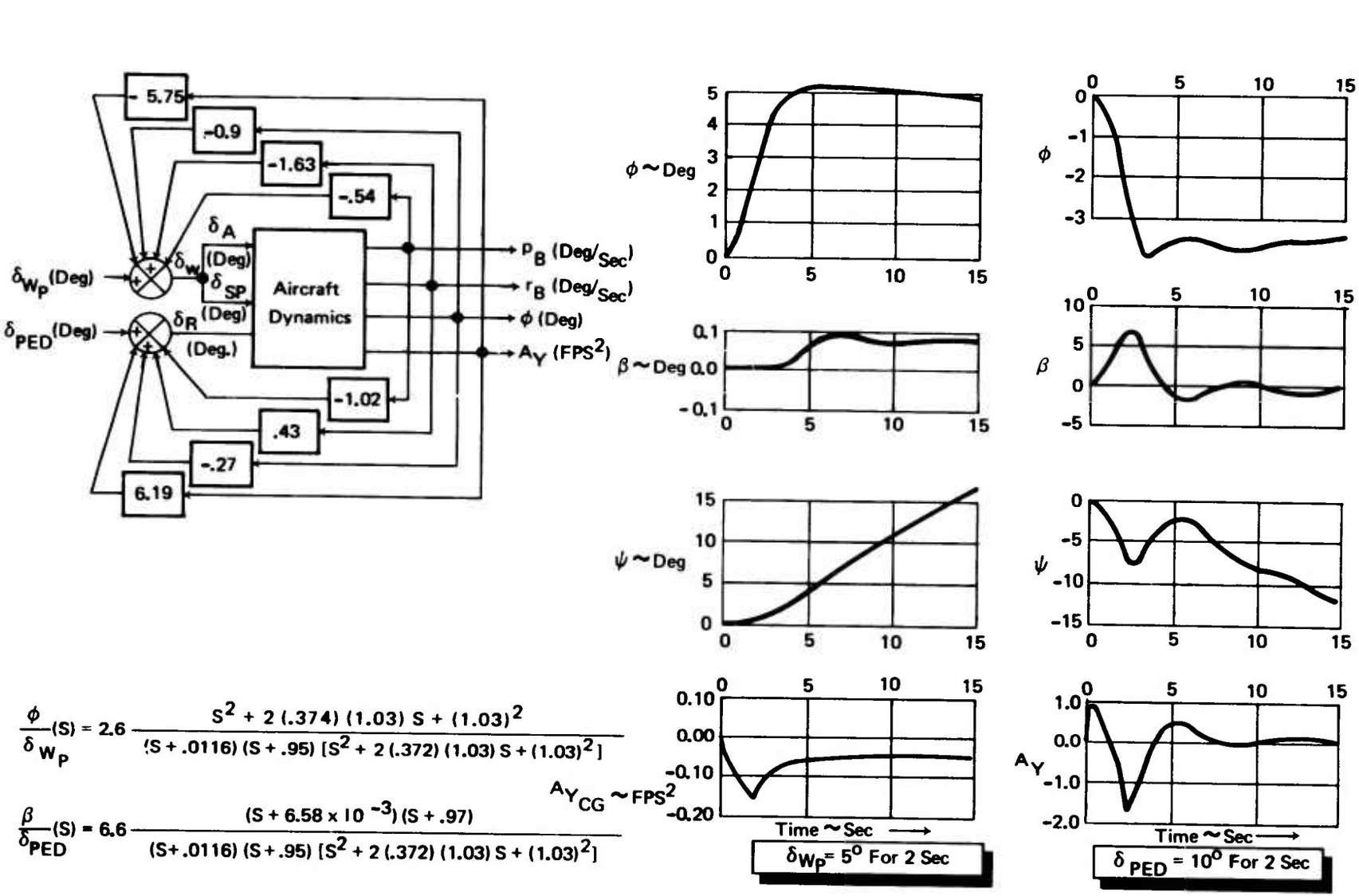

$$\frac{\phi}{\delta_{W_P}}(S) = 2.6 \frac{S^2 + 2(.374)(1.03)S + (1.03)^2}{(S + .0116)(S + .95)[S^2 + 2(.372)(1.03)S + (1.03)^2]}$$

$$\frac{\beta}{\delta_{PED}}(S) = 6.6 \frac{(S + 6.58 \times 10^{-3})(S + .97)}{(S + .0116)(S + .95)[S^2 + 2(.372)(1.03)S + (1.03)^2]}$$

Figure 26 : Block Diagram Transfer Functions and Time Histories for DR141

Computation of Failure Probability by "Q" Method [1]

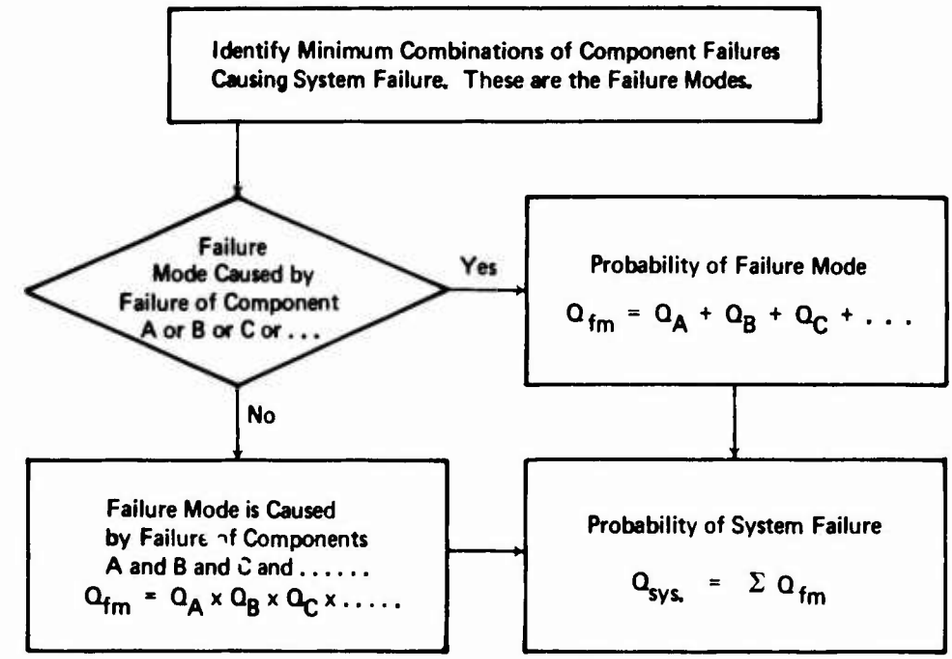

Examples :

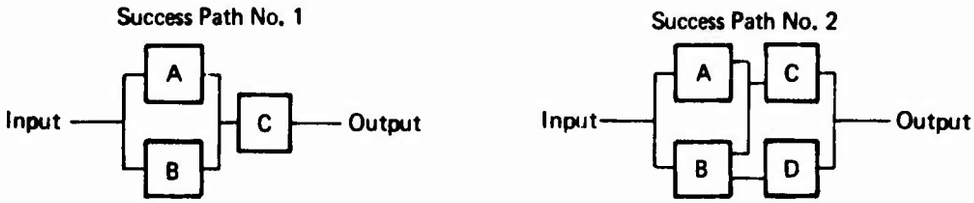

Success Path	Minimum Combinations of Component Failures	Q_{fm}	Q_{sys}
No. 1	A and B C	$Q_A \times Q_B$ Q_C	$Q_A \times Q_B + Q_C$
No. 2	A and B C and D B and C	$Q_A \times Q_B$ $Q_C \times Q_D$ $Q_B \times Q_C$	$Q_A \times Q_B + Q_C \times Q_D + Q_B \times Q_C$

[1] From AFFDL TR-70-135

Figure 27: Computation of Failure Probability By "Q" Method

of structural damage or the probability of excessive pilot workload).

In addition to analyzing the probability of failure occurance, the severity of the failure must be considered. The consequences of the first two failure conditions are catastrophic, whereas excessive pilot workload would generally not result in loss of aircraft. Therefore the failure probability data is combined in the following manner to obtain an overall safety rating.

$$S_R = .5\,(P_{LC}) + .4\,(P_{SD}) + .1\,(P_{EW}) \tag{51}$$

where: P_{LC} is a merit figure for the probability of loss of control, P_{SD} is a merit figure for the probability of structural damage, and P_{EW} is a merit figure for the probability of excessive pilot workload.

The values for the figures of merit were obtained using the procedure of section 3.1.2.5, where the following probabilities levels were used to establish the rating of 1 through 10:

$$(1)\quad Q_{LC} < 1 \times 10^{-10} \quad ; \quad P_{LC} = 1.0 \tag{52}$$

$$Q_{LC} = 1 \times 10^{-9} \quad ; \quad P_{LC} = 10.0 \tag{53}$$

$$(2)\quad Q_{SD} < 1 \times 10^{-15} \quad ; \quad P_{SD} = 1.0 \tag{54}$$

$$Q_{SD} = 1 \times 10^{-14} \quad ; \quad P_{SD} = 10.0 \tag{55}$$

$$(3)\quad Q_{EW} < 1 \times 10^{-5} \quad ; \quad P_{EW} = 1.0 \tag{56}$$

$$Q_{EW} = 1 \times 10^{-4} \quad ; \quad P_{EW} = 10.0 \tag{57}$$

The Q's are the computed failure probabilities. Linear variation of the P's was used for Q values above minimum for that category.

The task is thus reduced to identifying the specific failure modes applicable to a given mechanization and the calculating of the probability of these failure modes. Since several mechanization categories use common major system elements, this task was simplified by evaluating the failure probability of the major elements and combining them as appropriate for each specific mechanization. This procedure is discussed in Appendix III.

3.3.2 Analysis of Control System Performance

The analysis of control system performance was based on data obtained from piloted simulation studies. This data was of two kinds: First, Cooper-Harper pilot ratings provided a subjective evaluation of the control system performance. These ratings were obtained for special handling quality evaluation tasks, for an instrument flight task in turbulence, and for control performance considering the effects of engine and control system failures. During the instrument tracking task,

a second category of data was collected. This consisted of pilot controller RMS values, tracking error RMS values, and touchdown accuracy data. This second set of data provided quantitative indication of pilot workload, capability for precise tracking, and the ability to achieve accurate and repeatable touchdown performance.

A blend of the qualitative tracking performance data and the Cooper-Harper ratings was selected for the evaluation of control system performance, weighted as follows:

$$P_R = .5\ P_T + .25\ P_{HQ} + .25\ P_F \tag{58}$$

In this equation, P_T = Tracking performance rating factor
P_{HQ} = Handling quality rating factor (Cooper-Harper Ratings)
and P_F = Failure effect (Cooper-Harper Rating)
Details of computations of these quantities are discussed in Appendix III.

3.3.3 Complexity Analysis

To provide a quantitative basis for assessing relative complexity, a surface actuator using mechanical feedback and a mechanical control valve was used as a baseline element and given the complexity rating of 1. All of the other elements used in the system, bellcranks, cables, mechanical voters, clutches, jack screws, electronic voters, rate gyros, servo amplifiers, and etc. were then rated relative to this baseline system. The complexity of a given configuration then was obtained by summing up the element complexity for all of the components of the total system. This provided a means of eliminating a bias that would tend to work against either a mechanical or an electrical mechanization. The specific complexity values of each component are included in the Appendix III, Tables XLI and XLII. The relative ranking of the system complexities is included in the machanization trade study of Section 5.2.

3.3.4 Weight and Cost Evaluation

Both the weight and cost evaluation of the control systems relied heavily on statistacal data obtained from current Boeing aircraft. The schematics of the control systems provided an insight into the correlation of the proposed control systems and present Boeing aircraft of the 727/737 class. The actuation and mechanical paths were costed and weighed in relationship to these existing aircraft. The cost of the electronic systems required additional effort since the fly-by-wire techniques are not presently used in the existing production aircraft. For those components that are used in existing aircraft (e.g., rate gyros, attitude gyros, accelerometers, etc.) costs were obtained and used in the cost estimates of the electronic systems. For the electronic voters and other complicated systems, such as the strap down inertial sensors, cost and weight estimates were obtained from research groups that are evaluating these systems for future aircraft. These weights and costs were then summed up and are included

in the summary trade study charts of Section 5.2. For those items where the costs were broken out individually, such as rate gyros, attitude gyros, and INS, the costs were included in a summary data sheet of Appendix III (Table XLII). The costs of major portions of the mechanical control system were predicted by statistical methods. Incremental costs were not broken out for the elements of those major subsystems. The control system costs and weights include the following major elements:

- o Moment producer actuation systems
- o Composite mechanical control system (signal path)
- o Composite electronic control system (signal path)
- o Incremental factors for alternate moment producers (i.e., blown versus double hinge control surfaces)
- o Pneumatic system for blown surfaces.

3.3.5 Design Risk

The evaluation of design risk assigns a discrete value reflecting the degree of technical and/or production experience that exists for projected system mechanizations. Values of zero to five were assigned to the major system elements as follows:

Design Risk Value	Criteria
0	System elements where extensive technical and production capabilities exist.
1	System elements that have undergone extensive prototype evaluation and have been utilized in a limited number of production aircraft.
2	System elements similar to item 2 but which have been evaluated only on test aircraft.
3	System elements which have been evaluated in flight test but which lack extensive prototype development and have not been used in production aircraft.
4	System elements which have been evaluated in flight test programs where the difference in aircraft size or minimum operating speed results in uncertainty relative to the application for the AMST.
5	System elements which have been evaluated in laboratory and/or scaled wind tunnel tests but do not have flight test data available to verify performance.

The design risk values assigned to each major system element (e.g., electronic signal path, actuation, or moment producer system) are summed to obtain a total system design risk.

3.3.6 Control System Vulnerability Analysis

The vulnerability analysis considered the susceptibility of the proposed control systems to be disabled or significantly degraded by a single 9 mm projectile. The loss of control capability, for any single airplane axis was the criterion used to indicate that the system was disabled. In addition those "hostile-fire" induced failures causing control degradation to Level 2 and Level 3 were identified.

The failure modes used in the control law safety analysis were used to determine the impact of the loss of specific control elements. The vulnerability analysis then identified for each condition (i.e., loss of control, Level 2, and Level 3 operation), the number of places where a 9 mm hit would cause the specific degraded response.

Since the failure conditions were not of equal severity, the data was weighted. The vulnerability factor was therefore computed by:

$$R_V = 1.0\, N_{LC} + .4\, N_{L3} + .1\, N_{L2} \tag{59}$$

where N_{LC}, N_{L3}, and N_{L2} are the number of points where a 9 mm round can cause loss of control, Level 3 operation, or Level 2 operation respectively.

SECTION IV

CONTROL SYSTEM CHARACTERISTICS

4.1 General

The control system characteristics are divided into control law and control mechanization categories. The control law characteristics describe the aircraft response variations in STOL approaches for the alternate control laws studied. In addition, the high speed characteristics and the landing transition requirements are discussed. The control mechanization defines the physical characteristics of the systems required to implement the control laws.

4.2 Control Law Characteristics

4.2.1 Control Law Comparative Data

One of the objectives of the STAI was to define which control characteristics are most beneficial in providing good flying qualities and performance during the landing phase of a STOL mission. Accordingly, a list of potentially significant control parameters was established as a design guide for control law development. The list included data required for verifying compliance with military specifications and additional data applicable to the STOL landing task. By developing control laws in which the design parameters are systematically varied, the significant characteristics could then be isolated and optimized. Characteristics considered to have potential significance are indicated in the control system summary sheets, Tables VII and VIII. These data show the airplane response to control inputs in the landing/approach condition with the pilot out of the feedback control loop. System characteristics are shown for airplanes defined by two different sets of aerodynamic data. "Data Set 1" was used for preliminary selection of control laws, and was based on estimated derivatives. "Data Set 2" was based on derivatives confirmed by STAI wind tunnel test results, and was used for final control law selection. The data and equations of motion used for control law development, are given in Appendix II.

4.2.1.1 Longitudinal Control Systems

System characteristics in Table VII are listed under four subheadings; stability, coupling effects, maneuver characteristics, and system sensitivity. The stability column lists the roots of the characteristic equation, which can be resolved into complex pairs of "short period" and "phugoid" roots for the unaugmented systems only. The intent of this column was to confirm compliance with Paragraph 3.2.2 of MIL Spec. MIL-F-83300, which requires that for level 1 flying qualities, all roots be stable and the second-order pair of roots primarily determining the short term response be in a specific region of the S-plane. Most of the augmented systems did not have a short term response dominated by a second order pair of roots. The remaining requirement (that the roots be stable) can be easily checked by the listed stability data.

Parameters under "Coupling Effects" provide a measure of the cross-control inputs required of the pilot if he wishes to isolate airspeed perturbations from pitch attitude or flight path changes. Both attitude and flight path coupling are given since particular control systems attempted to minimize excursions in one variable at the expense of the other. Parameters $\Delta V_{Max}/\Delta\theta_{ss}$ and $\Delta V_{Max}/\Delta\gamma_{ss}$ give the ratio of the maximum speed excursion to the steady state attitude or flight path change induced by a control column pulse. A two-second duration was assumed for the pulse input and the maximum change of airspeed was defined as that occurring prior to the stabilization of pitch attitude and flight path. This restriction avoids penalizing a system which has an extremely slow speed divergence, not observable when under pilot control, but which would indicate misleadingly large velocity errors. The last two columns listed under coupling effects, $\Delta\theta max/\Delta V_{ss}$, $\Delta\gamma max/\Delta V_{ss}$, show the maximum attitude and flight path changes induced when the pilot commands a speed change by rotating the thrust vector angle (δ_{σ_p}). Again, attitude or flight path changes occurring after the speed change has stabilized are neglected since they would not affect the pilot's evaluation of the airplane's transient flying qualities.

The column headed "Maneuver Characteristics" provides a measure of the response of pitch rate and normal acceleration to column commands, and airspeed to thrust vector angle inputs. Parameters $T_{90\%\dot{\theta}_{ss}}$, $T_{90\%a_{n_{ss}}}$, and $T_{90\%V_{ss}}$ give the time required to reach 90 percent of steady state pitch rate, normal acceleration, and airspeed. $\dot{\theta}_{max}/\dot{\theta}_{ss}$ indicates the overshoot on commanded pitch rate. Military Specification MIL-F-83300 does not define requirements on any of these parameters. However, AGARD Report No. 577 (Reference 11) suggests a maximum value for $\dot{\theta}_{max}/\dot{\theta}_{ss}$ of 1.15. Bisgood (Reference 12) indicates that $T_{90\%a_{n_{ss}}}$ should not exceed 3 seconds for acceptable flying qualities.

The final column shows the sensitivity of the controls in terms of pitch rate and normal acceleration developed by a column command, and the airspeed change available from thrust vector rotation. With the exception of requiring that the value of pitch control force gradient with normal acceleration (F_s/a_n) never be less than 3 pounds per g, MIL-F-83300 does not place specific requirements on these parameters.

Block diagrams of each longitudinal control system studied are shown in Figures 28 through 38. Three basic types of systems were considered:

(1) Systems without feedback controls
(2) Systems with pitch attitude feedback
(3) Systems with flight path angle feedback

System Number	Data Set	Stability — Characteristic Roots	Coupling Effects — Response Coupling Due To δ_{COL} Pulse — $\frac{\Delta V_{max}}{\Delta \theta_{ss}}$ $\left(\frac{fps}{deg}\right)$
MP01	No.1	$[S^2 + 2(.263)(.0987)S + (.0987)^2][S^2 + 2(.804)(.791)S$	-3.26
MP02	No.1	Same as MP01-1	-3.36
MP03	No.1	Same as MP01-1	-3.36
SP01	No.2	$(S + .021)(S + .070)[S^2 + 2(.96)(.86)S + (.86)^2]$	-1.59
SP02A	No.2	$(S + .0016)(S + .958)[S^2 + 2(.93)(.53)S + (.53)^2]$	-.20
SP03	No.1	$(S + .002)(S + .15)(S + .522)(S + 1.39)$	-.06
SP04	No.2	$S(S + 3.3)[S^2 + 2(.9)(.45)S + (.45)^2]$	-.24
SP05	No.2	$S(S + .094)(S + 2.67)[S^2 + 2(.85)(.69)S + (.69)^2]$	-.14
DP02	No.1	$S(S + .379)[S^2 + 2(.942)(.606)S + (606)^2]$	-.05
DP03	No.1	$(S + .003)(S + 1.31)[S^2 + 2(.909)(.421)S + (.421)^2]$	-.06
DP05	No.1	$S(S + .243)(S + .764)[S^2 + 2(.826)(1.43)S + (1.43)^2]$	-.10
DP07	No.1	$(S + .003)(S + .278)[S^2 + 2(.759)(.854)S + (.854)^2]$	.04
AP01	No.1	$S(S + .243)[S^2 + 2(.805)(.735)S + (.735)^2]$	-.08
AP02	No.1	$S(S + .243)(S + .764)[S^2 + 2(.826)(1.43)S + (1.43)^2]$	-.10

*See Paragraph 2.7 of Reference 24.

Table VII: Control System Synthesis Data Sheet–Longitudinal

ects		Maneuver Characteristics						System Sensitivity			
Response Coupling Due To $\delta\sigma_p$ Step		Response To δ_{COL} Step				Response To $\delta\sigma_p$ Step	Response To δ_{Col} Step	Response To $\delta\sigma_p$ Step			
$\frac{\Delta V_{max}}{\Delta\theta_{ss}}$ $\left(\frac{fps}{deg}\right)$	$\frac{\Delta V_{max}}{\Delta\gamma_{ss}}$ $\left(\frac{fps}{deg}\right)$	$\frac{\Delta\theta\,max}{\Delta V_{ss}}$ $\left(\frac{deg}{fps}\right)$	$\frac{\Delta\gamma\,max}{\Delta V_{ss}}$ $\left(\frac{deg}{fps}\right)$	$T_{90\%\,\dot{\theta}_{ss}}$ (secs)	$T_{90\%\,a_{n_{ss}}}$ (secs)	$\frac{\dot{\theta}_{max}}{\dot{\theta}_{ss}}$	$T_{90\%\,V_{ss}}$ (secs)	$\left(\frac{\dot{\theta}}{\delta_{Col}}\right)_{ss}$ $\left(\frac{deg/sec}{inch}\right)$	$\left(\frac{F_s}{a_{11}}\right)_{\bullet}$ $\left(\frac{Lbs}{g}\right)$	$\left(\frac{V}{\delta\sigma_p}\right)_{ss}$ $\left(\frac{fps}{deg}\right)$
-3.26	-5.85	.01	.16	1.1	3.1	1.18	9.4	2.5	26	-1.5
-3.36	-5.73	.01	.16	1.3	2.9	1.14	9.4	2.3	28	-1.5
-3.36	-5.73	-.16	.05	1.3	2.9	1.14	20.3	2.3	28	-5.8
-1.59	-3.10	-.04	.15	1.5	2.9	1.00	15.0	2.1	33	-2.0
-.20	-.26	-.03	.11	1.2	4.1	1.08	5.6	2.0	28	-0.7
-.06	-.07	.02	.19	1.0	5.0	1.10	15.6	1.6	34	-1.9
-.24	-.28	-.02	.11	0.7	3.9	1.06	5.5	1.6	33	-0.6
-.14	-.18	-.01	-.04	0.8	3.7	1.06	2.6	1.6	34	-0.9
-.05	-.06	.04	.18	1.3	4.4	1.13	8.1	2.4	22	-1.0
-.06	-.07	.03	.16	1.0	4.8	1.14	6.7	1.9	27	-0.8
-.10	-.11	.08	.11	0.8	3.8	1.24	9.6	1.4	33	-0.9
.04	.04	-.05	.13	1.2	3.1	1.16	8.6	1.6	33	-0.7
-.08	-.09	-.27	-.02	1.1	4.0	1.19	9.7	2.3	22	-0.9
-.10	-.11	-.27	-.01	0.8	3.8	1.24	9.7	1.4	33	-0.9

(1) Systems Without Feedback Controls (MP01*, MP02, MP03, Figure 28)

As shown in Table VII and Figure 20, the short period and phugoid motions of the unaugmented systems are closely coupled. According to Reference 12, handling difficulties can arise if the ratio of the short period and phugoid frequencies $\frac{\omega_{SP}}{\omega_{PH}}$ is less than 20. In the landing approach condition the STAI airplane has a value 8, indicating potential problems.

System MP01 is a basic system in which the pilot can primarily control flight path by the elevator and speed by the thrust vector angle.

System MP02 is similar to MP01 except that elevator commands also provide direct lift control (DLC) via symmetrical spoiler deflections.

System MP03 adds an interconnect from thrust vector angle to elevator and DLC. As can be seen in Table VII this reduces the flight path excursions when changing airspeed, at the expense of increased attitude perturbations.

(2) Systems Which Include Pitch Attitude Feedback (SP01, SP02A, SP03, SP04, SP05, CP21, DP02, DP03)

Unless otherwise specified, these systems provide pitch attitude control from the column without airspeed excursions, and airspeed from the thrust vector angle controller without inducing pitch attitude changes. Pitch attitude rate is proportional to control column force.

System SP01 (Figure 29) is a basic feedback system using only pitch rate feedback to the elevator and DLC. The augmentation does not explicitly minimize speed excursions during pitch maneuvers, although some improvement over the unaugmented systems is evident from Table VII.

---

*System identification code:

1. First Letter
   - M - Mechanical
   - S - Stability Augmented
   - C - Control Augmented
   - F - Fly by Wire
   - D - Decoupled
   - A - Attitude Hold Feature Included
2. Second Letter
   - P - Longitudinal
   - R - Lateral/Directional
3. Numbers are arbitrarily assigned.
4. Final letters (if present):
   - A - Modification
   - R - Mechanical Revision

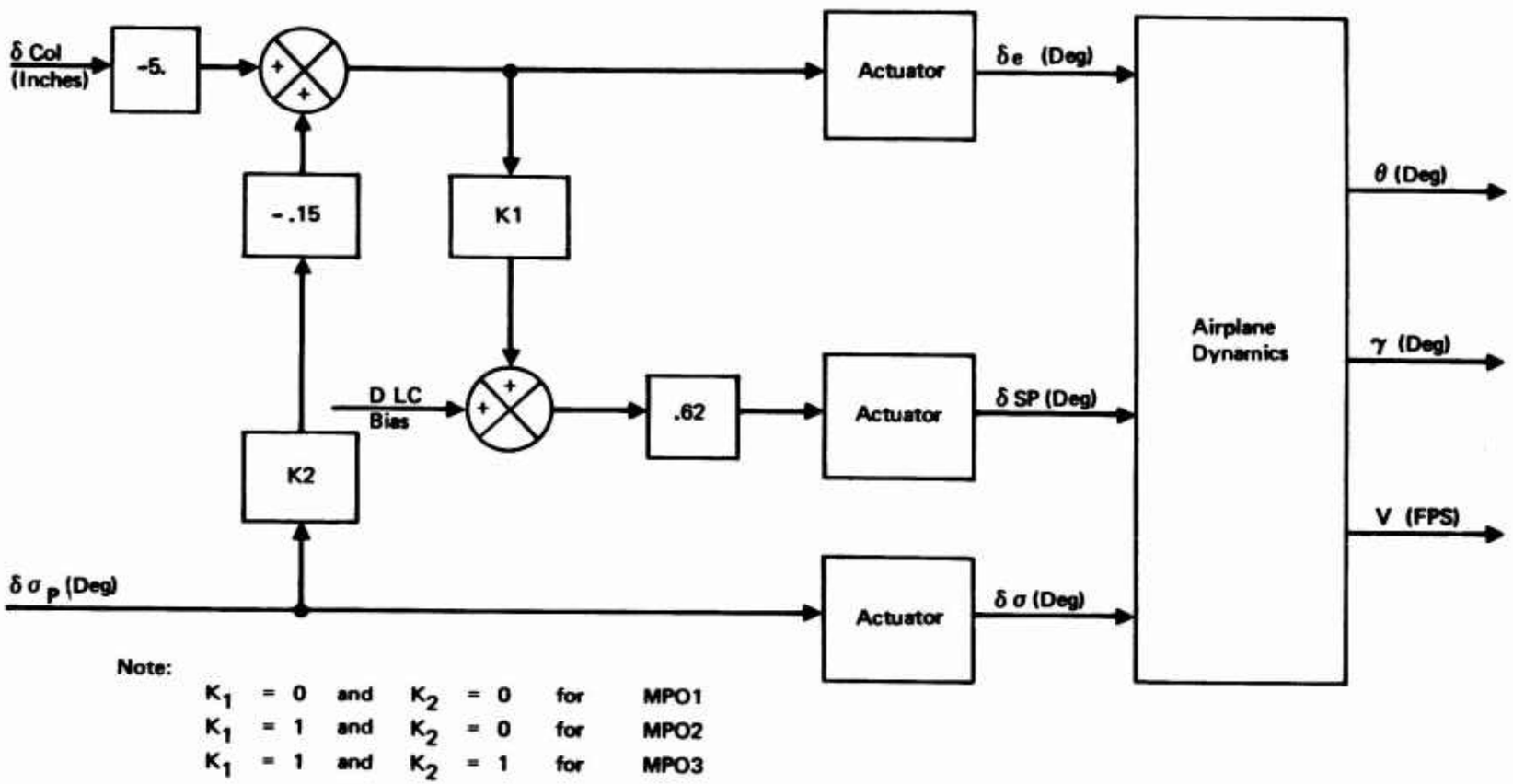

Figure 28 : Block Diagram for Control Systems -- MP01, MP02 and MP03

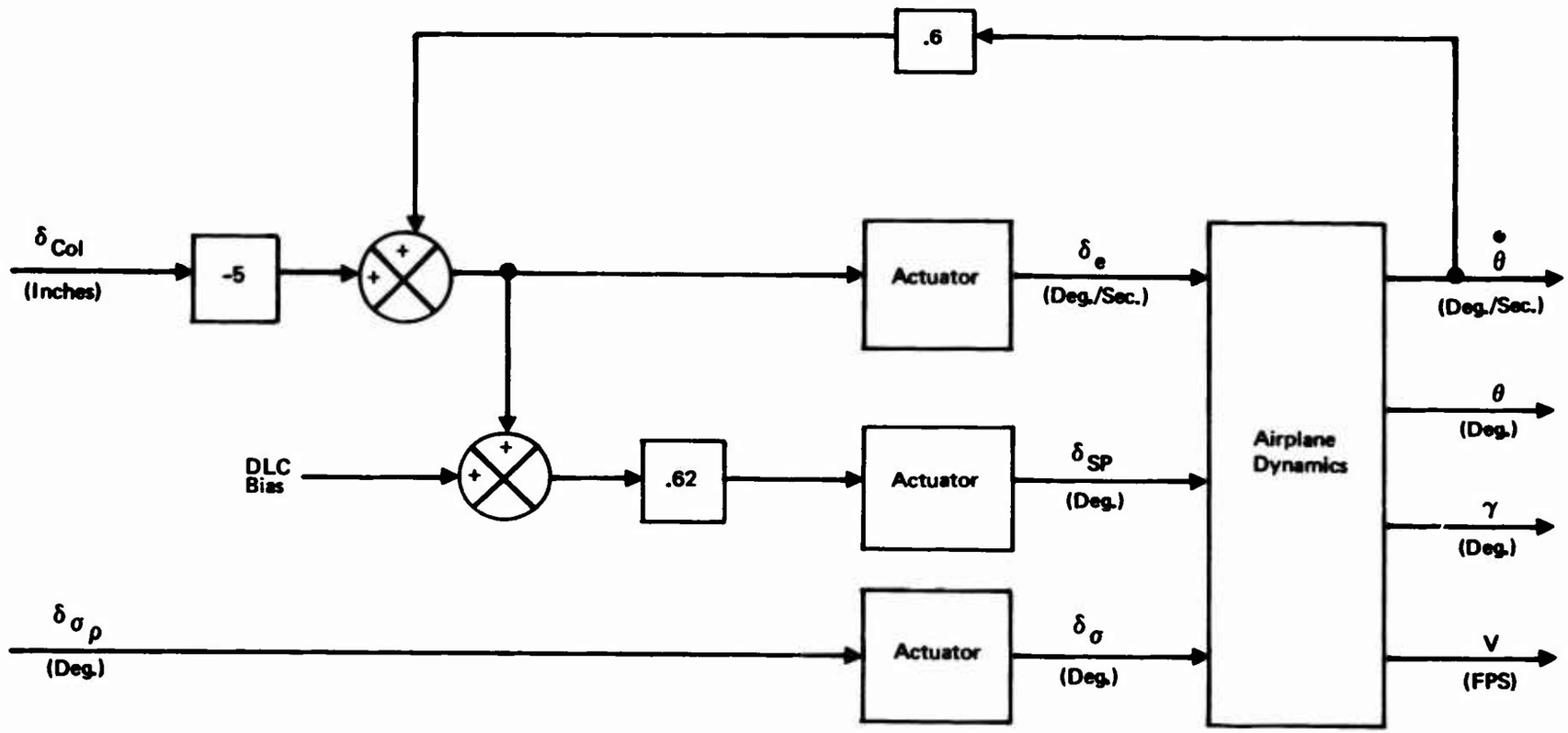

Figure 29 : Block Diagram for Control System SP01

System SPO2A (Figure 30) enables pitch maneuvers to be performed with minimum speed excursions. This is obtained by the feedback of attitude changes and airspeed error to the thrust angle controller. As can be seen in Table VII, the speed feedback provides a faster rise time on airspeed response than SPO1 at the expense of reduced speed sensitivity. Compensation for loss of lift in a banked turn is obtained by feeding back the absolute value of roll attitude to the direct lift controller. A simplified system without the lift compensator was tested and labelled SPO2. Systems APO3 and APO7 are basically the same as SPO2A but include pitch attitude hold circuits that are activated in the absence of pilot column inputs. A control augmented version of SPO2A, labelled CP21 and shown in Figure 30, was tested on the NASA Ames moving base simulator during the system validation phase of the study.

System SPO3 is a similar system to SPO2 but with an alternate speed-decoupling-from-column network. As shown in Figure 31, the speed decoupling is obtained by feeding back both attitude and attitude rate to the thrust angle controller. This enables pitch decoupling during airspeed changes comparable to that of SPO2 without the requirement of airspeed feedback.

System DPO2 decouples attitude from thrust angle system by feeding back airspeed and longitudinal acceleration to the column input, and is otherwise like SPO3 except for the airspeed feedback to δ_r. In addition, the pitch rate feedback to column signal of SPO3 is removed, resulting in a slightly more oscillatory system. The value of $\dot{\theta}_{MAX}/\theta_{SS}$ is still within the design goal of 1.15, however.

Systems SPO4 and SPO5 (Figure 32) are variants of System SPO2A but with higher gain pitch rate feedbacks and column gearing. As shown in Table VII, this increases the pitch rate response but at the expense of normal acceleration response.

System DPO3 (Figure 33) is basically similar to SPO3 except that direct lift control is removed. As shown in Figure 34, this results in a slower initial flight path response.

(3) Systems with Flight Path Angle Feedback (DPO5, DPO5A, DPO5B, DPO7, APO1, APO2, APO5)

These systems provided flight path angle rate proportional to column deflections with minimum airspeed changes, and airspeed proportional to thrust angle commands with little effect on flight path angle. Direct lift control is included in each system since it was not possible to realize the decoupling feedbacks required when DLC was not used.

DPO5 (Figure 35) is the basic flight path angle system, utilizing airspeed-from-column decoupling by the feedback of flight path and flight path rate to the thrust angle controller. Flight path angle is not decoupled from airspeed changes although flight path changes are reduced by adding flight path rate damping feedback

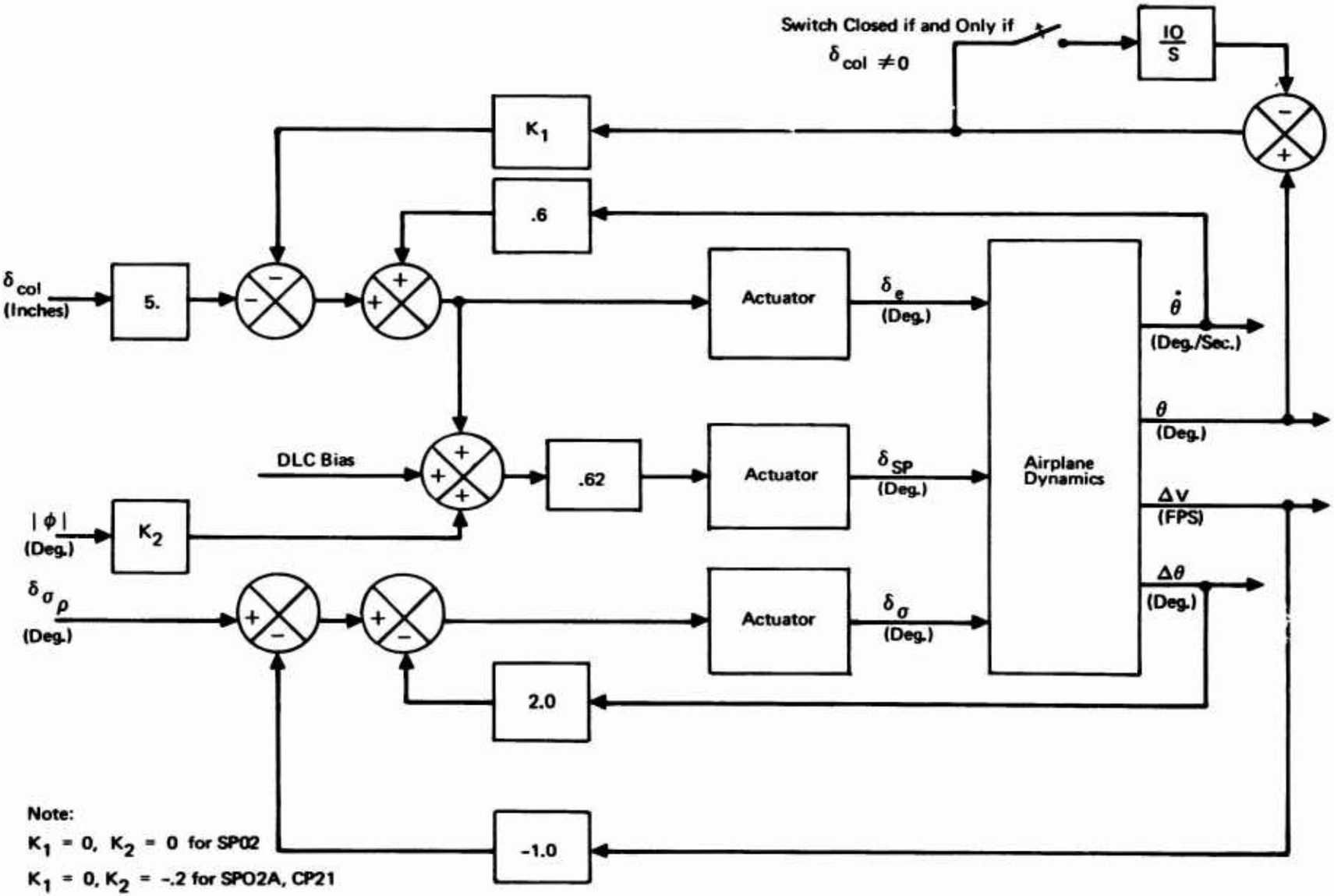

Note:

$K_1 = 0$, $K_2 = 0$ for SP02

$K_1 = 0$, $K_2 = -.2$ for SPO2A, CP21

$K_1 = -2.$, $K_2 = 0$ for AP03

$K_1 = -5.$, $K_2 = -.2$ for AP07

Figure 30 : Block Diagram for Control Systems SP02, SP02A, CP21, AP03 and AP07

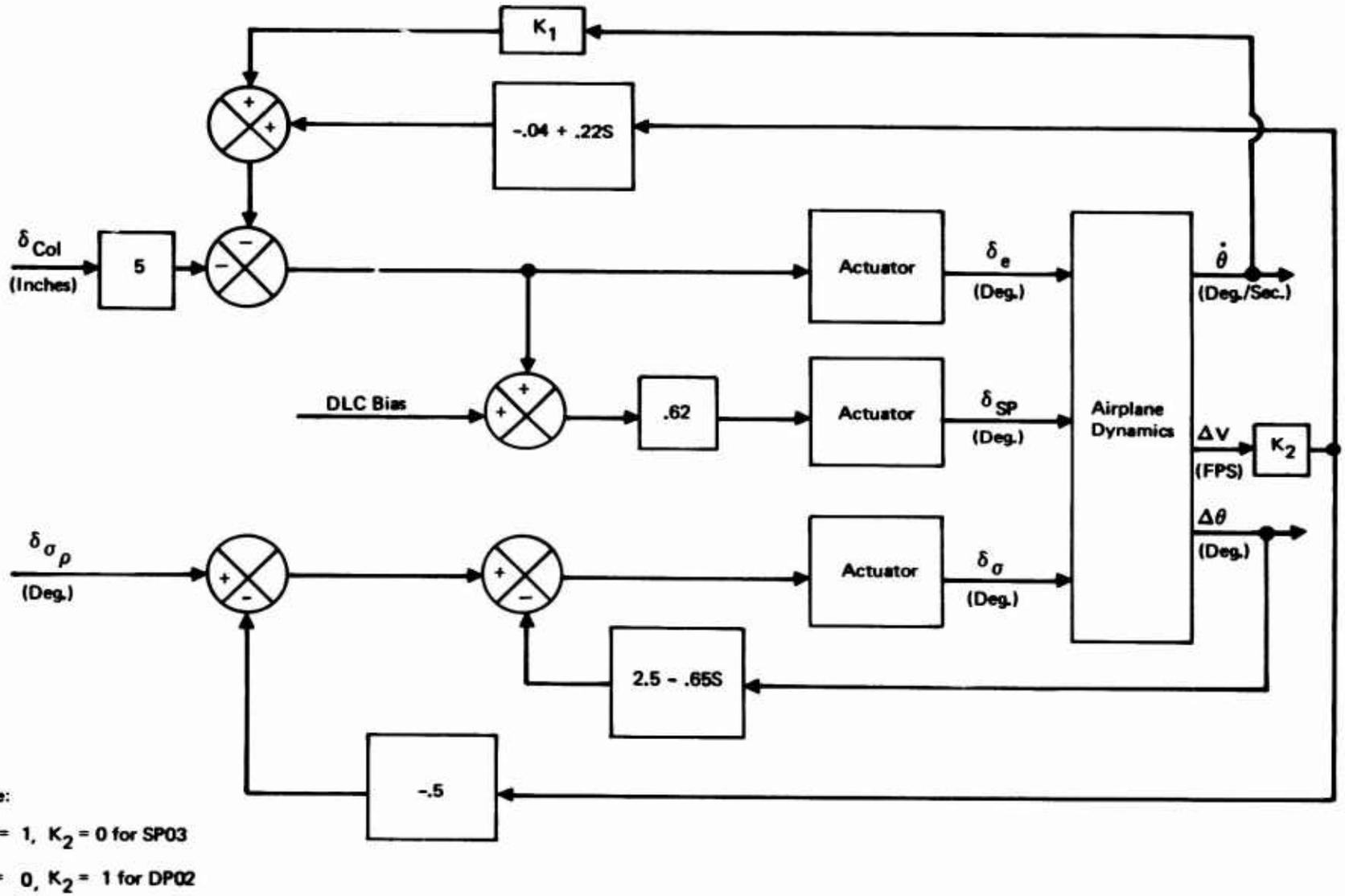

Figure 31: Block Diagram for Control Systems SPO3 and DPO2

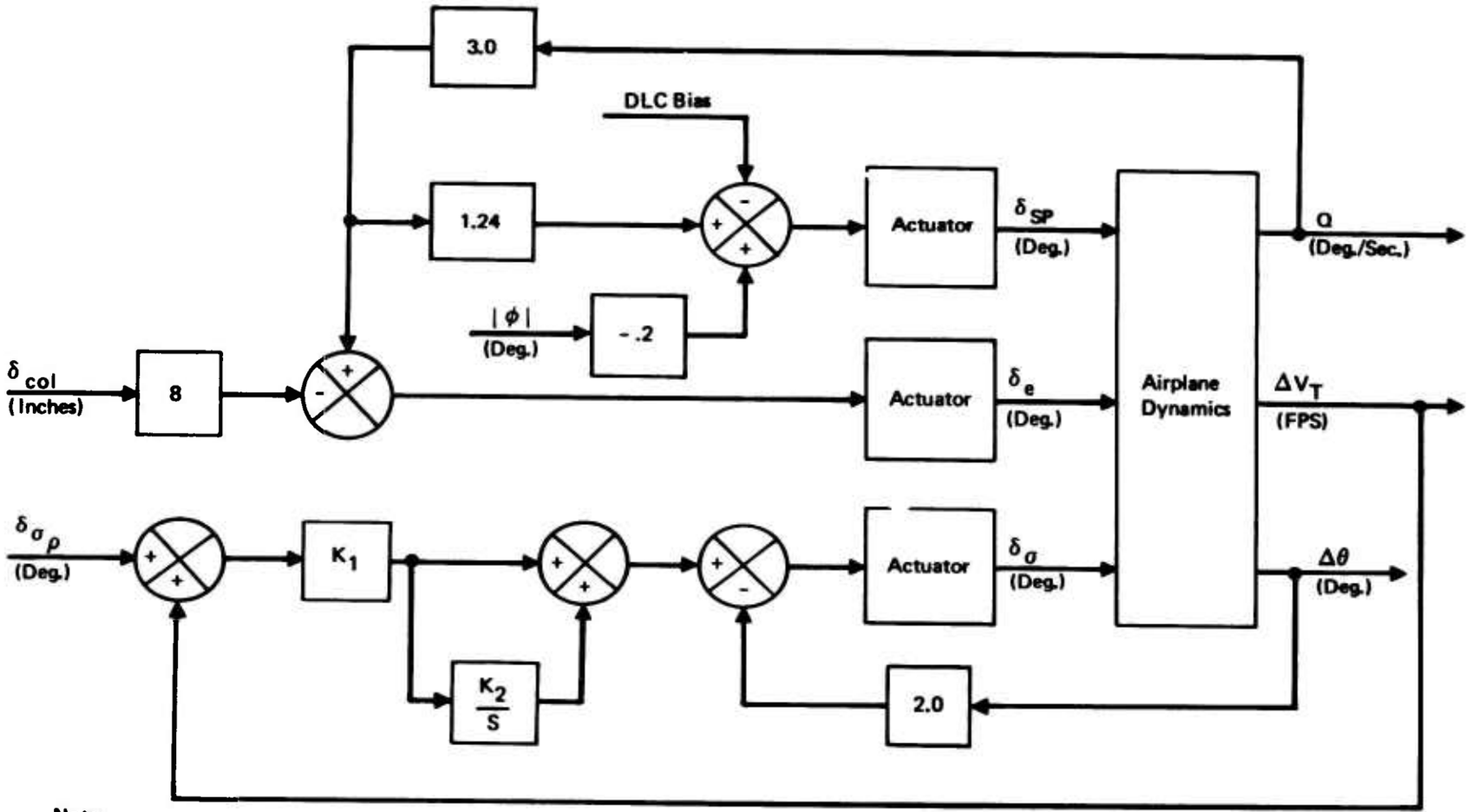

Note:

$K_1 = 1, K_2 = 0$ for SP04

$K_1 = 3, K_2 = .1$ for SP05

Figure 32 : Block Diagram for Control Systems SP04 and SP05

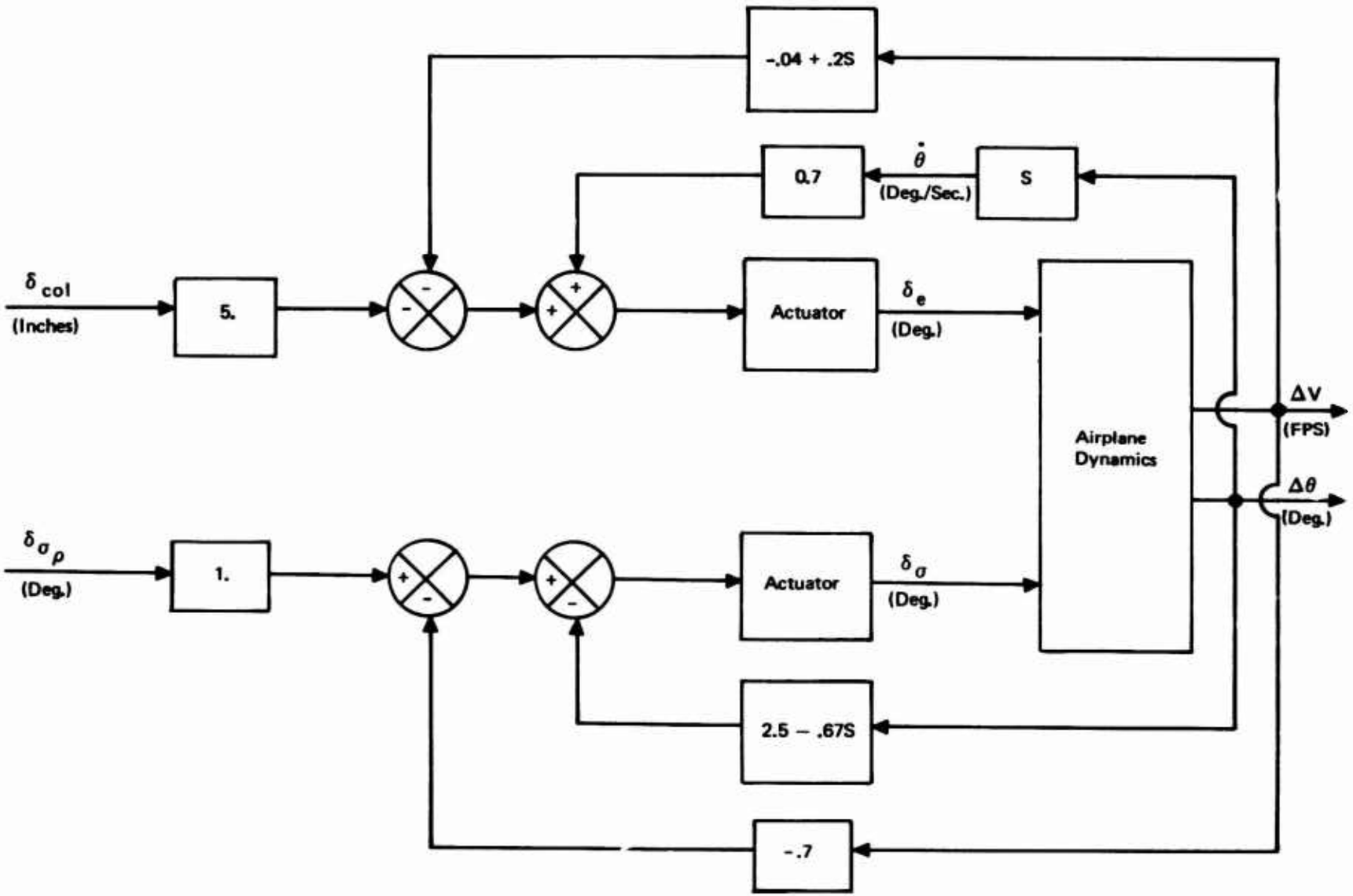

Figure 33 : Block Diagram for System DP03

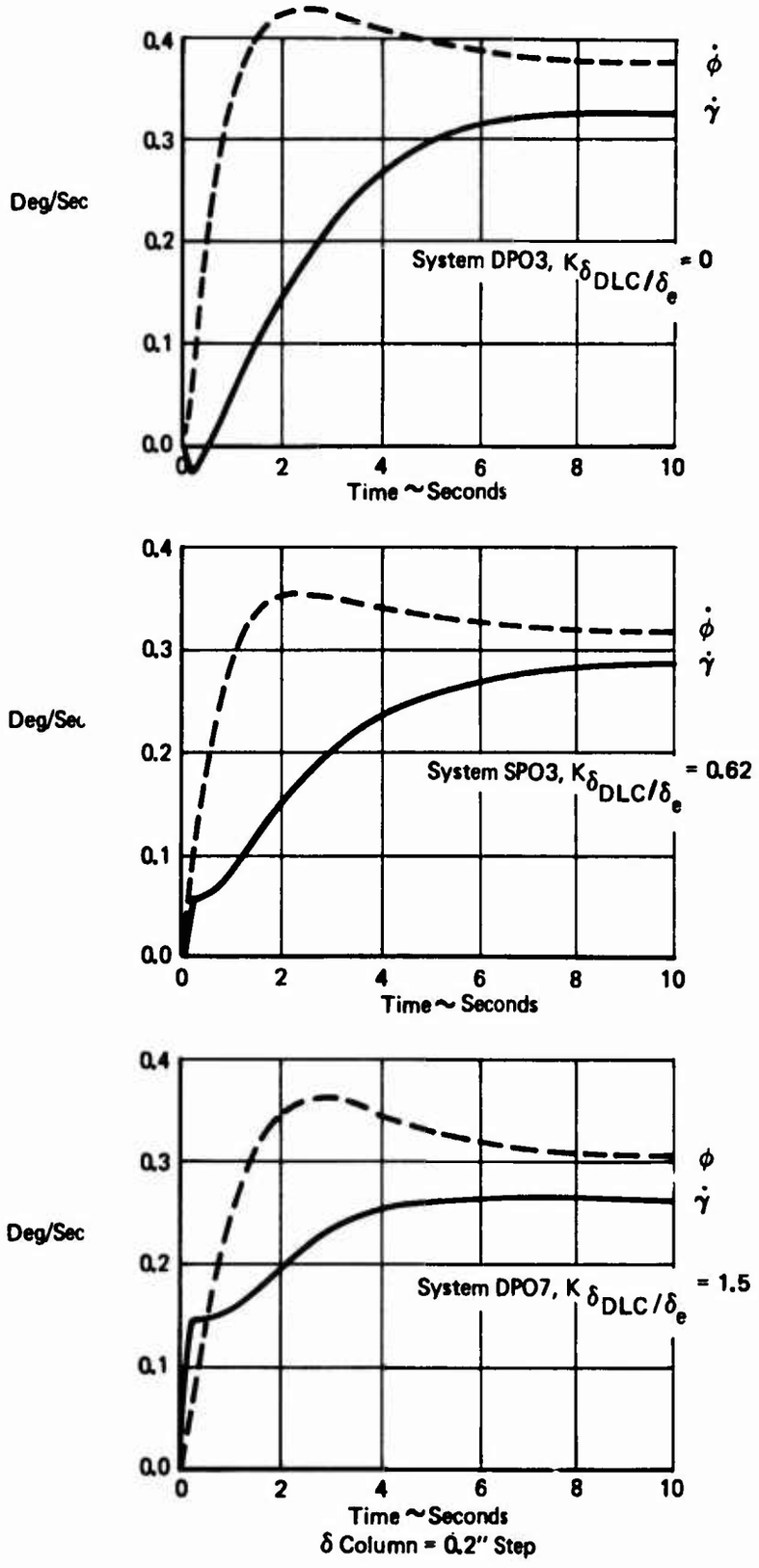

Figure 34 : Effect of Direct Lift Control on Response to Column Step

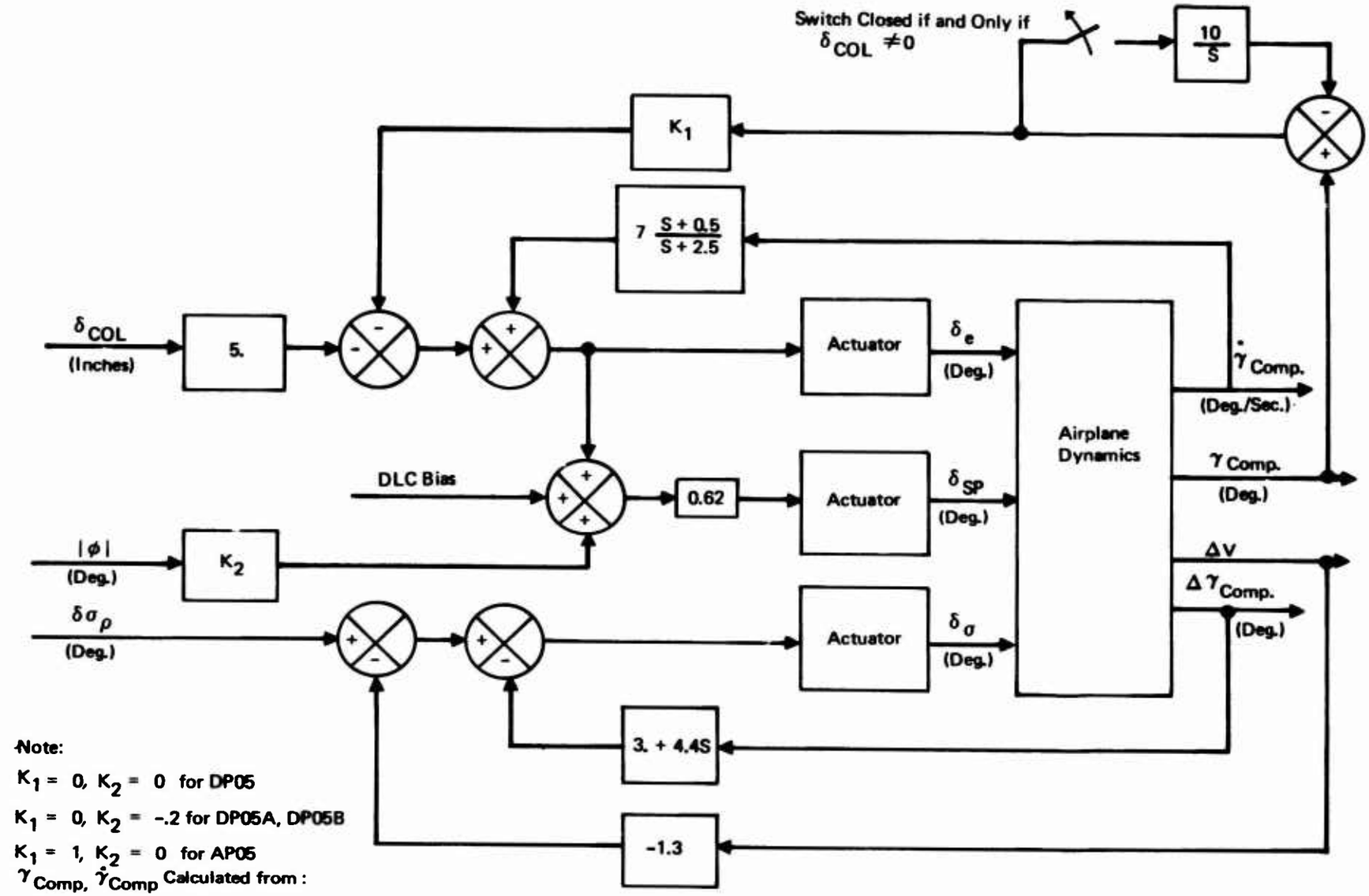

Note:

$K_1 = 0,\ K_2 = 0$ for DP05

$K_1 = 0,\ K_2 = -.2$ for DP05A, DP05B

$K_1 = 1,\ K_2 = 0$ for AP05

γ_{Comp}, $\dot{\gamma}_{Comp}$ Calculated from :

Ground Speed in DP05A

Air Speed in DP05B

Figure 35 : Block Diagram for Control Systems DP05, DP05A, DP05B, and AP05

to the column. DPO5A and DPO5B include a lift compensator for banked turns. DPO5B uses airspeed to compute flight path and flight path rate whereas all other flight path systems use groundspeed in the flight path and flight path rate calculations.

System APO2 is similar to DPO5 except that flight path perturbations are decoupled from airspeed commands by feeding back airspeed error and longitudinal acceleration to the elevator and DLC. As shown in Table VII, This lowers $|\Delta\gamma_{max}/\Delta V_{ss}|$ but increases $|\Delta\phi_{max}/\Delta V_{ss}|$, compared with DPO5.

System DPO7 (Figure 36) provides faster flight path response to column than DPO5 by increasing the direct lift gain. This can be seen from the value of $T_{90\%_{an}}$ in Table VII and is further illustrated in Figures 23, 24, and 37 which shows the $\dot{\gamma}$ and $\dot{\theta}$ response of systems DPO3, SPO3, DPO7.

System APO1 (Figure 38) augments the damping of $\dot{\gamma}$ from column by providing a flight hold mode instead of using $\dot{\gamma}$ feedback as in DPO5. Since the hold mode is disconnected when the column is out of detent, the transient response to column commands is similar to DOP5. However, the $\Delta\gamma_{max}/\Delta V_{ss}$ ratio is improved for APO1 at the expense of degraded $\Delta\dot{\theta}_{max}/\Delta V_{ss}$.

4.2.1.2 Lateral-Directional Systems

Characteristics of all lateral/directional stability augmentation systems evaluated are shown in Table VIII. This summary data was selected to check compliance with the flying quality requirements of MIL-F-83300 and to tabulate additional data considered useful in system selection. Characteristic roots of each system are listed in Table VIII under the heading "Stability". (MRO821 is the only control system showing MIL SPEC stability noncompliance.) The parameters listed under "Coupling Effects" in Table VIII are defined in MIL-F-83300 (dihedral effect is an exception). The nonresonant nature (minimal dutch roll response) of most of these control systems made the MIL-F-83300 time response evaluations of $\measuredangle_p/\beta$, ψ_β, and $|\phi/\beta|_d$ difficult if not impossible to apply. Therefore, alternate techniques are now described. To determine $|\phi/\beta|_d$; $\phi(s)/\beta(s)$ was evaluated at either dutch roll pole location ($s = \zeta_D\,\omega_D \pm j\omega_D\sqrt{1-\zeta_D^2}$). This results in a ratio of two complex numbers which yields $|\phi/\beta|_d$. The parameter $\measuredangle_p/\beta$ can be determined from the ratio $p(s)/\beta(s)$ evaluated at either dutch roll pole location. When the phase angle of the denominator complex number is subtraced from the phase angle of the numerator complex number, $\measuredangle_p/\beta$ is the result. These definitions of $|\phi/\beta|_d$ and $\measuredangle_p/\beta$ were obtained from Appendix V C of Reference 23. ψ_β was computed from an equation listed in "Airplane Flying Qualities Specification Revision", an article in Reference 13. This equation uses the angle between the dutch roll pole and the p/δ_w zero plus the dutch roll pole damping ratio to compute ψ_β. Requirements on these parameters ensure that sideslip and roll oscillations are not

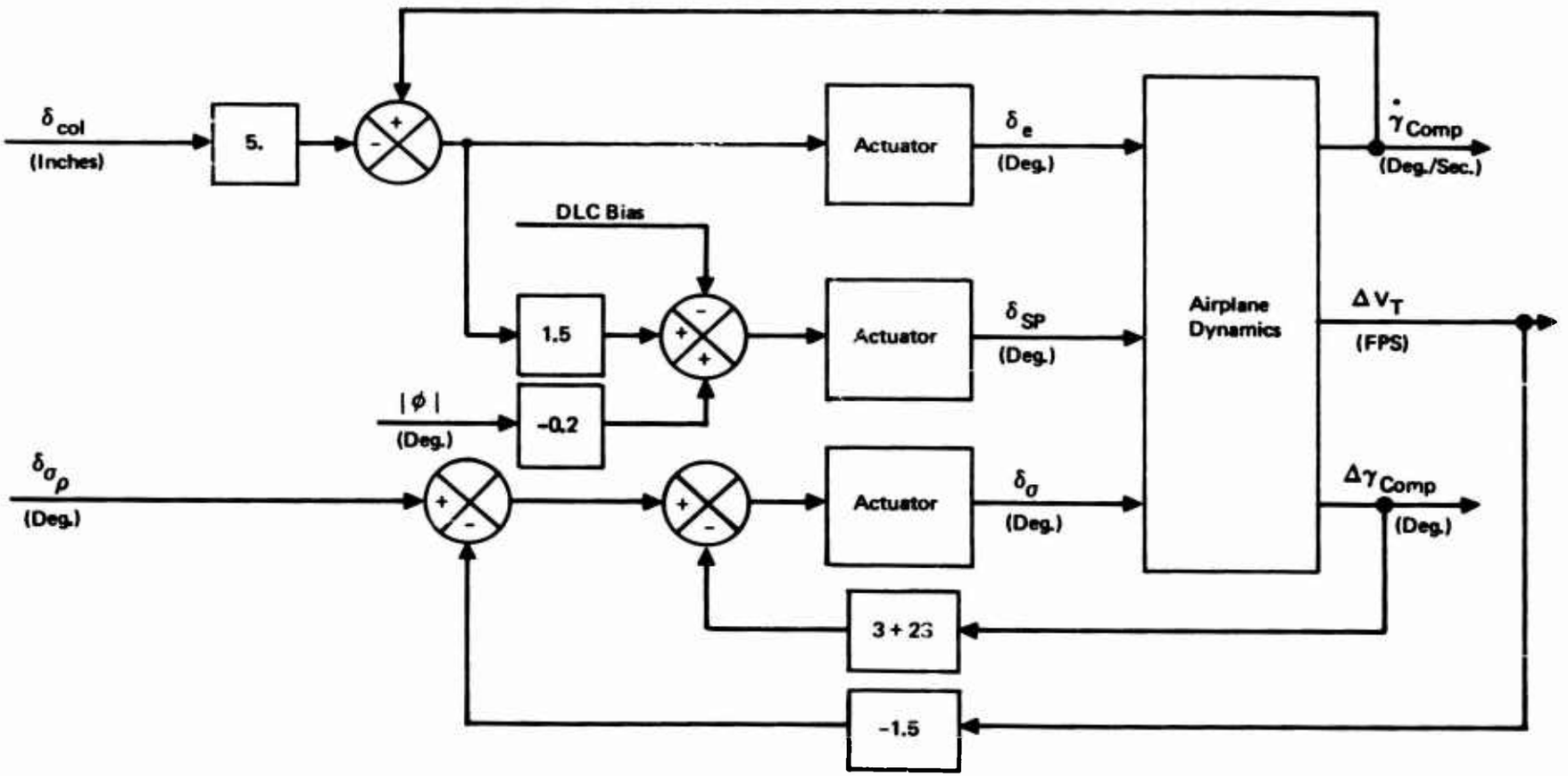

Figure 36 : Block Diagram for Control System DP07

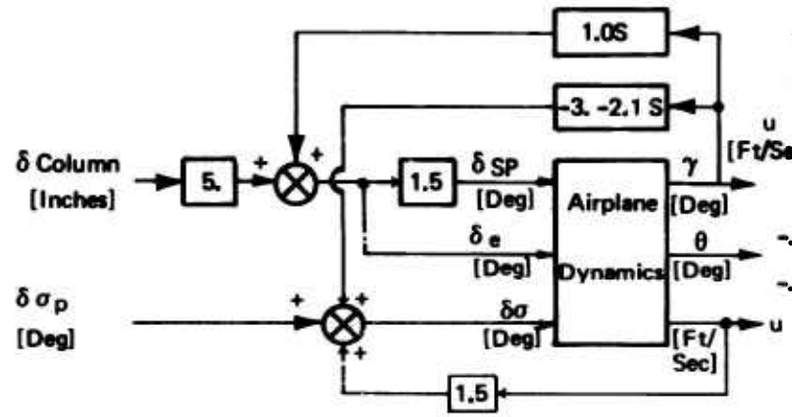

$$\frac{\gamma}{\delta \text{ Column}} = \frac{-.78\,[S^2 + 2\,(.45)\,(1.1)\,S + (1.1)^2]}{S\,[S^2 + 2\,(.76)\,(.84)\,S + (.84)^2]} \quad \frac{\text{Deg}}{\text{Inch}}$$

$$\frac{\theta}{\delta \text{ Column}} = \frac{-1.7\,[S + .65]}{S\,[S^2 + 2\,(.76)\,(.84)\,S + (.84)^2]} \quad \frac{\text{Deg}}{\text{Inch}}$$

$$\frac{u}{\delta \sigma_p} = \frac{-0.20}{S + 0.28} \quad \frac{\text{Ft/Sec}}{\text{Deg}}$$

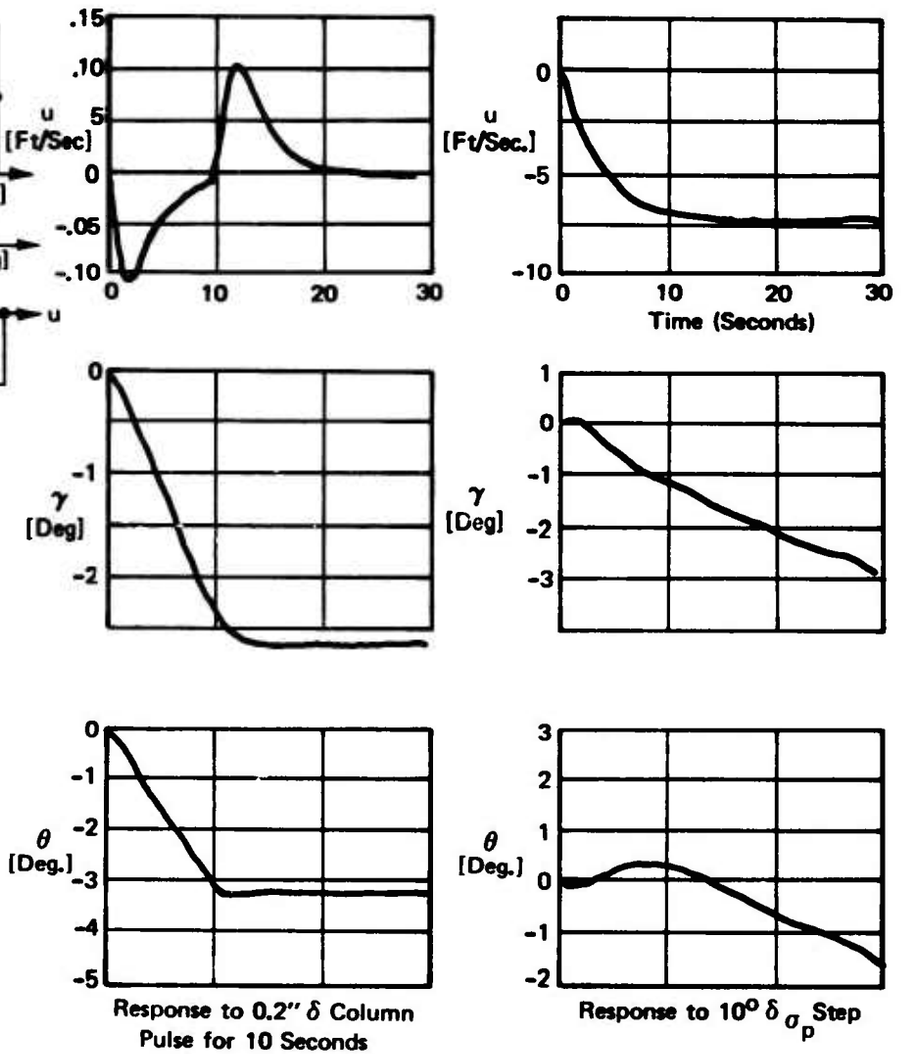

Figure 37 : Longitudinal System DP07 Response to Column Pulse and Thrust Vector Angle Step

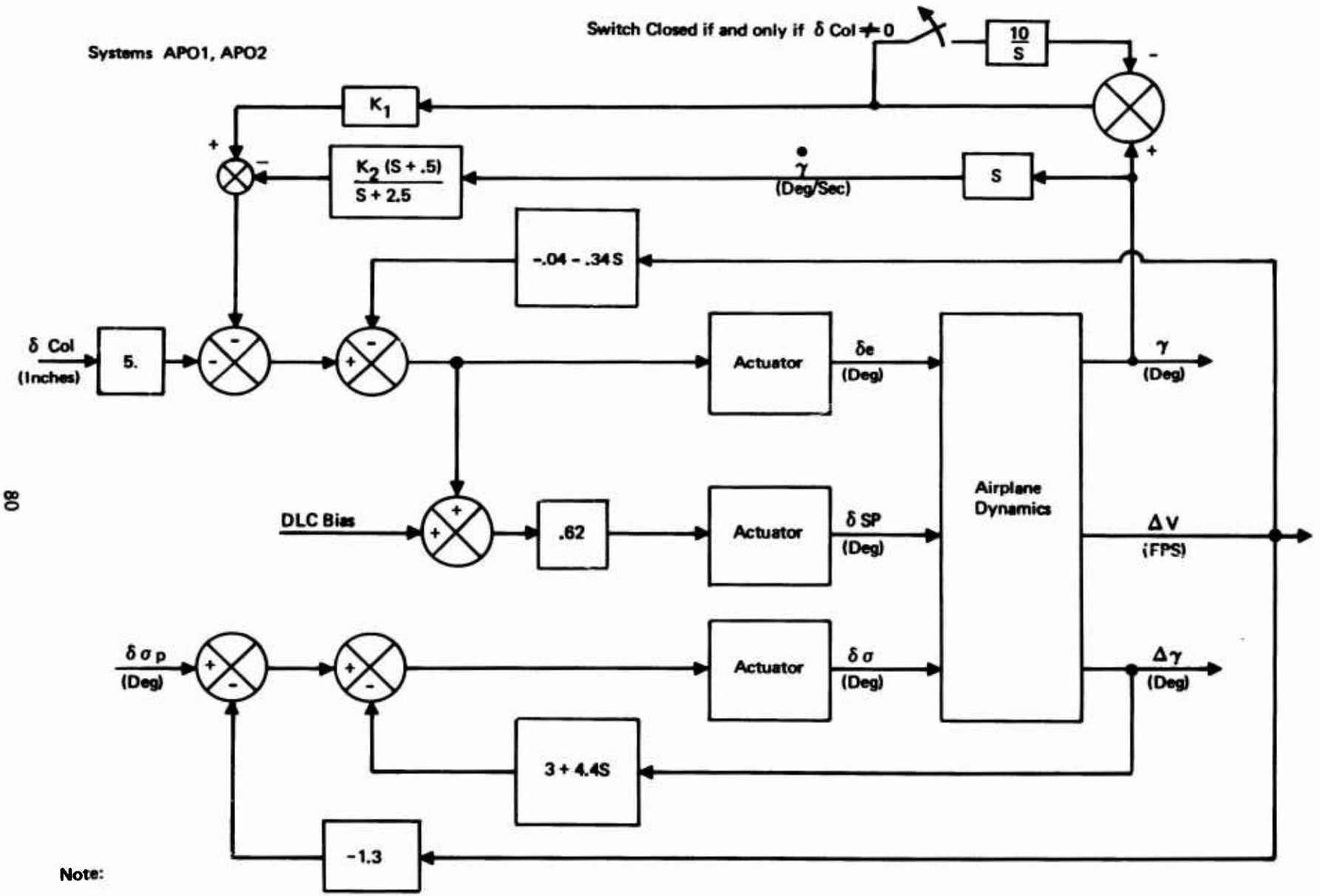

Note:

K_1 = .5 & K_2 = 0 for APO1

K_1 = 0 & K_2 = 7 for APO2

Figure 38 : Block Diagram for Control Systems APO1 and APO2

		Stability				
		Dutch Roll		Roll Time Constant	Spiral Time Constant	Turn Coordinat (Response δ W Puls
		ω_D	ζ_D	T_R	T_{SPIR}	$\frac{\Delta\beta}{\phi_1}$
System Number	Data Set	r/s		(secs)	(secs)	
MR0821	No.2	0.9	0.2	1.1	-7.5 [1]	
SR0721	No.1	0.7	0.2	0.8	406	
SR10	No.1	0.7	0.7	1.1	1100	
SR11	No.1	0.5	0.2	1.1	440	
SR20	No.2	0.9	0.6	1.1	-185	
SR21	No.2	1.5	0.4	0.3	177	
FR20, CR20	No.2	1.5	0.4	0.3	177	
DR141	No.1	1.0	0.4	1.0	62	
DR142	No.1	1.0	0.4	0.5	630	
FR21, CR21	No.2	1.0	0.4	0.5	630	

[1] Does Not Meet (MIL-F-83300) Level 2 Flying Quality Criterion But Meets Level 3

[2] Does Not Meet (MIL-F-833 for $\left|\frac{\Delta\beta}{\phi_1}\right| \times \left|\frac{\phi}{\beta}\right|_d$

A

Table VIII: Control System Synthesis Data Sheet – Lateral/Directional

Coupling Effects						System Sensitivity		
Turn Coordination (Response to δ W Pulse)			Dihedral Effect (Response to δ R Step)		Dutch Roll Excitation (Response to δ W Pulse)	Response to δ W Step	Response to δR_p Step	
$\frac{\Delta\beta}{\phi_1}$	$\left\lvert\frac{\Delta\beta}{\phi_1}\right\rvert \times \left\lvert\frac{\phi}{\beta}\right\rvert_d$	ψ_β	$\measuredangle P/\beta$	$\left(\frac{\phi}{\beta}\right)_{T=3\text{ secs}}$		$\frac{\phi_{OSC}}{\phi_{AVG}}$	$\frac{\dot{\phi}_{SS}}{\delta W_P}$	$\frac{\beta_{MAX}}{\delta R_{ped}}$
							(sec^{-1})	$\left(\frac{deg}{in.}\right)$
1 ▷	◀				Divergent			▶
0.58	0.337 2 ▷		-149°	184°	-0.41	0.140	1.0	-13.1
0.32	0.246		-70°	192°	-0.54	0.066	1.3	- 7.4
0.32	0.320		-142°	163°	-0.47	0.103	1.8	-19.0
0.34	0.269 2 ▷		-64°	166°	-0.85	0.034	0.6	- 6.4
0.26	0.118		-73°	127°	-0.56	0.046	0.3	- 6.6
0.18	0.081		-133°	124°	-0.56	0.	0.3	- 6.6
0.03	0.002		-48°	55°	-0.05	0.015	1.3	- 9.8
0.06	0.002		-40°	50°	-0.03	0.	0.7	- 9.8
0.06	0.005		-85°	57°	-0.03	0.	0.3	- 9.8

(MIL-F-83300) Level 1 Flying Quality Criterion

$\left\lvert\frac{\phi}{\beta}\right\rvert_d$

B

excessive during roll maneuvers. The coupling between rudder inputs and roll attitude is indicated by the parameter $[\phi/\beta]_{T=3}$, the ratio of roll attitude to sideslip measured three seconds after a step rudder input. Three seconds was chosen as the measurement time since this approximates the time delay between initiating a typical decrab maneuver and touchdown. It is therefore a measure of lateral control input required to keep wings level during decrab. Table VIII also shows the system sensitivity in terms of the steady state roll rate available from wheel and maximum sideslip available from rudder pedal. The usefulness of these parameters is discussed in Section 4, Part II of this volume.

Block diagrams of each lateral/directional control system evaluated are shown in Figures 39 through 47. System types included the basic unaugmented airplane, augmentation using roll and yaw rates only, and more complex systems using roll and yaw attitude and lateral acceleration feedbacks. A brief description of each system is given in the following:

System Number	Characteristics
MR0821 (Figure 39)	No stability augmentation. Control wheel (δw_ρ) provides roll control through ailerons and spoilers, rudder pedals (δ PED) operate the rudder only. The system has excessive spiral instability with a time-to-double-bank-angle of 5.2 seconds. This meets the MIL-F-83300 Level 3 flying quality requirement of greater than 4 seconds-to-double, but exceeds the Level 2 requirement of greater than 12 seconds to double amplitude.
SR11 (Figure 39)	Meets Level 1 spiral stability requirements by feedback of yaw rate to δw, and improved turn coordination by feeding back roll rate to δ_R. The required $r \rightarrow \delta_w$ gain is obtained by root locus studies. The necessary $p \rightarrow \delta_R$ gain is obtained from the simultaneous solution of the side force and yawing moment equations with $\beta = \dot{\beta} = 0$. (See Reference 14 for details.) This system meets Level 1 turn coordination requirements.
SR0721 (Figure 40)	Provides MIL-F-83300 Level 1 spiral stability and improved roll rate response by the feedback of yaw rate and roll rate to δ_w. Turn coordination is aided by a crossfeed from control wheel to rudder. This system barely exceeds the MIL-F-83300 Level 1 criterion for the ratio $\lvert\frac{\Delta\beta}{\phi_1}\rvert \times \lvert\frac{\phi}{\beta}\rvert_d$.

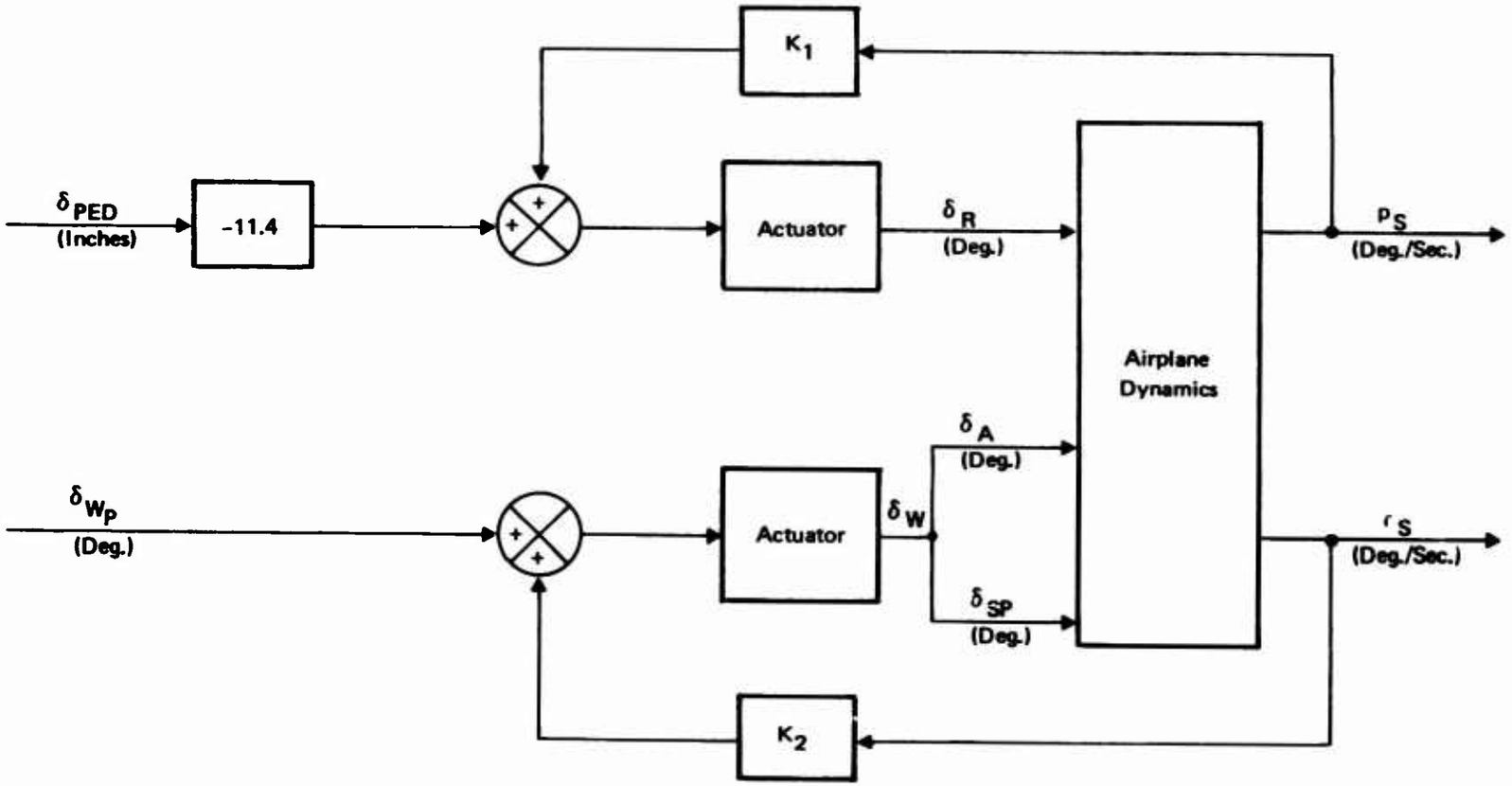

Note:

$K_1 = 0$, $K_2 = 0$ for MRO821

$K_1 = -1.4$, $K_2 = -.75$ for SR11

Figure 39: Block Diagram for Control Systems MRO821 and SR11

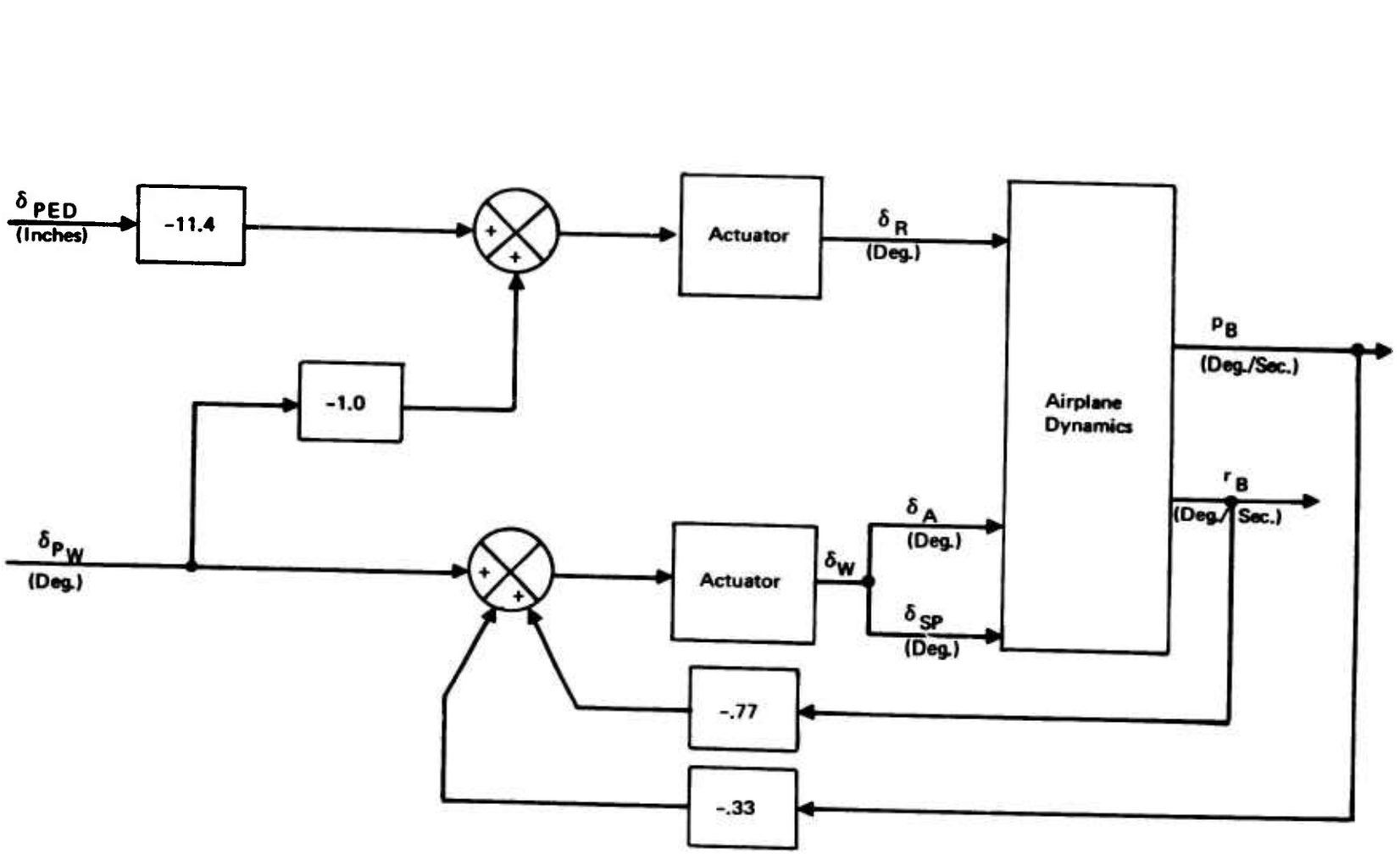

Figure 40 : Block Diagram for Control System SRO721

System Number	Characteristics
SR10 (Figure 41)	Provides Level 1 spiral stability by the feedback of yaw rate to δ_w. Turn coordination is improved by the feedback of a computed sideslip rate ($\hat{\beta}_{SAS}$) to rudder and a crossfeed of δ_w to rudder. The resultant turn coordination parameters meet Level 1 criteria. The required $r \rightarrow \delta_w$ and $\hat{\beta}_{SAS} \rightarrow \delta_R$ gains are obtained from root locus studies. The crossfeed gain is obtained as a low frequency approximation to the required crossfeed transfer function.
SR20 (Figure 42)	This control law is conceptually the same as SR10. The SR20 gains are different than the SR10 gains because the control derivatives were updated from Aero data set #1 to data set #2 (See Appendix II). The Level 1 criterion for the $\left\|\frac{\Delta\beta}{\phi_1}\right\| x \left\|\frac{\phi}{\beta}\right\|_d$ ratio is exceeded slightly.
SR21 (Figure 43)	Provides spiral stability by the feedback of yaw rate to δ_w. Turn coordination is improved by the feedback of a filtered approximation to sideslip rate to rudder and by a crossfeed from control wheel to rudder. The feedback of roll rate to δ_w increases the roll rate response to wheel inputs.
CR20, FR20 (Figure 44)	The significant difference between SR21 and these two control laws is the use of a closer approximation to the required δ_w to rudder crossfeed transfer function. CR20 is mechanized as a control augmentation system and FR20 is mechanized as a fly-by-wire system. (See Paragraph 3.2.1 for a detailed development of this control law and Paragraph 4.3.2 for mechanization details.)
AR20 (Figure 44)	This is the CR20 system with a heading hold loop activated in the absence of pilot inputs and a roll attitude hold loop which maintains roll altitude in a banked turn.
DR141 (Figure 45)	A decoupled system providing roll rate proportional to wheel deflection without sideslip, and sideslip proportional to rudder pedal deflection without roll. The system is neutrally stable with dutch roll frequency and damping at 1 rad/sec and 0.4 respectively, and a roll time constant of 1 second. Development of the decoupled systems is discussed in Paragraph 3.2.3.
DR142, CR21, FR21 (Figures 46 and 47)	Similar to system DR141 except that the roll time constant is reduced to 0.5 seconds. CR21, FR21 are alternative mechanization of the basic DR142 system.

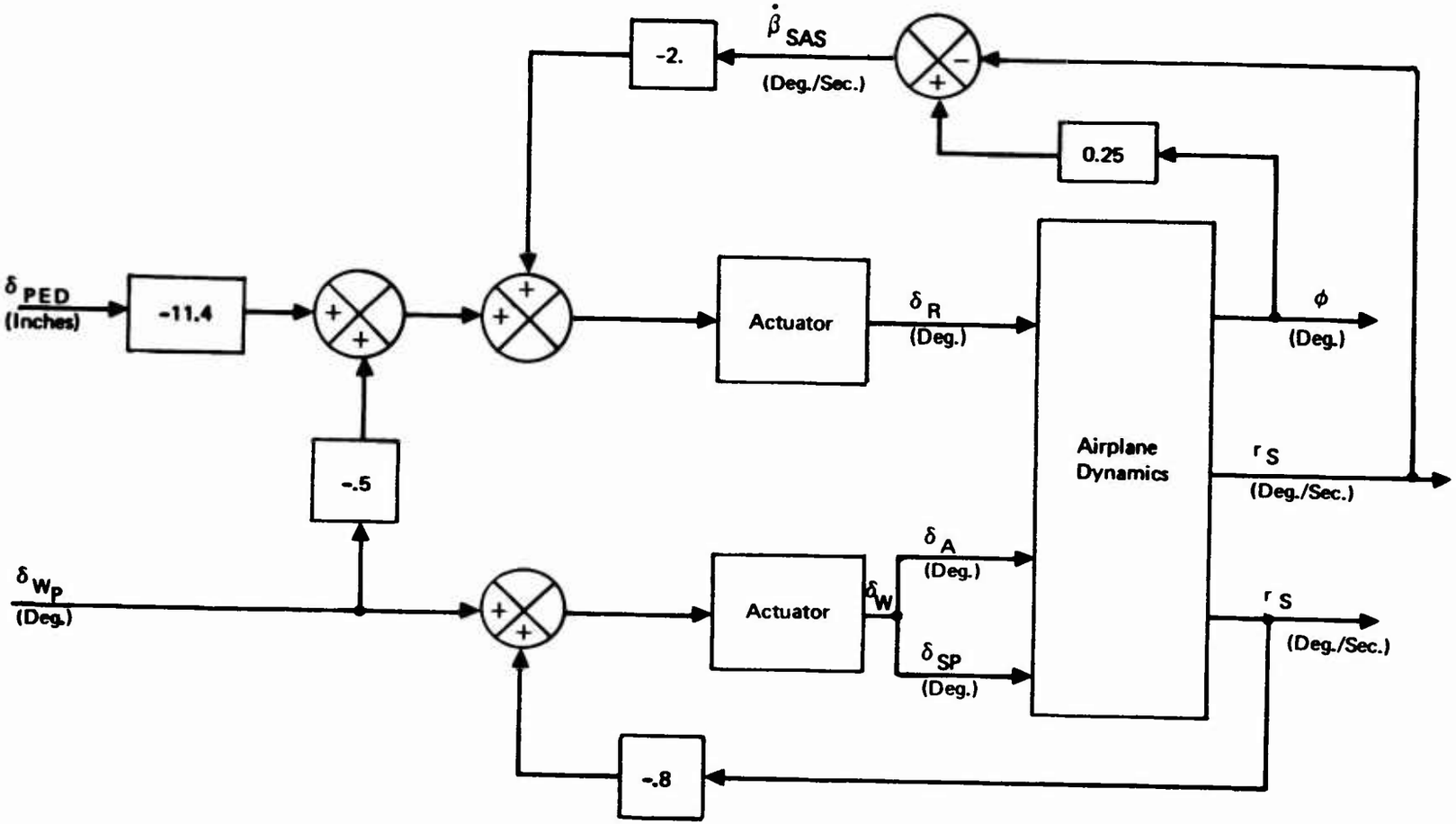

Figure 41 : Block Diagram for Control System SR10

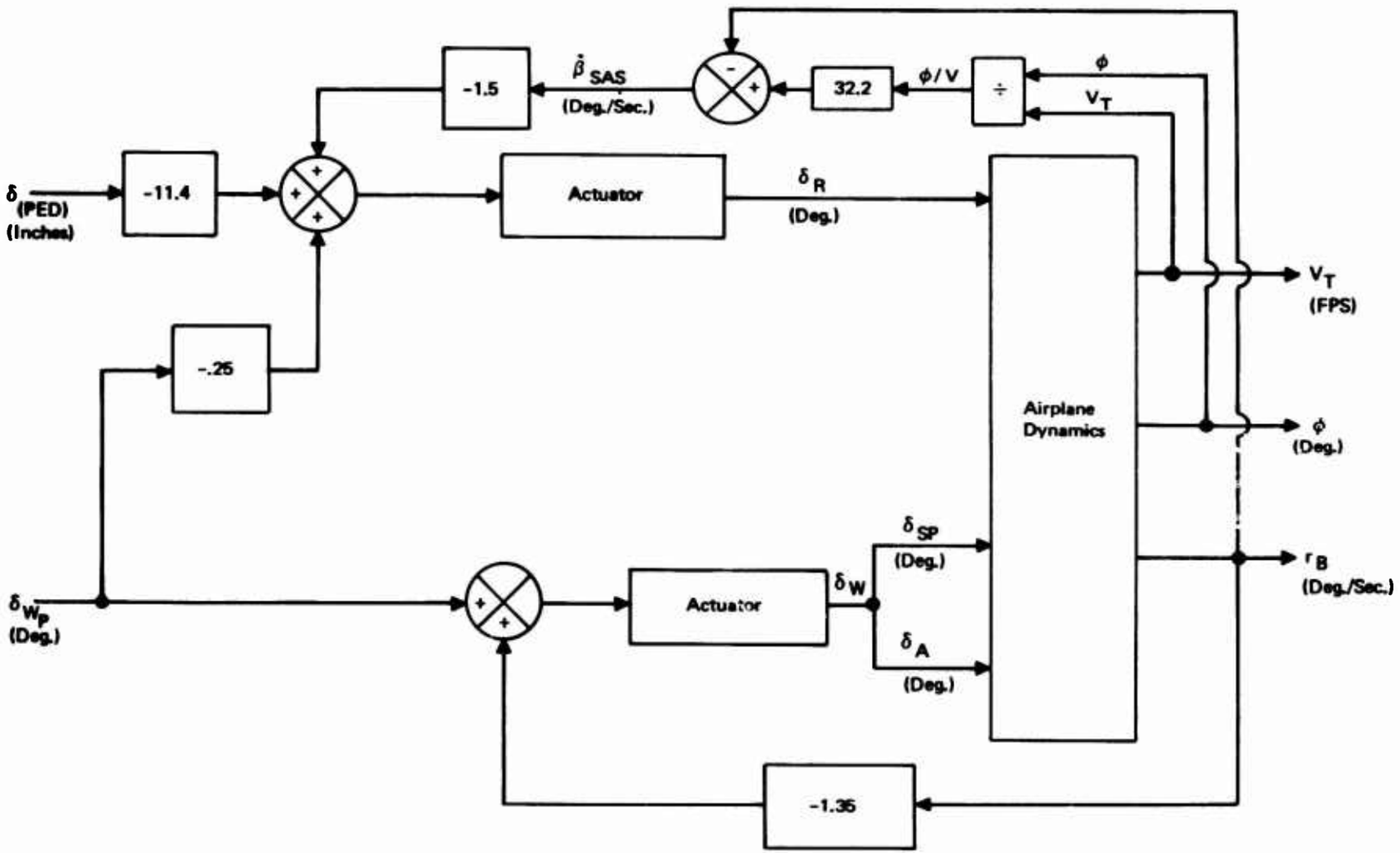

Figure 42 : Block Diagram for Control System SH20

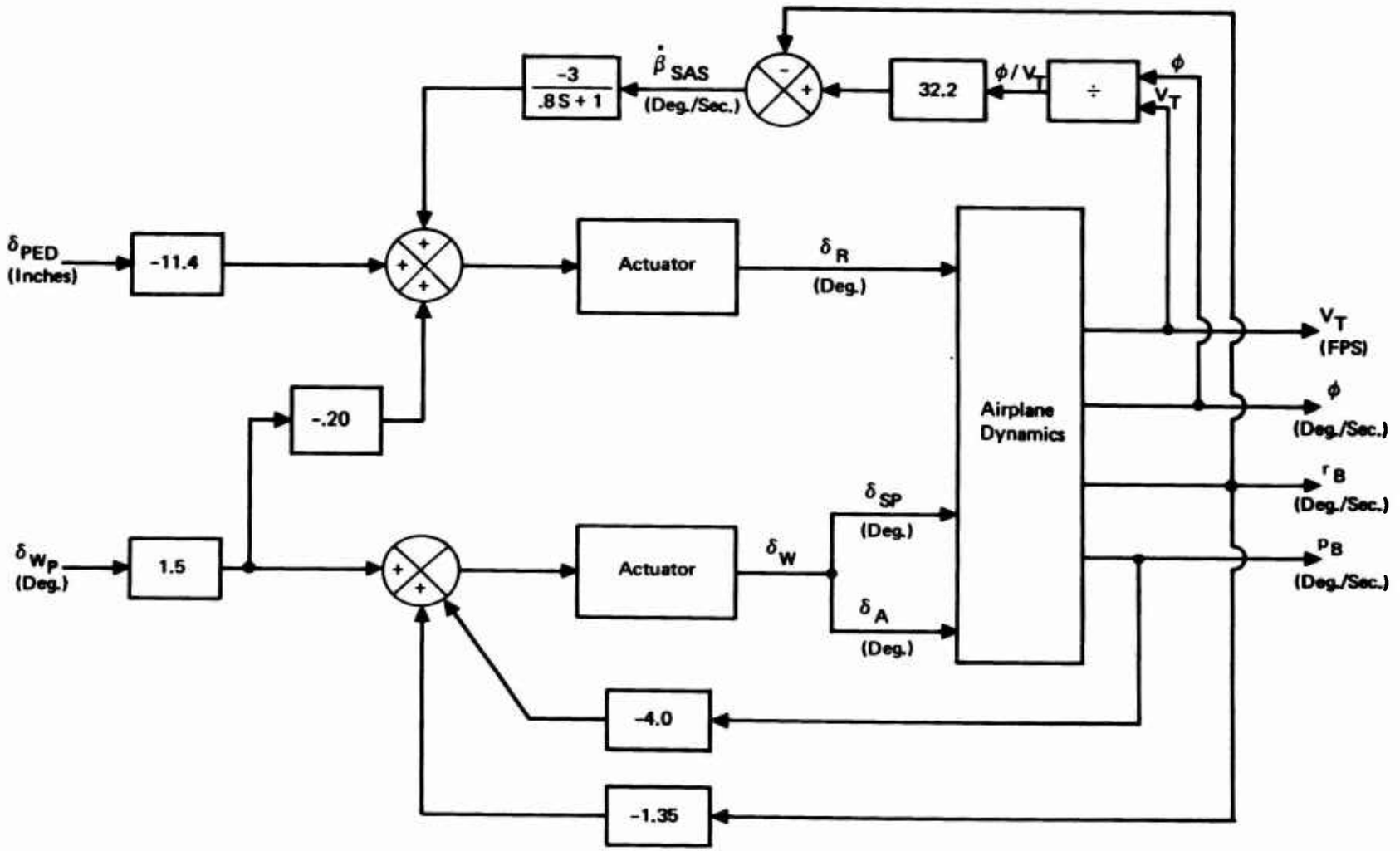

Figure 43 : Block Diagram for Control System SR21

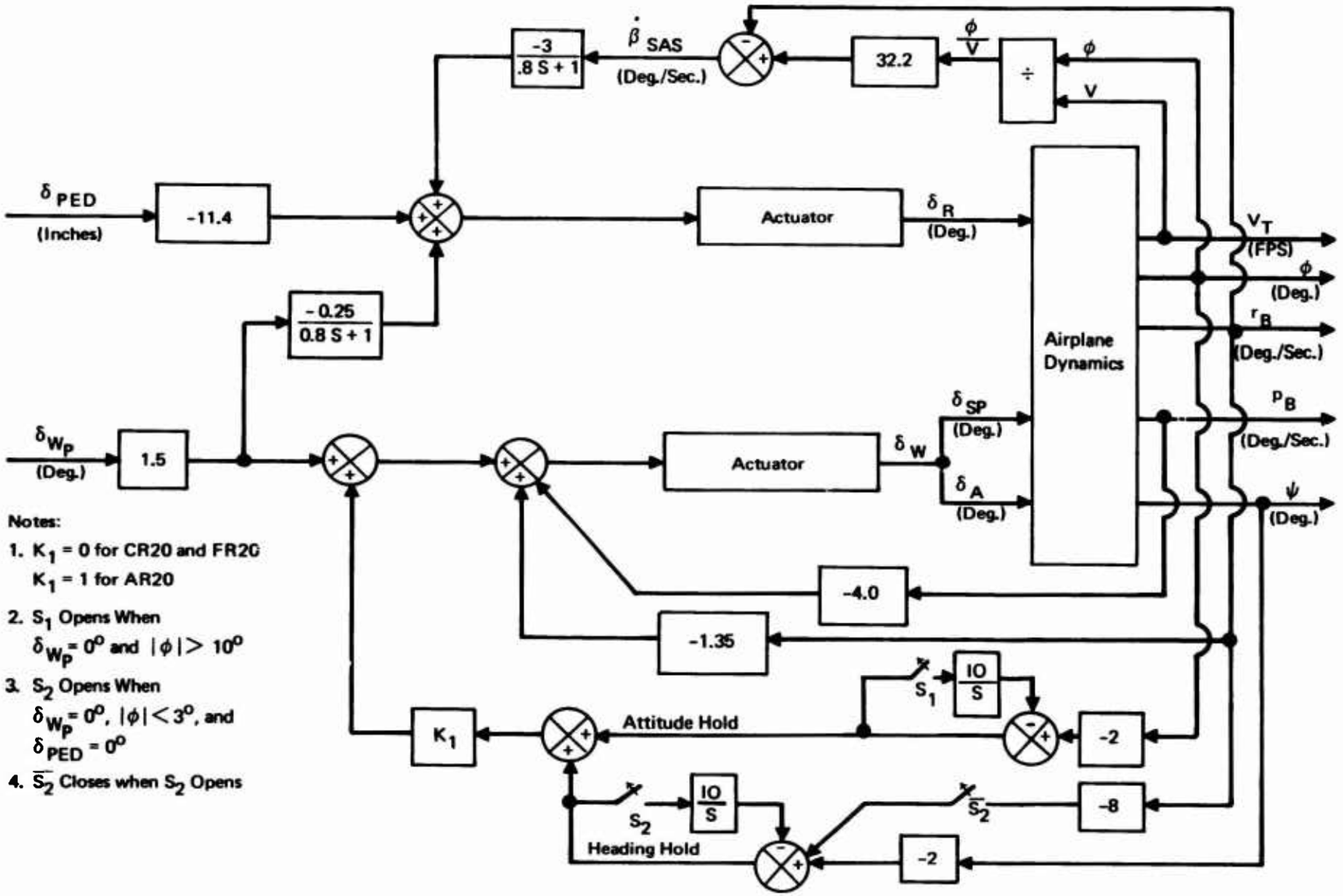

Figure 44 : Block Diagram for Control Systems CR20, FR20, and AR20

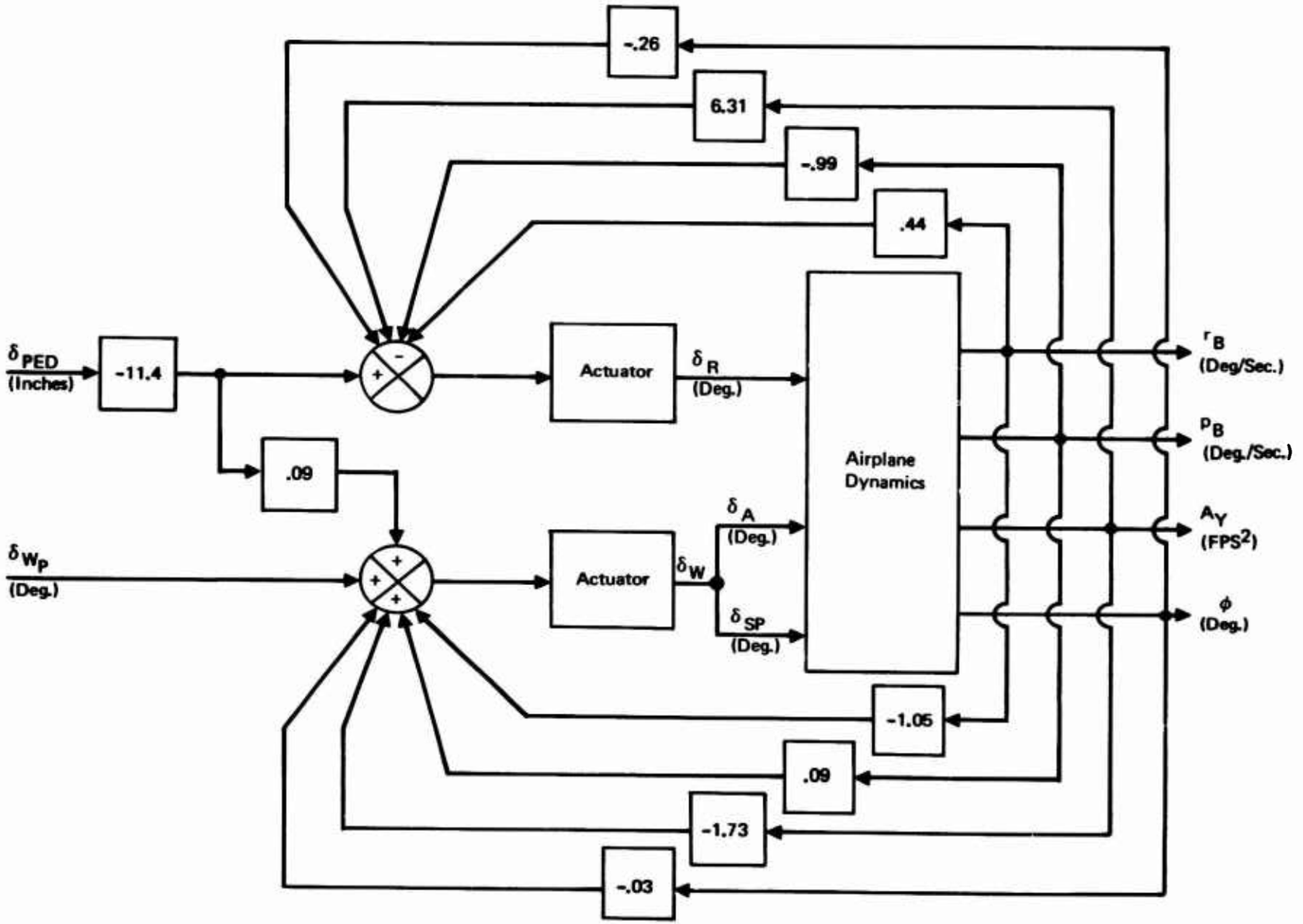

Figure 45 : Block Diagram for Control System DR 141

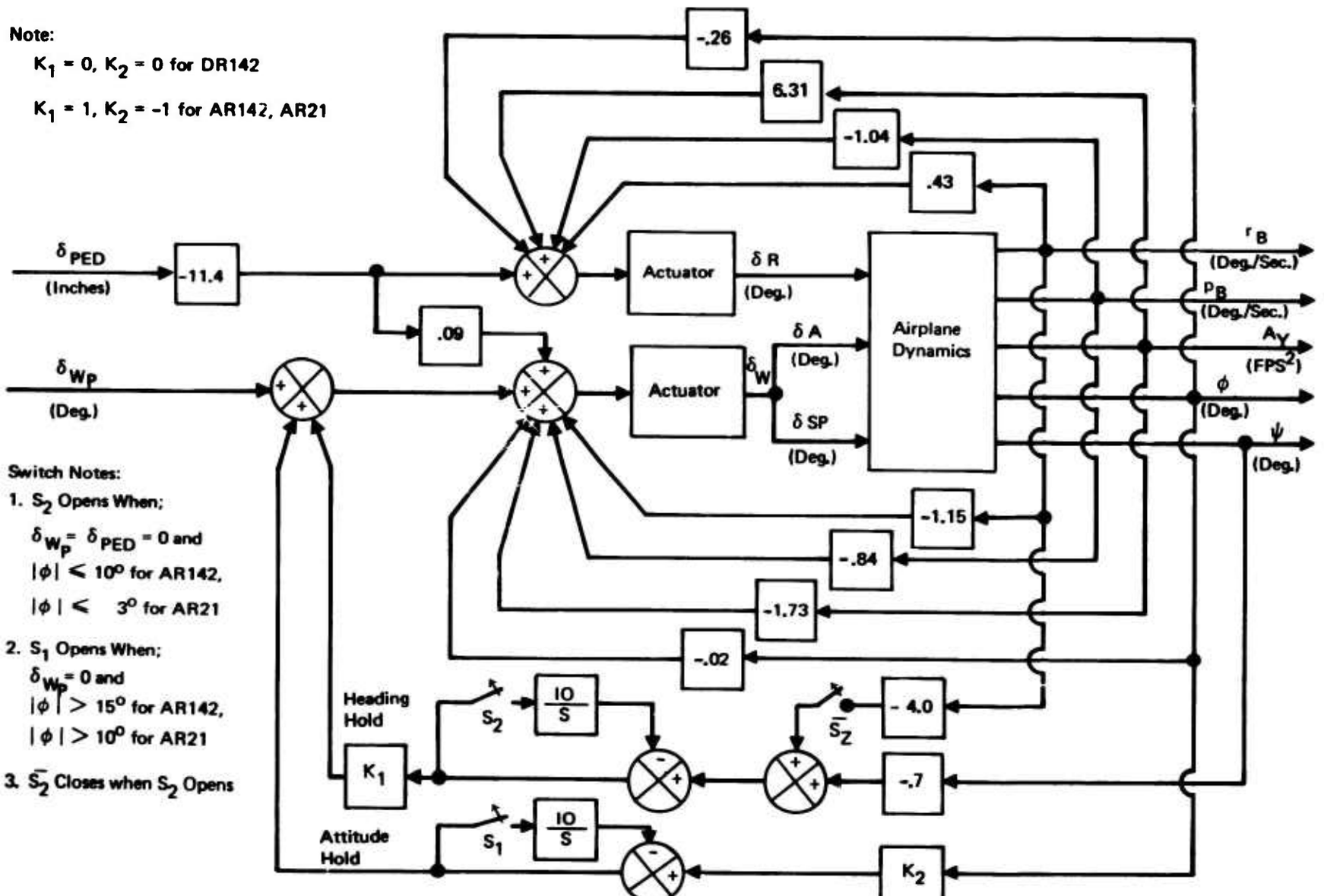

Figure 46 : Block Diagram for Control Systems DR142, AR142, and AR21

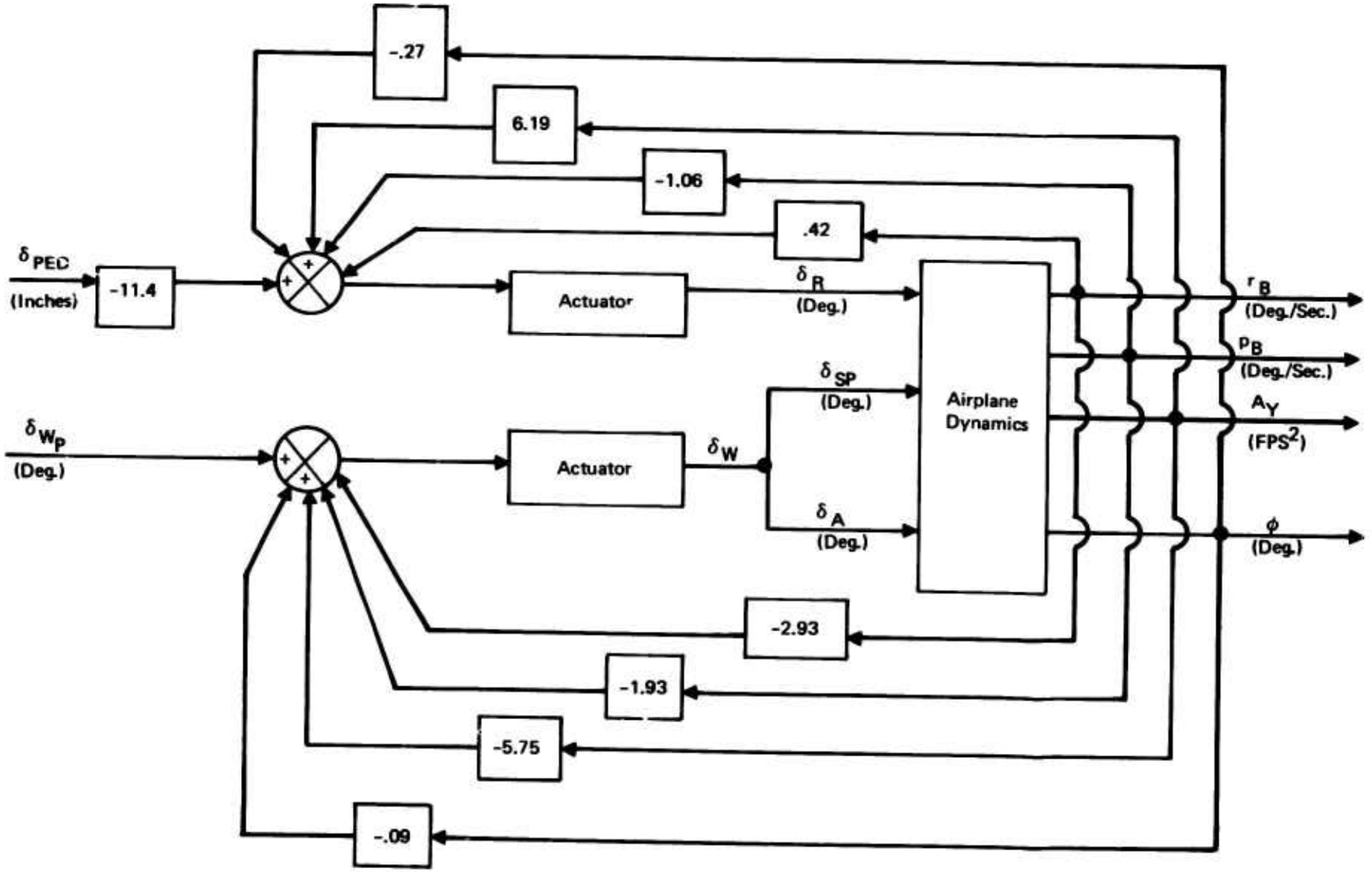

Figure 47 : Block Diagram for Control Systems CR21 and FR21

System Number	Characteristics
AR142, AR21 (Figure 46)	System DR142 with a heading hold loop activated in the absence of pilot inputs and a roll attitude hold loop which maintains roll attitude in a banked turn. The systems differ only in the logic used to activate the hold circuits. (i.e., heading hold is disconnected when bank angle exceeds 10° for AR142 and 3° for AR21; roll attitude hold is not activated until the bank angle is greater than 15° for AR142, and 10° for AR21.) Dynamic response characteristics are not included in Table VIII since they are identical to DR142 for pilot inputs.

4.2.2 High Speed Characteristics

Although the emphasis of this study was on handling qualities in the landing approach condition, stability was also checked at higher speeds to determine the requirements for stability augmentation throughout the flight profile. Flight conditions evaluated are shown on the mission profile of Figure 48. These were: 20,000 feet altitude at M = .78 (maximum q): 40,000 feet at M = .64 (low q at maximum altitude); and sea level, V = 469 knots (V = 1.2 V_S, flaps up). Since these flight conditions were at the extremes of the flight profile, it is probable that if handling quality requirements are satisfied at these conditions, the requirements will be satisfied throughout the profile.

4.2.2.1 Longitudinal Stability

Figures 49 and 50 compare the short period and phugoid characteristics of the unaugmented airplane with the Level 1 handling quality requirements of Military Specification F-8785B. As shown, Level 1 requirements are met at each flight condition. Thus the stability augmentation system developed for landing approach is not required for flaps-up flight.

4.2.2.2 Lateral/Directional Stability

Stability augmentation requirements at the extremes of the flight profile were determined by comparing the system characteristic roots with the "Level 1" handling quality requirements defined in Military Specification MIL-F-8785B. These requirements and the system roots are plotted in Figure 51. As shown, all requirements are met by the unaugmented airplane at each flight condition, with the exception of low dutch roll damping at Flight Condition 3a. (H = 40,000 feet, M = .64). By including a yaw damper consisting of yaw rate (r) fed back to the rudder (δ_R) through a washout circuit,

$$\frac{\delta_R}{r} = \frac{0.2\,s}{s + 0.2} \quad \left(\frac{deg.}{deg./sec.}\right) \tag{60}$$

the Level 1 requirements are satisfied at all conditions. Loss of the yaw damper would then degrade handling qualities to Level II only at the high altitude, low dynamic pressure, flight conditions.

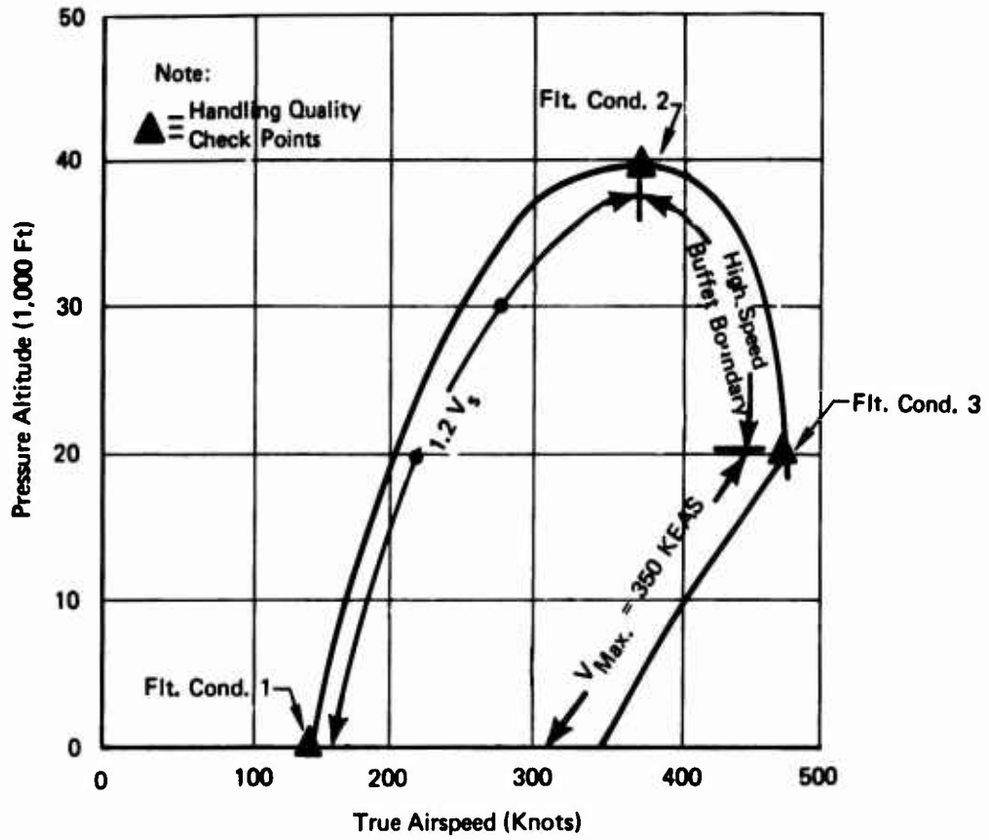

Flt Cond.	Altitude	V_{TAS}/Mach No. (Knots/Dimensionless)	Purpose
1	Sea Level	169/.26	V = 1.2 V_s, Flaps Up
2	40,000'	370/.64	Low q at Max. Alt.
3	20,000'	478/.78	Maximum q

Figure 48 : Speed – Altitude Envelope

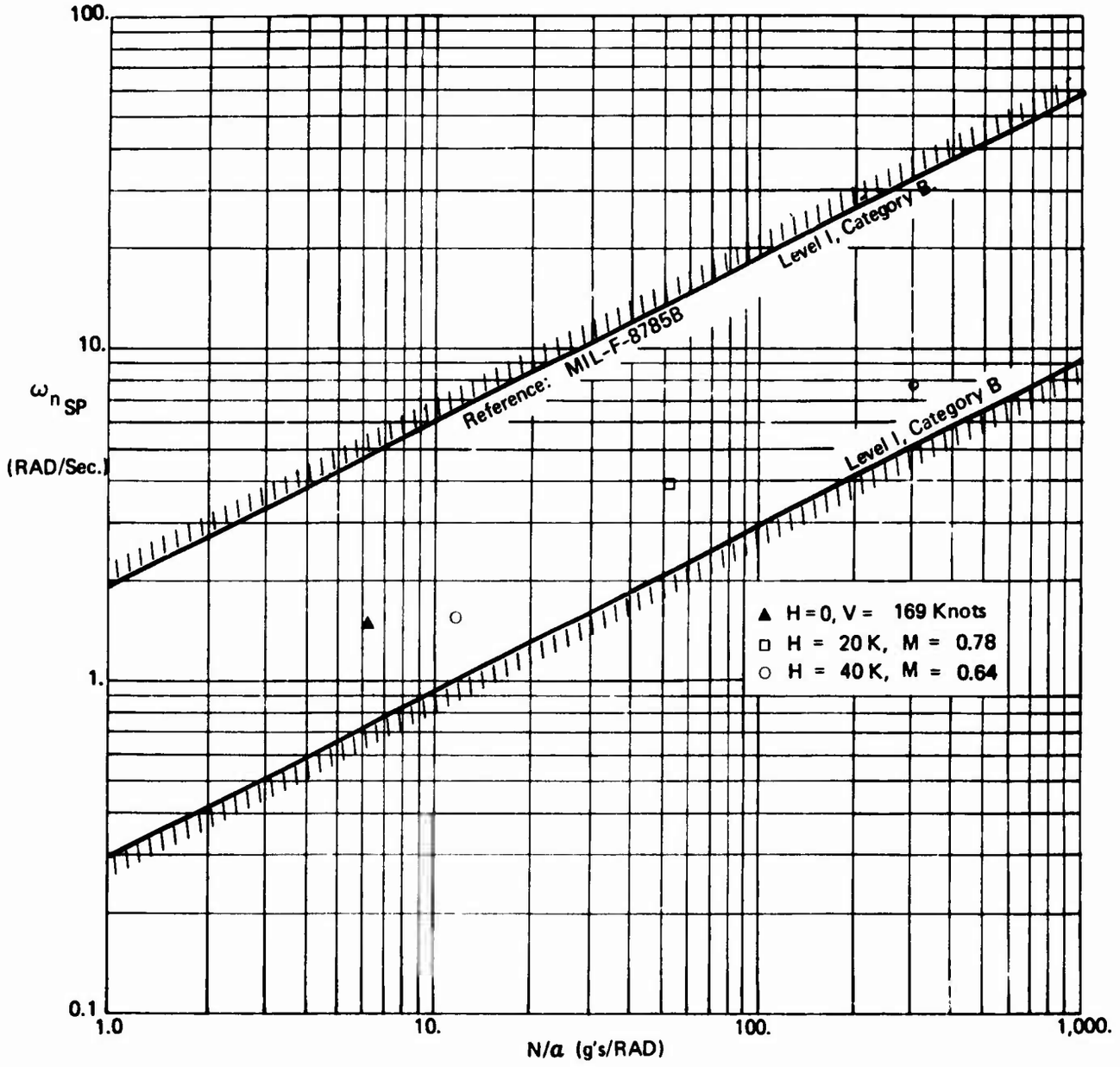

Figure 49 : Short Period Dynamics at Flight Profile Extremes

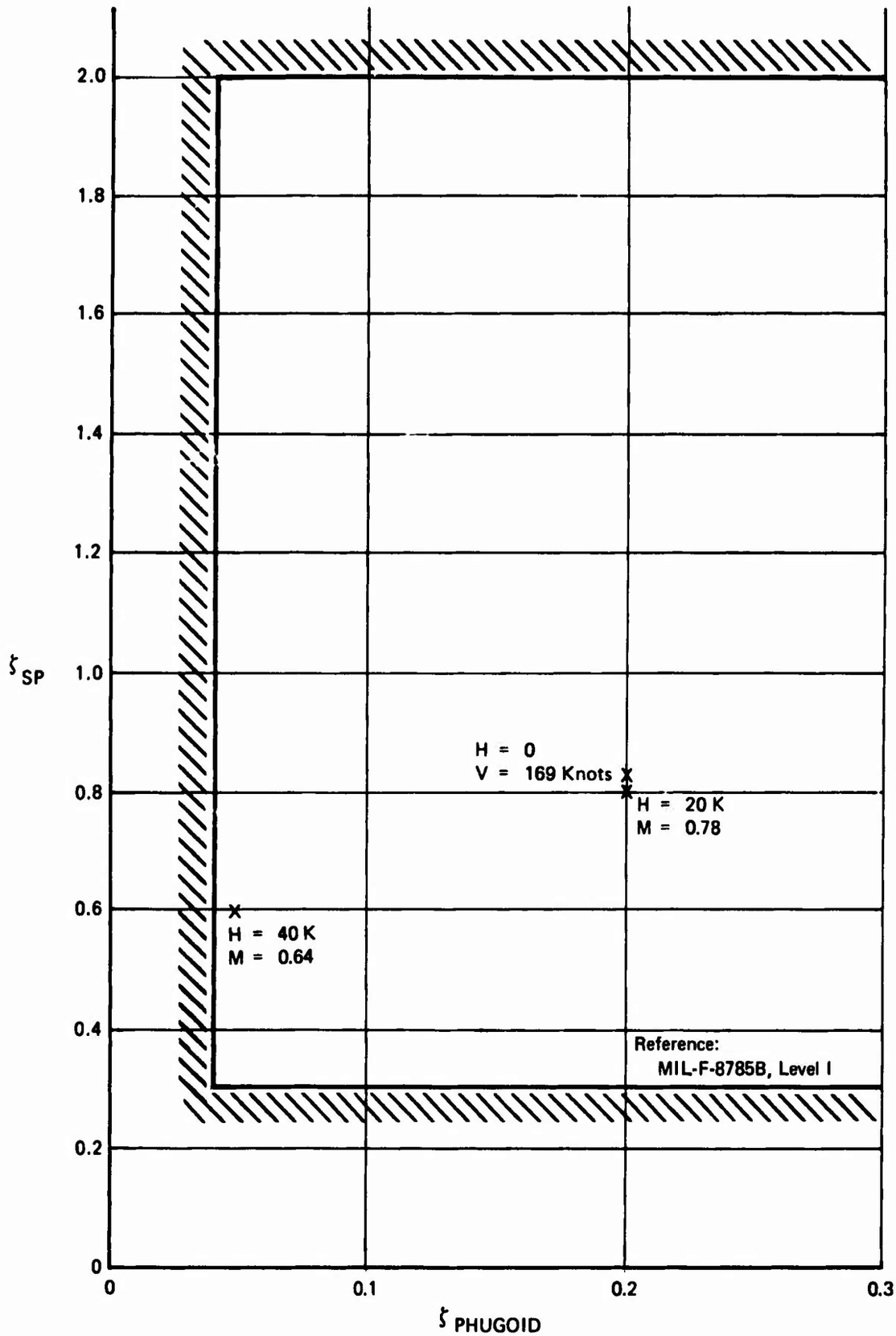

Figure 50 : Short Period and Phugoid Damping Ratios at Flight Profile Extremes

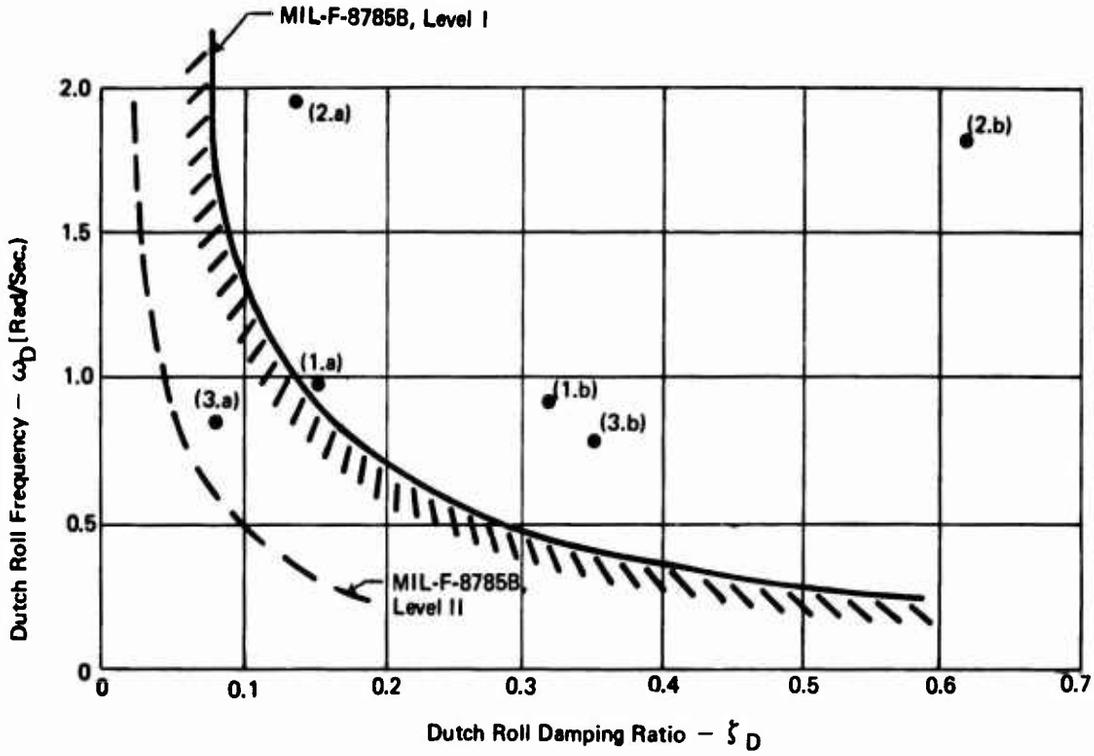

Note:

1.a	H = 0, V = 169 Knots, Yaw Damper Off	3.a	H = 40,000 Ft, M = 0.64, Yaw Damper Off
1.b	H = 0, V = 169 Knots, Yaw Damper On	3.b	H = 40,000 Ft, M = 0.64, Yaw Damper On
2.a	H = 20,000 Ft, M = 0.78, Yaw Damper Off		
2.b	H = 20,000 Ft, M = 0.78, Yaw Damper On		

Yaw Damper; $\frac{\delta_R}{r} = \frac{0.2S}{S + 0.2}$ $\frac{\text{Deg's}}{\text{Deg/Sec.}}$

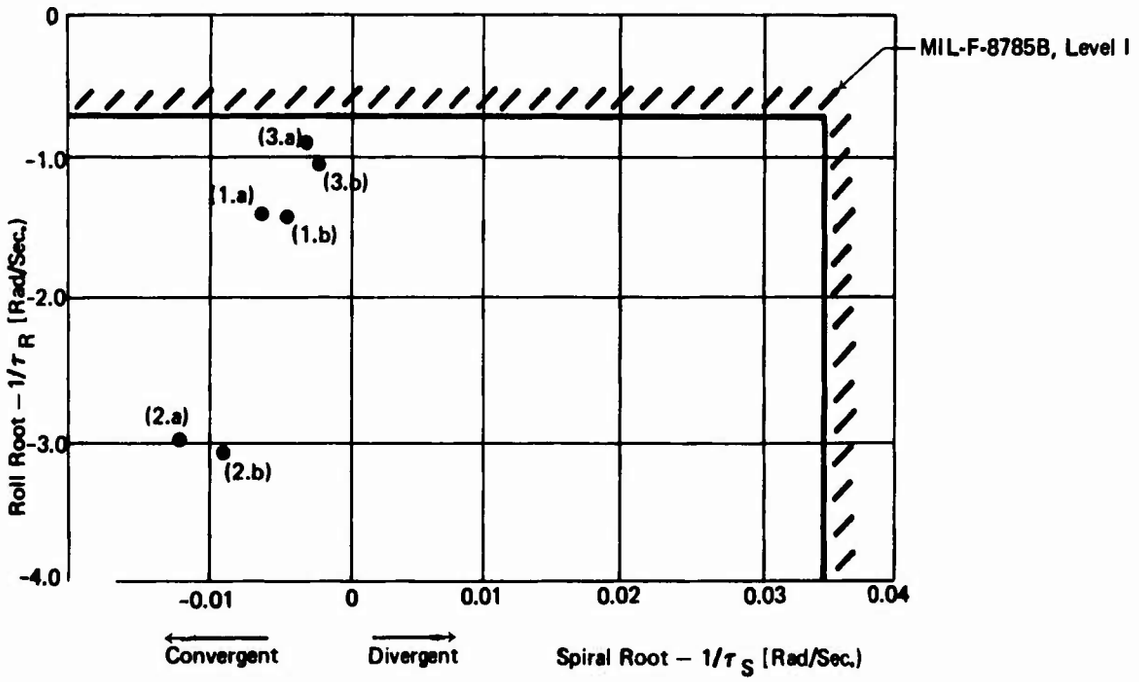

Figure 51 : Lateral/Directional Stability at Flight Profile Extremes

4.2.3 Augmentation Requirements During Transition to Landing Approach

4.2.3.1 Longitudinal Axis

As airspeed is reduced from the "clean" cruise condition, the STOL configuration can be reached by first lowering flaps and deploying spoilers and then finally rotating the thrust vector while increasing thrust. The proposed longitudinal CAS for landing (System CP21) uses pitch rate feedback to the elevator/spoilers and attitude/airspeed feedbacks to the thrust vector angle. Thus if a longitudinal augmentation is required prior to rotating the thrust vector, the simplest system would be to use pitch rate feedback only and add the thrust vector commands after thrust rotation.

Figures 52 and 53 show the short period and phugoid characteristics, augmentation on and augmentation off as airspeed is reduced. The augmentation consists of pitch rate feedback to the elevator and spoilers ($K_{\delta_{e/\dot{\theta}}}$ = 0.6 deg/deg/sec, $K_{\delta_{SP/\dot{\theta}}}$ = 0.37 deg/deg/sec) and is assumed to be switched on when flap deployment is initiated at V = 169 knots. Flaps are fully deployed at V = 93 knots at which point the thrust vector is rotated to reach the landing approach condition. It can be seen from Figures 52 and 53 that MIL-8785B and MIL-83300 Level 1 requirements are met augmentation on and augmentation off as airspeed is reduced from 265 knots to 93 knots.

4.2.3.2 Lateral/Directional Stability

As shown in Section 5.2, lateral/directional control systems FR20 and FR21 were selected as the best lateral/directional systems evaluated. Transition from low speed, flaps up flight to the landing/approach condition was therefore studied for both control laws. A feasible procedure for transition to landing is shown in Figure 54, which compares the characteristic roots with MIL-F-8785B and MIL-F-83300 Level 1 requirements. Both landing augmentation systems are assumed to be switched on when flap deployment is initiated at V = 1.2 V_{STALL} (169 knots). Before the landing augmentation system is switched on, the yaw damper must be in operation. Alternatively, Level 1 requirements are also met at this flight condition without the yaw damper as shown in Figure 51. Flight conditions 2b and 3b of Figure 54 show lateral/directional stability at V = 1.2 V_{STALL} = 93 knots with flaps fully extended, but with the thrust vector along the x-axis (σ = 0 degrees). The normal landing approach configuration with V = 75 knots and σ = 70 degrees is shown as flight conditions 2c and 3c. The data of Figure 54 assumes that the feedback gains of the lateral/directional systems are inversely proportional to the dynamic pressure. For example, when the landing augmentation system is switched on at V = 169 knots, the feedback gains are $\frac{q\ (75\ knots)}{q\ (169\ knots)} \simeq 0.2$ of their value at 75 knots. As shown in Figure 54, Level 1 requirements are met by both augmentation systems throughout the transition.

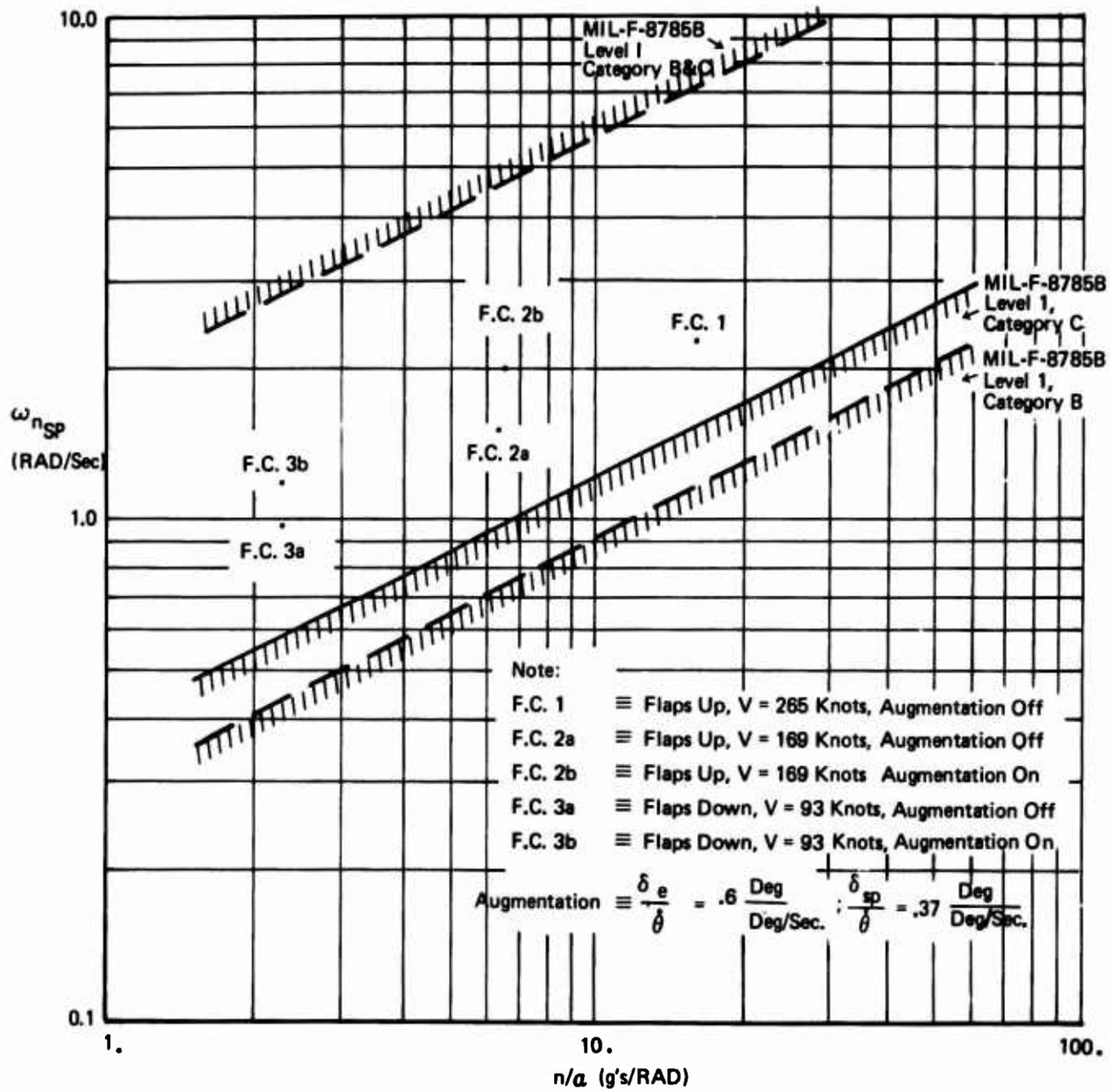

Figure 52 : Short Period Dynamics During Transition to Landing

Note:

F.C. 1 ≡ Flaps Up, V = 265 Knots, Augmentation Off

F.C. 2a ≡ Flaps Up, V = 169 Knots, Augmentation Off

F.C. 2b ≡ Flaps Up, V = 169 Knots, Augmentation On

F.C. 3a ≡ Flaps Down, V = 93 Knots, Augmentation Off

F.C. 3b ≡ Flaps Down, V = 93 Knots, Augmentation On

$$\text{Augmentation} \equiv \frac{\delta_e}{\dot{\theta}} = .6 \frac{\text{Deg}}{\text{Deg/Sec}} ; \frac{\delta_{sp}}{\dot{\theta}} = .37 \frac{\text{Deg}}{\text{Deg/Sec.}}$$

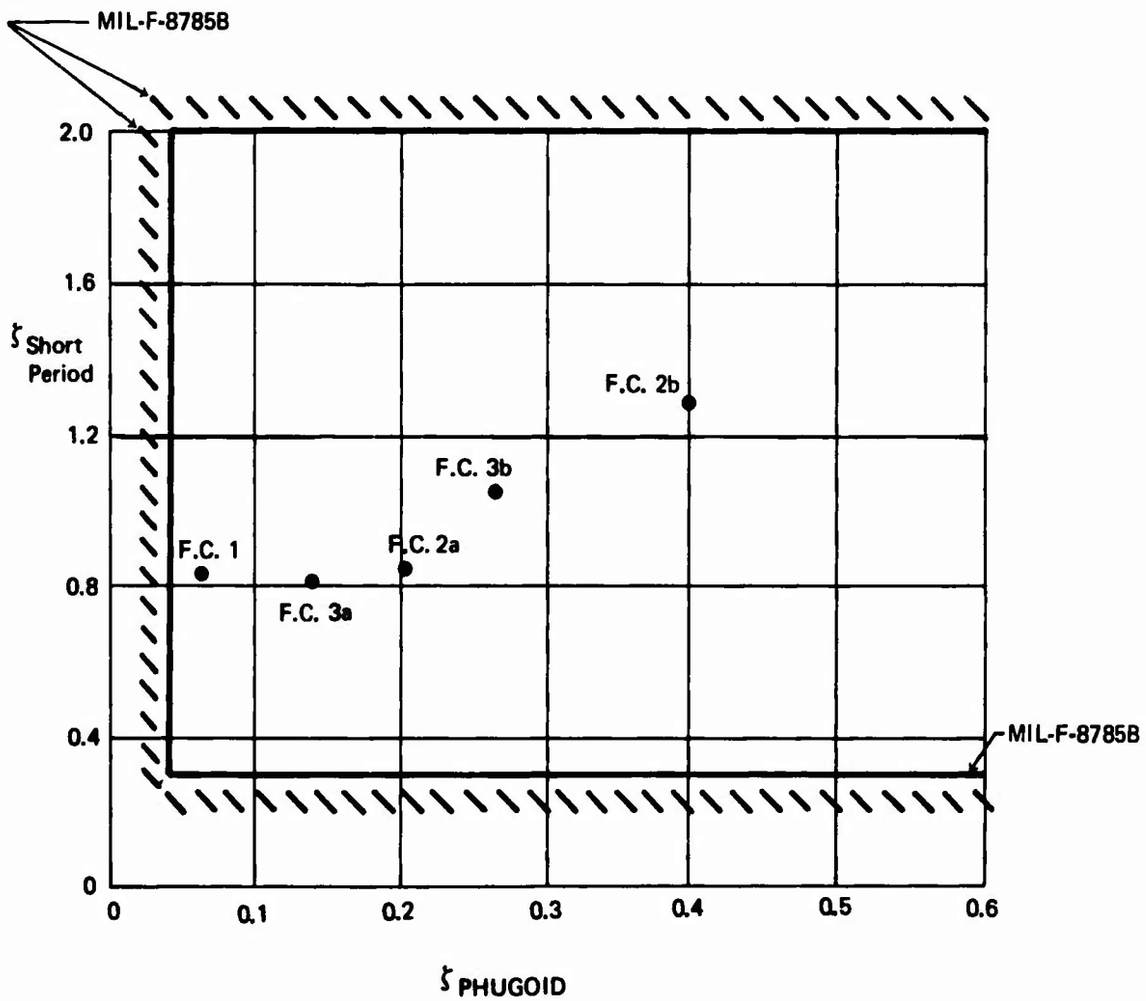

Figure 53 : Short Period and Phugoid Damping Ratios During Transition to Landing

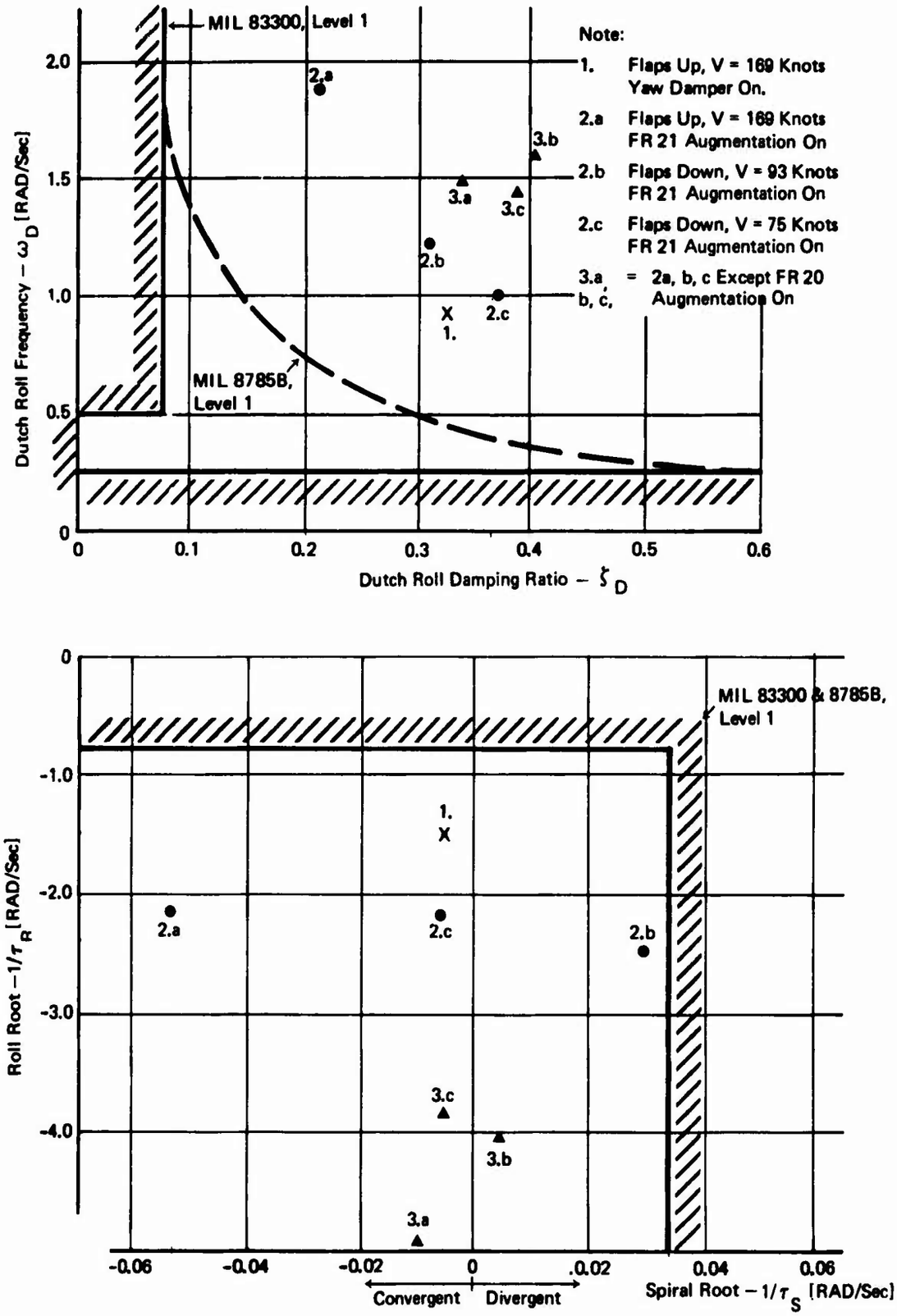

Figure 54 : Lateral/Directional Dynamics During Transition to Landing

4.2.4 Response to Atmospheric Turbulence

Atmospheric turbulence affected the longitudinal and lateral/directional control laws in different manners. For the former case, the turbulence-induced variations in the pitch attitude display caused the pilots to resort to flight path display data for inner loop closures. The turbulence-induced lateral accelerations proved undesirable for an otherwise superior lateral/directional system.

4.2.4.1 Longitudinal Turbulence

During the piloted simulation studies it was determined that the airplane response to atmospheric turbulence affected the pilot's ability to achieve precise flight path control and resulted in altered piloting techniques. To gain insight into this phenomenon, both axial and vertical gust turbulence were evaluated. For the landing/approach case considered, the gust models used were:

Head Wing Gusts

$$\Phi_{u_g}(\Omega) = \sigma_u^2 \frac{2L_u}{\pi\left[1 + (L_u \cdot \Omega)^2\right]} \tag{61}$$

Vertical Gusts

$$\Phi_{w_g}(\Omega) = \sigma_w^2 \frac{L_w\left[1 + 3(L_w \cdot \Omega)^2\right]}{\pi\left[1 + (L_w \cdot \Omega)^2\right]^2} \tag{62}$$

where

σ_u = R.M.S. level of Clear Air Turbulence at 300 ft. altitude

σ_u = 12 ft/sec

σ_w = 6.7 ft/sec

L_u = 970 ft.

L_w = 300 ft.

Data was obtained for the unaugmented airplane, decoupled (θ, u) and (γ, u) systems defined in Figures 22, 23, 24, and 37 respectively. As indicated in Figure 35, a flight path angle hold loop was added to a basic (γ, u) system. The hold loop is disconnected when the pilot is commanding flight path rate and holds the current flight path when the pilot releases the stick. In addition the (γ, u) system with the lowest DLC gain was evaluated both with and without the u to δ_e DLC feedback decoupling, to check the benefit of this feedback in turbulence.

Table IX summarizes the results of turbulence effects. The data shows that:

1. The (γ, u) systems reduce flight path gust sensitivity at the expense of pitch attitude excursions, and vice versa for the (θ,u) systems.

2. Deleting the $u \rightarrow \delta_e$, δ_{SP} feedback gains in a (γ, u) system produces a large percentage increase in flight path sensitivity to gusts.

3. A flight path hold outer loop, at the gain levels considered, does not significantly reduce system response to turbulence.

4.2.4.2 Lateral Turbulence

System gust sensitivities were obtained by computing the response to the Dryden continuous random gust model defined in MIL-F-8785B. For the landing approach case considered, a crosswind gust model with the following characteristics was assumed:

$$\Phi_{V_g}(\Omega) = \sigma_V^2 \frac{L_V}{\pi} \frac{1+3(L_V \cdot \Omega)^2}{[1+(L_V \cdot \Omega)^2]^2} \qquad (63)$$

where:

σ_V = R.M.S. level of Clear Air Turbulence at 300 ft. altitude

σ_V = 12 ft/sec

L_V = 970 ft.

The fixed base simulation studies of control law DR142 indicated that the excellent turn coordination and precise control capabilities of this system made it superior to the other candidates. However, after evaluating the mechanized version of DR142 (CR21) on the NASA Ames Moving Base Simulator, it was discovered that CR21 was noticeably more sensitive to turbulence than was the alternative CR20 system. An additional decoupled system (DR172) was therefore developed which was similar to DR142 but with the dutch roll damping ratio increased from ζ_D= 0.4 to ζ_D= 0.7. Transient responses and block diagrams of the decoupled systems are shown in Figures 26, 55, and 56. A comparison of the turbulence response of the decoupled systems plus system CR20 is given in the following paragraph.

Since adverse pilot comments regarding system DR142 were concerned with turbulence sensitivity, the r.m.s. lateral acceleration at the pilot station ($A_{yP.S.}$) was computed for clear air turbulence levels of random gusts. A plot of the power spectral density of $A_{yP.S.}$ showed that a large percentage of the gust energy was concentrated around the dutch roll frequency of 1 rad/sec. Therefore the effect of including a notch filter on the feedback of lateral acceleration to both the rudder and roll controls was evaluated. The transfer function of the filter considered was:

TABLE IX LONGITUDINAL SYSTEM RESPONSE TO RANDOM TURBULENCE

SYSTEM NAME	SYSTEM CHARACTERISTICS	RESPONSE TO u_{GUST} = 12 ft/sec RMS			RESPONSE TO w_{GUST} = 6.7 ft/sec RMS		
		$\sigma_{u_{air}}$ [FPS]	σ_γ [DEGS]	σ_θ [DEGS]	$\sigma_{u_{air}}$ [FPS]	σ_γ [DEGS]	σ_θ [DEGS]
MP02	UNAUGMENTED AIRPLANE	14.1	2.5	1.9	3.2	1.8	1.1
SP03	(θ, u) DECOUPLED: $K_{\delta DLC/\delta e} = 0.62$	10.4	2.3	0.4	1.1	1.8	0.5
DP05	(γ, u) DECOUPLED: $K_{\delta DLC/\delta e} = 0.62$, $K_{\delta COL/u} = K_{\delta COL/\dot{u}} = 0$, $K_{\delta COL/\gamma} = 0$	8.9	1.0	1.6	4.1	2.5	3.1
DP05*	(γ, u) DECOUPLED: $K_{\delta DLC/\delta e} = 0.62$, $K_{\delta COL/u} = .04$, $K_{\delta COL/\dot{u}} = .34$, $K_{\delta COL/\gamma} = 0$	8.9	0.5	2.5	4.1	1.0	2.5
AP05*	(γ, u) DECOUPLED: $K_{\delta DLC/\delta e} = 0.62$, $K_{\delta COL/u} = .04$, $K_{\delta COL/\dot{u}} = .34$, $K_{\delta COL/\gamma} = 0.5$	8.9	0.5	2.5	4.0	1.1	2.9
DP07*	(γ, u) DECOUPLED: $K_{\delta DLC/\delta e} = 1.5$, $K_{\delta COL/u} = .04$, $K_{\delta COL/\dot{u}} = .40$, $K_{\delta COL/\gamma} = 0$	7.9	0.4	2.3	3.4	0.7	2.6
AP08*	(γ, u) DECOUPLED: $K_{\delta DLC/\delta e} = 1.5$, $K_{\delta COL/u} = .04$, $K_{\delta COL/\dot{u}} = .40$, $K_{\delta COL/\gamma} = 1.0$	7.9	0.4	2.3	3.4	0.7	2.9

NOTES:

1. The addition of * to a System name implies $u, \dot{u} \rightarrow \delta_e$, DLC Feedback included.
2. The airplane/augmentation System does not include a pilot.
3. AD08* is DOP7* with an additional flight path angle hold loop.

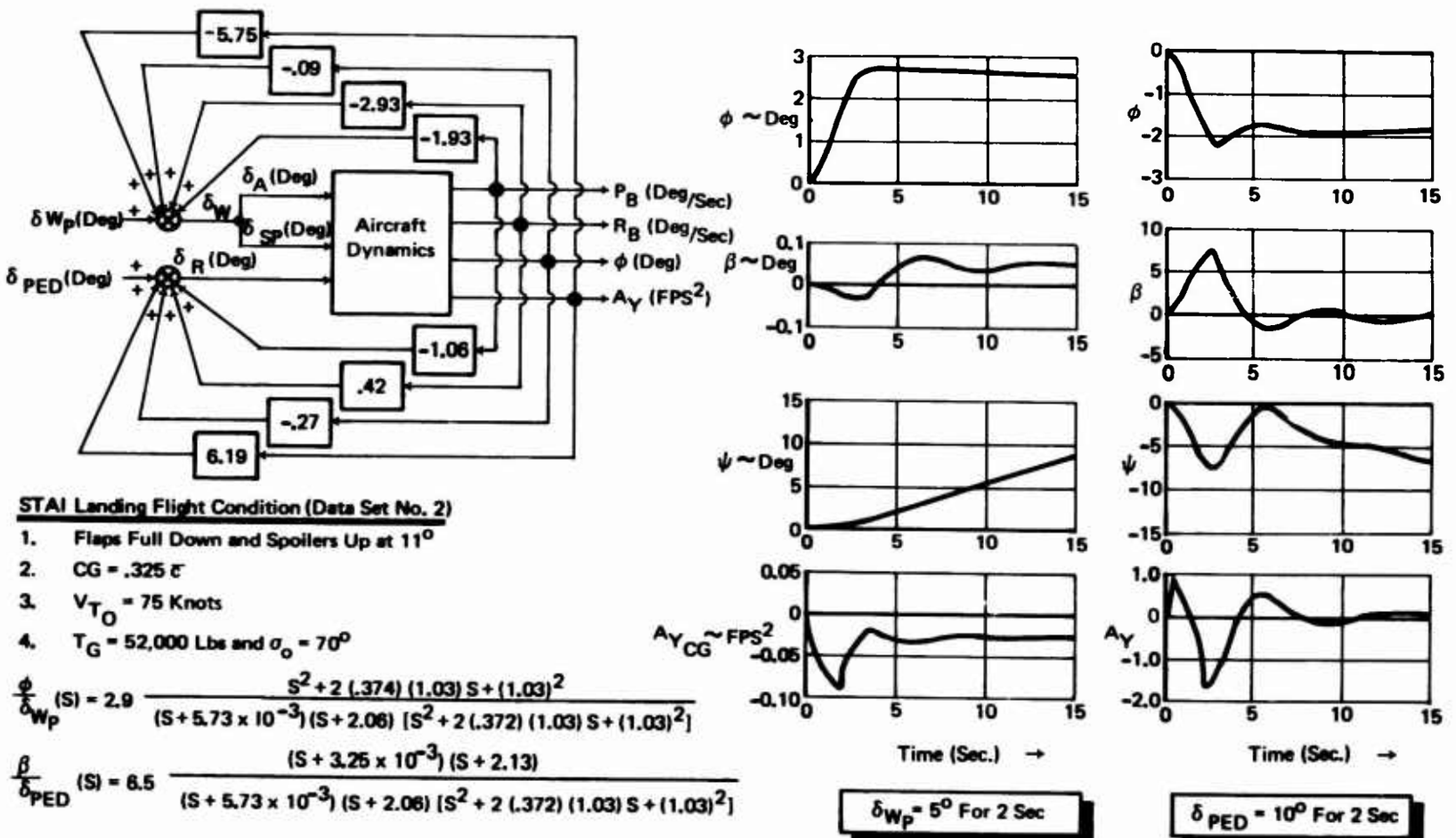

STAI Landing Flight Condition (Data Set No. 2)

1. Flaps Full Down and Spoilers Up at 11°
2. CG = .325 $\bar{c}$
3. V_{T_O} = 75 Knots
4. T_G = 52,000 Lbs and σ_o = 70°

$$\frac{\phi}{\delta_{W_P}}(S) = 2.9\,\frac{S^2 + 2(.374)(1.03)S + (1.03)^2}{(S + 5.73 \times 10^{-3})(S + 2.06)[S^2 + 2(.372)(1.03)S + (1.03)^2]}$$

$$\frac{\beta}{\delta_{PED}}(S) = 6.5\,\frac{(S + 3.25 \times 10^{-3})(S + 2.13)}{(S + 5.73 \times 10^{-3})(S + 2.06)[S^2 + 2(.372)(1.03)S + (1.03)^2]}$$

Figure 55: Block Diagram, Transfer Functions, and Time Histories for DR142

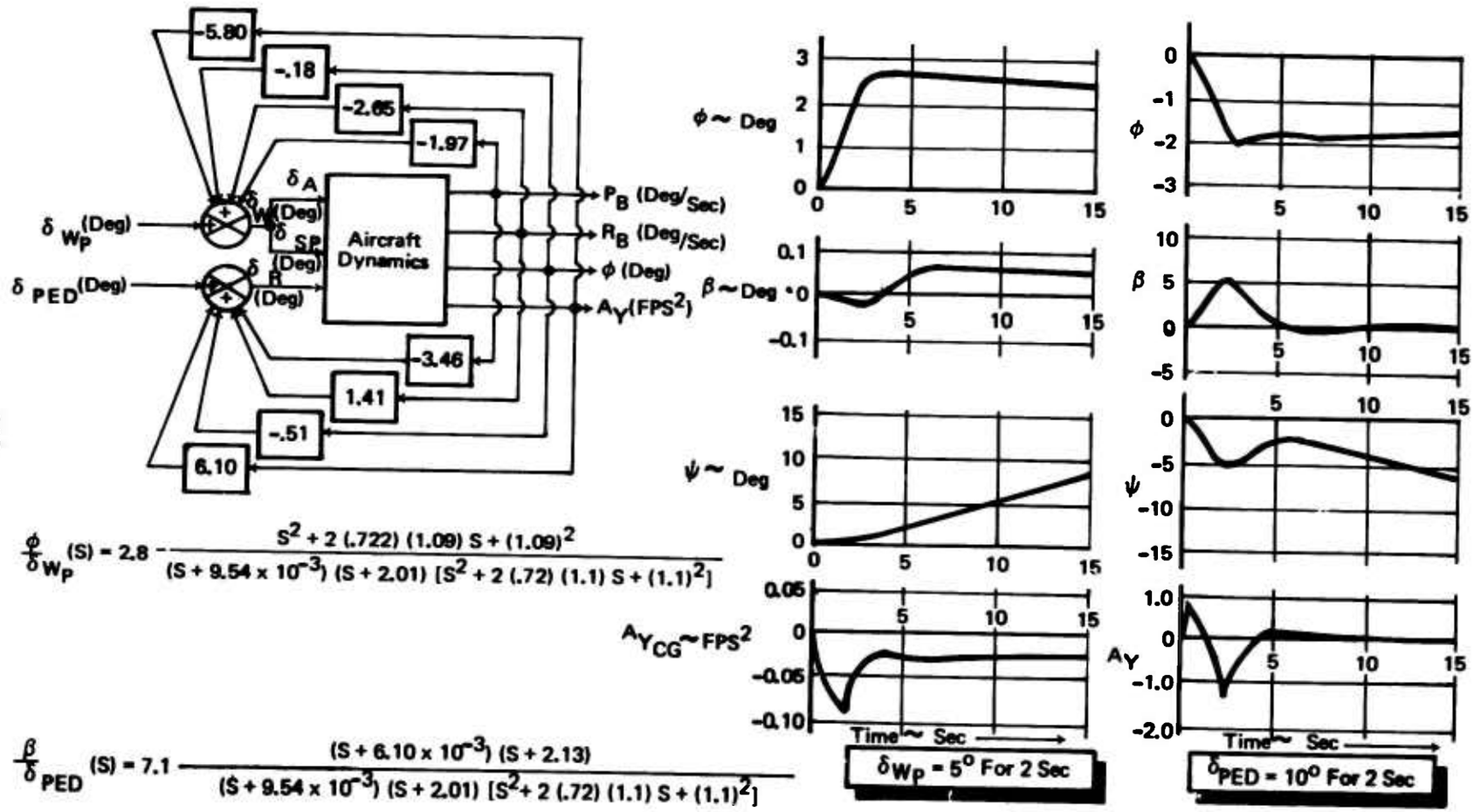

$$\frac{\phi}{\delta_{W_P}}(S) = 2.8 \frac{S^2 + 2(.722)(1.09)S + (1.09)^2}{(S + 9.54 \times 10^{-3})(S + 2.01)[S^2 + 2(.72)(1.1)S + (1.1)^2]}$$

$$\frac{\beta}{\delta_{PED}}(S) = 7.1 \frac{(S + 6.10 \times 10^{-3})(S + 2.13)}{(S + 9.54 \times 10^{-3})(S + 2.01)[S^2 + 2(.72)(1.1)S + (1.1)^2]}$$

Figure 56: Block Diagram, Transfer Functions, and Time Histories for DR172

$$\frac{A_{y_{Filtered}}}{A_y} = \frac{S^2 + 2\ (.1)\ S + 1}{S^2 + 2\ (.7)\ S + 1} \qquad (64)$$

When included in system DR142, this filter provided a significant reduction in acceleration at the pilot station, as shown in Table X, without affecting the response to pilot control inputs. The same filter was also beneficial in System DR172, but to a lesser extent since the resonant peak of gust energy at the dutch roll frequency was lower because of increased dutch roll damping.

4.3 Control Mechanization

4.3.1 General Considerations

Control laws are linearized conceptual definitions of the control and feedback signals required to provide adequate flight path control at low speed. In the mechanization study the effects of control device nonlinearities, redundancy requirements for safe and reliable operation, and sensor characteristics were included.

The following mechanization concepts were investigated:

(1) Mechanical Control System (MCS)

(2) Stability Augmentation System (SAS)

(3) Control Augmentation System (CAS)

(4) Fly-By-Wire with Mechanical Reversion System (FBW + Rev.)

(5) Fly-By-Wire System (FBW)

These mechanization concepts are shown schematically in Figure 57.

Automated flight path control systems can be integrated with any of the last four mechanizations and were not considered a separate mechanization category. The weight, cost, and complexity of the automatic path feature differs with the specific mechanization and will be identified incrementally.

4.3.2 Synthesis Procedure

The synthesis of control system mechanization deals with the physical properties of the elements for a prospective implementation of a control law. In this, it greatly differs from the control law synthesis which was concerned with the mathematical representation of the system elements.

The control mechanization analysis consisted of the identification of those factors critical to satisfactory performance (e.g. signal path nonlinearities, dynamic characteristics and sensor

TABLE X: LATERAL/DIRECTIONAL SYSTEM RESPONSE TO RANDOM TURBULENCE

SYSTEM	A_y FILTER	RESPONSE TO SIDEGUST, V_{GUST} = 12 FT/SEC, R.M.S.
		RMS $A_{y_{(PILOT\ STATION)}}$ [Ft/Sec^2]
DR142	None	6.3
DR141	None	6.2
DR172	None	4.6
DR142	$\frac{S^2 + 2\,(.1)\,S + 1}{S^2 + 2\,(.7)\,S + 1}$	3.8
DR172	$\frac{S^2 + 2\,(.1)\,S + 1}{S^2 + 2\,(.7)\,S + 1}$	3.4
FR20	None	3.0

NOTE: The airplane/augmentation system does not include a pilot.

A) Mechanical Control System (MCS)

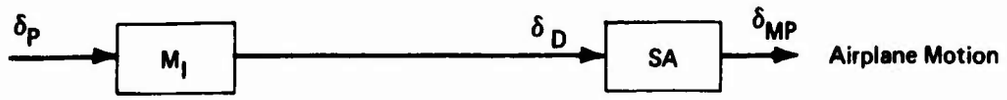

B) Stability Augmentation (SAS)

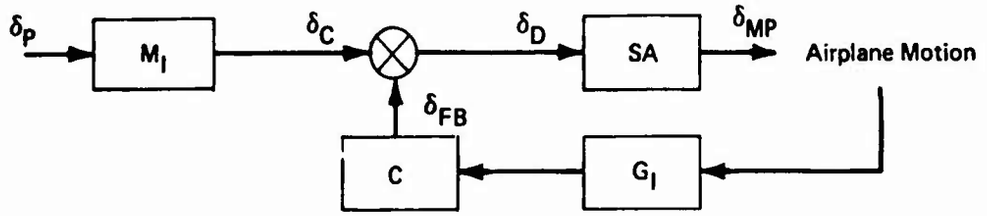

C) Control Augmentation (CAS)

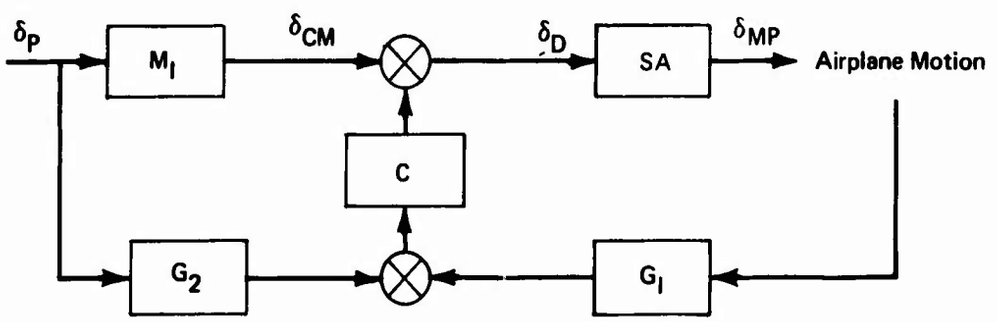

D) Fly-By-Wire (FBW)

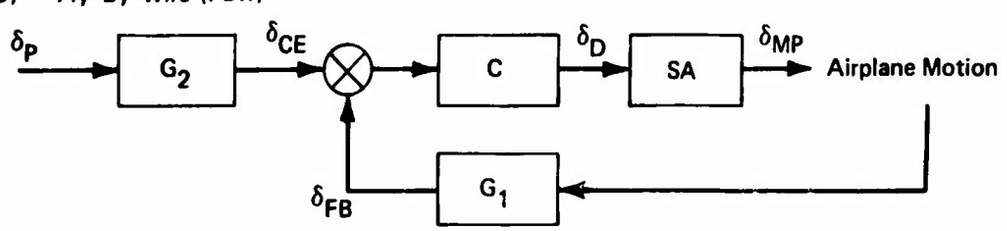

E) Fly-By-Wire With Mechanical Reversion (FBW + Rev.)

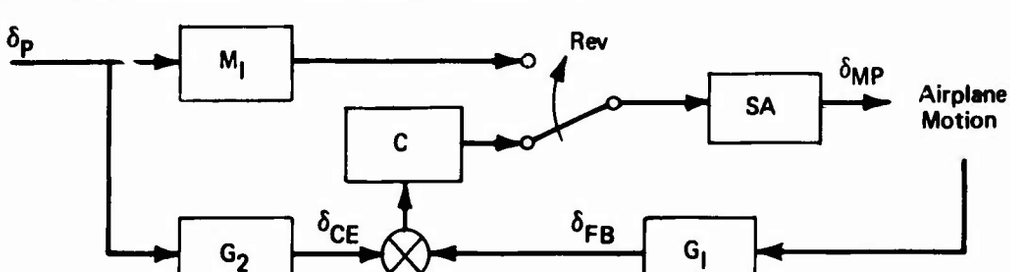

M_I = Mechanical signal path including feel system
G_I = Electrical feedback path
G_2 = Electrical feed forward path

C = Computation plus conversion to signals compatible with surface actuator
SA = Surface actuator
MP = Moment Producer

Figure 57: Control Mechanization Description

characteristics). Those factors that have a major impact on safety, weight, cost, and complexity were identified. The required sensors, unique control elements, and redundancy levels were specified for those control laws that offered the best performance. Finally, the elements were integrated into candidate systems.

4.3.2.1 Mechanization Design Criteria and Objectives

The initial step in the mechanization study was to identify the critical mechanization areas and to establish uniform criteria that could be applied to all mechanization categories. The following criteria were established as mandatory requirements:

(1) Actuation systems shall incorporate means of controlling failures induced transients consistent with structural limitations.

(2) Mechanization shall be designed to preclude inadvertent structural damage for normal pilot demands.

(3) The signal path and control actuation elements shall be mechanized to preclude a catastrophic single point failure and must satisfy the criteria relating to loss of axis control. Alternate paths may be considered if they allow safe CTOL landing or the successful completion of a STOL landing if failure occurs below the minimum decision altitude.

(4) Failure modes must conform to the following restrictions:

    (a) Failure during a STOL operation must permit either safe completion of the landing or safe transition to CTOL capabilities.

    (b) The probability of Level 3 STOL operation shall be less than 1×10^{-4} per flight.

    (c) No single point failure resulting in loss of control shall exist for either normal failure modes or small arms vulnerability.

The following design objectives were also established as goals to be sought for the mechanized systems.

(1) Piloting techniques learned for CTOL operation should be applicable for STOL operation to minimize pilot retraining.

(2) Speed should be controlled by a throttle-like lever (levers) where aft motion of the lever would reduce the airplane speed and forward motion of the lever would increase it.

(3) Advances in the state of the art should not be required for sensors or for the integration of mechanical or electrical signal paths.

(4) Failures in the thrust vector control actuation system should result in passive behavior. I.e., in the event of a failure the vector nozzle would remain fixed at its last commanded position.

(5) Control of the engine thrust level should be done by conventional throttle levers, control cables, and engine control devices.

(6) Failure modes precluding safe CTOL landing capability should have a probability less than 10^{-9} per flight.

4.3.2.2 Initial Definition of Mechanized Control Laws

The identification of those mechanization constraints that impact system performance, cost, and weight involves consideration of projected failure effects, the determination of allowable signal nonlinearities, and the establishment of special control system characteristics necessary for mission performance. During the control law definition phase the following major control system characteristics for the STOL landing approach task were identified:

(1) The aircraft speed in the STOL approach was controlled by modulating the thrust vector angle.

(2) Direct Lift Control (DLC) improved flight path response.

(3) Augmented airplane characteristics were required to achieve Level 1 response in both the longitudinal and the lateral/directional degrees-of-freedom.

(4) Lateral control sensitivity requires special attention because of the larger rate of heading change for a given bank angle.

(5) The lateral-to-longitudinal coupling was very noticeable. Bank angles in excess of approximately ten degrees resulted in noticeable changes to flight path.

Each of these characteristics presented unique mechanization problems. In addition, the problems cited in the design criteria section had to be solved. Specifically, these problems affected the design of the mechanical and electrical signal paths, the surface actuators, and selection of aircraft sensors.

The total mechanization task was very complex. Therefore the problem was separated into four tasks. The first three dealt with specific design problems regarding signal path mechanization, surface actuation mechanization, and sensor selection. Next, the job of integrating the elements from the first three tasks into a composite system was undertaken. At this time the different requirements for landing approach, transition, and high speed flight were integrated to provide a system satisfactory for the entire flight regime.

Signal Path Mechanization

The signal path consists of feedforward elements (for pilot controlled signals), feedback elements (for sensed response signals), and the elements necessary to convert these signals into a format compatible with the surface actuation system. Thus the signal path may include mechanical, hydraulic, and electrical components. The linear analysis and piloted simulation studies showed that feedforward signal paths in themselves are not adequate to control the spiral instability and flight path/speed coupling characteristics of the study airplane. The feedback signals required for satisfactory characteristics are difficult to sense and mechanize using only mechanical components, and would result in a system of questionable reliability. Therefore the mechanical-only signal path implementation was limited to that which would provide adequate CTOL flying qualities. The improvement of flying qualities by stability augmentation, control augmentation, or fly-by-wire techniques was done using analogue electronic components for the feedback paths. The reliability and performance of these are well known and the techniques for implementing them have been proven in operation.

For the definition of the signal path characteristics necessary for control system validation using piloted simulation, the following assumptions were made:

(1) The mechanical signal path lost motion was represented by a single hysteresis block by combining the effects of friction, cable compliance, and mechanical back lash as shown in Figure 58.

(2) The electrical path hysteresis was insignificant.

(3) The dynamic response, for those elements having high band pass characteristics compared to the augmentation or basic airplane dynamics, was considered unimportant to system definition. In this category were the dynamics of the rate gyros, the accelerometers, and the electrohydraulic servos that are the interface between electronic and mechanical systems.

Solution of the lateral control sensitivity and the lateral-to-longitudinal coupling problems discussed above required new designs for the mechanization validation studies.

During the conceptual phase of the control law study the aileron displacement was varied linearly with lateral control demand. The spoiler displacement versus lateral demand utilized a two-segment nonlinearity to correct for the aerodynamic nonlinearity of the rolling moment to spoiler deflection. The resulting rolling moment coefficient (ΔC_ℓ) is shown in Figure 59. The initial high slope (high gain) of the conceptual phase ΔC_ℓ/lateral demand curve was caused by the displacement doubling effect of differential spoiler operation in conjunction with a DLC bias. This high gain region caused objectionable lateral control sensitivity. Figure 59 also shows that this problem was corrected during the mechanization phase by improving the linearity of the spoiler lateral control in the presence of simultaneous DLC operation. This was done by

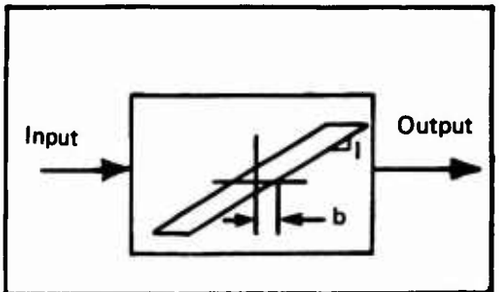

Control Surface	Lost Motion (2 x b)
1. Elevators	.4 Deg
2. Rudders	.4 Deg
3. Ailerons	.4 Deg
4. Spoilers	.7 Deg
5. Thrust Vector Angle	1.0 Deg

Figure 58: Mechanical System Lost Motion

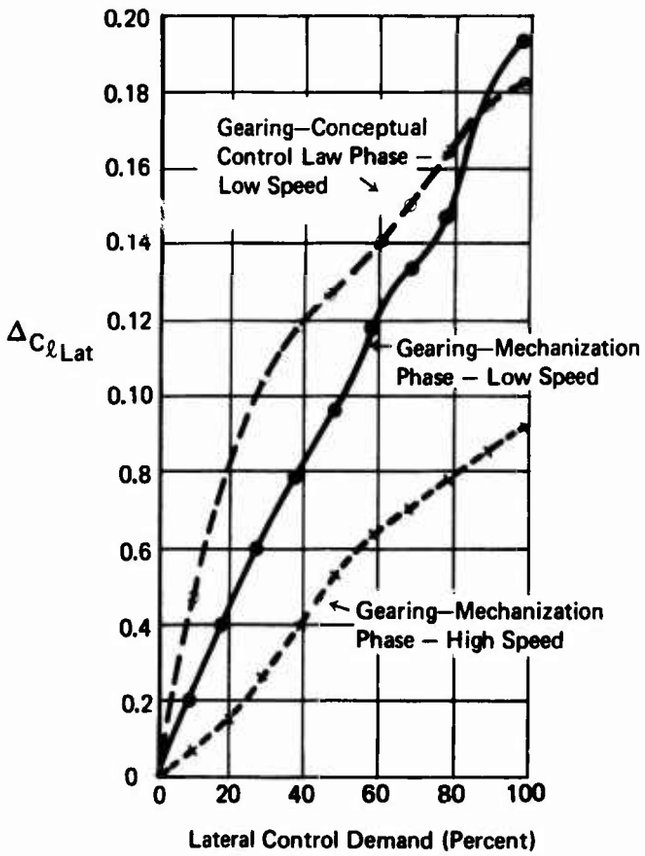

Figure 59: Lateral Control Rolling Moment Coefficient

revising the lateral control gearing and adding a spoiler gain changer to alter spoiler gain when used with DLC. The lateral control system gearing characteristics for both the conceptual and mechanized control law studies are shown in Figure 60. This figure also shows the schematic of the gain changer used to control spoiler gain during differential operation.

It can be seen in Figure 60 that two aileron gearing gradients were used for the mechanized lateral systems. At low speed the aileron is fully deployed for a twenty percent lateral demand while a fifty percent demand is required for the same deflection at high speed. This gain change was done by:

(1) Removing the electrical feedforward portion of the signal path in control augmented systems, or

(2) Incorporating a mechanical gain changer driven by flap position for mechanical systems, or

(3) Reducing the gain of the feedforward portion of the signal path for fly-by-wire systems.

The electrical spoiler signal path incorporated a dead-zone that delayed the use of these elements until twenty percent of the lateral control was demanded. This reduced the lift loss resulting from spoiler deployment. The electrically controlled spoilers utilized the two-segment gain curve to improve linearity. This can be accomplished with electronic summing amplifiers.

The lateral-to-longitudinal coupling problem was corrected by a cross feed from bank angle into the spoiler direct lift control. This partially compensated for the loss of lift due to bank angle. The incremental load factor as a function of bank angle is shown in the following equations (angle of attack, flight path, and speed are assumed constant):

$$\Delta L = L\ (1 - \cos \phi) = mg\ (1 - \cos \phi) \tag{65}$$

$$\Delta g = \frac{\Delta L}{m} = g(1 - \cos \phi) \text{ and} \tag{66}$$

$$\Delta n = \frac{\Delta g}{g} = (1 - \cos \phi) = \text{versine } \phi \tag{67}$$

To determine possible compensation techniques, cos ϕ is replaced by the first two terms of the series:

$$\cos \phi = 1 - \frac{\phi^2}{2!} + \frac{\phi^4}{4!} + \ldots\ldots \text{ where } \phi \text{ is in radians.} \tag{68}$$

thus:

$$\Delta n \tilde{=} \frac{\phi^2}{2} \text{ where } \phi \text{ is in radians.} \tag{69}$$

In the range of interest (i.e., bank angles up to 30 degrees), this term approximates the ideal versine correction. A simpler correction uses

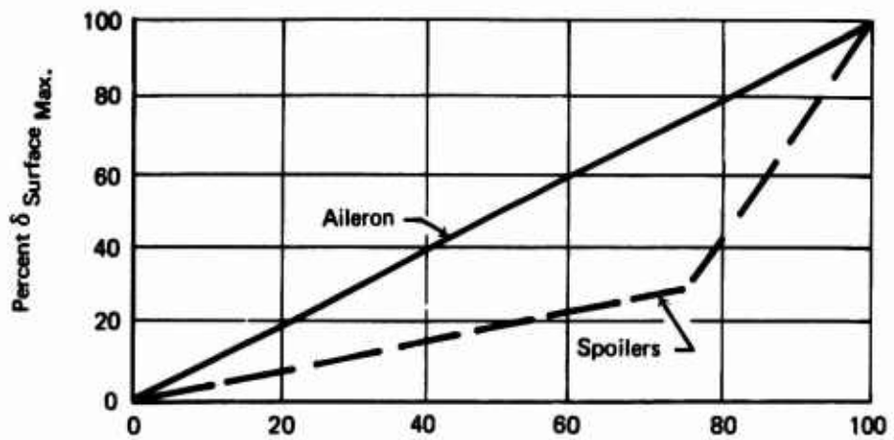

(a) Percent Maximum Lateral Demand
Conceptual Phase Gearing

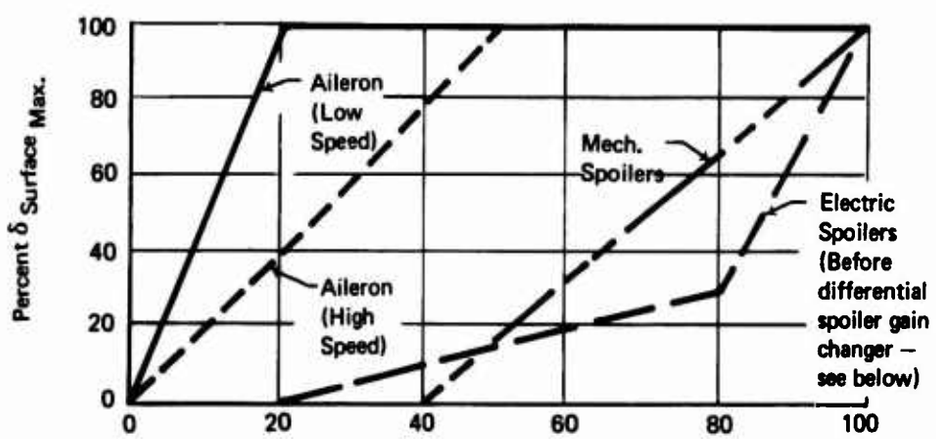

(b) Percent Maximum Lateral Demand
Mechanization Phase Gearing

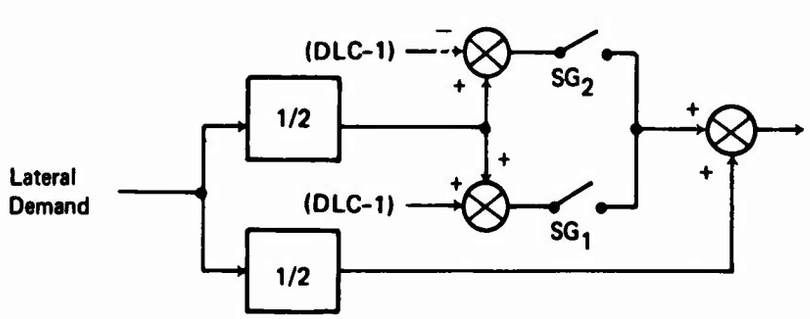

(c) Differential Spoiler Gain Changer for DLC Operation

Switch Logic:

SG_1 (Closed): δ_{SP_R} < 1 Deg.

SG_2 (Closed): δ_{SP_L} < 1 Deg.

Figure 60: Lateral Control Gearing

uses the absolute value of bank angle for correction. Noting that .1g acceleration is available from the direct lift control, two proposed corrections were defined:

$$\Delta n_1 = .016\,(\Delta_n/\delta_{sp})\,\phi^2 \tag{70}$$

or

$$\Delta n_2 = .2\,(\Delta_n/\delta_{sp})\,|\phi| \tag{71}$$

where

$$\Delta n/\delta_{sp} = .01/\text{degree} \quad \text{and} \quad \phi \text{ is in degrees} \tag{72}$$

The lift losses with and without compensation are shown in Figure 61. Although the ϕ^2 compensation provides a better correction than the $|\phi|$ compensation, the latter was chosen because it did not saturate the DLC, it maintained lift within two percent at bank angles up to twenty degrees.

Automated Flight Path Control

The incorporation of automatic path modes can be accomplished with minimal impact for FBW, FBW with reversion, and CAS systems. These systems have the necessary pilot demand transducers and electrically controlled surface actuators. The system modifications required for automatic flight path modes are the addition of:

(1) A "synchronizing" integrator for each path mode desired (e.g., pitch attitude or flight path, bank angle hold, and heading hold).

(2) The synchronizer control logic.

(3) A pitch trim "off-load" system.

The mechanizations of the automatic path modes considered during the simulation study are shown in Figure 62.

Surface Actuation Mechanization

The surface actuation system uses fully powered irreversable actuators. 1972 state of the art technology was used throughout. The SAS and CAS actuation systems utilized limited authority series servos. This actuation approach has been proven in both single channel and redundant channel applications.

The actuation system for the fly-by-wire and fly-by-wire with mechanical reversion utilized 1972 technology servos, but applied it in a new manner. A typical "parallel" type servo actuator was used: The normal mode is controlled by an electro-hydraulic control loop. A mechanically positioned control valve, connected in parallel with the servo valve (see Figures 63 and 64) is normally held in the "null" or

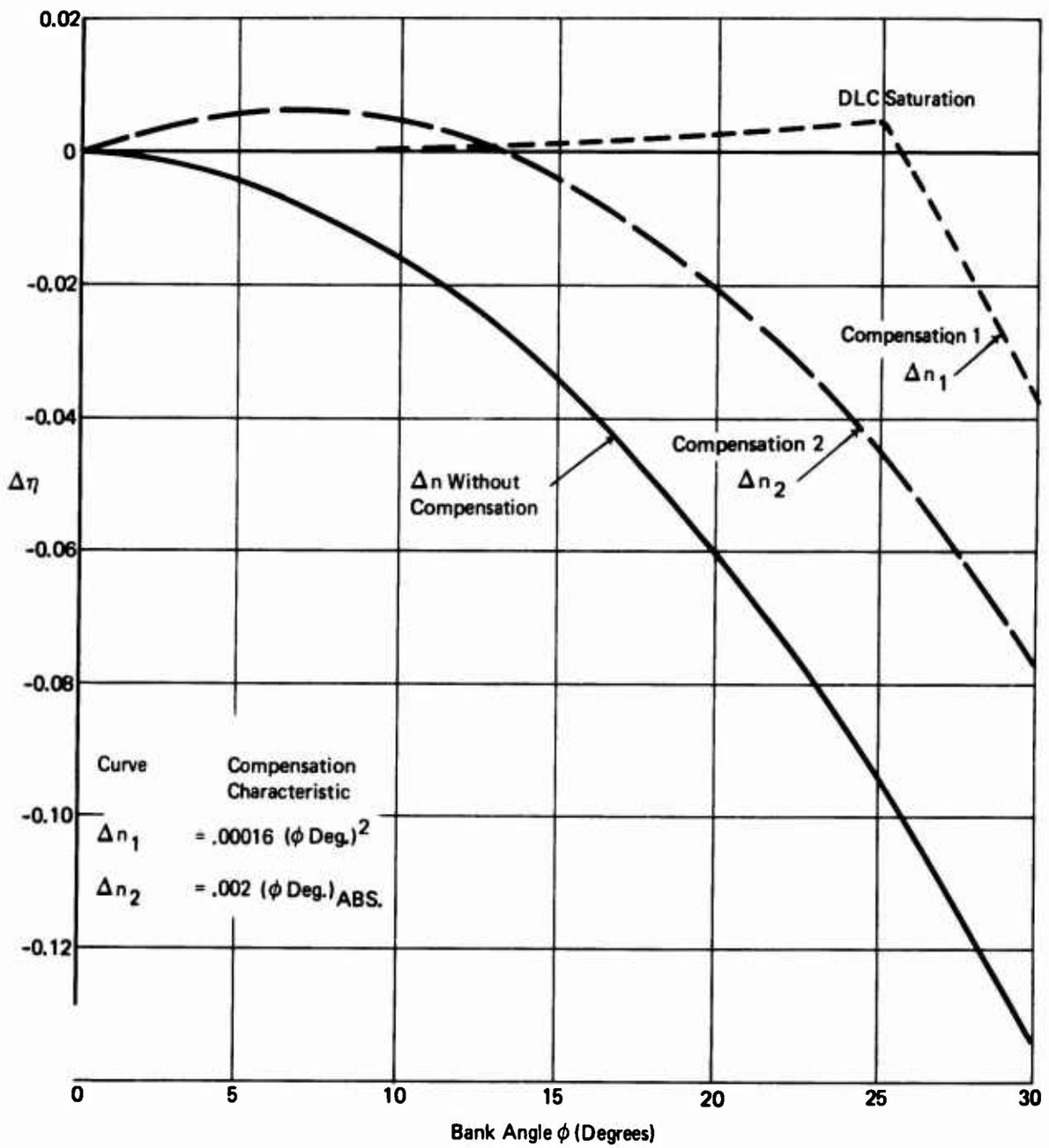

Figure 61: Incremental Lift Loss Due to Bank Angle

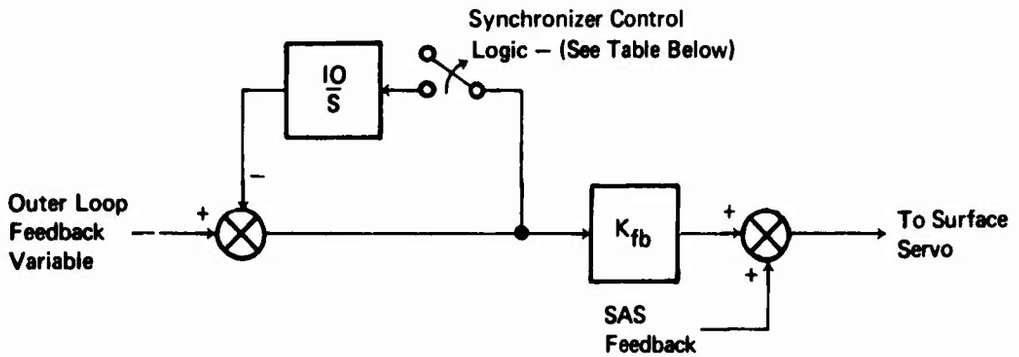

(a) Synchronizing Integrator (Pitch Attitude Hold, Bank Angle Hold, or Heading Hold)

Automatic Path Modes

Automatic Mode	Feedback Variable	Synchronizer Mode Control Logic		k_{fb}
		Closed	Open	
Pitch Attitude	θ	$F_{col} > 3$ Lbs	$F_{col} < 3$ Lbs and Q $< .5$ Deg/Sec.	Gains Varied With Specific Control Law
Flight Path	γ	$F_{col} > 3$ Lbs	$F_{col} < 3$ Lbs and Q $< .5$ Deg/Sec.	
Bank Angle Hold	ϕ	$F_W > 2$ Lbs or $F_{ped} > 7$ Lbs or $\phi > 3$ Deg	$F_W < 2$ Lbs and $F_{ped} < 7$ Lbs and $\phi < 3$ Deg	
Heading Hold	R and Ψ Compass	$F_W > 2$ Lbs or $\phi < 10$ Deg	$F_W < 2$ Lbs and $\phi > 10$ Deg.	

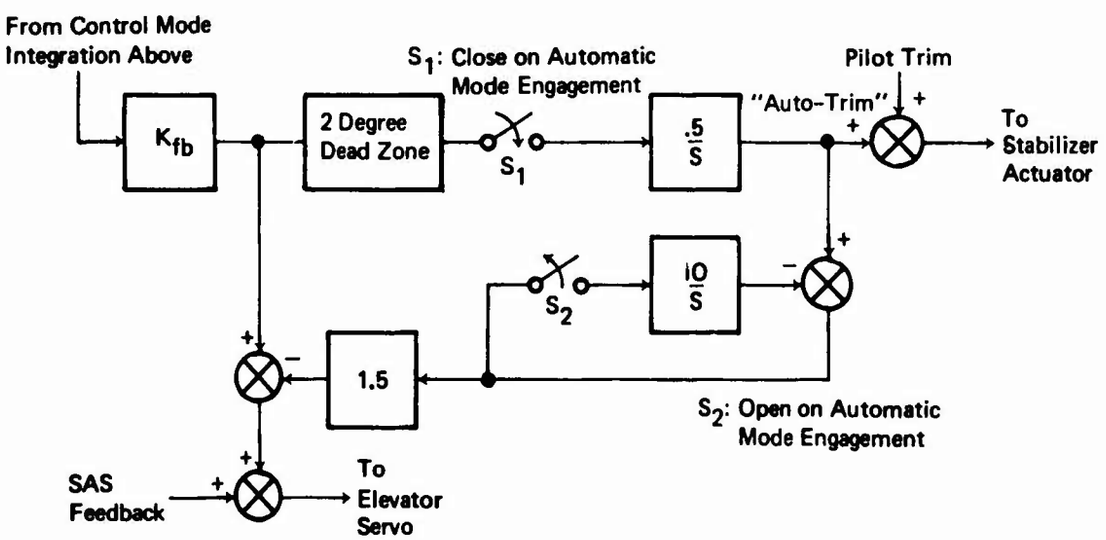

(b) Pitch Auto-Trim

Figure 62: Mechanization Modification for Automatic Path Modes

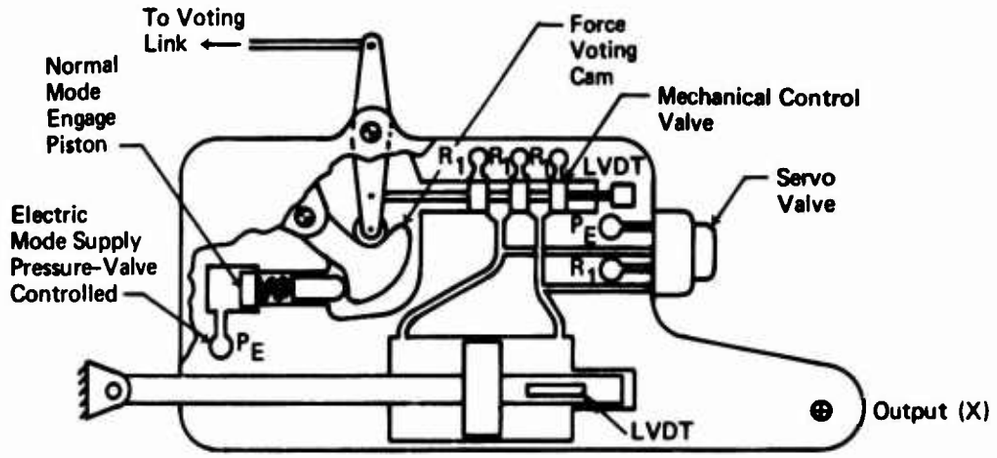

Fly-By-Wire Surface Actuator
(Single Hydraulic System)

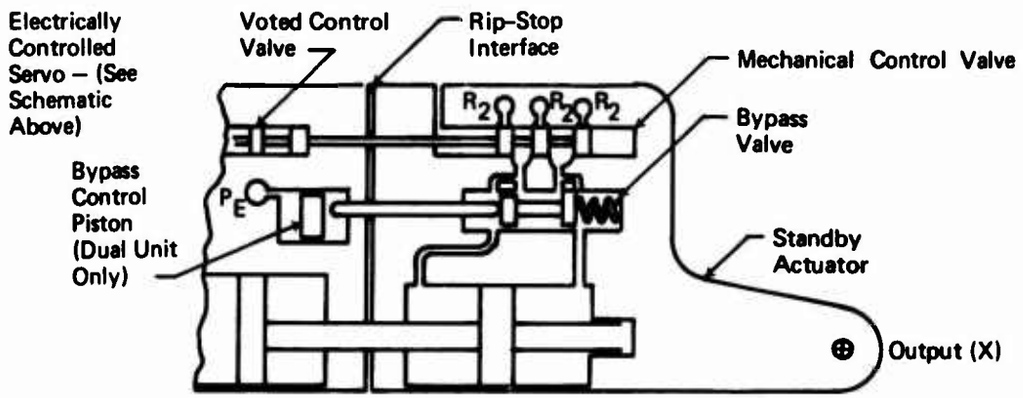

Fly-By-Wire Surface Actuator
(Modification for Dual Hydraulic System)

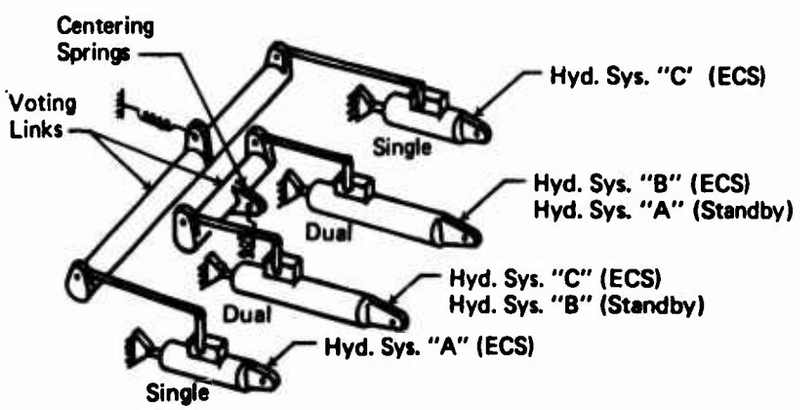

Fly-By-Wire Elevator System
(Voting and Hydraulic Distribution)

Figure 63: Fly-By-Wire Actuation Systems

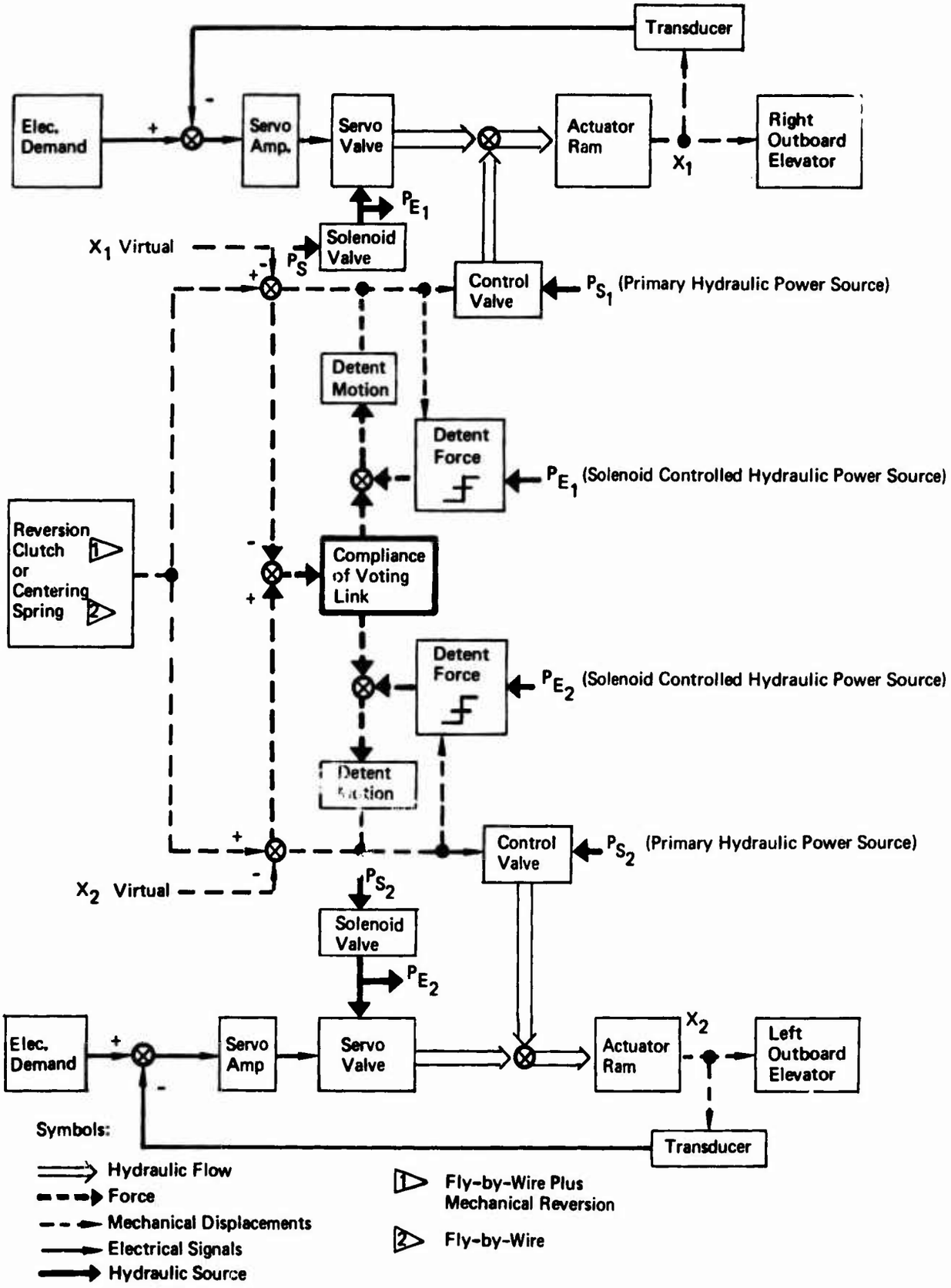

Figure 64: Schematic of Typical Fly–By–Wire Voting Actuators

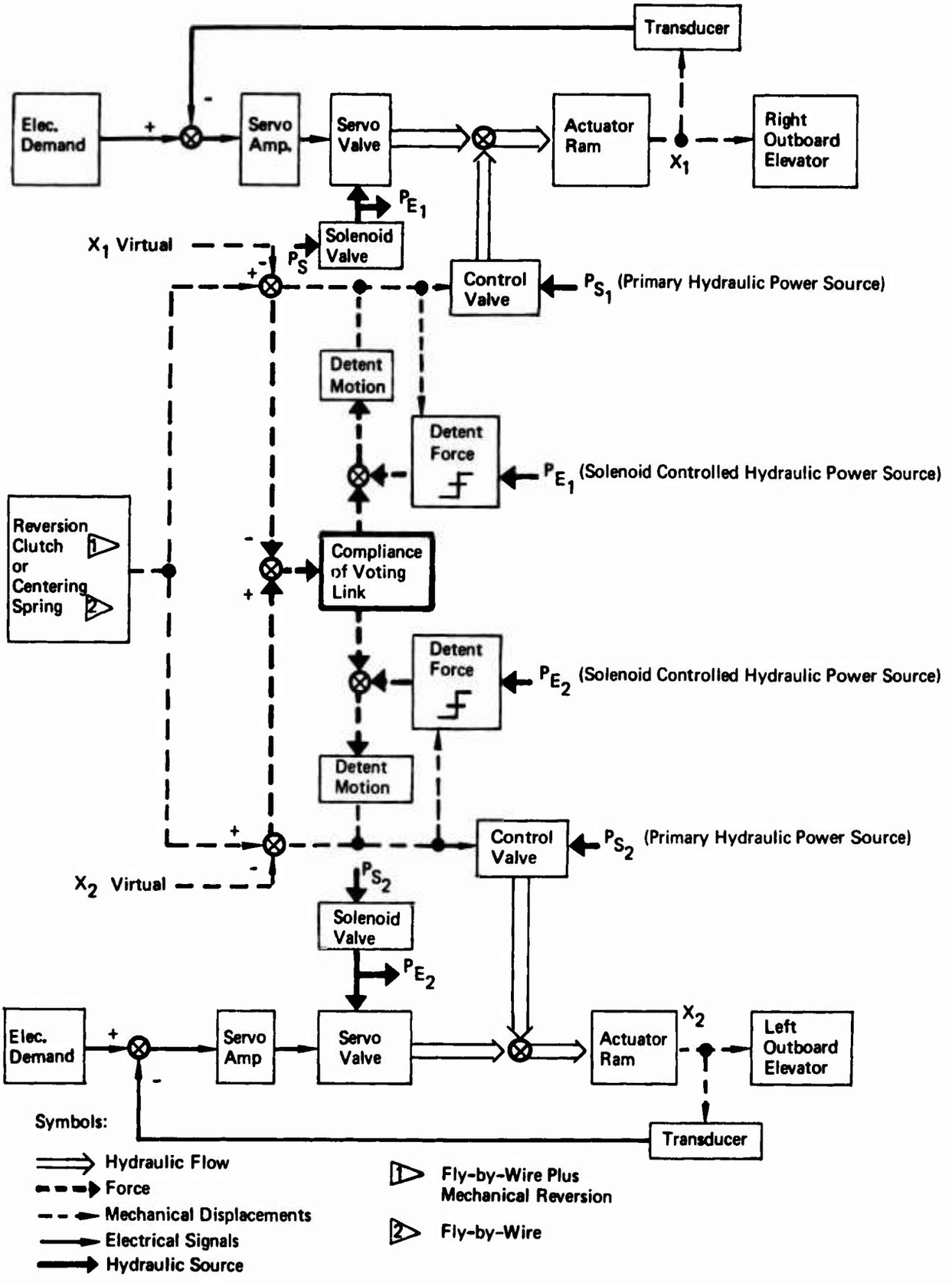

Figure 64: Schematic of Typical Fly–By–Wire Voting Actuators

centered position by the force voting cam. In the usual "parallel" servo application, the output motion of the electrically controlled actuator "back-drives" the feel system to provide the pilot with a surface motion cue. When the feel system force exceeds the "detent" force level of the voting cam, the mechanical valve moves to counteract the servo valve thus stopping actuator motion. For the proposed fly-by-wire actuation system, the override force is provided by a compliant voting link that interconnects two or more actuators. Once the output positions of the interconnected actuators vary by more than a fixed magnitude, the force generated by the voting link will override the voting cam and oppose further surface motion. Failures are monitored by the difference in sensed surface position or by the deflection of the mechanical control valve. Electronic voters were used in generating commands to each actuator to reduce the output misalignment due to channel-to-channel tracking errors.

The dual tandem actuators used on the inboard elevator panels require additional explanation. Only one servo valve was used for each elevator actuator. Thus, in the normal mode, only one of the dual actuator segments can be directly controlled by the electrical loop. The remaining segment is held in a bypass mode until a failure has been detected and the electric mode hydraulic pressure (P_E) is removed. At this time both segments of the actuator revert to a "slave" condition and are driven through the voting link by the remaining operational electric command servo.

For fly-by-wire with mechanical reversion, the centering springs on the voting links are replaced by a reversion link that connects the voting links to the mechanical path. This reversion link would be similar to that used in the Air Force Survivable Flight Control Program (Ref. 15) and would disconnect the mechanical path during normal mode operation.

Thrust Vector Actuation

In the thrust vector actuation systems, shown in Figure 65, hydraulic servo motors, shafts, gear boxes, and power hinges were selected to move the deflector segments and the vector ramp area match panel (see Figure 5). The drive path is irreversible so the vector angle will remain at its last commanded position when drive capability is lost because of hydraulic power or signal failures. Friction drums restrain the mechanical path to maintain a fixed demand until altered by the pilot.

Stabilizer Angle Actuation

The stabilizer displacement is controlled both by pilot demands and by the "auto-trim off-load" system shown in Figure 62. A stabilizer trim actuation using a position servo system was investigated. This type of actuation system has the following advantages over the normal integrating servo actuation system:

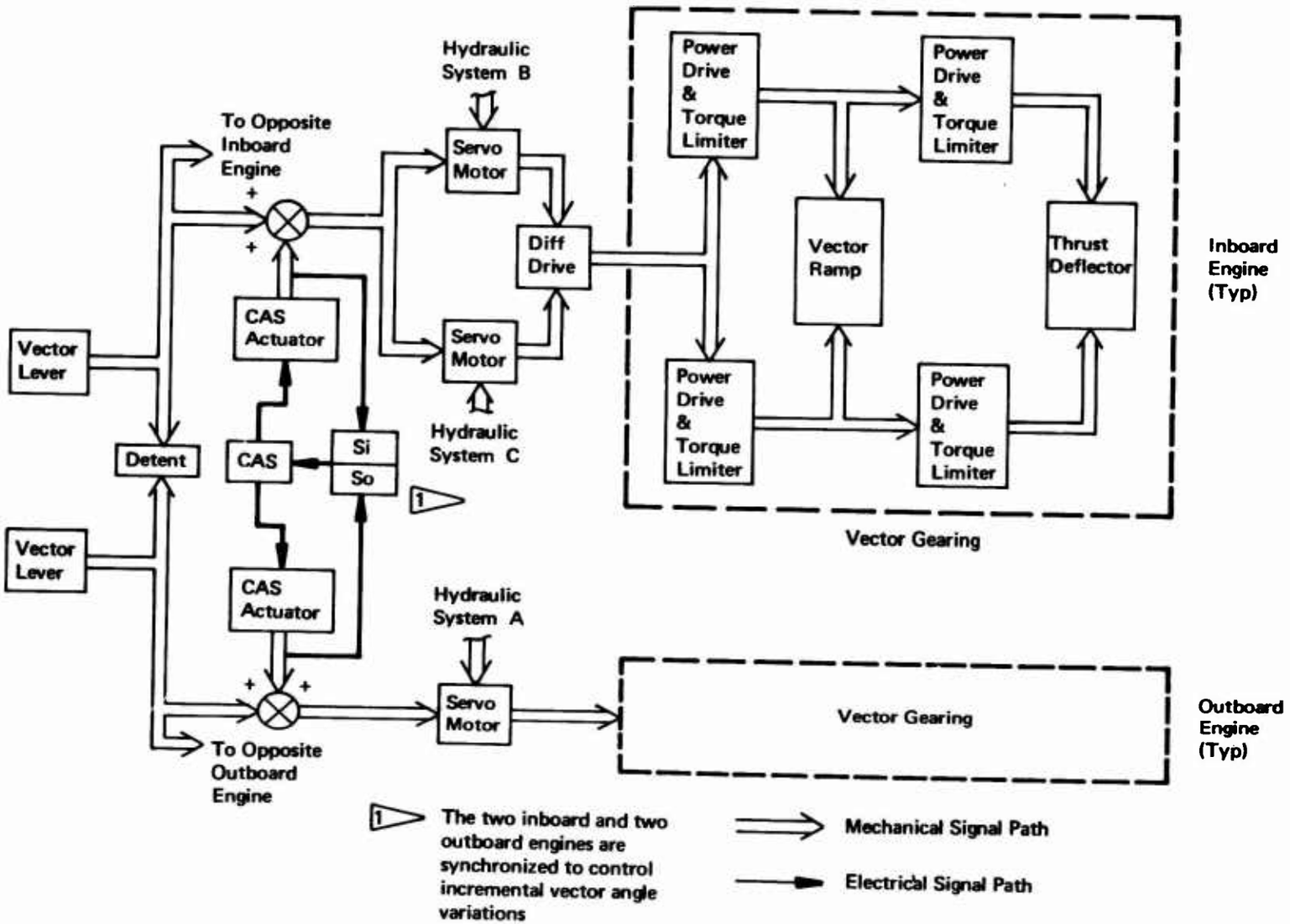

Figure 65: Thrust Vector Actuation System

(1) The position servos used in the actuation system provide a backup to the trim jack screw brake system. If the trim jack screw brakes fail, the position servos will provide a hard point and prevent the stabilizer from moving.

(2) Automatic monitoring systems can be easily implemented to prevent stabilizer runaway in the event one of the servo systems fails. This ability to detect and prevent trim runaways eliminates the need for the control column brake used in the existing trim systems.

(3) Dual redundancy is provided for the cockpit electrical trim system.

This actuator system is detailed in Figure 66. One contact on the pilot and co-pilot trim switches provides the input to the trim integrators while the other contact on the trim switches is used to enable integrator operation. Thus, trim cannot be accomplished unless both trim switch contacts are operating. Each of the two integrators feeds a separate electric servo actuator which drives a wormgear and differential gear box to provide an output to the stabilizer actuator. The mechanical override clutch provides a means for pilot input via the mechanical trim path.

The output of the two integrators is monitored to assure sufficient synchronization. These integrators should be able to track within 4°. A monitor is provided that compares the output of each servo actuator with the output of the differential gear box. When this magnitude exceeds a preset value (e.g., $\pm 2°$ of surface command) the servo actuator will be disabled. The output of the differential gear box is compared with the integrator demand so that a runaway servo loop will be opposed by the remaining servo loop. These feedback loops reduce the transient caused by any servo actuator runaway to one half the monitor limit. Thus the $\pm 2°$ limit will limit the stabilizer transient to $\pm 1°$. Operational capability can be maintained at one half the normal trim rate even though one electric servo actuator has failed. The worm gear that connects the servo actuator to the differential gear box acts as an irreversable mechanical link and allows the motion from the other servo actuator to drive the stabilizer trim system.

Sensor Selection

In the conceptual control law analysis, idealized airplane response rates, ground speed, flight path, and sideslip rate were used in the feedback systems. During the mechanization phase these signals were derived using sensors representative of those available for existing aircraft. Several of the desired signals could not be measured directly and were computed by blending other signals to obtain an approximation of the desired response. For example, the determination of flight path angle, flight path angle rate, and sideslip rate utilized approximation techniques. The approximation equations for these signals are shown below:

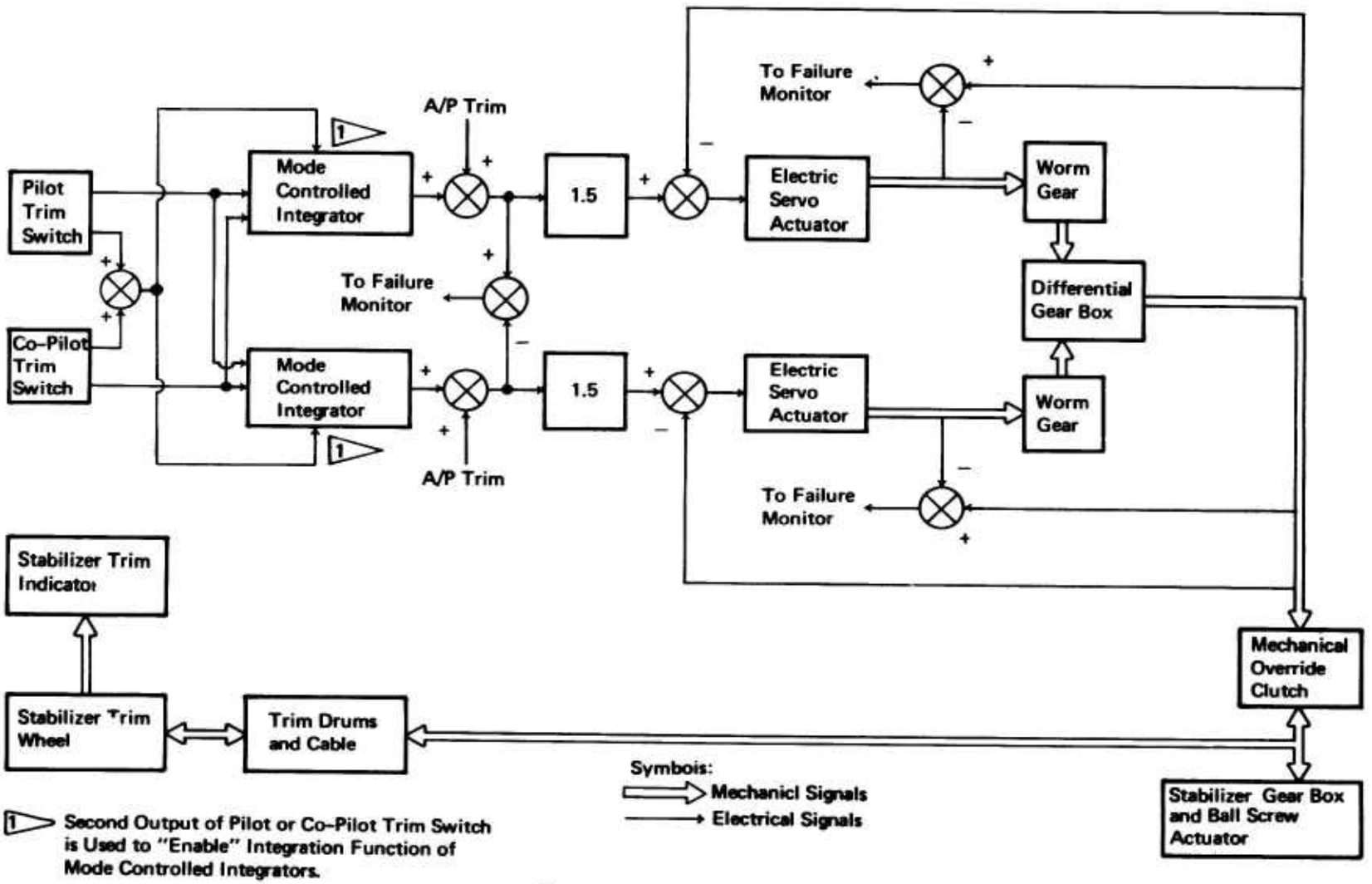

Figure 66: Proposed Stabilizer Trim Actuation System

Inertial reference flight path angle:

$$\gamma_{I_{(Deg)}} = \sin^{-1}\left(\frac{\dot{h}}{V_G}\right) \cong \left(\frac{\dot{h}}{V_G}\right)(57.3) \tag{73}$$

True airspeed reference flight path angle:

$$\gamma_{T_{(Deg)}} = \sin^{-1}\left(\frac{\dot{h}}{V_T}\right) \cong \left(\frac{\dot{h}}{V_T}\right)(57.3) \tag{74}$$

Inertial reference flight path angle rates (by taking the time differential of $\cong \gamma_I$):

$$\dot{\gamma}_{I_{(Deg/Sec)}} \cong \frac{57.3}{V_G^2}\left[-\dot{h}\,\dot{V}_G - V_G\,\ddot{Z}\right] \tag{75}$$

Since $-\dot{h}\,\dot{V}_G$ is small,

$$\dot{\gamma}_{I_{(Deg/Sec)}} = -57.3\,\ddot{Z}/V_G \tag{76}$$

and true airspeed reference flight path angle rate ($\dot{\gamma}_T$ derivation analogous to $\dot{\gamma}_I$ derivation):

$$\dot{\gamma}_{T_{(Deg/Sec)}} = -57.3\,\ddot{Z}/V_T \tag{77}$$

The sideslip rate approximation used in the development of lateral systems was

$$\dot{\beta}_{SAS} = -r + \frac{g}{V_T}\,\phi \tag{78}$$

Another signal that was derived from the blend of two signals was the altitude rate signal. The limited band pass of air data altitude rate sensors requires that a complementary filter be used to obtain an altitude rate signal with adequate band pass. This complementary filter uses a blend of barometric altitude rate and vertical acceleration to obtain a high band pass signal, given by

$$\dot{h} = \frac{\dot{h}_{baro} - \ddot{Z}\tau}{\tau s + 1}, \tag{79}$$

where

$$\tau = \frac{1}{\text{bandpass } \dot{h}_{baro}}$$

The specific sensors used in this study are listed in Table XI which states the idealized aircraft response parameter, the sensed aircraft response parameter, and the device used to measure the aircraft response. Off-the-shelf sensors are proposed in all control systems except those using flight path angle (γ) and flight path angle rate ($\dot{\gamma}$) feedback signals. The computation of γ and $\dot{\gamma}$ can be accomplished in an "inertial-space" reference frame or relative to the air mass. The first requires the computation of ground speed (inertial reference) while the latter uses airspeed (V_T). It was found in piloted simulation that ground speed was required to achieve acceptable touchdown dispersion. Therefore a "strapped-down" inertial sensor was selected to compute this term.

TABLE XI

FLIGHT CONTROL SENSORS

Idealized Design Parameter	Sensed Aircraft Response	Sensor
θ	θ	Two axis vertical gyro or INS
ϕ	ϕ	Two axis vertical gyro or INS
ψ	ψ	Gyro Compass or INS
r_s	r_B	Rate gyro
P_s	P_B	Rate gyro
$\dot{\theta}$	Q	Rate gyro
V_T	P_S and P_T	Total and static pressure transducers plus partial air data computer.
$\dot{h}_{baro}$	P_S and P_T	Same as for V_T
$\ddot{Z}$	$\ddot{Z}$	INS - accelerometer
V_G	$\ddot{Z}$, $\ddot{X}$, and $\ddot{Y}$	INS - computed
$\dot{\beta}$	r_B, ϕ	Two axis vertical gyro plus rate gyro
$\ddot{y}$	$\ddot{y}_B$	Accelerometer

Control System Integration

The definition of candidate system mechanization was required to determine the appropriate simulation model and to allow evaluation of system safety, weight, cost, complexity, design risks, and vulnerability. The establishment of an acceptable redundancy level was an iterative process where the safety of a proposed system redundancy was evaluated and the redundancy adjusted when inadequate safety was found.

The definition of a control mechanization must satisfy several requirements. It must indicate the functional and dynamic relationship of the various elements and it must provide a physical representation of the mechanization. In general, the physical and functional relationships of electrical elements are easily visualized by block diagram techniques. This is not always possible with mechanical systems, where a pictorial representation most often provides better insight into the physical properties of a proposed system.

The general characteristics of mechanical control systems can easily be visualized by referring to thrust vector angle control system (Figure 67). This shows the following features that are common to the mechanical elements of all MCS, SAS and CAS systems:

(1) Dual pilot/co-pilot controllers.

(2) Dual mechanical signal paths connected with a single "cross-tie" detent. (For the lateral system, the cable from each inter-tied aft quadrant goes to one wing only.)

(3) Feel (or friction) elements located in close proximity to surface actuation. (Except for the lateral system, which uses a central feel system.)

(4) The use of cables, quadrants, push rods, and bellcranks to transmit pilot demands.

The design of the mechanical systems was conventional with the exception of the "cross-tie" detent which allows isolation of each mechanical path in the event that one mechanical path "jams". This detent was designed to exhibit a "shear-out" characteristic, where there is an initial force to override a "jam" and then a residual force approaching zero. For the MCS, SAS and CAS control mechanizations, the longitudinal and lateral feel systems incorporated a pneumatic/hydraulic feel computer using dynamic pressure (q) as the control variable. This feel unit provides a variable force gradient for normal operation and reverts to a simple spring/cam "fixed feel" system upon failure of the hydraulic system. Dual feel units are used where one unit is associated with each independent path.

The feel units for the directional axis and for all axes with FBW or FBW + Reversion mechanization used dual spring/cam "fixed feel" units. The FBW + Rev. mechanization use a single cable system with a declutch mechanism to isolate the FBW voting actuators during normal operation.

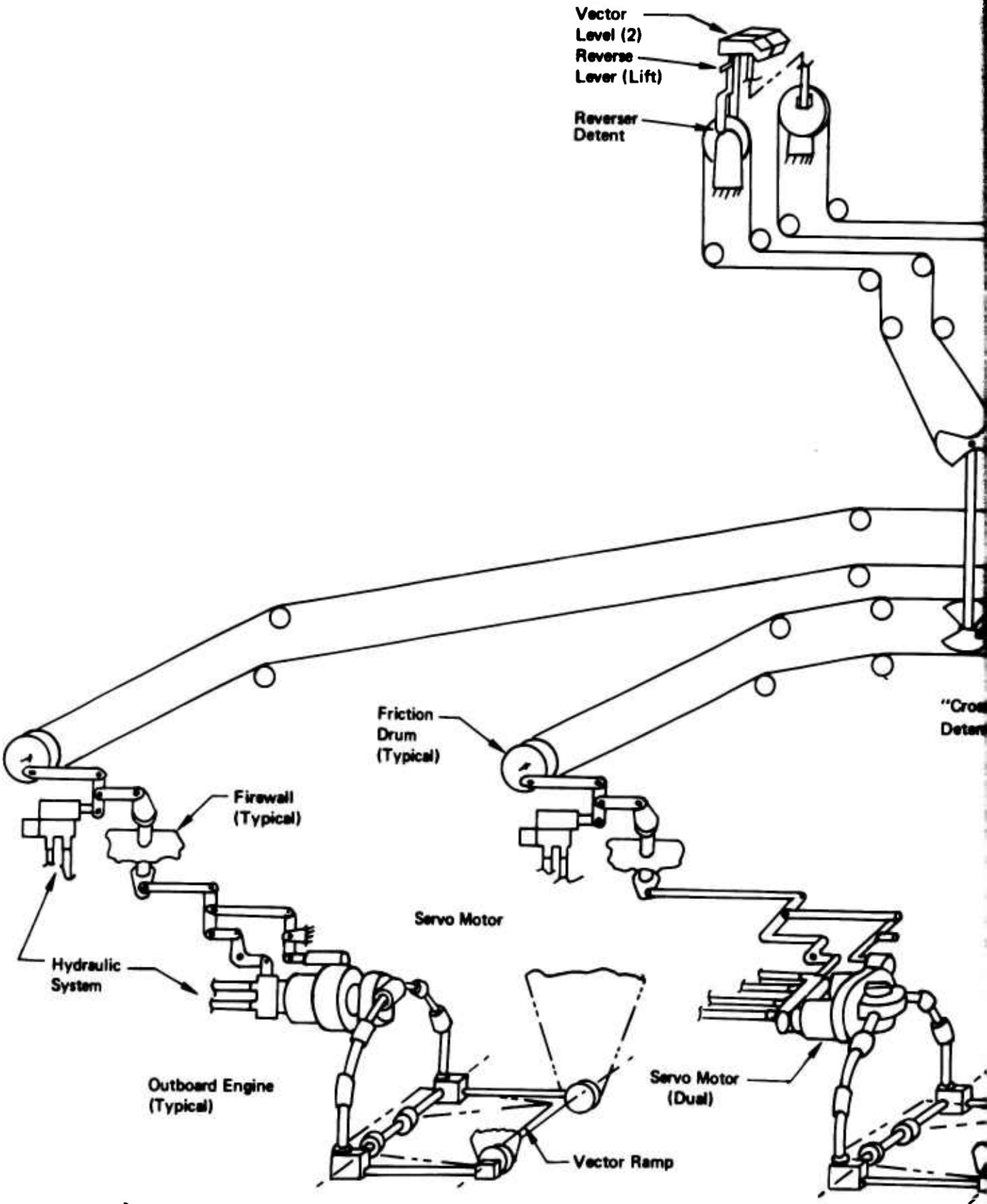

1 The CAS actuator is used for series inputs for electrically computed signals.

A

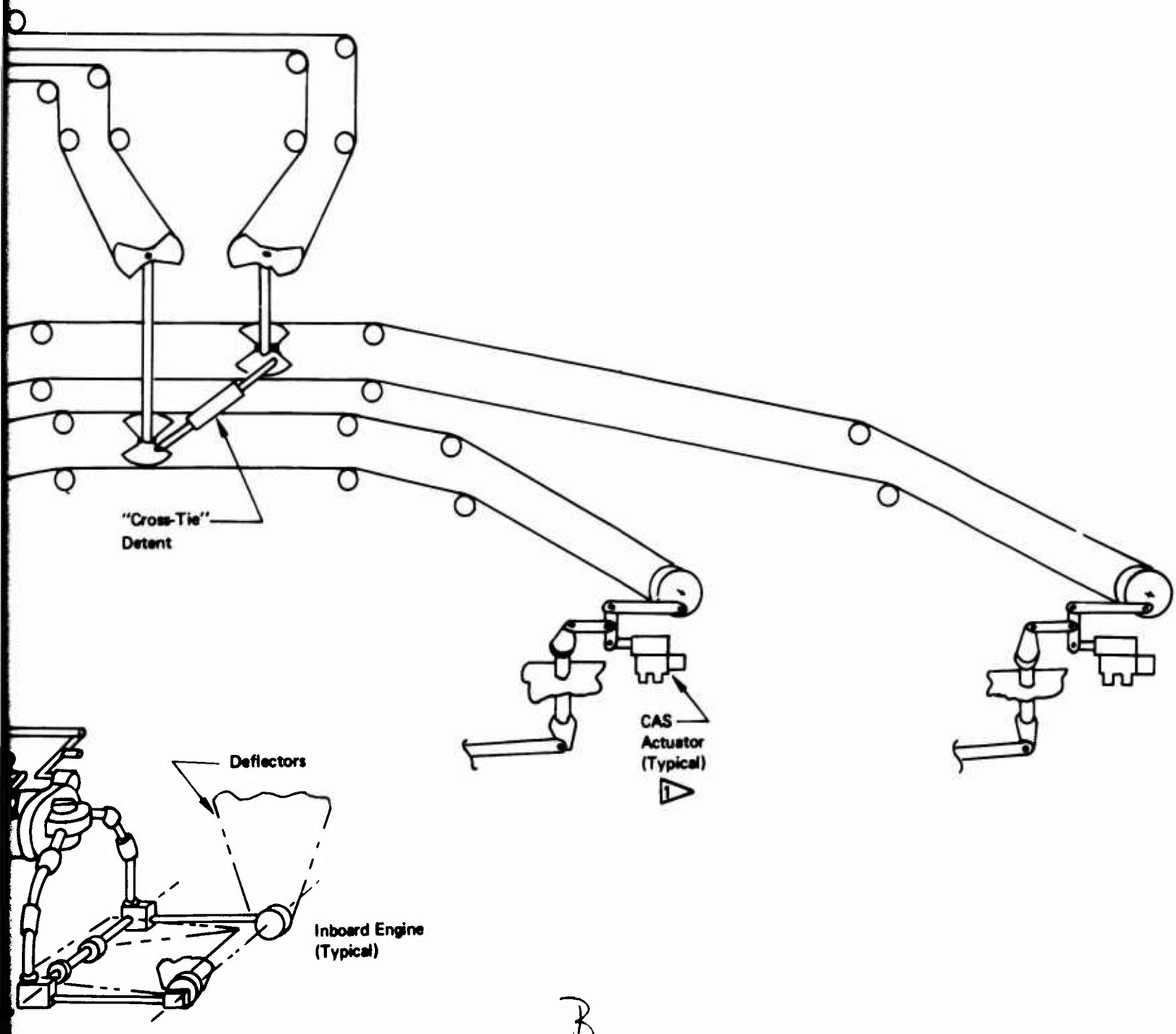

Figure 67. Thrust Vector Angle Control System

In the functional block diagrams (Figures 68 through 79), only the redundancy, lost-motion, and the reversion aspects of the mechanical systems are depicted. These functional diagrams concentrate on system redundancy and the interface between electrical and mechanical systems. This allows the determination of failure modes as they apply to specific mechanizations.

In Figure 68 the longitudinal CAS mechanization (CP21) is shown. The salient features of this system are:

(1) A triple redundant electronic system for fail-operational capability.

(2) Series summed surface actuation with redundant control surfaces.

(3) Dual mechanical signal path for cruise and STOL reversion control.

The cruise control is accomplished with control techniques equivalent to existing transport aircraft. (i.e., the throttles and elevators provide speed and attitude control.) As the aircraft transitions to the STOL mode, the speed brakes are employed to provide additional drag and in so doing provide the spoiler bias needed for DLC operation. The pilot presets the thrust level with the throttle controls and controls speed during the landing approach with the vector angle lever. The pilot activates the landing approach control mode after the deployment of flaps, and the speed hold mode when the approach speed has been obtained. The transition control is the same for all control axes and all mechanizations.

The major changes between control system candidates are in the mechanization details. Thus, the FBW +Reversion system (SP02R) and the FBW system (SP02A) are based upon the same control law as CP21. However, the mechanizations differ in the following areas:

(1) Normal control is FBW. The command/response characteristics inherent in the fly-by-wire feedbacks plus the gain changing provisions assure good feel characteristics over the complete range of dynamic pressures with a simple spring/cam feel unit.

(2) The actuation system is capable of 100 percent authority for both electrical and mechanical signals, yet failure transients are limited to an acceptable level.

(3) A single mechanical path provides for reversion control (SP02R only).

Both the FBW and FBW +Reversion systems use gain schedules to control "normal mode" feel characteristics. These gain schedule devices can be mechanized in either of two methods shown in Figure 70. The first method, using a servo driven potentiometer, reflects the technology used in existing autopilots. The improvement in integrated circuit reliability make the second option, using an electronic divider, a viable candidate.

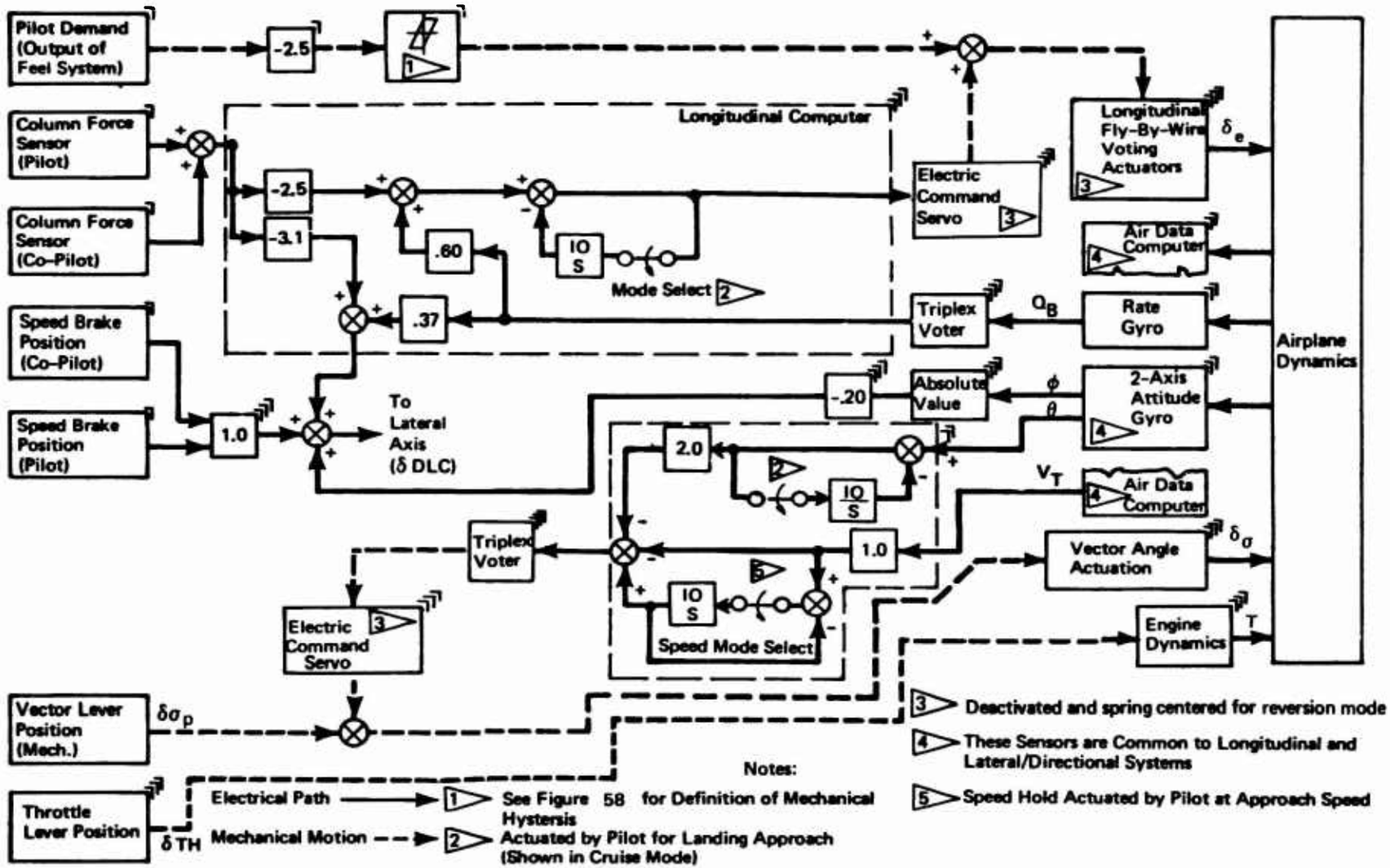

Figure 68: Longitudinal Control System Mechanization Diagram System CP21

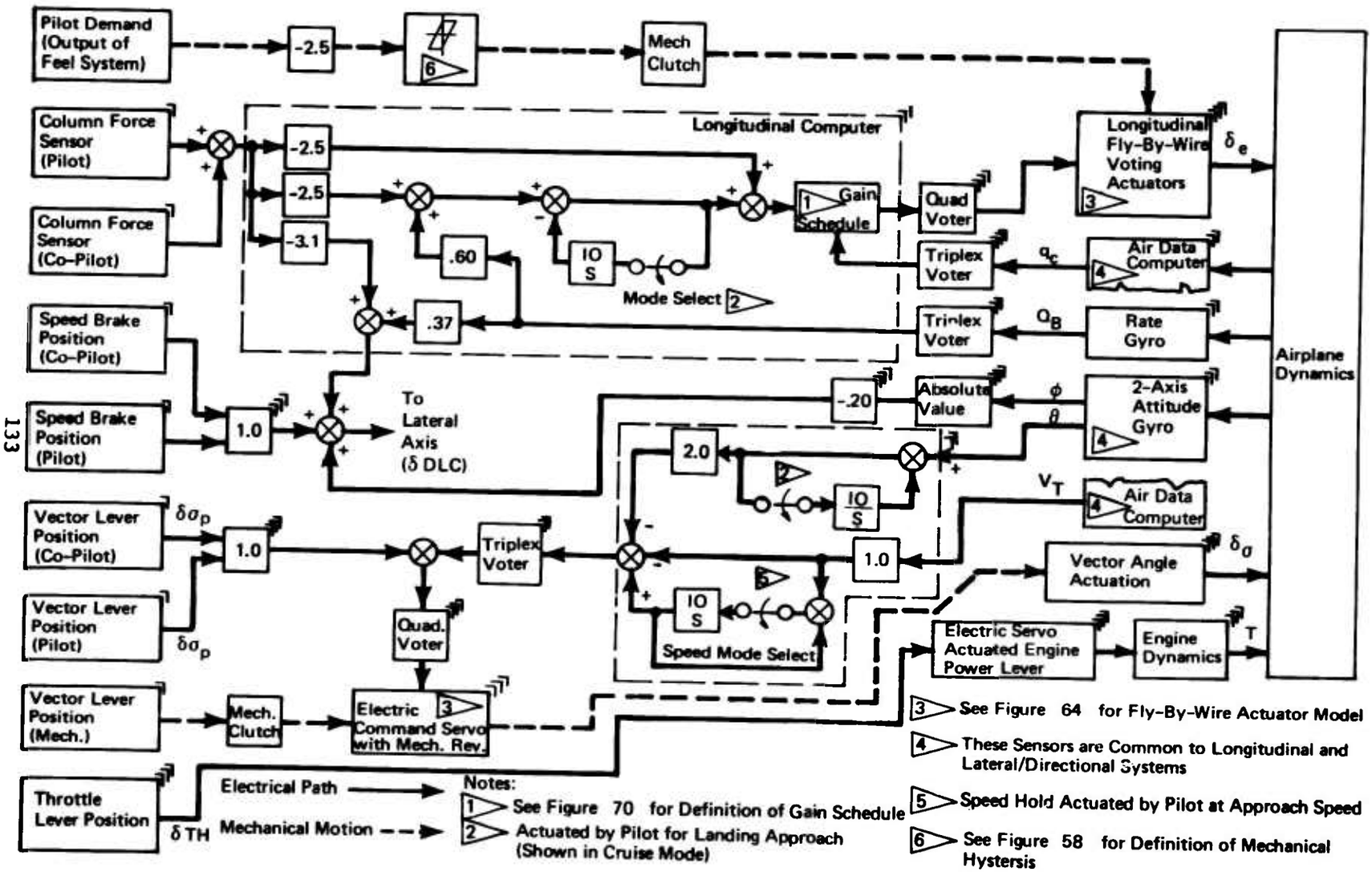

Figure 69: Longitudinal Control System Mechanization Diagram System SPO.2R

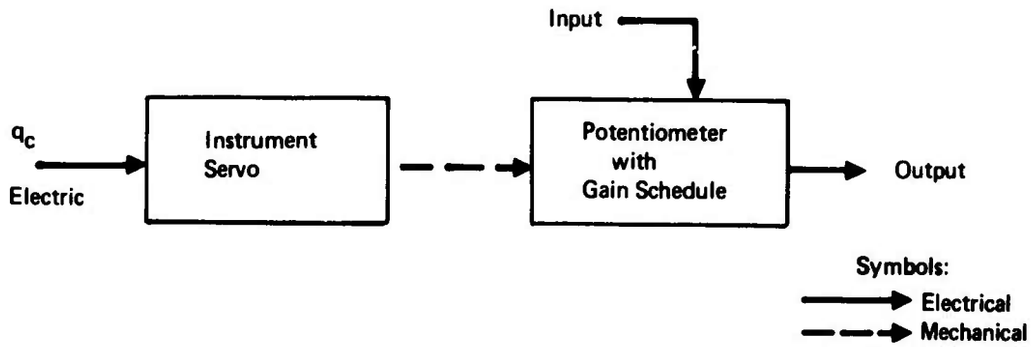

A) SERVO DRIVEN POTENTIOMETER

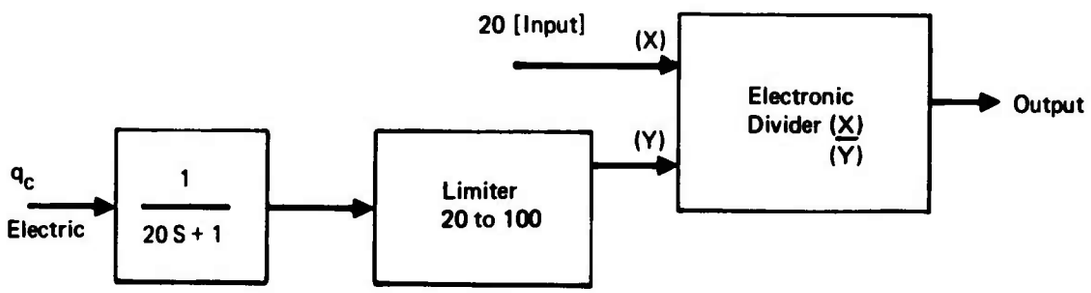

B) ELECTRONIC MULTIPLIER NETWORK

Figure 70: Gain Schedule Mechanization

The FBW mechanization (SPO2A, Figure 71) differs from the FBW + Revision by the addition of a fourth electrical signal path and the deletion of the mechanical reversion path. This electronic redundancy was required because the electrical system comprises the only signal path.

The mechanization diagrams for the lateral/directional mechanization are shown in Figures 72 through 76. The same general variations between the mechanization categories (i.e., CAS, FBW and FBW + Revision) are apparent in the lateral/directional axes. The use of blended aileron and spoiler surfaces for lateral control plus the general use of electrical spoiler servos requires additional examination of the mechanization impact on the lateral actuation system. In Figure 77, it will be noted that the SAS and CAS mechanization use a series servo to convert electrical inputs to mechanical displacements compatible with the aileron and outboard spoiler actuators. The remaining spoilers are controlled by electrical servos. For the FBW + Reversion system (see Figure 78), the voting type servos are utilized to be compatible with both the normal mode electrical signals and the reversion mode mechanical control. These same actuators are used with the FBW mechanization to achieve the transient limiting characteristics required with a 100 percent authority servo system.

In all of the above cases, a single conceptual control law has been mechanized in varying degrees of complexity. The major impact of mechanizing an alternate control law relates to specific sensors and the gains used in the electrical signal paths. This is most easily seen by comparing the FBW + Reversion mechanization of conceptual control laws FR20R and FR21R shown in Figures 76 and 79.

The preceeding subsections have considered the specific details of the mechanized control laws that were evaluated in the control system trade study. Using these details as the configuration baseline, the analysis methodology was used to determine quantitative values for safety, cost, weight, complexity, design risk, and vulnerability.

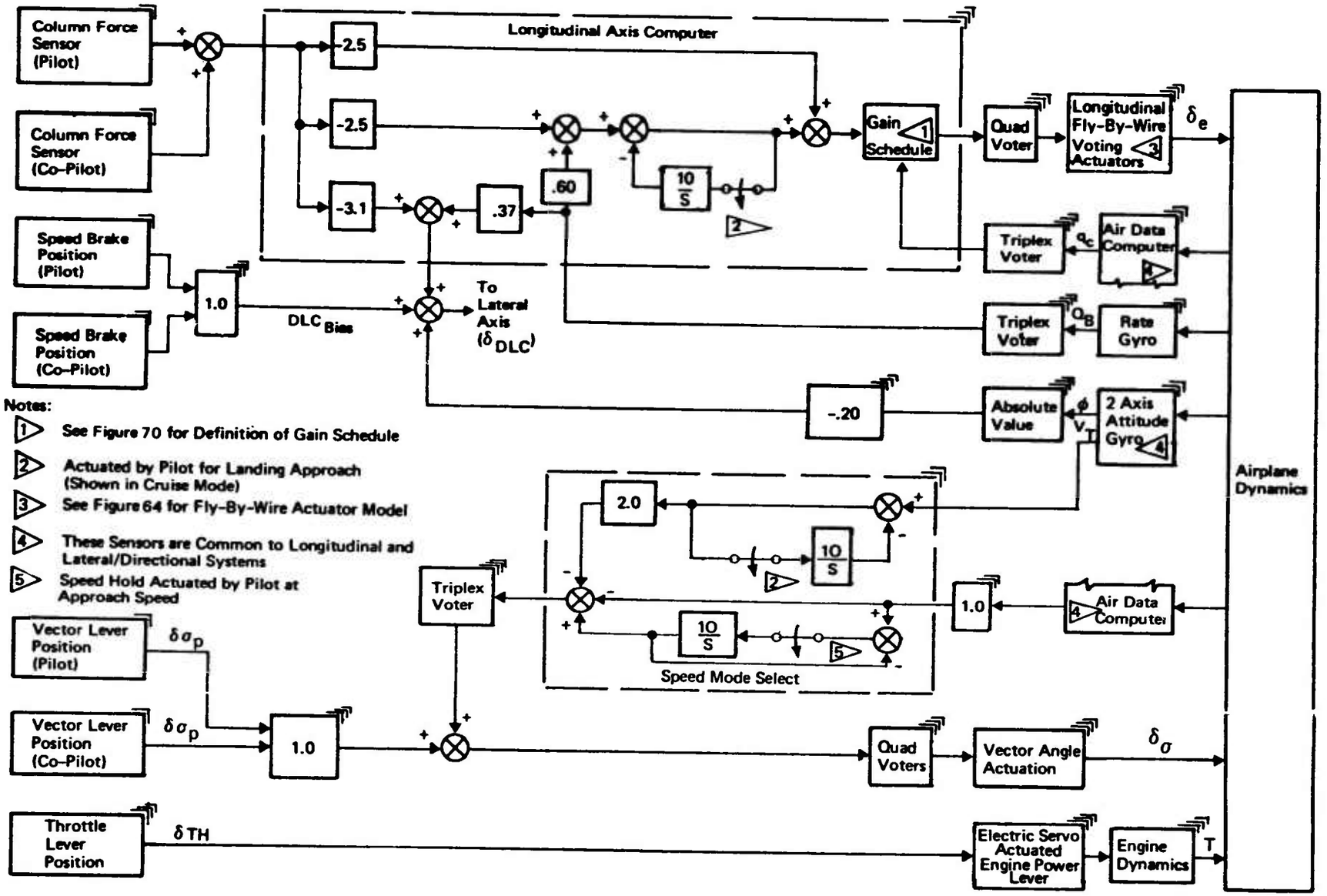

Figure 71: Longitudinal Control System Mechanization Diagram System SPO2A

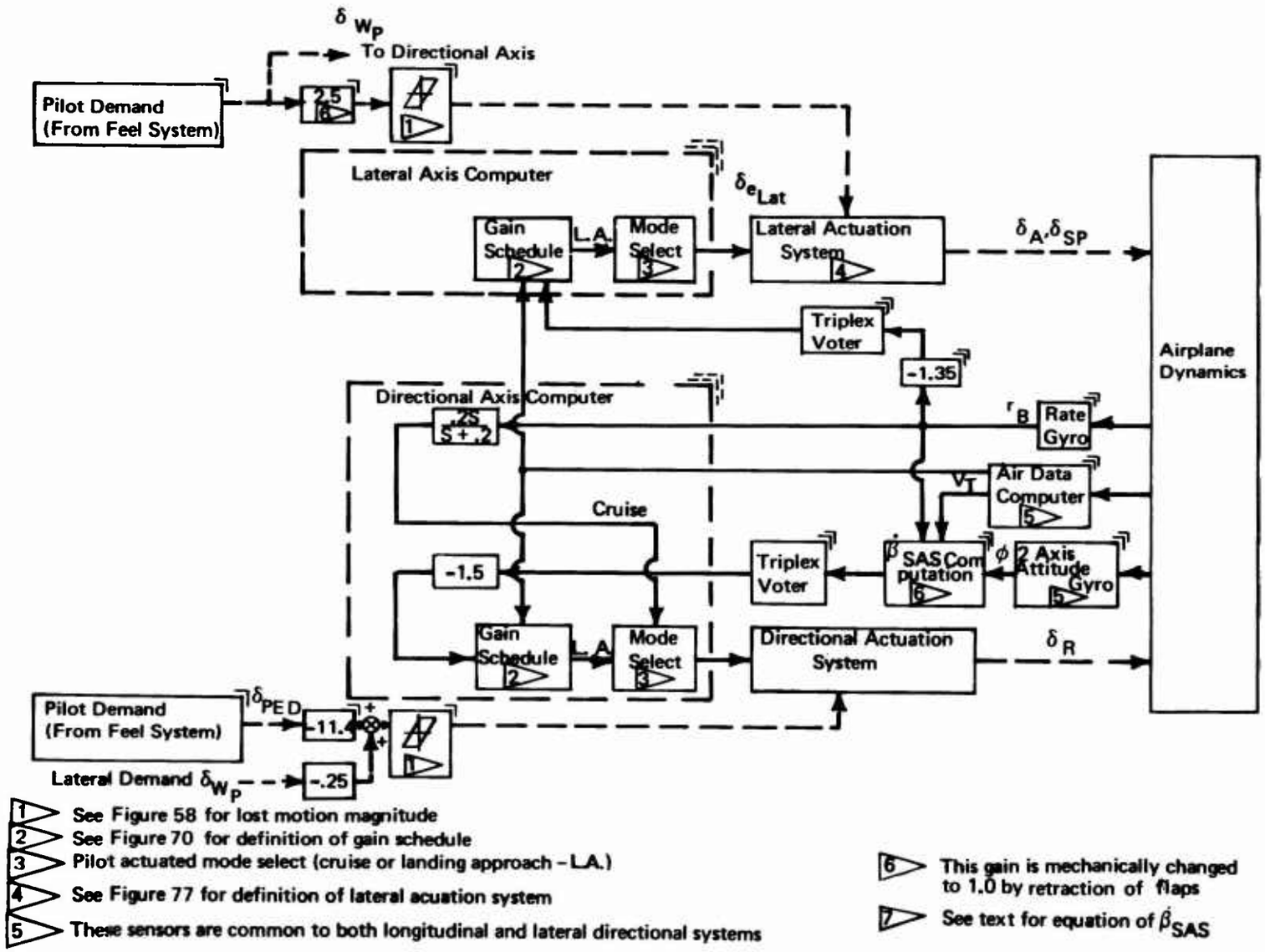

Figure 72: Mechanization Diagram SR20

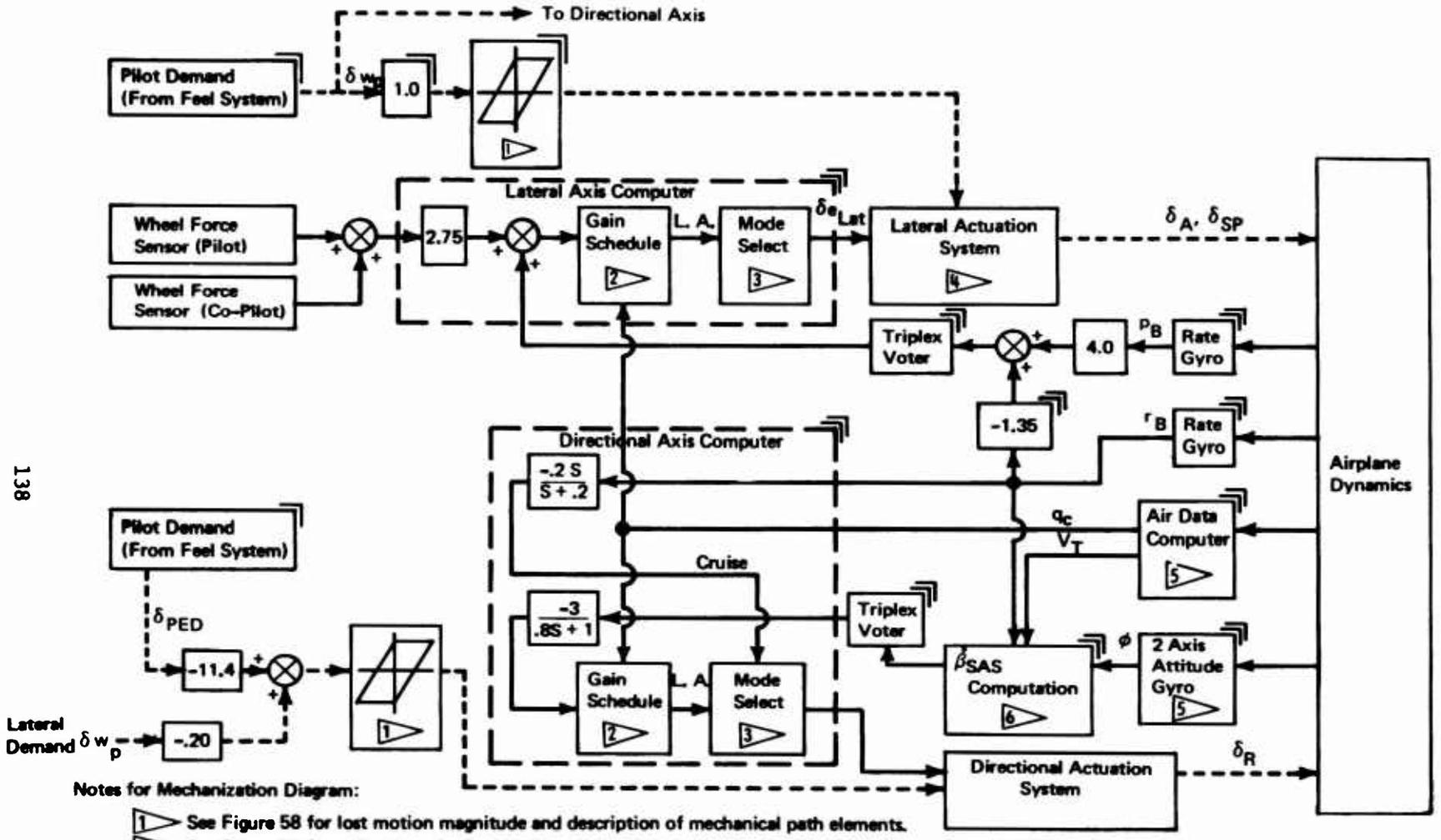

Notes for Mechanization Diagram:

1. See Figure 58 for lost motion magnitude and description of mechanical path elements.
2. See Figure 70 for definition of gain schedule.
3. Pilot actuated mode select (cruise or landing approach – L.A.)
4. See Figure 77 for definition of lateral actuation system.
5. These sensors are common to both longitudinal and lateral directional systems.
6. See text for equation of $\dot{\beta}_{SAS}$.

Figure 73: Mechanization Diagram SR21

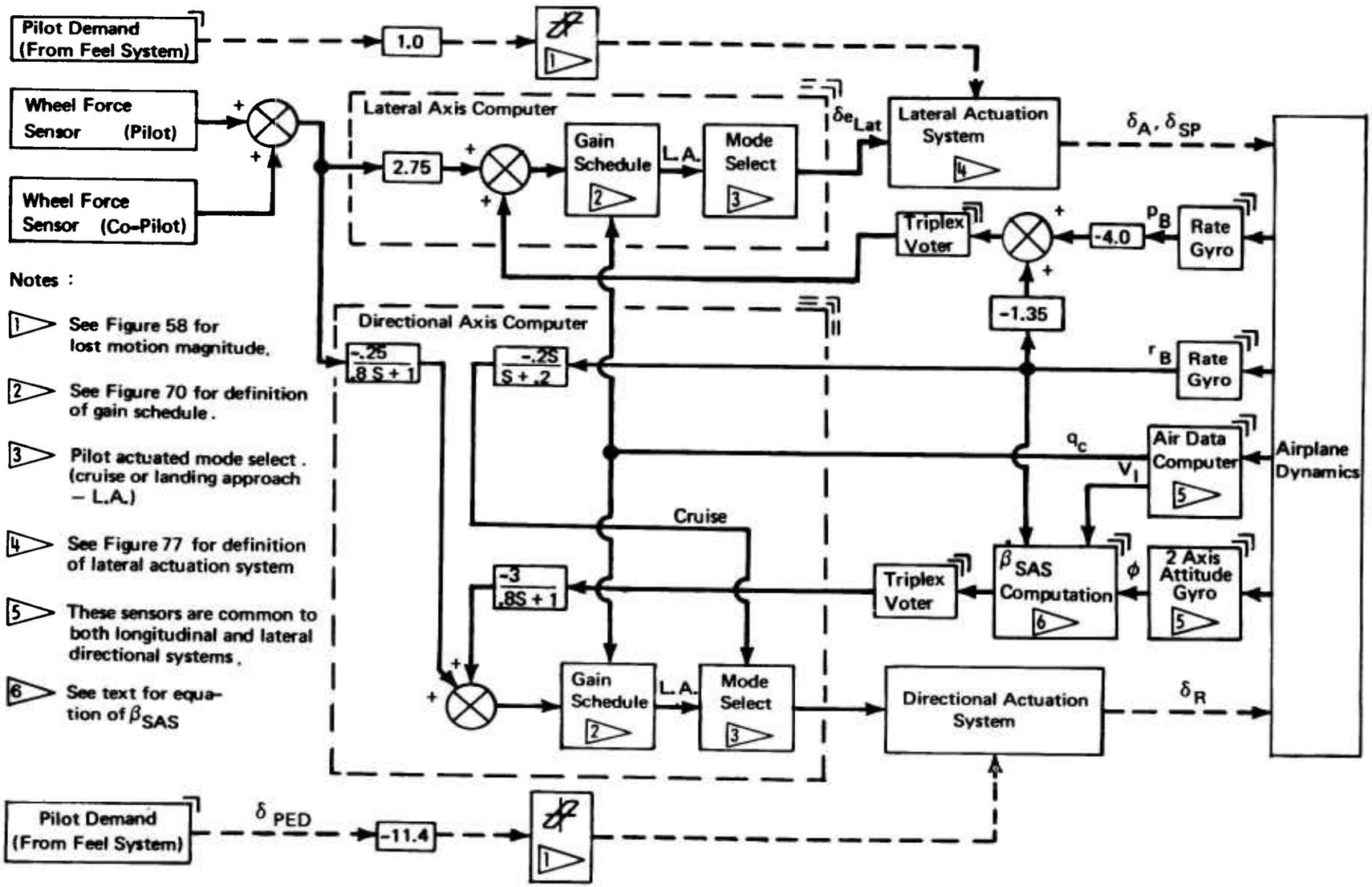

Figure 74 : Mechanization Diagram CR20

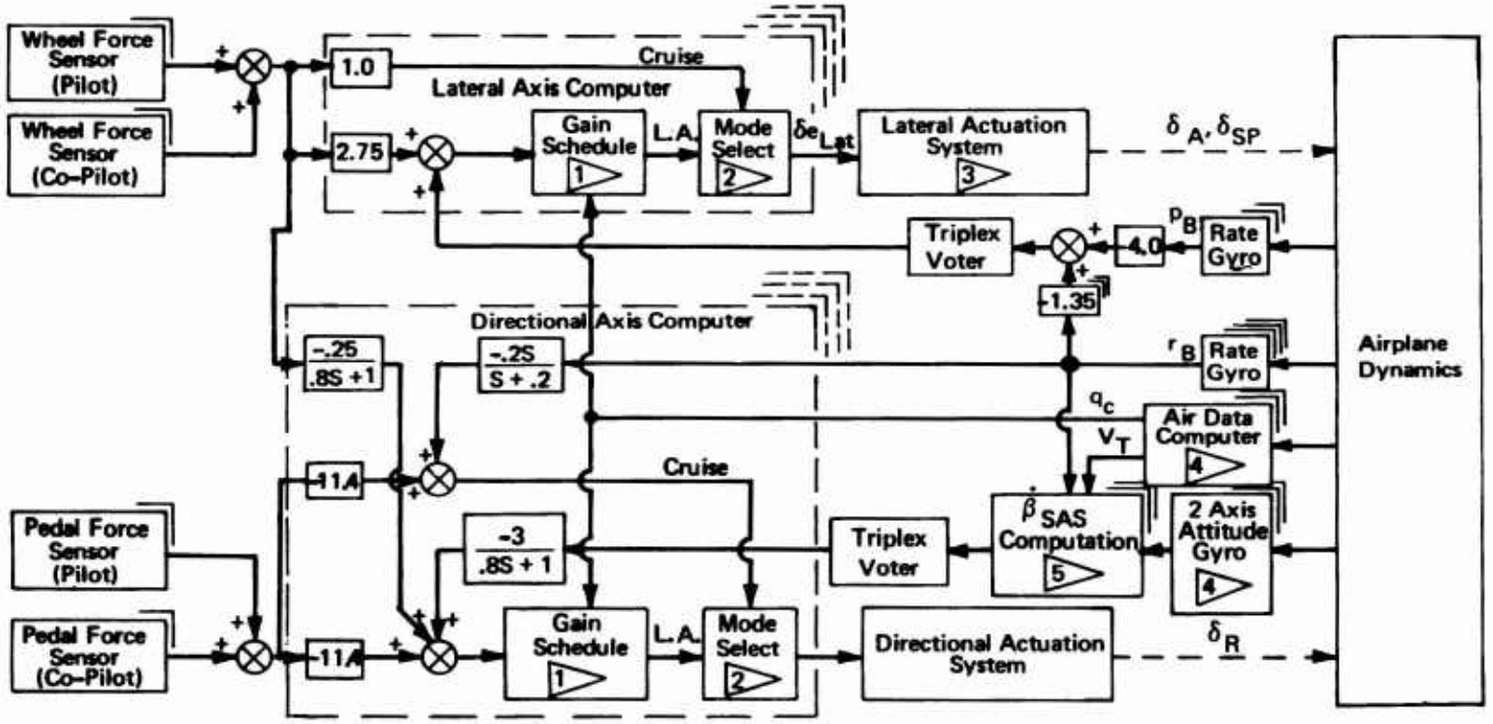

Notes for Mechanization Diagram:

1. See Figure 70 for definition of gain schedule
2. Pilot actuated mode select (cruise or landing approach – L.A.)
3. See Figure 78 for definition of lateral actuation systems
4. These sensors are common to both longitudinal and lateral directional systems
5. See text for equation of $\dot{\beta}_{SAS}$

Figure 75: Mechanization Diagram FR20

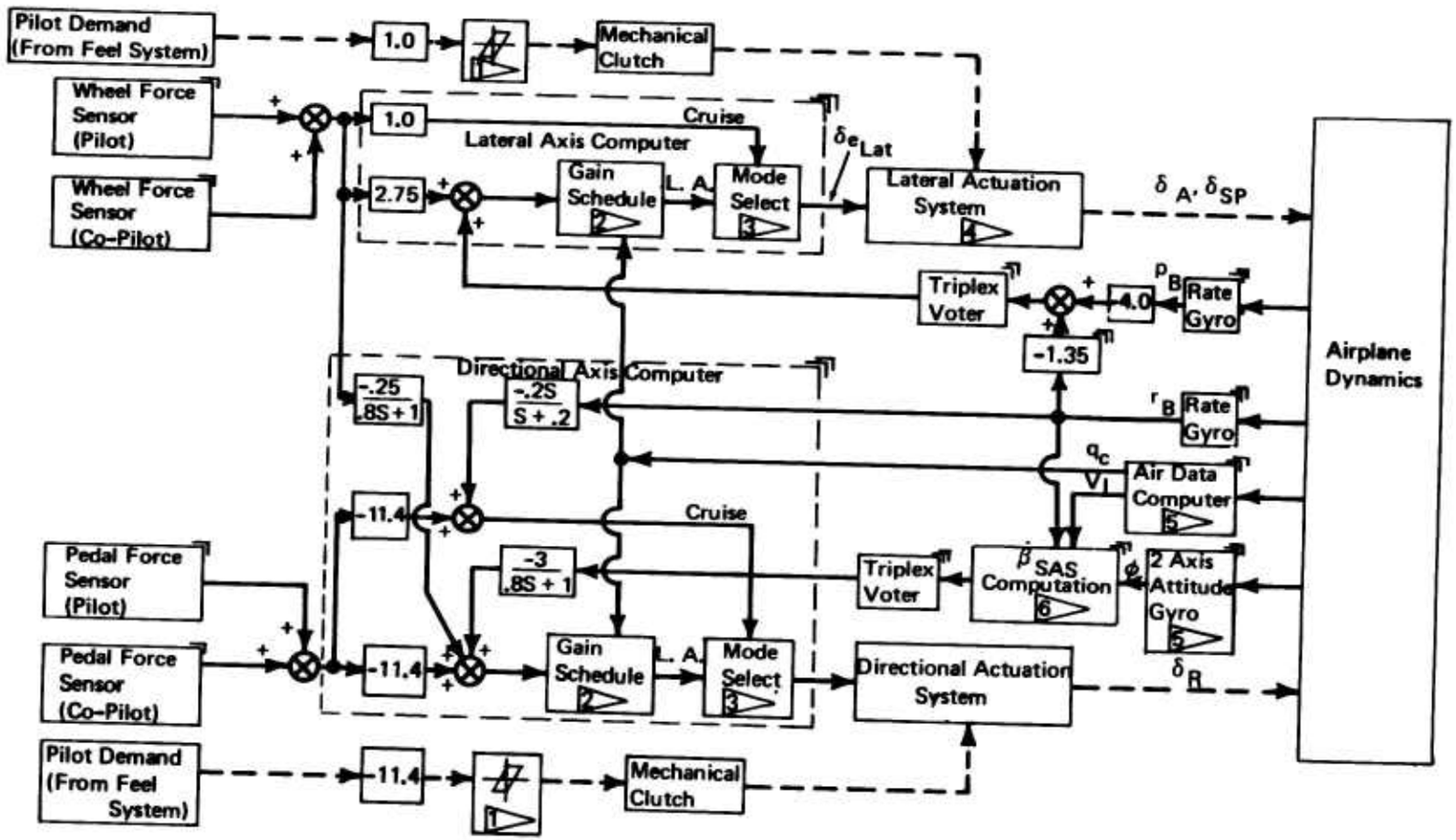

Notes for Mechanization Diagram:

1. See Figure 58 for lost motion magnitude
2. See Figure 70 for definition of gain schedule
3. Pilot actuated mode select (cruise or landing approach – L.A.)
4. See Figure 78 for definition of lateral actuation system
5. These sensors are common to both longitudinal and lateral directional systems
6. See text for equation of $\dot{\beta}_{SAS}$

Figure 76: Mechanization Diagram FR20R

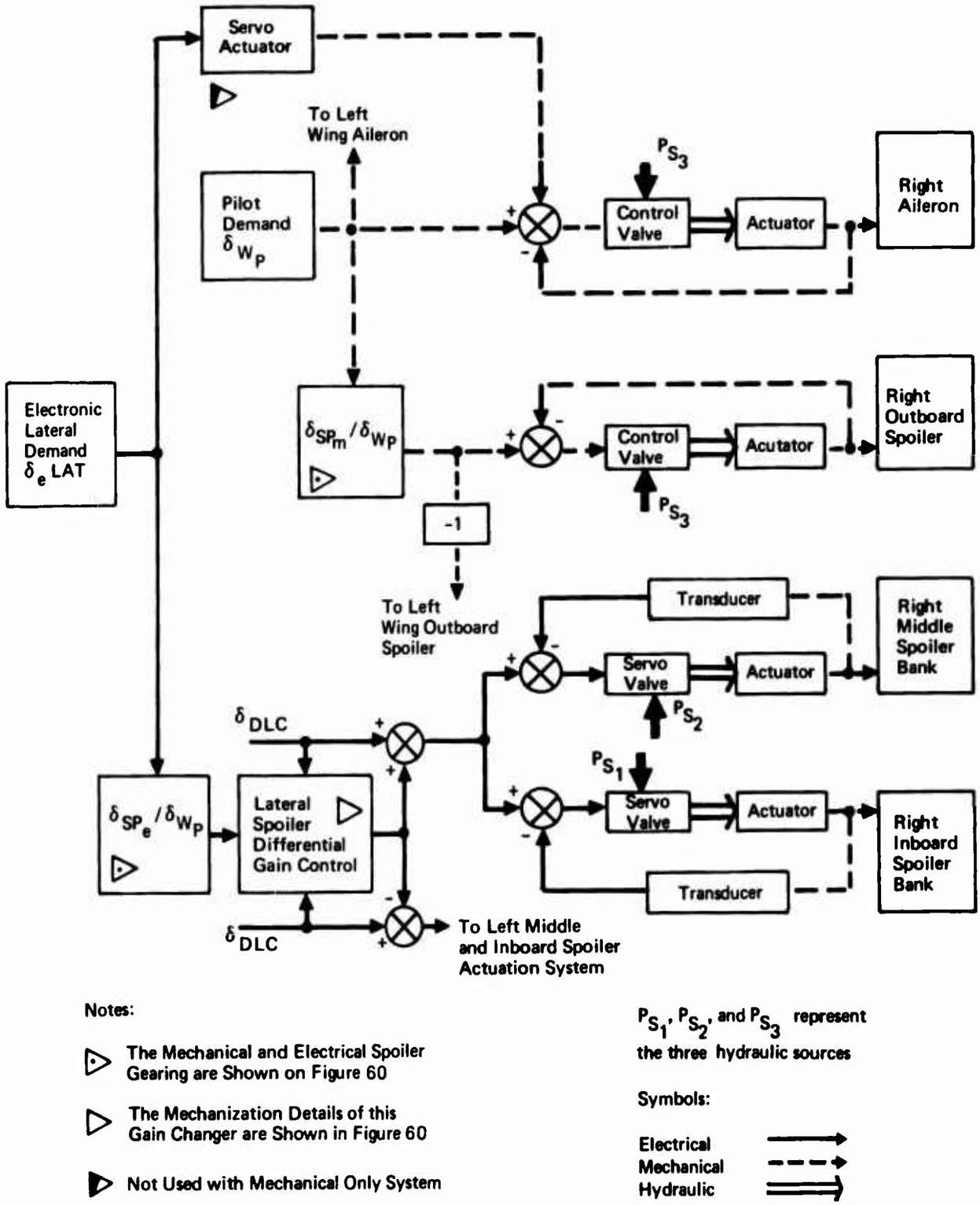

Figure 77: Lateral Actuation SAS, CAS and Mechanical Systems

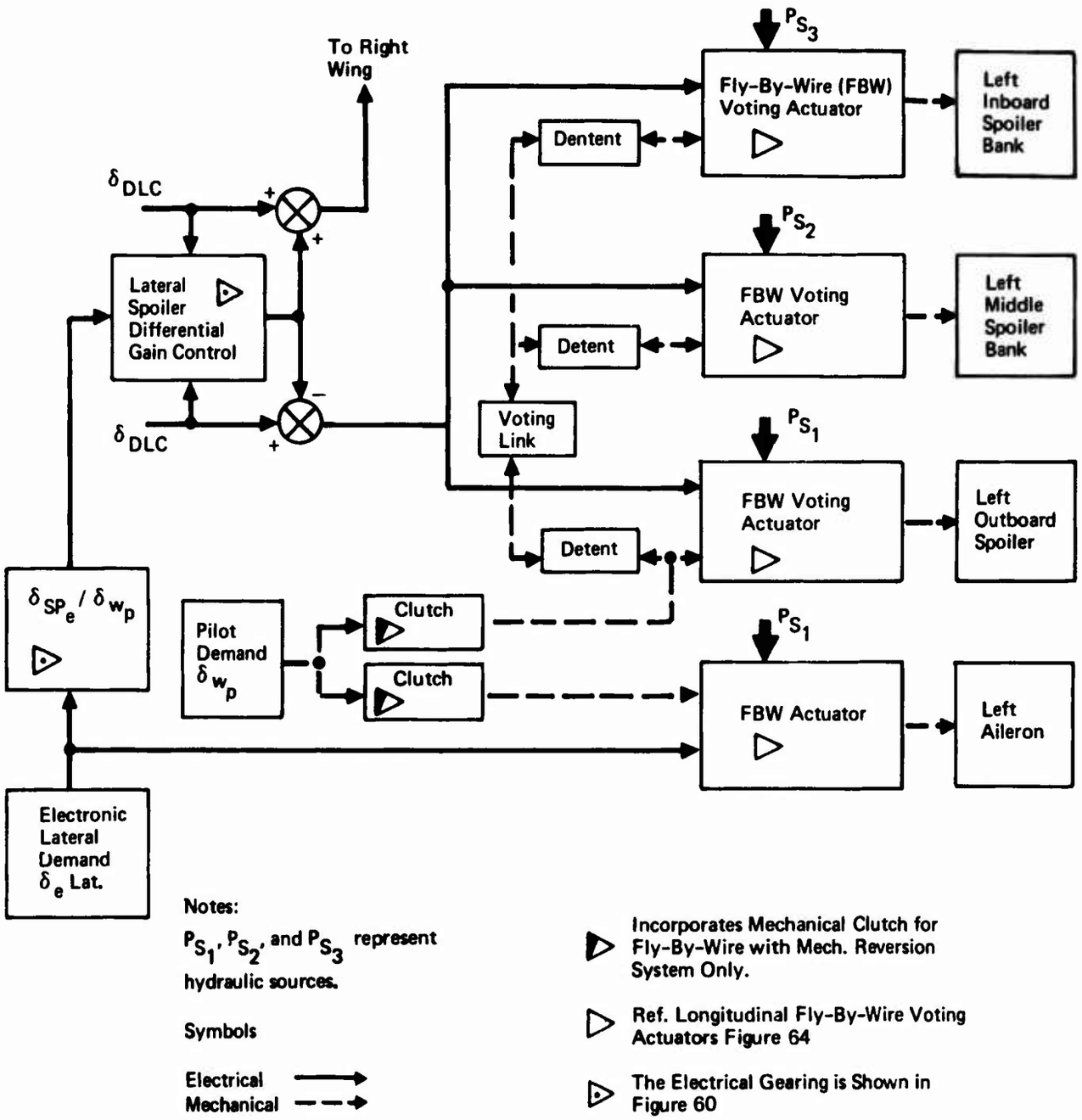

Figure 78: Lateral Fly-By-Wire and Fly-By-Wire With Reversion Actuation System

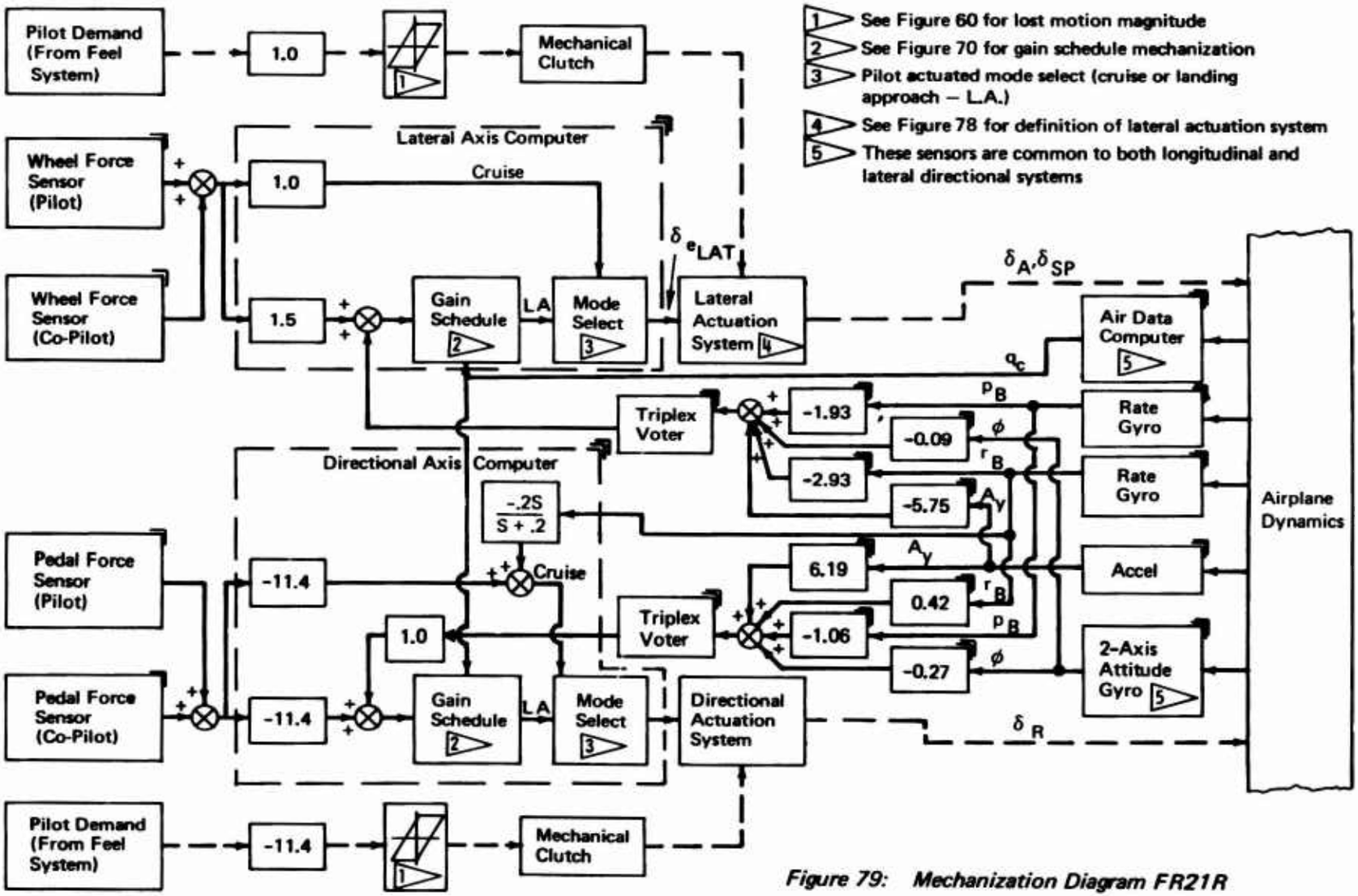

Figure 79: Mechanization Diagram FR21R

SECTION V

TRADE STUDIES

As part of the STAI two trade studies relating to control systems were performed. These were the evaluation of low "q" moment producers and the evaluation of mechanizations of potential STOL control systems. The end product of these trade studies was the selection of a control system for validation using a moving base piloted simulator.

5.1 Moment Producer Trade Study

Moment producers were first evaluated for their ability to generate rotational accelerations at low q's. Potential mechanizations of these producers were then postulated and the complexity, weight, and cost were estimated. The results are presented in Tables XII through XVI.

The first row of Tables XII and XIII identifies the candidate's ability to provide rotational acceleration in the desired axis of control. The second through fourth rows reflect the incremental weight, complexity, and cost associated with postulated candidate implementation. The computed data for the weight, cost, and complexity of each control element was normalized by its ability to develop rotational acceleration. Thus, the basic weight, cost, and complexity data are given in units of pounds/radian/sec^2, dollars/radian/sec^2, and complexity/radian/sec^2. The remaining rows contain the appropriate "control" or "cross-axis" coupling data.

The data in these tables (XII through XVI) are presented in two forms. The first number represents weighted figures-of-merit (see Section 3.1.2.5) for each parameter. The weighting factors are identified at the left of the table. Directly below these numbers, enclosed in parentheses, are the computed "row-data" for each parameter. The "row-data" have not been weighted or "normalized" by a figure-of-merit.

Those systems using blown control surfaces were evaluated by two methods. Initially it was assumed that sufficient bleed air would be available from the engines to provide the necessary blowing for any single candidate control surface. The appropriate data for this assumption are identified as "engine bleed" blown systems. When multiple surface blowing is contemplated or engine bleed is not adequate, an auxiliary air source is required. In the alternate analysis of the blown control elements, an auxiliary power unit (APU) was included in the postulated system. The data for this alternative is identified as "APU" blown systems.

It has been previously noted that a mechanical flap/vectored thrust airplane requires the reservation of a large portion of the wing trailing edge for high-lift flaps. Therefore, the performance of lateral control candidates has been separated into three groups. In Table XII, those candidates that can be mounted outboard of the flaps are identified and their relative performance is compared. Although spoilers and flaperons were investigated in this outboard region, they were not as effective as the ailerons. When the blown ailerons are drooped to maintain high-lift capability, the control power drops drastically.

TABLE XII

MOMENT PRODUCER TRADE STUDY SUMMARY
LATERAL CONTROL CANDIDATES MOUNTED OUTBOARD OF HIGH LIFT FLAPS

TRADE STUDY PARAMETERS	WEIGHTING FACTOR	AILERONS				SPOILERS			FLAPERONS	
		BLOWN (2)	DOUBLE HINGE	DROOPED 50 DEG BLOWN (2)	SINGLE HINGE	SLOTTED DEFLECT.	VENTED	PANEL	TRIPLE SLOTTED	DOUBLE SLOTTED
Control Power ($\dot{p}$)	1.0	1.00 (.302)	5.29 (.199)	7.33 (.150)	8.38 (.125)	5.08 (.204)	7.17 (.154)	9.79 (.091)	9.50 (.098)	10.0 (.086)
Weight ($\Delta W/\dot{p}$)	.6	1.43 (4305)	2.18 (5658)	4.09 (9113)	2.49 (6222)	.60 (2812)	.68 (2960)	1.49 (4414)	5.80 (12205)	6.0 (12563)
Complexity ($Cx/\dot{p}$)	.4	1.79 (20.53)	2.15 (24.12)	4.0 (42.6)	3.07 (33.33)	.40 (6.68)	.51 (7.76)	.95 (12.16)	1.44 (17.02)	1.50 (17.69)
Cost ($\$/\dot{p}$ x10^{-3})	.3	1.20 (146)	.72 (102)	2.83 (294)	3.00 (310)	.31 (64.4)	.35 (68.7)	.30 (63.7)	1.67 (189)	1.54 (177)
Control Coupling										
($\dot{U}/\dot{p}$)	1.0	.52 (.868)	.32 (.529)	.24 (.394)	.39 (.646)	.43 (.721)	.37 (.621)	.34 (.557)	.03 (.050)	.09 (.1511)
($\dot{W}/\dot{p}$)	1.0	0 (0)	0 (0)	0 (0)	0 (0)	6.16 (6.22)	6.14 (6.20)	6.16 (6.23)	6.02 (6.08)	5.96 (6.02)
($\dot{R}/\dot{p}$)	1.0	0 (0)	0 (0)	6.53 (.147)	0 (0)	.29 (.0065)	.17 (.0039)	.33 (.0074)	1.59 (.0357)	1.14 (.0257)
$\dot{Q}/\dot{p}$	1.0	0 (0)	0 (0)	0 (0)	0 (0)	.58 (.0313)	.62 (.0335)	.86 (.0467)	0 (0)	0 (0)
Rating Factor (1)		5.94	10.66	25.02	17.33	13.85	16.01	20.22	26.05	26.23
Rank		1	2	7	5	3	4	6	8	9

(1) The lower rating factors indicate best operation.
(2) "Engine Bleed" blowing system.

TABLE XIII

MOMENT PRODUCER TRADE STUDY SUMMARY -
LATERAL CONTROL CANDIDATES COMPATIBLE WITH "HIGH-LIFT" MECHANICAL FLAPS

TRADE STUDY PARAMETERS	WEIGHTING FACTOR	SPOILERS			FLAPERONS	
		Slot Deflector	Vented	Panel	Triple Slot	Double Slot
$\dot{P}$	1.0	1.00 (.636)	4.82 (.479)	9.49 (.289)	9.10 (.303)	10.00 (.266)
$\Delta W/\dot{P}$	.6	.60 (2812)	.68 (2960)	1.49 (4414)	5.80 (12,205)	6.0 (12,563)
$C_X/\dot{P}$	.4	.4 (6.68)	.75 (7.76)	2.19 (12.16)	3.78 (17.02)	4.0 (17.69)
Cost/$\dot{P}$	.3	.54 (64.4)	.30 (52.2)	1.76 (63.7)	3.00 (189)	2.77 (177)
$\dot{U}/\dot{P}$	1.0	.81 (1.35)	.69 (1.15)	.62 (1.04)	.05 (.09)	.17 (.28)
$\dot{W}/\dot{P}$	1.0	11.53 (11.65)	11.50 (11.62)	11.56 (11.68)	11.34 (11.45)*	11.24 (11.35)*
$\dot{R}/\dot{P}$	1.0	.29 (.0065)	.17 (.0039)	.33 (.0074)	1.59 (.0357)	1.14 (.0257)
$\dot{Q}/\dot{P}$	1.0	.58 (.0313)	.62 (.0335)	.88 (.0467)	0 (0)	0 (0)
Rating Factor		15.75	19.53	28.32	34.66	35.32
Rank		1	2	3	4	5

*The lift/roll penalty for flaperons reflects the reduction in operating $C_{L_{MAX}}$ caused by not deploying the flaps to the normal "high-lift" operating point.

In Table XIII, those roll moment producers that can be used concurrently with high-lift flaps are shown. For these candidates it is seen that all spoilers out perform the flaperons. The best spoiler is a slot deflector which is the most complicated design. The least effective is the panel spoiler which is the simplest design. It should be noted, however, that when a panel spoiler is used with a flap incorporating Fowler action, the panel spoiler acts as a vented spoiler following Fowler motion.

Further explanation is required for the control power and application of the flaperons shown in this table. At large deflections, flaps tend to increase drag more rapidly than they increase lift. Thus, the flaperons used in this study were deflected to an intermediate displacement. The roll control was obtained by differential displacements of the flaperons about this intermediate point. Since both flaps were never simultaneously deflected to their maximum lift point, some lift capability of the wing was lost. A larger wing would be required to obtain the same total lift capability that could be obtained by full symmetrical flap development. To indicate the penalty associated with this loss of lift capability, a lift-to-roll acceleration coupling term was identified that reflected the incremental loss of lift for partial versus full flap deflection.

Table XIV gives the evaluation of lateral control systems which are full span spoilers or flaperons or partial span spoilers blended with ailerons. The use of blown high-lift ailerons plus high performance spoilers provided the two best systems. Next came the system using double hinge ailerons and slot deflector spoilers, followed by slot deflector spoilers only. The all-wing flaperon provides the least control capability. Thrust modulating devices were not included in this summary table since they were incapable of providing adequate roll control power for engine failures.

It should be noted at this point that the effectiveness of control elements for generating roll acceleration are dependent on the wing taper ratio as well as wing location. For wings with taper ratios larger than four-tenths, the most effective wing location is near the wing tip. As the taper ratio is reduced, the point of maximum effectiveness moves inboard. Thus, the percent of total roll power provided by tip mounted elements varies with wing taper ratio. [Note: The relative performance of each alternate candidate shown in Tables XII and XIII would remain the same for all wing taper ratios. However, the absolute control capability would be changed.]

Table XV compares the performance of the candidate directional moment producer systems. Here the best performance was obtained using a double hinged rudder with increased surface area. This included an incremental weight and cost increase associated with the surface area increase. All other candidates wre compared with the smaller surface area that was proposed for the study airplane. The blown rudder system using engine bleed gave a second best rating and the blown system with auxiliary power rated fourth. The vectoring systems using vector angle modulation were not included because they could not provide adequate directional control in the event of engine failure.

TABLE XIV

MOMENT PRODUCER TRADE STUDY SUMMARY -
LATERAL CONTROL SYSTEMS

TRADE STUDY PARAMETERS	WEIGHTING FACTOR	ALL SPOILER		ALL FLAPERON	ENGINE BLEED BLOWN AILERON		APU BLEED BLOWN AILERON		DOUBLE HINGE AILERON	
		Slot Deflector	Vented	Triple Slot	S/D Spoiler	Vented Spoiler	S/D Spoiler	Vented Spoiler	S/D Spoiler	Vented Spoiler
$\dot{p}$	1.0	2.34 (.898)	5.81 (.683)	10.00 (.423)	1.00 (.981)	3.66 (.816)	1.00 (.981)	3.66 (.816)	2.66 (.878)	5.37 (.713)
$\Delta W/\dot{p}$	.6	.60 (2802)	.68 (2960)	6.00 (12,205)	.92 (3366)	1.03 (3558)	1.78 (4864)	2 06 (5359)	1.03 (3563)	1.18 (3827)
$C_x/\dot{p}$	.4	.44 (6.68)	.82 (7.76)	4.00 (17.02)	.48 (6.77)	.71 (7.46)	.54 (6.94)	.78 (7.66)	.40 (6.55)	.66 (7.29)
Cost/$\dot{p}$	.3	.53 (64.4)	.30 (52.2)	2.90 (189.2)	.54 (64.6)	.38 (56.1)	2.72 (179.5)	3.00 (194.2)	.74 (75.6)	.62 (68.7)
$R/\dot{p}$	1.0	.29 (.0065)	.17 (.0039)	1.59 (.0357)	.20 (.0044)	.15 (.0034)	.20 (.0044)	.15 (.0034)	.35 (.0078)	.17 (.0039)
$Q/\dot{p}$	1.0	.58 (.0313)	.62 (.0335)	0 (0)	.60 (.0323)	.54 (.0293)	.60 (.0323)	.54 (.0293)	.71 (.0382)	.62 (.0335)
$U/\dot{p}$	1.0	.69 (1.15)	.58 (.97)	.05 (.08)	.71 (1.19)	.62 (1.04)	.71 (1.19)	.62 (1.04)	.69 (1.15)	.58 (.97)
$W/\dot{p}$	1.0	9.78 (9.88)	9.75 (9.85)	9.61 (9.71)	7.81 (7.89)	7.05 (7.12)	7.81 (7.89)	7.05 (7.12)	7.81 (7.89)	8.13 (8.21)
Rating Factor		15.25	18.73	34.15	12.26	14.14	15.36	17.86	14.39	17.33
Rank		4	8	9	1	2	5	7	3	6

TABLE XV

MOMENT PRODUCER TRADE STUDY SUMMARY -
DIRECTIONAL CONTROL ELEMENTS

TRADE STUDY PARAMETER	WEIGHTING FACTOR	RUDDERS				
		BLOWN		DOUBLE HINGED		CONVEN-TIONAL
		Engine Bleed	APU Bleed	Increased Surface Area	Baseline Surface Area	
$\dot{R}$	1.0	1.00 (.158)	1.00 (.158)	2.43 (.145)	5.53 (.117)	10.00 (.076)
$\Delta W/\dot{R}$	.6	1.56 (129.7)	6.00 (207.2)	2.15 (140.0)	.60 (113.0)	1.41 (127.1)
$C_x/\dot{R}$	.4	3.30 (63.29)	4.00 (68.35)	.40 (42.40)	1.40 (49.57)	3.83 (67.10)
$Cost/\dot{R}$	.3	.30 (290.6)	3.00 (1012.6)	.57 (363.0)	.50 (344.3)	.45 (331.6)
$\dot{U}/\dot{R}$	1.0	.17 (1.24)	.17 (1.24)	.10 (.68)	.10 (.68)	.12 (.83)
$\dot{W}/\dot{R}$	1.0	0 (0)	0 (0)	0 (0)	0 (0)	0 (0)
$\dot{P}/\dot{R}$	1.0	1.40 (.608)	1.40 (.608)	1.71 (.745)	1.42 (.615)	1.36 (.592)
$\dot{Q}/\dot{R}$	1.0	.83 (.203)	.83 (.203)	.31 (.076)	.26 (.064)	.11 (.026)
Rating Factor		8.56	16.40	7.67	9.81	17.28
Rank		2	4	1	3	5

Table XVI compares the moment producing capability of the longitudinal moment producer systems. The double slotted elevator and the blown (engine bleed) elevator ratings were very close. If an auxiliary air bleed source was required, the rating of the blown elevator dropped drastically. T-tail double hinged elevators ranked third among longitudinal moment producers. The difference between T-tail and low-tail installation for moment producers is also shown in this table. The increased weight and cost of the geared flying T-tail elevator system resulted in this system being rated fourth.

This moment producer trade study provides a means of determining the relative ability of moment producers to satisfy the low q control capability. The basic computed data (follows figure-of-merit data in parentheses) has been included to allow a future user to assign alternate weighting factors to change the rating emphasis to suit his needs.

The user is cautioned that low q control power capability alone does not provide an adequate basis to select a specific moment producer. The unique integration considerations, which vary application to application, must be evaluated. Among these are:

(1) Linearity and resolution at low and high q.

(2) Simultaneous satisfaction of low and high q control requirements.

(3) The ability to achieve high frequency response with the candidates system.

(4) The design risks associated with relatively unproven concepts.

5.2 Control Mechanization Trade Study

Each candidate control system had many attributes. It was the purpose of the control trade study to isolate and use the important attributes as evaluation parameters in the comparison of control systems for the following general mechanization categories:

(1) Mechanical Control System (MCS)

(2) Stability Augmentation System (SAS)

(3) Control Augmentation System (CAS)

(4) Fly-by-Wire with Mechanical Revision (FBW + Rev,)

(5) Fly-by-Wire (FBW)

The specific parameters that have been selected for this evaluation are performance, safety, cost, weight, complexity, design risk, and vulnerability. Section 3.3 discussed the analytical technique used to assign a quantitative value to each of these parameters. Section 4.3 discussed the specific mechanization details for each mechanization category.

The same figure-of-merit analysis technique used in the moment producer trade study has been used in the analysis of the control system relative performance. This process provides a common quantitative base so that weighting factors, indicating relative importance for each parameter, can be used in the summation of a composite rating factor. The tabular data in this section reflect the weighted figures-of-merit for each parameter, the composite rating factors, and the relative rank of each candidate.

In several instances only one candidate has been selected for analysis in a specific mechanization category. This happened whenever performance capability was the only differentiating characteristic between the various potential mechanizations investigated. Thus, early piloted simulation studies indicated that MP02 provided better performance than MP01 or MP03. The characteristics of these and other alternate mechanizations are shown in Table VII of Section 4.2.

The separation of longitudinal from lateral/directional control candidates reduced the total selection task since only the best candidate in each mechanization category was combined to obtain the final candidate control systems. The evaluation of the longitudinal candidates is discussed first.

The tabulated values for the longitudinal control system trade study parameters are contained in Table XVII. From this data, it is seen that the SP02R (FBW + Rev) system has the best rating (i.e., lowest cumulative rating factor). The differences between this system and the second system, SP02A (FBW), were improved safety, lower complexity, and less design risk. The major factor causing the CP21 (CAS) system to be ranked third was higher weight and complexity. The MCS safety rating of 10 was due to the fact that this mechanization can only provide Level 3 flying qualities even when no failures occur:

Table XVIII contains the relative performance data for the lateral/directional control candidates. In contrast to the longitudinal axis, the lateral/directional FBW (FR20) mechanization rates better than the FBW + Rev. (FR20R) mechanization. The low rating for the FR20R system is caused by the retention of a large degree of mechanical control in the lateral axis, adversely affecting cost, weight, and complexity. The control augmented CR20 system rated third behind the two FBW systems. As in the longitudinal axis, the increased weight and complexity of the control augmented system more than offset advantages in safety, cost and design risk.*

---

*The data in these tables reflect a particular set of moment producers. The computational data in Appendix III show the impact of alternate lateral moment producers.

TABLE XVI

MOMENT PRODUCER TRADE STUDY SUMMARY -
LONGITUDINAL CONTROL ELEMENTS

TRADE STUDY PARAMETER	WEIGHTING FACTOR	TEE TAIL							LOW TAIL						
		ELEVATORS					FLYING TAIL		ELEVATORS					FLYING TAIL	
		Double Slot	Blown Engine Bleed	APU Bleed	Double Hinge	Conven-tional	Geared Elevator	Slab	Double Slot	Blown Engine Bleed	APU Bleed	Double Hinge	Conven-tional	Geared Elevator	Slab
$\dot{Q}$	1.0	3.06 (.581)	1.00 (.674)	1.00 (.674)	4.63 (.510)	8.83 (.320)	3.41 (.565)	7.04 (.401)	5.18 (.485)	3.45 (.563)	3.45 (.563)	6.48 (.426)	10.00 (.267)	5.41 (.472)	8.47 (.336)
$\Delta W/\dot{Q}$	.6	.73 (4225)	.60 (4162)	4.07 (5900)	.82 (4270)	2.65 (5187)	3.61 (5669)	2.59 (5158)	2.39 (5062)	1.87 (4795)	6.00 (6868)	2.50 (5114)	4.69 (6212)	5.84 (6788)	4.62 (6177)
$C_x/\dot{Q}$	.4	.53 (11.19)	2.49 (15.43)	2.83 (16.17)	.81 (11.76)	2.87 (16.25)	.40 (10.90)	1.78 (13.90)	1.08 (12.38)	3.48 (17.58)	3.89 (18.47)	1.65 (13.62)	4.00 (18.71)	.65 (11.44)	2.13 (14.64)
Cost/$\dot{Q}$	.3	.40 (103.6)	.61 (121.6)	2.48 (282.8)	.26 (99.9)	.30 (94.7)	1.48 (196.6)	1.06 (160.4)	.53 (114.1)	.79 (136.7)	3.00 (328.2)	.48 (110.0)	.43 (106.1)	1.66 (212.1)	1.23 (175.0)
$\dot{U}/\dot{Q}$	1.0	.08 (.24)	.20 (.62)	.20 (.62)	.11 (.34)	.14 (.41)	.10 (.30)	.06 (.18)	.09 (.28)	.25 (.76)	.25 (.76)	.14 (.41)	.17 (.50)	.11 (.32)	.07 (.22)
$\dot{W}/\dot{Q}$	1.0	3.06 (5.65)	3.06 (5.65)	3.06 (5.65)	3.06 (5.65)	3.06 (5.65)	3.06 (5.65)	3.06 (5.65)	3.68 (6.85)	3.68 (6.85)	3.68 (6.85)	3.68 (6.85)	3.68 (6.85)	3.68 (6.85)	3.68 (6.85)
Rating Factor		7.86	7.96	13.64	9.79	17.85	12.06	15.59	12.95	13.52	20.27	14.93	22.97	17.35	20.20
Rank		1	2	7	3	11	4	9	5	6	13	8	14	10	12

(Page 154 Blank)

TABLE XVII

CONTROL MECHANIZATION TRADE STUDY SUMMARY LONGITUDINAL SYSTEMS

Evaluation Parameters	Weighting Factor	Candidate Systems									
		MP02 (MCS)	SP03 (SAS)	CP21 (CAS)	SP02A (FBW)	SP04 (FBW)	SP05 (FBW)	DP05 (FBW)	DP07 (FBW)	SP02R (FBW+Rev)	DP05R (FBW+Rev)
Performance	1.0	9.93	10.00	2.18	2.32	3.64	3.54	1.00	2.96	2.18	1.00
Safety	1.0	10.00	1.08	2.34	2.41	2.41	2.41	2.33	2.33	1.08	1.00
Cost	.6	.60	3.19	3.34	4.54	4.54	4.54	6.00	6.00	3.79	5.24
Weight	.6	.60	3.74	4.01	.91	.91	.91	5.20	5.20	1.72	6.00
Complexity	.4	.40	3.91	4.00	3.27	3.27	3.27	3.56	3.56	2.98	2.74
Design Risk	.4	.40	1.12	1.12	2.56	2.56	2.56	4.00	4.00	1.84	3.28
Vulnerability	.2	1.0	1.0	1.0	1.0	1.0	1.0	1.0	1.0	1.0	1.0
Rating Factor		22.93	24.04	17.99	17.01	18.33	18.23	23.09	25.05	14.59	20.26
System Rank		7	9	3	2	5	4	8	10	1	6

TABLE XVIII

CONTROL MECHANIZATION TRADE STUDY SUMMARY

LATERAL/DIRECTIONAL SYSTEMS - (DOUBLE HINGE AILERON)

Evaluation Parameters	Weighting Factor	Candidate System								
		MRO821 (MCS)	SR20 (SAS)	SR21 (SAS)	CR20 (CAS)	CR21 (CAS)	FR20 (FBW)	FR21 (FBW)	FR20^{R} (FBW+Rev)	FR21^{R} (FBW+Rev)
Performance	1.0	10.00	5.90	2.56	1.00	1.40	1.14	1.57	1.14	1.57
Saftey	1.0	10.00	1.01	1.00	1.01	1.06	3.78	3.83	1.04	1.10
Cost	.6	.60	4.37	4.81	4.81	4.72	5.75	5.66	6.00	5.91
Weight	.6	2.90	5.48	6.00	6.00	5.82	.80	.60	5.55	5.35
Complexity	.4	.40	2.93	3.40	3.37	3.64	2.08	2.36	3.89	4.00
Design Risk	.4	.40	1.30	1.30	1.30	1.30	4.00	4.00	4.00	4.00
Vulnerability	.2	2.0	2.0	2.0	2.0	2.0	.2	.2	.2	.2
Rating Factor		26.30	22.99	21.07	19.49	19.94	17.75	18.22	21.82	22.13
System Rank		9	8	5	3	4	1	2	6	7

The following general conclusions summarize the tables:

(1) Poor performance and safety of purely mechanical control systems preclude their selection for STOL vehicles.

(2) FBW systems possess a definite weight advantage over SAS and CAS systems.

(3) Difficulty attendant to the combination of mechanical and electrical signal paths make SAS and CAS systems more complex than FBW systems.

5.3 Final Control System Selection

The best candidates for longitudinal and lateral/directional control systems were identified and then combined to examine the best candidate systems for each mechanization category. These candidates are:

(1) Mechanical Control System - MCS (MP02/MR0821)

(2) Stability Augmentation System - SAS (SP03/SR21)

(3) Control Augmentation System - CAS (CP21/CR20)

(4) Fly-by-Wire with Mechanical Reversion - FBW + Rev. (SP02R/FR20R)

(5) Fly-by-Wire - FBW (SP02A/FR20)

The individual axis performance, cost, weight, complexity, design risk, and vulnerability data was summed to obtain the system analysis data. The system safety data had to be recomputed because some failure modes that disabled one axis of control are in reality common to several axes.

The weighted figure-of-merit data are shown in Table XIX. The control augmented system (CP21/CR20) rated above the fly-by-wire with reversion system (SP02R/FR20R). This result was initially surprising since the composite fly-by-wire system (SP02A, FR20) ranks third whereas an averaging of the individual axis ratings would have lead to the conclusion that the fly-by-wire system would be first. However, the design risk and safety scores of these mechanizations were poor. The fly-by-wire system's probability of encountering Level 3 (1.23×10^{-4} versus the target of 1.0×10^{-4}) and the probability of encountering loss of control (1.11×10^{-9} versus target of 1.0×10^{-9}) were larger than the remaining mechanizations. The differences between the various parameter rating of the first two systems were approximately offsetting, with the CAS ratings better for cost, design risk, and safety while the FBW + Rev. ratings were better for weight, complexity and vulnerability.

The fact that the MCS was ranked better than the SAS was due to the cost, weight, complexity, and design risk of the SAS. This indicates the need to exercise engineering judgment in addition to the numerical comparison. The MCS is not adequate for the mission, whereas the SAS provides a minimum of Level 2 capability.

TABLE XIX

CONTROL MECHANIZATION TRADE STUDY

Evaluation Parameters	Weighting Factor	CANDIDATE SYSTEMS				
		Mechanical (MP02/MR0821)	SAS (SP03/SR21)	CAS (CP21/CR20)	FBW (SP02A/FR20)	FBW + Rev. (SP02R/FR20R)
Performance	1.0	10.00	5.30	1.00	1.09	1.09
Safety	1.0	10.00	2.58	1.00	6.06	1.88
Cost	.6	.60	4.60	4.69	6.00	5.64
Weight	.6	1.76	5.83	6.00	.60	4.20
Complexity	.4	.40	3.95	4.00	2.87	3.75
Design Risk	.4	.40	1.43	1.43	4.00	3.48
Vulnerability	.2	2.00	2.00	2.00	.20	.20
Total Score		25.16	25.69	20.12	20.82	20.24
Rank		4*	5*	1	3	2

*See text discussion.

The nearly identical ratings of the first three systems also requires engineering judgment to determine which system is to be selected for validation by piloted simulation. For this study, the control augmented system (CP21, CR20) was selected because the failure modes of the control augmented system cause larger aircraft "upsets" than the other two mechanizations. Since the same basic control law was embodied in all three mechanizations, a successful validation of the CAS was sufficient to validate all three mechanizations. Prior to validation, the selected control systems were investigated using linear analysis to determine the sensitivity to airplane parameter variations.

The landing approach flight condition at which control system comparisons were made assumed a center of gravity at $0.32\bar{c}$ and an airspeed of 75 knots. To determine the sensitivity of the selected longitudinal CAS, System CP21, the stability was checked at fore and aft c.g. ($0.20\bar{c}$; $0.40\bar{c}$) and at airspeeds of 65 and 85 knots.

Military Specification MIL-F-83300 defines short period flying quality requirements in terms of "the second order pair of roots that primarily determine the short-term response of angle-of-attack following an abrupt pitch control input". As shown in Table XX, which lists the angle of attack to column displacement transfer function for speed and c.g. variation, the predominant poles include a root close to the origin of the s-plane. Therefore, compliance with the specification was checked by fitting the time response of an equivalent second-order pair of roots to the system time response rather than by using the poles directly. These data are plotted in Figure 80 which includes the Level 1 flying quality requirement from MIL-F-83300. As can be seen, Level 1 requirements are met throughout the c.g. and airspeed range considered.

Insight into the lateral/directional control system sensitivity was obtained by plotting the locus of the system roots for the aircraft parameter variations noted above. Root locations are compared in Figure 81 with Level 1 flying quality requirements of Military Specification MIL-F-83300. Control system gains were assumed to be fixed as airspeed and c.g. varied. It is seen that Level 1 requirements were met throughout the airspeed and c.g. range considered.

TABLE XX

ANGLE-OF-ATTACK RESPONSE OF SYSTEM SPO2

Center of Gravity (% $\bar{c}$)	Airspeed (Knots)	Angle-of-Attack/Column Position Transfer Function Degs/inch
20	75	$\frac{-.033(S-8.7)[S^2+2(.91)(.22)S+(.22)^2]}{(S+.038)(S+.31)[S^2+2(.77)(1.14)S+(1.14)^2]}$
30	75	$\frac{-.033(S-84)[S^2+2(.91)(.22)S+(.22)^2]}{(S+.028)(S+.36)[S^2+2(.87)(.98)S+(.98)^2]}$
40	75	$\frac{-.033(S-8.1)[S^2+2(.90)(.22)S+(.22)^2]}{(S+.014)(S+1.10)[S^2+2(.93)(.51)S+(.51)^2]}$
30	65	$\frac{-.027(S-7.5)[S^2+2(.90)(.24)S+(.24)^2]}{(S+.044)(S+.48)[S^2+2(.81)(.79)S+(.79)^2]}$
30	85	$\frac{-.038(S-9.4)[S^2+2(.91)(.21)S+(.21)^2]}{(S+.025)(S+-30)[S^2+2(.88)(1.16)S+1.16^2]}$

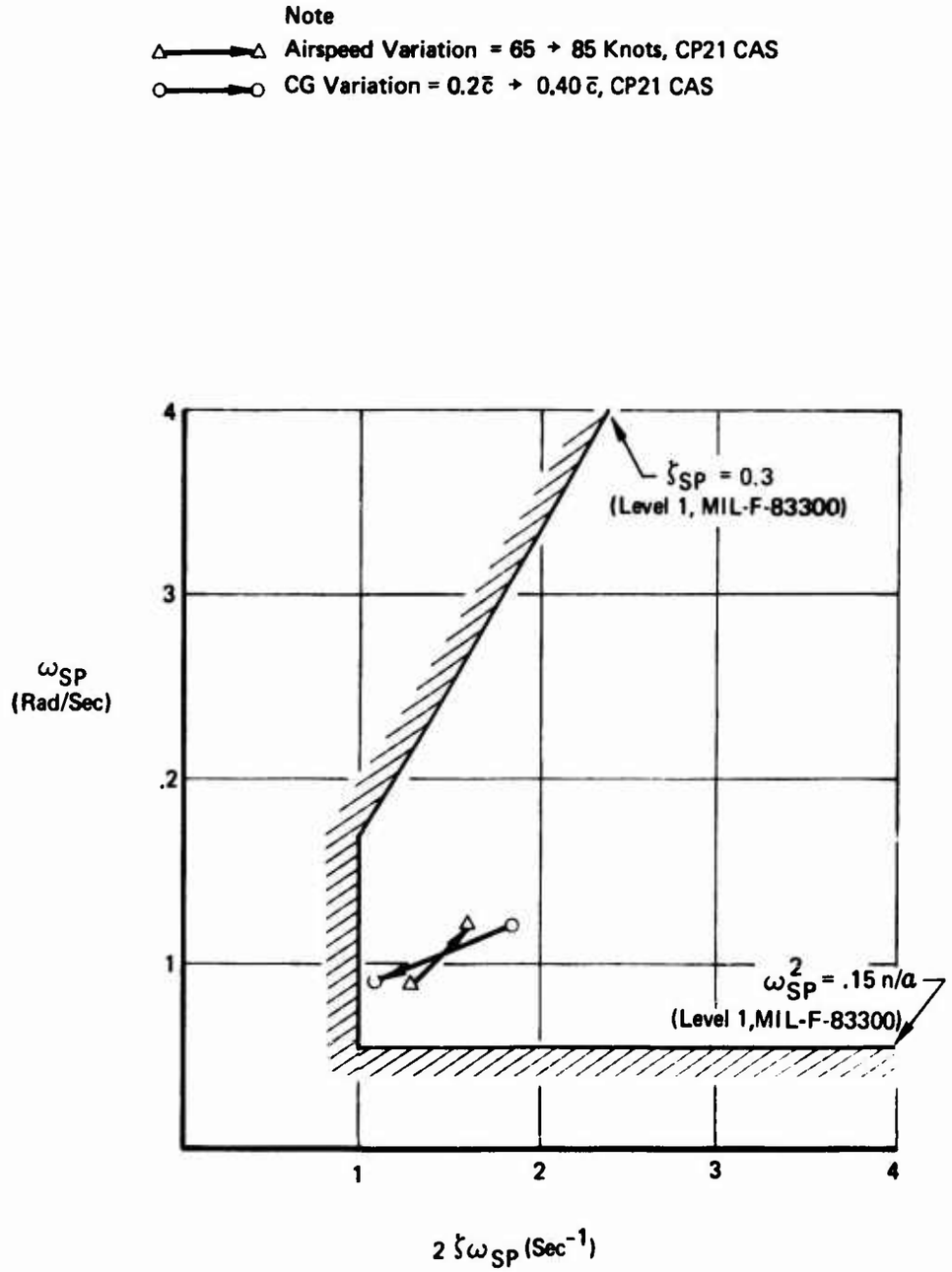

Figure 80: Sensitivity of System CP21 to Airspeed and Center of Gravity Variations

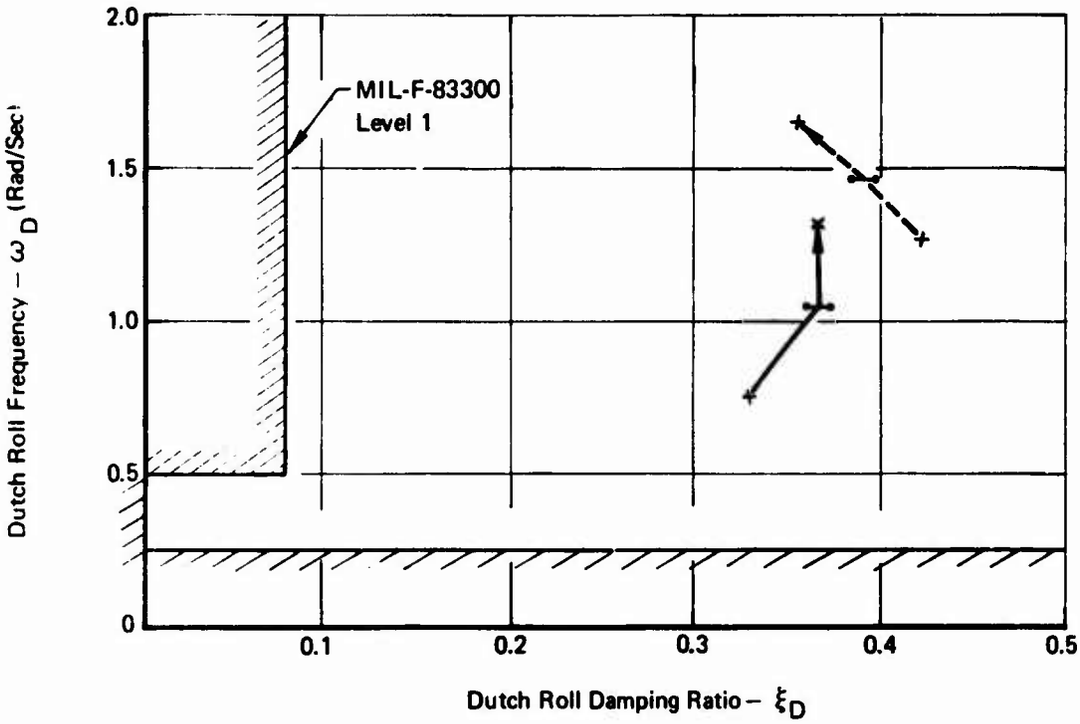

Note:

x– – –→x Airspeed Variation = 65, 75, 85 Knots, System CR 20
·– – – –· CG Variation = 0.2, 0.3, 0.4$\bar{c}$, System CR 20
x————→x Airspeed Variation = 65, 75, 85 Knots, System FR21
·————· CG Variation = 0.2, 0.3, 0.4$\bar{c}$, System FR21

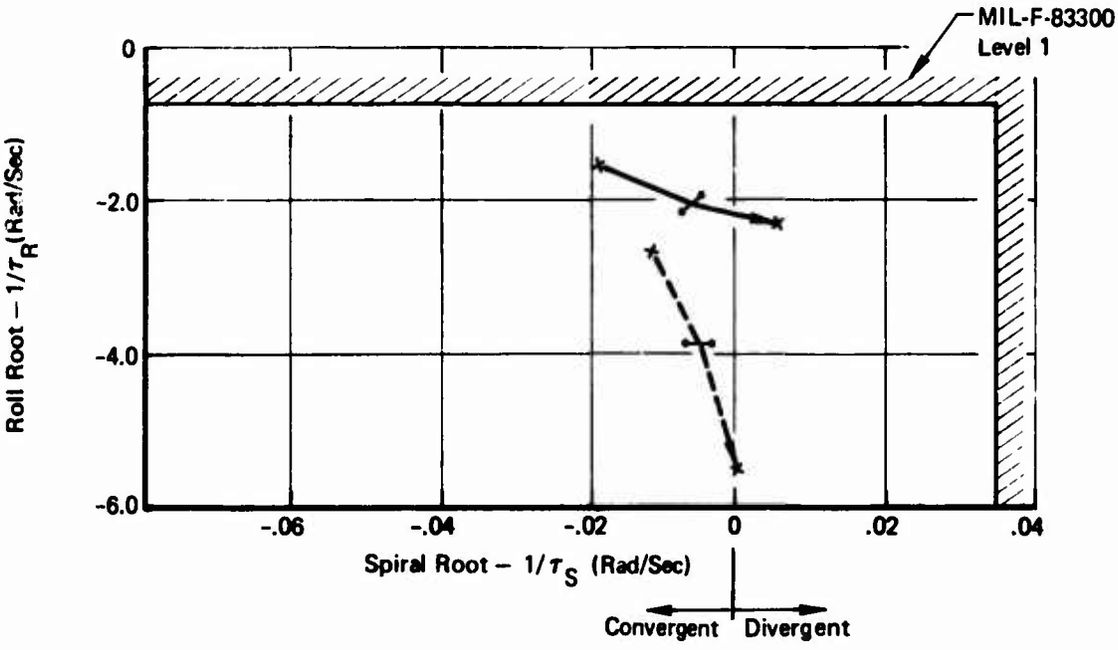

Figure 81: Sensitivity of Systems CR20, FR21 to Airspeed and Center of Gravity Variations

SECTION VI

CONCLUSIONS AND RECOMMENDATIONS

6.1 Conclusions

The control technique developed in this study, based on modulation of thrust vector angle to control speed and on modulation of elevator in conjunction with direct lift control to control flight path, can provide excellent flying qualities despite the problems of low dynamic pressure and severe aerodynamic cross coupling inherent in the high performance STOL flight condition. No special piloting technique is required for the STOL landing task, as would have been the case if vector angle were not modulated. Furthermore, this control technique can be applied to airplanes using powered lift concepts other than Vectored Thrust/Mechanical Flaps.

In particular, the Boeing AMST Prototype airplane will be equipped with Upper Surface Blowing (USB) flaps to provide powered lift and augmented aerodynamic lift. This airplane can use a very similar control concept, in which the USB flap angle is modulated (like the thrust vector angle in the system studied in this report) to control speed.

6.1.1 Moment Producer Study

Aerodynamic moment producers compatible with the high-lift requirements of the STOL mission are sufficient, and out perform the propulsive candidates. This is because:

(1) Engine bleed air can be used more effectively to develop control moments by augmenting the aerodynamic lift by BLC than by directing the air flow through a reaction nozzle.

(2) Differential engine thrust modulation or differential vector angle modulation prove unsatisfactory when engine-out control and sustained propulsive lift are required simultaneously.

In this study, the roll control power was designed to provide the capability of rolling 30 degrees in 1.8 seconds as required by military specification. This resulted in a difficult mechanization task to provide a roll sensitivity acceptable to the pilots.

(1) The rate of change in airplane heading, for a given bank angle, is inversely proportional to airspeed. Bank angles below 20 degrees satisfied heading rate requirements for all maneuvers including lateral offsets prior to touchdown. If there is no other factor dictating a large roll power requirement (i.e., engine out trim plus minimum maneuver), the requirement for 30 degrees in 1.8 seconds would not seem justified.

(2) The use of certain control systems greatly reduces the magnitude of aircraft "upset" caused by atmospheric disturbances or system failures. Thus, the control power needed to correct an upset is reduced.

The moment producers were rated considering control power, weight, cost, complexity, and undesired "coupled-response." The specific comparative ratings are shown in sub-section 5.1.

6.1.2 Control Law Development

Satisfactory control laws were defined for both longitudinal and lateral/directional control. This study indicated:

(1) In the longitudinal case, speed control must be decoupled from flight path control. As for lateral/directional control, turn coordination must exist concurrently with good "de-crab" characteristics.

(2) Compliance with MIL-F-83300 requirements does not guarantee satisfactory handling qualities. This was evident in the lateral/directional axes where satisfactory systems required turn coordination characteristics superior to MIL-F-83300 requirements. (See Paragraph 4.2.3 of Volume V, Part II.)

(3) The design philosophy used herein is superior for the definition of control systems. In this philosophy:

(a) The airplane characteristics were established based upon a configuration developed for maximum STOL performance and,

(b) Control laws were defined using suitable feedback techniques to achieve the desired control system/aircraft response characteristics.

This philosophy led directly into the mechanization phase, since the required feedback paths were defined at the same time as acceptable aircraft response characteristics. This contrasts with the other commonly used philosophy where the aircraft characteristics are analytically modified one at a time until a satisfactory response is obtained. It is then necessary to determine how feedback techniques can be employed to obtain aircraft characteristics equivalent to those achieved by arbitrary parameter modification. This is extremely difficult when multiple feedback loops are used.

(4) The STOL airplane requires substantial augmentation in the longitudinal and lateral/directional control axes.

6.1.3 Control System Mechanization

The comparative analysis of section 5.3 shows that three different mechanization techniques provide approximately the same rated performance. The control augmented system (CAS) exhibited a superior safety rating, good cost and design risk characteristics, and inferior weight and complexity ratings. The fly-by-wire with reversion (FBW + Rev) system exhibited good safety characteristics with intermediate cost, weight, complexity, and design risk ratings. The fly-by-wire (FBW) system had

inferior safety, cost, and design risk rating while exhibiting the best complexity and weight characteritics. Since safety is extremely important, either the CAS or the FWB + Rev. systems were considered preferable.

The definitions of control system mechanizations, depicted in Figure 57, were based upon current industry and Air Force practice which combines the definition of control law and mechanization techniques into a single descriptive phrase. The task of this study was somewhat ambiguous because of these combined definitions.

This ambiguity could be eliminated from future studies if the control law techniques were completely separated from the control mechanization techniques. This separation can be accomplished by independent definitions of these two characteristics. Control law techniques could be: 1) stability augmentation; 2) control augmentation; 3) response command; and 4) automatic. These control law techniques consider only the sensed variables required to define the control process and do not include mechanization techniques which could be: 1) electromechanical with continuous "series" or "parallel" summation; 2) electromechanical with single or redundant standby systems (this includes normally isolated mechanical paths); and 3) fly-by-wire. The electromechanical integration can occur prior to the control surface (signal path summation) or can utilize separate control surfaces (aerodynamic summation).

6.2 Recommendations

Additional study is required in the following three areas:

(1) Lateral/Directional systems were acceptable to the pilots even though they did not satisfy the heading response requirements of six degrees in one second. (See Paragraph 3.3.10.1 of MIL-F-83300.) It is possible that the specification requirement may be overly stringent.

(2) The turn coordination requirements (Paragraphs 3.3.8 through 3.3.8.4) of MIL-F-83300 may require alteration to assure satisfactory handling qualities for the lateral/directional systems. As an example, the specification allows an $|\Delta\beta/\phi_1|$ ratio of .8 to 1.65 for varying values of sideslip phase angle ψ_β. All control systems in this study with pilot ratings of three or less had $|\Delta\beta/\phi_1|$ ratios of .3 or less. (See Paragraph 4.2.3 of Volume V, Part II.)

(3) The Air Force can provide a key role in establishing separate definitions for control law techniques and control mechanization techniques. These definitions could be used by all contractors. Such industry standardization would improve the Air Force's ability to compare control systems proposed by different potential suppliers.

APPENDIX I
MOMENT PRODUCER BACKGROUND DATA

I.1 Purpose

This appendix contains the background data used to analyze potential moment producer capabilities. Also included herein are the computed data for the purpose of comparing moment producer relative rating. A brief discussion of the data is included to provide further insight in the analysis processes used in this study.

I.2 Aerodynamic Characteristics of Moment Producer Candidates

The complete aerodynamic definition of the candidate moment producers are shown in Tables XXI through XXV. This data was obtained from several sources which are identified in the following paragraph.

For the rudder, aileron, flaperon, and horizontal tail elements, two-dimensional unblown estimates of control surface lift coefficient were based on the C_L from Section 4.1.1.2 of Reference 16 and control effectiveness from Reference 17. Two-dimensional drag estimates and hinge moments were obtained from Reference 16 (Sections 6.1.7 and 6.1.3). Blown control surface data (C_L and C_μ) were obtained from Reference 18. Potential flow estimates using data from Reference 19 were used to predict hinge moments for blown control surfaces at deflections greater than 30°. Spoiler lift coefficients were obtained from Reference 16 (Section 6.1.1.1) for a panel spoiler with wing flaps undeflected. A "flap effect" correction factor was obtained from Reference 20. Correction factors for the plug, vented spoiler, and spoiler-slot-deflector were obtained from Reference 21 and hinge moments from References 20 and 21.

Definition of chord ratios and aileron droop angles are shown in Figures 82 and 83. The definition of the flaperon droop and control angles are shown in Figure 84.

I.3 Initial Computation of Moment Producer Relative Control Power Capability

The relative performance capability of the aerodynamic candidates was derived using the two-dimension infinite span characteristics (i.e., aerodynamic section properties) defined in Section I.2 above. The effective control area used in computing the net aerodynamic force was computed by dividing the total control surface area into incremental areas proportional to control element span and spanwise location. In Figure 8 the major geometric characteristics are identified. The equation for computing effective area is derived below.

TABLE XXI

MOMENT PRODUCTER STUDY DATA SHEET - FORM 1

NORMALIZED CAPABILITY

(1) CANDIDATE MOMENT PRODUCER	(2) % CHORD / SEGMENT RATIO	(3) CONTROL $\frac{\delta_{MAIN}}{\delta_{AFT}}$ (Degs)	(4) DROOP $\frac{\delta_{MAIN}}{\delta_{AFT}}$ (Degs)	(5) SECTION ΔC_{L}/deg.	(6) SECTION ΔC_{D}/deg.	(7) SECTION $\Delta C_{L_{Max}}$	(8) SECTION $\frac{\Delta C_{L_{Max}}}{C_{\mu}}$	(9) SECTION $C_{\mu_{Max}}$	(10) SECTION $\Delta C_{D_{Max}}$	(11) SECTION ΔC_{D} DUE TO BLC THRUST RECOVERY		(12) CRITICAL FLIGHT CONDITION FOR HINGE MOMENT COEFF.	(13) HINGE LINE LOCATION % CHORD	(14) SECTION MAXIMUM HINGE MOMENT COEFF. C_{h} Max.
										$\delta_{r} \leq 10°$	δ_{r}=Max			
A. Rudder														
1. Single Hinged	20/0	30/0	0/0	.0494	.00045	1.015	- - -	0	.042	- - -	- - -	G.E.O.	20	± .244
	35/0	30/0	0/0	.0665	.00165	1.54	- - -	0	.107	- - -	- - -	G.E.O.	35	± .305
	50/0	30/0	0/0	.0800	.0040	1.96	- - -	0	.192	- - -	- - -	G.E.O.	50	± .363
2. Double Hinged	20/20	30/30	0/0	.0675	.00047	1.28	- - -	0	.047	- - -	- - -	G.E.O.	20	± .420
	20/35	30/30	0/0	.0748	.00048	1.40	- - -	0	.052	- - -	- - -	G.E.O.	20	± .460
	20/50	30/30	0/0	.0812	.00051	1.585	- - -	0	.057	- - -	- - -	G.E.O.	20	± .470
	35/20	30/30	0/0	.0910	.00168	1.940	- - -	0	.117	- - -	- - -	G.E.O.	30	± .55
	35/35	30/30	0/0	.1020	.00175	2.2	- - -	0	.127	- - -	- - -	G.E.O.	30	± .59
	35/50	30/30	0/0	.1115	.00195	2.45	- - -	0	.142	- - -	- - -	G.E.O.	30	± .594
	50/20	30/30	0/0	.1115	.00406	2.53	- - -	0	.287	- - -	- - -	G.E.O.	50	± .587
	50/35	30/30	0/0	.1250	.00430	2.88	- - -	0	.227	- - -	- - -	G.E.O.	50	± .670
	50/50	30/30	0/0	.1360	.00470	3.17	- - -	0	.252	- - -	- - -	G.E.O.	50	± .700
3. Chordwise Blowing	20/0	60/0	0/0	.0494	.00045	2.64	19.4	.0590	.140	-.0590	-.0470	G.E.O.	20	± .66
	35/0	60/0	0/0	.0665	.00165	3.26	13.4	.0590	.340	-.0590	-.0470	G.E.O.	35	± .66

SEE TABLE XXV FOR NOTES

TABLE XXII

MOMENT PRODUCTER STUDY DATA SHEET - FORM 1

NORMALIZED CAPABILITY

(1) CANDIDATE MOMENT PRODUCER	(2) % CHORD SEGMENT RATIO	(3) CONTROL $\frac{\delta_{MAIN}}{\delta_{AFT}}$ (Degs)	(4) DROOP $\frac{\delta_{MAIN}}{\delta_{AFT}}$ (Degs)	(5) SECTION ΔC_{L}/deg.	(6) SECTION ΔC_{D}/deg.	(7) SECTION $\Delta C_{l_{Max}}$	(8) SECTION $\frac{\Delta C_{l_{Max}}}{C_{\mu}}$	(9) SECTION $C_{\mu_{Max}}$	(10) SECTION $\Delta C_{D_{Max}}$	(11) SECTION ΔC_{D} DUE TO BLC THRUST RECOVERY		(12) CRITICAL FLIGHT CONDITION FOR HINGE MOMENT COEFF.	(13) HINGE LINE LOCATION % CHORD	(14) SECTION MAXIMUM HINGE MOMENT COEFFICIENT C_{h} Max.
										$\delta_r \leq 10°$	δ_r =Max			
	50/0	60/0	0/0	.0800	.0040	3.62	6.56	.0590	.62	-.059	-.047	G.E.O.	50	±.66
4. Spanwise Blowing	20/0	60/0	0/0	.0494	.00045	2.64	15.70	.0743	.14	---	---	G.E.O.	20	±.66
	35/0	60/0	0/0	.0665	.00165	3.26	10.7	.0743	.34	---	---	G.E.O.	35	±.66
	50/0	60/0	0/0	.0800	.0040	3.62	5.24	.0743	.62	---	---	G.E.O.	50	±.66
B. Aileron/ Flaperon														
1. Conventional Aileron	15/0	30/0	0/0	.0406	.0001	.800	---	0	.03	---	---	L.F.	15	±.215
	25/0	30/0	0/0	.0545	.00075	1.17	---	0	.060	---	---	L.F.	25	±.257
	35/0	30/0	0/0	.0650	.00165	1.49	---	0	.106	---	---	L.F.	35	±.292
2. Double Hinged Aileron	15/50	30/30	0/0	.0665	.00013	1.21	---	0	.04	---	---	L.F.	15	±.42
	25/50	30/30	0/0	.0910	.00085	1.85	---	0	.08	---	---	L.F.	25	±.52
	35/50	30/30	0/0	.110	.00195	2.37	---	0	.141	---	---	L.F.	35	±.60
3. Drooped Convent. Aileron	15/0	±30/0	30/0	.0117	0	.552	---	0	.042	---	---	L.F.	15	-.275
	25/0	±30/0	30/0	.0186	.0005	.895	---	0	.077	---	---	L.F.	25	-.382
	35/0	±30/0	30/0	.0303	.0014	1.210	---	0	.124	---	---	L.F.	35	-.470

SEE TABLE XXV FOR NOTES

(Page 172 Blank)

TABLE XXIII

MOMENT PRODUCTER STUDY DATA SHEET - FORM 1

NORMALIZED CAPABILITY

(1) CANDIDATE MOMENT PRODUCER	(2) % CHORD SEGMENT RATIO	(3) CONTROL δ_{MAIN} / δ_{AFT} (Degs)	(4) DROOP δ_{MAIN} / δ_{AFT} (Degs)	(5) SECTION ΔC_{L}/deg.	(6) SECTION ΔC_{D}/deg.	(7) SECTION $\Delta C_{l_{Max}}$	(8) SECTION $\frac{\Delta C_{l_{Max}}}{C_{\mu}}$	(9) SECTION $C_{\mu_{Max}}$	(10) SECTION $\Delta C_{D_{Max}}$	(11) SECTION ΔC_{D} DUE TO BLC THRUST RECOVERY		(12) CRITICAL FLIGHT CONDITION FOR HINGE MOMENT COEFF.	(13) HINGE LINE LOCATION % CHORD	(14) SECTION MAXIMUM HINGE MOMENT COEFFICIENT C_{h} Max.
										$\delta_r \leq 10°$	δ_r=Max			
4. Chordwise Blown Aileron	15/0	60/0	0/0	.0405	.0001	2.28	17.2	.070	.10	-.07	-.056	L.F.	15	±.66
	25/0	60/0	0/0	.0545	.00075	2.80	14.5	.070	.20	-.07	-.056	L.F.	25	±.66
	35/0	60/0	0/0	.0650	.00165	3.17	10.80	.070	.337	-.07	-.056	L.F.	35	±.66
5. Chordwise Blown Drooped Aileron	15/0	±30/0	50/0	.0351	0	1.036	9.6	.097	.02	-.097	-.058	L.F.	15	-.66
	25/0	±30/0	50/0	.0404	.0005	1.21	8.22	.097	.035	-.097	-.058	L.F.	25	-.66
	35/0	±30/0	50/0	.0441	.0015	1.30	5.90	097	.044	-.097	-.058	L.F.	35	-.66
6. Flaperon-Double Slotted														
(a) Deflection of Main + Aft	30/50	40/20 10/10	20/20	.0792	.0002	.785	---	0	.019	---	---	L.F.	Leading Edge of Main	-1.00
(b) Deflection of Aft	30/50	20/70 20/20	20/20	.025	0	.412	---	0	0	---	---	L.F.	Leading Edge of Aft	- .30
7. Flaperon Triple Slotted														
(a) Deflection of Fore, Main Aft	30/50	40/20 10/10	20/20	.0792	.0001	.900	---	0	.007	---	---	L.F.	Leading Edge of Main	-1.07
(b) Deflection of Aft	30/50	20/70 20/20	20/20	.025	0	.412	---	0	0	---	---	L.F.	Leading Edge of Aft	- .30
C. Spoilers														
1. Panel Spoilers	12/0	60/0	0/0	.00955	.0008	. 828	---	0	.082	---	---	L.F.	70	+.45
	20/0	60/0	0/0	.0239	.0020	.994	---	0	.137	---	---	L.F.	70	+.54

SEE TABLE XXV FOR NOTES

(Page 174 Blank)

TABLE XXIV

MOMENT PRODUCER STUDY DATA SHEET - FORM 1

NORMALIZED CAPABILITY

(1) CANDIDATE MOMENT PRODUCER	(2) % CHORD SEGMENT RATIO	(3) CONTROL $\frac{\delta_{MAIN}}{\delta_{AFT}}$ (Degs)	(4) DROOP $\frac{\delta_{MAIN}}{\delta_{AFT}}$ (Degs)	(5) SECTION ΔC_{L}/deg.	(6) SECTION ΔC_{D}/deg.	(7) SECTION $\Delta C_{L_{Max}}$	(8) SECTION $\frac{\Delta C_{L_{Max}}}{C_{\mu}}$	(9) SECTION $C_{\mu_{Max}}$	(10) SECTION $\Delta C_{D_{Max}}$	(11) SECTION ΔC_{D} DUE TO BLC THRUST RECOVERY		(12) CRITICAL FLIGHT CONDITION FOR HINGE MOMENT COEFF.	(13) HINGE LINE LOCATION % CHORD	(14) SECTION MAXIMUM HINGE MOMENT COEFF. C_{h} Max.
										$\delta_{r}<10°$	δ_{r}=Max			
2. Plug Spoiler	10.4/0	90/0	0/0	.00955	.0008	.828	- - -	0	.082	- - -	- - -	L.F.	70	+.45
	17.4/0	90/0	0/0	.0239	.0020	.994	- - -	0	.137	- - -	- - -	L.F.	70	+.54
3. Vented Spoiler	12/0	60/0	0/0	.0138	.001	.932	- - -	0	.103	- - -	- - -	L.F.	70	+.506
	20/0	60/0	0/0	.0346	.0025	1.125	- - -	0	.172	- - -	- - -	L.F.	70	+.608
4. Spoiler-Slot-Deflection	12/0	60/0	0/0	.0244	.0016	1.24	- - -	0	.161	- - -	- - -	L.F.	70	*+.675,0
	20/0	60/0	0/0	.0615	.0040	1.49	- - -	0	.269	- - -	- - -	L.F.	70	*+.810,0
D. Horizontal Tail														
1. Conventional Elevator	20/0	30/0	0/0	.0474	.00045	.968	- - -	0	.042	- - -	- - -	L.F.	20	±.218
	35/0	30/0	0/0	.0634	.00165	1.47	- - -	0	.107	- - -	- - -	L.F.	35	±.318
	50/0	30/0	0/0	.0758	.0040	1.87	- - -	0	.192	- - -	- - -	L.F.	50	±.411
2. Double Hinged Elevator	35/50	30/30	0/0	.1070	.00195	2.35	- - -	0	.142	- - -	- - -	L.F.	35	±.66
3. Double Slotted Elevator	35/50	40/30	0/0	.1240	.00137	3.43	- - -	0	.143	- - -	- - -	L.F.	35	±.68
4. Blown Conventional Elevator	20/0	60/0	0/0	.0474	.00045	2.53	16.90	.0665	.14	-.0665	-.0530	L.F.	20	±.593
	35/0	60/0	0/0	.0634	.00165	3.10	11.0	.0665	.34	-.0665	-.0530	L.F.	35	±.602
	50/0	60/0	0/0	.0758	.0040	3.47	5.96	.0665	.62	-.0665	-.0530	L.F.	50	±.618

SEE TABLE XXV FOR NOTES

(Page 176 Blank)

TABLE XXV

MOMENT PRODUCER STUDY DATA SHEET - FORM 1

NORMALIZED CAPABILITY

(1) CANDIDATE MOMENT PRODUCER	(2) CHORD SEGMENT RATIO	(3) CONTROL $\delta_{MAIN}/\delta_{AFT}$ (Degs)	(4) DROOP $\delta_{MAIN}/\delta_{AFT}$ (Degs)	(5) SECTION $[\Delta C_{L/deg.}]$	(6) SECTION $[\Delta C_{D/deg.}]$	(7) SECTION $\Delta C_{L_{Max}}$	(8) SECTION $\Delta C_{L_{Max}}/C_{\mu}$	(9) SECTION $C_{\mu_{Max}}$	(10) SECTION $\Delta C_{D_{Max}}$	(11) SECTION ΔC_D DUE TO BLC THRUST RECOVERY		(12) CRITICAL FLIGHT CONDITION FOR HINGE MOMENT COEFF.	(13) HINGE LINE LOCATION % CHORD	(14) SECTION MAXIMUM HINGE MOMENT COEFF. $C_{h_{Max}}$
										$\delta_{r-}<10°$	δ_r=Max			
5. Slab Tail	100/0	16/0	0/0	.1010	0	1.23	- - -	0	.04	- - -	- - -	L.F.	25	±.045
6. Slab Tail + Geared Elev.	100/20	13/30	0/0	.172	.000676	1.81	- - -	0	.092	- - -	- - -	L.F.	25	±.249
	100/35	13/30	0/0	.197	.00248	1.98	- - -	0	.157	- - -	- - -	L.F.	25	±.316
	100/50	13/30	0/0	.212	.00600	2.08	- - -	0	.242	- - -	- - -	L.F.	25	±.368
7. Slab Tail + Gear Elev. + L.E. Flap	100/35	21/30	0/0	197	.00248	2.56	- - -	0	.137	- - -	- - -	L.F.	25	±.30

NOTE:

1. $[C_L/deg]$ & $[C_D/deg]$ are based on a 10° deflection, Columns (5) & (6).
2. $C_{\mu_{Max}}$ was determined at the maximum deflection, Column (9).
3. δ_{AFT} is measured relative to the main surface deflection, δ_{MAIN}, Columns (3) & (4), Figure A-2.
4. Drooped aileron and Flaperons lift and drag characteristics are obtained by averaging the individual wing's contribution, Columns (7) & (10). The applicable surface deflections were determined using differential displacements for the ailerons. The differential deflections of the flaperons are represented by the double entry values for $(\delta_{MAIN}/\delta_{AFT})$. Thus an entry of 40/20, 10/10 indicates that the main flap segment on one wing is deflected 40 degrees relative to the reference plane with the aft segment deflected 20 degrees relative to the main flap segment. On the other wing, the main flap is deflected 10 degrees from the reference plane and the aft segment is deflected 10 degrees relative to the main flap segment (see Figure A-3).
5. Spoiler data are based on the flaps-up configuration. Multiply the panel and plug data by a factor of 2 and the vented and spoiler-slot-deflector data by 3.0 for flaps down, Columns (7) & (10).
6. The section maximum hinge coefficient is taken at the maximum deflection angle, Column (14).
7. C_D due to BLC thrust recovery is not included in the $C_{D_{Max}}$, Column (10).
8. G.E.O. is Ground Engine Out, V=90 KEAS, L.F. is Landing Flare; Column (12).
9. *When spoiler and deflector are geared together, then C_h = 0, Column (14).

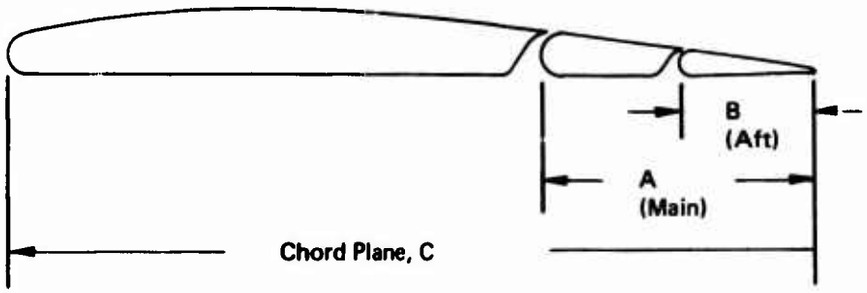

Figure 82: Specification of Chord Ratios

Example of % chord specification of multi-segment control surface. The ratio shown in column 2 (Tables XXI through XXV) reflects the % chord of the main control segment and a factor depicting the aft control segment as a % of the main control segment. These factors are computed as shown below:

$$\% \text{ CHORD} = A/C \times 100 \quad (81)$$

$$\text{SEGMENT RATIO} = B/A \times 100 \quad (82)$$

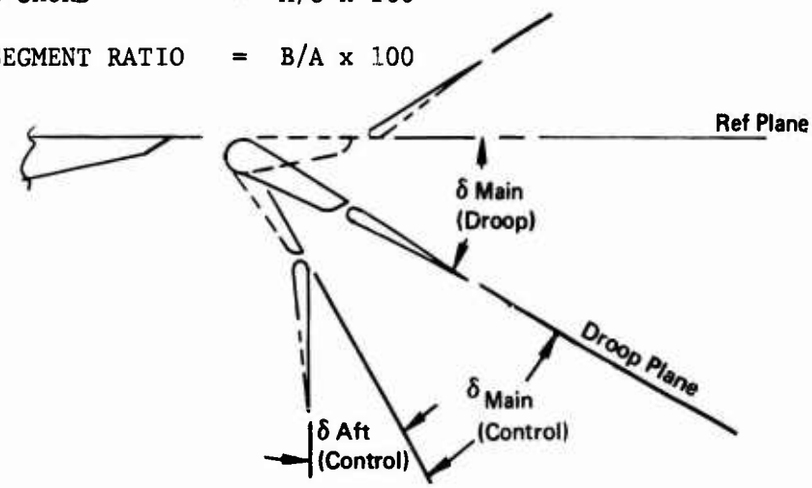

Figure 83: Specification of Multi-Segment Contro and Droop Deflections for Ailerons, Elevators, and Rudders

Example of the specification of surface control and droop deflections. (Columns 3 and 4 of Tables XXI through XXV.)

Droop (Aileron only) ($\delta Main_{Droop}$) - This specification is a ratio depicting the deflection of the front segment relative to a reference plane.

Control (Aileron elevator, or rudder) $\left(\frac{\delta Main_{Control}}{\delta Aft_{Control}}\right)$ - This specification is a ratio depicting the deflection of the front control element segment relative to the droop or reference plane (i.e., no droop) and the deflection of the aft segment relative to the front segment (shown in dashed lines).

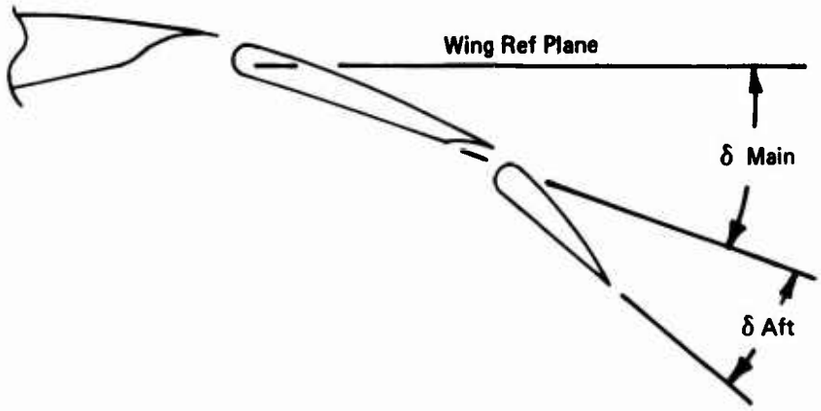

Figure 84: Specification of Flaperon Control and Droop Deflections

Droop - This is the "neutral" position of the flaperon and is specified as a ratio of the main segment deflection relative to the wing reference plane and the deflection of the aft segment relative to the main segment.

$$\delta DROOP = \frac{\delta MAIN}{\delta AFT} \text{ where a specification of 20/20 represents} \quad (83)$$

Flaperon in droop (Neutral) position: $\delta MAIN = 20°$ relative to reference plane; $\delta AFT = 20°$ relative to $\delta MAIN$

Control - This specifies the position of the main and aft segments for both extremes of the control deflections. The first ratio reflects the maximum deflection of the main segment relative to the wing reference plane and the aft segment deflection relative to the main segment. The second ratio reflects the minimum deflection of the main segment relative to the wing reference plane and the aft segment deflection relative to the main segment.

$$CONTROL = \frac{\delta MAIN}{\delta AFT} \text{ MAX} ; \frac{\delta MAIN}{\delta AFT} \text{ MIN} \quad (84)$$

where a specification of 40/20, 10/10 represents

Flaperon in down control position: $\delta MAIN = 40°$ relative to ref. plane; $\delta AFT = 20°$ relative to $\delta MAIN$

Flaperon in up control position: $\delta MAIN = 10°$ relative to ref. plane; $\delta AFT = 10°$ relative to $\delta MAIN$

$$C_T = \lambda C_R \tag{85}$$

$$S_W = 2 \cdot [\frac{C_R + C_T}{2}] \cdot [b/2] \text{ or } C_R = \frac{2S_w}{b(1 + \lambda)} \tag{86}$$

$$C_i = C_R - \frac{(C_R - C_T)}{(b/2)} \; y_i \tag{87}$$

Letting $K_i = y_i/(b/2)$ and substituting for C_R and C_T

$$C_i = \frac{2S_w}{b(1 + \lambda)} \; [1 + (\lambda - 1)K_i] \tag{88}$$

$$\text{Since } S_{ik} = [\frac{C_i + C_k}{2}] \cdot [y_i - y_k] \text{ substituting for } y_i, y_k, C_i, C_k \tag{89}$$

$$\text{we find } S_{ik} = [\frac{S_w}{(1 + \lambda)}] \cdot [1 + \frac{(\lambda - 1)}{2} (K_i + K_k)] \; [K_i - K_k] \tag{90}$$

The applicable aerodynamic force is then:

$$F_{(aero)} = qS_{ik}C_{(section\ property)}$$

$$\text{where the } C_{(section\ property)} \text{ is } C_{L_{max}} \text{ or } C_{D_{max}} \text{ as applicable.} \tag{91}$$

These aerodynamic forces were used with the general equations of Section 3.1.2.1 to determine control capability. During the phase one moment producer study, the aerodynamic control capability was normalized per foot of span. The control capability of the candidates, normalized as noted above, are shown in Tables XXVI and XXVII. These tables indicate the relative control power capabilities for each candidate and also indicate the magnitude of control or "cross-axis" coupling.

The reaction control candidates considered the use of powerplant thrust and vector modulation plus the use of engine bleed reaction jets. The applicable powerplant forces were obtained from Figure 9 for varying thrust magnitude and vector angle. The control power of these elements was normalized by the applied engine thrust. Table XXVIII shows the control capability for thrust vector angle variations and Table XXIX shows the control capability for variations of thrust magnitude. Several vectoring schemes restricted the maximum excursion of the vector angle which limited the usefulness of these vectoring systems.

I.4 Computation of Implementation Penalty Factors

The weight and complexity of alternate moment producers varies considerably. The values of weight and complexity were computed as described in Sections 3.1.2.2 and 3.1.2.3. The incremental and

Table XXVI: Moment Producer Trade Study — Performance

CANDIDATE MOMENT PRODUCER	TYPE		ELEMENT CONFIGURATION						CONTROL POWER FACTOR ④						PERFORMANCE COST FACTORS			
	CONFIG-URATION	FORCE	LOCATION % b/2	CHORD % MAIN	CHORD % AFT	AUGMENTATION BLOWN	AUGMENTATION DROOP,°	SPAN % b/2	FT/SEC^2 /FT $\dot{U}$	$\dot{V}$	W	RAD/SEC2/FT $\dot{Q}$①	$\dot{P}$②	$\dot{R}$③	SECTION LIFT/ DRAG	COUPLING $\dot{U}/^*$	$\dot{W}/^*$	$\Sigma C/^*$
AILERON	DOUBLE HINGE	AERO	97	25	50	0	0	12	.0092	0	0	0	.0174	0	107.1	.529	0	0
					50	0		17	.0096				.0175		107.1	.529		
					50	0		22	.0098				.0176		107.1	.557		
	CONVENTIONAL				0	0		12	.0230				.0264		72.67	.871		
								17	.0236				.0265		72.67	.868		
							0	22	.0244				.0266	0	72.67	.917		0
							30	12	.0050				.0132	.00038	92.00	.379		.029
							30	17	.0052				.0132	.000351	92.00	.394		.029
							30	22	.0053				.0133	.000382	92.00	.398		.029
							50	12	.0046				.0114	.000340	80.78	.404		.030
							50	17	.0046				.0114	.000339	80.78	.404		.030
						0	50	22	.0047				.0115	.000339	80.78	.409		.029
						0	0	12	.0070				.0110	0	72.67	.636		0
							0	17	.0072				.0110	0	72.67	.655		0
							0	22	.0074				.0111	0	72.67	.833		0
							30	12	.0044				.0084	.00034	41.41	.524		.041
							30	17	.0046				.0085	.00033	41.41	.541		.039
AILERON	CONVENTIONAL	AERO	97	25	0	0	30	22	.0047	0	0	0	.0085	.00034	41.41	.553	0	.039
FLAPERON	TRIPLE SLOT	AERO	85	30	50	0	20	25	.0005	0	0	0	.0084	.00003	47.19	.0595	0	.00357
			60						.0006				.0071	.00003	47.19	.0854		.00423
			35						.0008				.0041	.00001	47.19	.1951		.00244
	DOUBLE SLOT		85						.0014				.0074	.00008	33.69	.1892		.01081
			60						.0017				.0062	.00007	33.69	.2742		.01129
FLAPERON	DOUBLE SLOT	AERO	35	30	50	0	20	25	.0021	0	0	0	.0035	.00004	33.69	.6000	0	.01143

ΣC = SUMMATION OF PRIME CONTROL INDUCED ROTATIONAL ACCELERATIONS

* = PRIME CONTROL POWER

① PRIME FOR HORIZONTAL TAIL

② PRIME FOR WING

③ PRIME FOR VERTICAL TAIL

④ BASED UPON TWO DIMENSIONAL SECTION DATA

Table XXVII: Moment Producer Trade Study — Performance

CANDIDATE MOMENT PRODUCER	TYPE		ELEMENT CONFIGURATION						CONTROL POWER FACTOR ④						PERFORMANCE COST FACTORS			
									FT/SEC²/FT			RAD/SEC²/FT			SECTION	COUPLING		
	CONFIG-URATION	FORCE	LOCATION % b/2	CHORD % MAIN	CHORD % AFT	AUGMENTATION BLOWN	AUGMENTATION DROOP*	SPAN %b/2	$\dot{U}$	$\dot{V}$	$\dot{W}$	$\dot{Q}$ ①	$\dot{P}$ ②	$\dot{R}$ ③	LIFT/ DRAG	$\dot{U}/^*$	$\dot{W}/^*$	$\Sigma C/^*$
SPOILER	SLOTTED	AERO	95	15	0	0	0	10	.0336	0	.2307	.00087	.0375	.0026	13.88	.897	6.163	.093
			85					20	.0408		.2778	.00081	.0378	.0026		1.08	7.35	.032
			65					20	.0508		.3405	.00060	.0339	.0023		1.47	10.04	.039
			45					20	.0591		.4032	.00025	.0255	.0017	13.88	2.32	15.81	.076
	VENTED		95					10	.0216		.1734	.00066	.0282	.0017	12.58	.77	6.15	.034
			85					20	.0261		.2088	.00061	.0285	.0017		.915	7.333	.031
			65					20	.0321		.2559	.00045	.0255	.0015		1.26	10.04	.076
			45					20	.0378		.3030	.00019	.0192	.0011	12.58	1.963	15.78	.037
	PANEL		95					10	.0115		.1028	.00059	.0168	.0008	11.04	.690	6.12	.033
			85					20	.0140		.1238	.00054	.0168	.0008		.834	7.37	.033
			65					20	.0170		.1518	.00041	.0152	.0007		1.118	9.93	.073
	PANEL		45	15	0	0	0	20	.0202	0	.1798	.00017	.0114	.0006	11.04	1.772	15.77	.003
ELEVATOR	DOUBLE SLOT		TEE TAIL	35	50	0	0	100	.0091	0	.219	.0387	0	0	90.50	.235	5.659	0
	CONVENTIONAL				0	0			.018		.198	.0350			38.46	.514	5.057	
	DOUBLE HINGE				50	0			.00907		.150	.0265			54.88	.342	5.033	
	CONVENTIONAL			35	0	0			.00683		.094	.0166			38.46	.411	5.033	
SLAB TAIL	CONVENTIONAL			100	0	0			.0026		.079	.0139			–	.187	5.033	
	GEARED ELEVATOR		TEE TAIL	100	35	0	0	100	.0100	0	.126	.0224	0	0	79.43	.445	5.525	
ELEVATOR	DOUBLE SLOT		LOW TAIL	35	50	0	0	100	.0091	0	.219	.0321	0	0	90.50	.205	6.022	
	CONVENTIONAL				0	0			.018		.198	.0269			38.46	.623	6.031	
	DOUBLE HINGE				50	0			.00907		.150	.0219			54.83	.414	6.033	
	CONVENTIONAL			35	0	0			.00683		.094	.0137			33.46	.400	6.031	
SLAB TAIL	CONVENTIONAL			100	0	0			.0026		.079	.0115			–	.225	6.075	
	GEARED ELEVATOR		LOW TAIL	100	35	0	0	100	.0100	0	.126	.0185	0	0	79.43	.511	6.011	0
RUDDER	DOUBLE HINGE		–	35	50	0	0	100	.0155	.2678	0	.00068	.01419	.023	57.18	.674	0	.033
	CONVENTIONAL		–	35	0	0	0	100	.0117	.1683	0	.00051	.00892	.015	40.30	.709	0	.023
	CONVENTIONAL	AERO	–	35	0	0	0	100	.031	.3564	0	.00136	.01888	.031	40.30	1.060	0	1.053

ΣC = SUMMATION OF PRIME CONTROL INDUCED ROTATIONAL ACCELERATIONS

* = PRIME CONTROL POWER b = WING SPAN

① PRIME FOR HORIZONTAL TAIL

② PRIME FOR WING

③ PRIME FOR VERTICAL TAIL

④ BASED UPON TWO DIMENSIONAL SECTION DATA

Table XXVIII: Moment Producer Trade Study — Performance

CANDIDATE MOMENT PRODUCER	CONFIG-URATION	DEFLECTION Δσ DEG	CONTROL POWER PER 1,000 LB THRUST					COUPLING				
			$\dot{U}$	$\dot{W}$	$\dot{P}$	$\dot{R}$	$\dot{Q}$	$\dot{U}/°$	$\dot{W}/°$	$\Sigma C/°$		
ENGINE-	ROTAT.	72 → 8 ①	.1887°	.1456	0	0	.0023	1.0	.7786	.0212		
THRUST	VALVE	72 → 8 ②	.1887	.1456	.013 °	.0037	.0023	8.36	11.2	.4615		
VECTOR	③	72 → 72 ①	0	0	0	0	0	0	0	0		
CONTROL		72 → 72 ②	0	0	0	0	0	0	0	0		
	ROTAT.	75 → 8 ①	.1773°	.1998	0	0	.0030	1.0	1.1	.02		
	CASCADE	75 → 8 ②	.1773	.1998	.0144°	.0061	.0030	12.3	13.9	.63		
	④	75 → 90 ①	.0625	.0063°	0	0	.0013	7.5	1 ^	.16		
		75 → 90 ②	.0625	.0063	.00075	.0019°	.0013	83.3	11.1	1.06		
	THREE	75 → 8 ①	.1762°	.1936	0	0	.0031	1.0	1.1	.02		
	BEARING	75 → 8 ②	.1762	.1936	.0142°	.0050	.0031	12.4	13.6	.63		
		75 → 90 ①	.0611	.0064°	0	0	.0013	9.6	1.0	.20		
		75 → 90 ②	.0611	.0064	.00053	.0021°	.0013	115.3	12.1	.87		
	DUAL	75 → 8 ①	.1773°	.1748	0	0	.0031	1.0	1.0	.02		
	SWIVEL	75 → 8 ②	.1773	.1748	.0127°	.0050	.0031	14.0	13.8	.71		
		75 → 90 ①	.0564	.0057°	0	0	.0012	9.9	1.0	.21		
		45 → 90 ②	.0564	.0057	.00031	.0019°	.0012	181.9	18.1	.79		
	EYEBALL	45 → 8 ①	.0752°	.1311	0	0	.0011	1.0	1.7	.01		
	③	45 → 8 ②	.0757	.1311	.0096°	.0025	.0011	7.9	13.7	.38		
		45 → 45 ①	0	0°	0	0	0	0	0	0		
		45 → 45 ②	0	0	0	0	0	0	0	0		

ΣC = SUMMATION OF PRIME CONTROL INDUCED ROTATIONAL ACCELERATIONS

° PRIME CONTROL POWER

① ALL FOUR ENGINES ARE DISPLACED THROUGH ANGLE Δσ. CONTROL POWER FACTORS ARE NORMALIZED BY USING THRUST OF FOUR ENGINES.

② TWO ENGINES ON ONE SIDE OF AIRPLANE ARE DISPLACED THROUGH ANGLE Δσ. VECTORS ON OPPOSITE SIDE REMAIN AT 75 DEGREES. CONTROL POWER FACTORS ARE NORMALIZED BY USING THRUST OF TWO ENGINES.

③ CONFIGURATION DEFLECTION LIMITED

④ $\alpha = 0°$, $\phi = 90°$

⑤ APPROACH THRUST AT 75% MAXIMUM FOR ALL DEFLECTIONS

Table XXIX: Moment Producer Trade Study — Performance

CANDIDATE MOMENT PRODUCER	CONFIG URATION	DEFLECTION DEGREE σ	CONTROL POWER PER 1 000 LB THRUST ③					COUPLING			
			$\dot{J}$	$\dot{W}$	$\dot{P}$	$\dot{R}$	$\dot{Q}$	$\dot{U}/^*$	$\dot{W}/^*$	$\Sigma c/^*$	
ENGINE	ROTAT.										
THRUST	VALVE	72 ④	.0254	.0467*	0	0	.000327	.544	1.0	—	
MODULATION	②	⑤	.0254	.0467	.00318*	.00090	.000327	8.0	14.7	.4	
	ROTAT.①										
	CASCADE	75 ④	.0157	.0582*	0	0	.000425	.27	1.0	—	
		⑤	.0157	.0582	.00436*	.00064	.000425	3.6	13.3	.2	
	THREE										
	BEARING	75 ④	.0152	.0568*	0	0	.000421	.27	1.0	—	
		⑤	.0152	.0568	.00416*	.00051	.000421	3.7	13.7	.2	
	DUAL	75 ④	.0140	.0519*	0	0	.000379	.27	1.0	—	
	SWIVEL	⑤	.0140	.0519	.00376*	.00051	.000379	3.7	13.8	.2	
	EYEBALL	45 ④	.0414	.0414*	0	0	.000304	1.0	1.0	—	
	②	⑤	.0414	.0414	.00301*	.00139	.000304	13.8	13.8	.6	
REACTION	BLEED	ROLL	—	—	.043*	—	—	—			
JET	AIR	PITCH	—	.246	—	—	.043*	—			
		YAW	—	—	—	.024*	—	—	—		

Σc = SUMMATION OF PRIME CONTROL INDUCED ROTATIONAL ACCELERATIONS

* = PRIME CONTROL POWER

① $\alpha = 0^0$, $\phi = 90^0$

② CONFIGURATION LIMITED DEFLECTION

③ THRUST IS VARIED FROM 75% TO 100% MAXIMUM FOR APPLICABLE ENGINES.

④ THRUST OF FOUR ENGINES IS VARIED. CONTROL POWER FACTORS ARE NORMALIZED BY THRUST FOR FOUR ENGINES

⑤ THRUST FOR TWO ENGINES ON ONE SIDE OF AIRPLANE IS VARIED. CONTROL POWER FACTORS NORMALIZED BY THRUST FOR TWO ENGINES.

composite weights are shown in Tables XXX and XXXI to provide insight into the division of the incremental weight between structure and the control/actuation elements. Also the incremental complexity factors (PG, PD, and FC) and the total complexity value (Cx) are also shown in these tables.

I.5 Computation of Parametric Values For Moment Producer Comparative Rating

The phase one moment producer data presented in Sections I.2 through I.4 provided a means of comparing the relative performance of the individual candidates. During the second phase, the finite span effects were included in the computation of aerodynamic candidate control power. At this time, the approach speed was projected to be eighty knots rather than the ninety knots originally projected. Therefore, the control capability shown in the final study phase reflects control power at eighty knots.

During this final phase, the costs of the various systems were computed. The statistical cost procedures were based upon the control system structural weight, weight of the pneumatic systems for blown surfaces, and a lump sum estimation for actuation components. These cost increments are shown in Table XXXII. The actuation costs assume that:

(1) The surfaces are controlled by mechanical displacements representing the desired response.

(2) Each spoiler panel uses an individual actuator and each aileron is controlled by a "dual" actuator.

These assumptions represent the conventional means of implementing surface actuation.

The moment producer system comparisons, tabulated herein, used the airplane mass and geometric properties of Tables III and IV, the lateral control axis constraint restricting the use of trailing edge control devices (except where these were integrated with the flap function), an eighty knot speed, and finite span effects to derive the basic moment producer parameter data. All the comparative data, except control power, were divided by the control power derived from the applicable moment producer candidate. This provides a common basis for the comparison of these parameters (e.g., pounds/rad. sec^2, cost/rad. sec^2, and complexity/rad. sec^2).

The data in Tables XXXIII through XXXVI include the comparative data in the dimensional form and the unweighted "figure-of-merit" values derived from the dimensional data using equations 19 and 20 The lateral control elements and control systems are shown in Tables XXXIII and XXXIV respectively. The lateral elements in Table XXXIII have been separated into two categories for evaluating the specific figure of merits. These were: 1) control elements compatible with high-lift flaps and 2) elements installed outboard of the high

Table XXX: Implementation Penalty Factors

CANDIDATE MOMENT PRODUCER	b_θ or B_T ②	$\frac{\dot{}}{\alpha}$ ③	f ①	$\frac{\Delta W_{Strut}}{f}$	$\frac{\Delta W_{Cont.}}{f}$	$\Delta W/f$	P_G	P_D	F_c	C_x
AILERON										
DOUBLE HINGE	12	.0174	6.35	36.8	34.2	71.0	1.6	0.8	2.4	4.8
	17	.0175	9.00	36.8	25.8	62.6	1.6	0.8	2.4	4.8
	22	.0176	11.63	36.8	21.3	58.1	1.6	0.7	2.6	4.9
BLOWN										
CONVENTIONAL	12	.0264	6.35	23.0	65.9	88.9	3.2	1.6	4.3	9.1
	17	.0265	9.00	23.0	48.2	71.2	3.2	1.6	4.3	9.1
	22	.0266	11.64	23.0	40.4	63.4	3.6	1.6	3.9	8.7
CONVENTIONAL	12	.0110	6.35	23.0	28.1	51.1	1.6	0.8	1.8	4.2
	17	.0110	9.00	23.0	20.6	43.6	1.6	0.8	1.8	4.2
	22	.0111	11.64	23.0	16.6	39.6	1.6	0.7	1.8	4.1
BLOWN	12	.0132	6.35	23.0	67.4	90.4	3.2	1.6	4.5	9.4
DROOP 30°	17	.0132	9.00	23.0	50.4	73.4	3.2	1.6	4.5	9.3
	22	.0133	11.64	23.0	41.3	64.3	3.2	1.6	4.1	8.9
BLOWN	12	.0114	6.35	23.0	67.4	90.4	3.2	1.6	4.5	9.3
DROOP 50°	17	.0114	9.00	23.0	50.4	73.4	3.2	1.6	4.5	9.3
	22	.0115	11.64	23.0	41.3	64.3	3.2	1.6	4.1	8.9
UNBLOWN	12	.0084	6.35	23.0	29.6	52.6	1.6	0.8	2.1	4.5
DROOP 30°	17	.0085	9.00	23.0	21.7	44.7	1.6	0.8	2.1	4.5
	22	.0085	11.94	23.0	17.4	40.4	1.6	0.8	2.0	4.4
FLAPERON										
TRIPLE SLOTTED	85	.0084	13.23	36.9	19.6	56.5	1.7	1.4	4.1	7.2
	60	.0071	13.23	36.9	22.7	59.6	1.7	1.4	4.1	7.2
	35	.0041	13.23	36.9	25.5	62.4	1.7	1.2	4.4	7.3
DOUBLE SLOTTED	85	.0074	13.23	31.9	19.2	51.1	1.7	1.3	3.5	6.5
	60	.0062	13.23	31.9	22.0	53.9	1.7	1.3	3.6	6.6
	35	.0035	13.23	31.9	25.0	56.9	1.7	1.1	3.8	6.6
SPOILER										
SLOT DEFLECTOR	95	.0375	5.29	13.7	15.4	29.1	1.6	1.0	3.4	6.0
	85	.0378	10.58	13.7	15.3	29.0	1.6	1.0	3.3	5.9
	85	.0339	10.58	13.7	15.4	29.1	1.6	1.0	3.4	6.0
	45	.0256	10.58	13.7	15.6	29.2	1.6	0.9	3.3	5.8
VENTED	95	.0282	5.29	8.6	14.9	23.6	1.6	1.0	2.7	5.3
	85	.0285	10.58	8.6	14.6	23.2	1.6	1.0	2.7	5.3
	85	.0255	10.58	8.6	14.6	23.2	1.6	0.9	2.8	5.3
	45	.0192	10.58	8.6	14.7	23.3	1.6	0.9	2.8	5.3
PANEL	95	.0198	5.29	6.9	13.9	20.8	1.6	1.0	2.3	4.9
	85	.0188	10.58	6.9	13.6	20.5	1.6	1.0	2.3	4.9
	85	.0152	10.58	6.9	13.6	20.5	1.6	0.9	2.4	4.9
	45	.0114	10.58	6.9	13.7	20.8	1.6	0.9	2.4	4.9

① f = SPAN FOR AERODYNAMIC UNITS OR 1,000 LB FOR THRUST UNITS

② b_θ = AILERON SPAN (% b/2)

B_T = FLAPERONS AND SPOILERS ELEMENT TIP LOCATION (PERCENT b/2)

③ $\frac{\dot{}}{\alpha}$ IS PRIME CONTROL POWER PER FOOT OR PER 1,000 LB OF THRUST

$C_x = P_G + P_D + F_c$

$\Delta W/f = \frac{\Delta W_{Struct.}}{f} + \frac{\Delta W_{Control}}{f}$

Table XXXI: Impelementation Penalty Factors

CANDIDATE MOMENT PRODUCER	PRIME CONTROL AXIS	$\dot{a}$ ②	f ①	$\frac{\Delta W \text{ Strut}}{f}$	$\frac{\Delta W \text{ Cont.}}{f}$	$\frac{\Delta W}{f}$	P_G	P_D	F_C	C_x
RUDDER										
DOUBLE HINGE	$\dot{R}$	.823	16.19	48	34.4	82.4	1.6	1.1	3.1	5.8
CONVENTIONAL	$\dot{R}$	.815	16.19	30	30.2	60.2	1.6	1.1	2.4	5.1
BLOWN										
CONVENTIONAL	$\dot{R}$	.831	16.19	30	97	127.7	3.2	1.9	4.9	7.5
ELEVATOR (TEE TAIL)										
DOUBLE SLOT	$\dot{Q}$	.8367	36.48	33	34.3	67.3	1.6	1.3	3.6	6.5
BLOWN										
CONVENTIONAL	$\dot{Q}$	.8360	36.48	18	58.9	76.9	3.2	2.4	4.8	7.6
DOUBLE HINGE	$\dot{Q}$	.8285	33.48	28	31.7	59.7	1.6	1.3	3.1	6.0
CONVENTIONAL	$\dot{Q}$	.8186	36.48	18	27.5	45.5	1.6	1.3	2.3	5.2
SLAB TAIL (TEE TAIL)										
CONVENTIONAL	$\dot{Q}$	.8138	36.48	30	17.7	56.7	1.7	1.2	2.7	5.6
GEARED ELEVATOR	$\dot{Q}$	.8224	36.48	60	27.8	87.8	1.7	1.2	3.3	6.2
ELEVATOR (LOW TAIL)										
DOUBLE SLOT	$\dot{Q}$	.8321	36.48	33	34.1	67.1	1.6	1.1	3.3	6.0
BLOWN										
CONVENTIONAL	$\dot{Q}$	.8288	36.48	18	56.9	73.7	3.2	2.0	4.7	7.2
DOUBLE HINGE	$\dot{Q}$	.8219	36.48	28	31.5	59.5	1.6	1.1	3.1	5.8
CONVENTIONAL	$\dot{Q}$	.8137	36.48	18	23.9	41.9	1.6	1.1	2.3	5.0
SLAB TAIL (LOW TAIL)										
CONVENTIONAL	$\dot{Q}$	.8115	36.48	30	17.5	56.5	1.7	1.0	2.2	4.9
GEARED ELEVATOR	$\dot{Q}$	.8185	36.48	60	27.7	87.7	1.7	1.0	2.7	5.4
REACTION JET										
ROLL	$\dot{P}$	.843	1.15			647.8	2.1	1.2	3.5	6.8
YAW	$\dot{R}$	.824	1.15			1278.3	2.1	1.3	3.3	6.7
PITCH	$\dot{Q}$	.843	1.15			1278.3	2.1	1.3	3.3	6.7

C_x = COMPLEXITY FACTOR

① f = SPAN FOR AERODYNAMIC UNITS OR
f = 1,000 LB FOR THRUST UNITS

② $\dot{a}$ IS PRIME CONTROL POWER PER FOOT OR PER 1,000 LB OF THRUST

TABLE XXXII

MOMENT PRODUCER COST INCREMENTS

Control Surface	($/#$_{struct.}$) ①	($/#$_{pneu.}$)	Number of Actuators	$/Actuator
AILERONS:				
Double Hinge	40.00	---	4	1800
Blown Undrooped ②	34.00	20.00	4	1500
Single Hinge (Conventional)	34.00	---	4	1500
FLAPERON:				
Triple Slotted	45.00	---	4	2000
Double Slotted	42.00	---	4	2000
SPOILERS:				
Slot Deflector	67.00	---	16 ④ 20 ⑤	900
Vented	58.00	---	16 ④ 20 ⑤	700
Panel	39.00	---	16 ④ 20 ⑤	700
RUDDER:				
Blown ②	43.00	20.00	3	1500
Double Hinge	51.00	---	3	1500
Single Hinge (Conventional)	43.00	---	3	1500
HORIZONTAL TAIL: ③				
ELEVATORS				
Double Slotted	45.00	000	4	1500
	41.00	000	4	1500
Blown ②	37.00	20.00	4	1500
	34.00	20.00	4	1500
Double Hinge	44.00	---	4	1800
	40.00	---	4	1800
Conventional	37.00	---	4	1500
	34.00	---	4	1500
Slab Tail	41.00	---	4	2000
	37.00	---	4	2000
Slab Plus	48.00	---	4	2500
Geared Elevator	43.00	---	4	2500

① The dollar per structural weight included installation of control linkages and miscellaneous parts.
② For APU blown surface systems the weight was adjusted for different duct routing and $112,000 was added for APU.
③ Two entries are shown for the horizontal tail. The first entry applies to tee tail installations and the second to low tail installations.
④ Partial span spoilers integrated with aileron (8 panels per wing).
⑤ Full span spoilers (10 panels per wing).

(Page 190 Blank)

TABLE XXXIII

BASIC MOMENT PRODUCER DATA-LATERAL ELEMENTS

TRADE STUDY PARAMETER	LATERAL ELEMENTS OUTBOARD OF HIGH-LIFT FLAPS									LATERAL CONTROL ELEMENTS COMPATIBLE WITH HIGH-LIFT FLAPS				
				BLENDED						SPOILERS			FLAPERONS	
	ALL SPOILER SLOT DEFLECTOR	VENTED	ALL FLAPERON TRIPLE SLOTTED	ENGINE BLEED BLOWN AILERON S/D SPOILER	ENGINE BLEED BLOWN AILERON VENTED SPOILER	APU BLEED BLOWN AILERON S/D SPOILER	APU BLEED BLOWN AILERON VENTED SPOILER	DOUBLE HINGE AILERON S/D SPOILER	DOUBLE HINGE AILERON VENTED SPOILER	SLOTTED DEFLECTOR	VENTED	PANEL	TRIPLE SLOT	DOUBLE SLOT
$\dot{P}$	2.34 (.898)	5.81 (.683)	10.00 (.418)	1.00 (.981)	3.66 (.816)	1.00 (.981)	3.66 (.816)	2.66 (.878)	5.32 (.713)	1.00 (.636)	4.82 (.479)	9.49 (.287)	9.10 (.303)	10.00 (.266)
$\Delta W/\dot{P}$	1.00 (2812)	1.14 (2960)	10.00 (12,765)	1.53 (3366)	1.71 (3558)	2.97 (4864)	3.44 (5354)	1.72 (3563)	1.97 (3827)	1.00 (2812)	1.14 (2960)	2.48 (4414)	9.62 (12205)	10.00 (12563)
$C_X/\dot{P}$	1.11 (6.68)	2.04 (7.76)	10.00 (17.02)	1.19 (6.77)	1.78 (7.46)	1.34 (6.94)	1.95 (7.66)	1.00 (6.55)	1.64 (7.29)	1.00 (6.68)	1.88 (7.76)	5.48 (12.16)	9.45 (17.02)	10.00 (17.69)
COST/$\dot{P}$	1.77 (64.4)	1.00 (52.2)	9.68 (189.2)	1.79 (64.6)	1.25 (56.1)	9.07 (179.5)	10.00 (194.6)	2.48 (75.6)	2.05 (68.7)	1.80 (64.4)	1.00 (52.2)	5.87 (63.7)	10.00 (189)	9.23 (177)
$\dot{U}/\dot{P}$	.69 (1.15)	.58 (.97)	.05 (.05)	.71 (1.19)	.62 (1.04)	.71 (1.19)	.68 (1.04)	.69 (1.15)	.58 (.97)	.81 (1.35)	.69 (1.15)	.62 (1.04)	.05 (.09)	.17 (.28)
$\dot{W}/\dot{P}$	9.78 (9.88)	9.75 (9.85)	9.61 (9.71)	7.81 (7.89)	7.05 (7.12)	7.81 (7.89)	7.05 (7.12)	7.81 (7.89)	8.13 (8.21)	11.53 (11.65)	11.50 (11.62)	11.56 (11.68)	11.34 (11.45)*	11.24 (11.35)*
$\dot{R}/\dot{P}$	.29 (.0065)	.17 (.0039)	1.59 (.0357)	.20 (.0044)	.15 (.0034)	.20 (.0044)	.15 (.0034)	.35 (.0078)	.17 (.0039)	.29 (.0065)	.17 (.0039)	.33 (.0074)	1.59 (.0357)	1.14 (.0257)
$\dot{Q}/\dot{P}$	.58 (.0313)	.62 (.0335)	0 (0)	.60 (.0323)	.54 (.0293)	.60 (.0323)	.54 (.0293)	.71 (.0382)	.62 (.0335)	.58 (.0313)	.62 (.0335)	.88 (.0467)	0 (0)	0 (0)

NOTE: Numbers enclosed in parenthesis ( ) are the raw data used to evaluate the normalized parameter.

* The lift/roll penalty for flaperons reflects the reduction in operating C_{LMAX} caused by not deploying the flaps to the normal "high-lift" operating point as a means of controlling drag coupling.

151

(191 tank)

Table XXXIV

BASIC MOMENT PRODUCER DATA - LATERAL SYSTEMS

TRADE STUDY PARAMETER	ALL SPOILERS		ALL FLAPERON	BLENDED					
				ENGINE BLEED BLOWN AILERON		APU BLEED BLOWN AILERON		DOUBLE HINGE AILERON	
	SLOT DEFLECTOR	VENTED	TRIPLE SLOTTED	S/D SPOILER	VENTED SPOILER	S/D SPOILER	VENTED SPOILER	S/D SPOILER	VENTED SPOILER
$\dot{P}$	2.34 (.898)	5.81 (.683)	10.00 (.423)	1.00 (.981)	3.66 (.8.16)	1.00 (.981)	3.66 (.816)	2.66 (.878)	5.32 (.713)
$\Delta\dot{W}/\dot{P}$	1.00 (2812)	1.14 (2960)	10.00 (12205)	1.53 (3366)	1.71 (3558)	2.97 (4864)	3.44 (5359)	1.72 (3563)	1.97 (3827)
$\dot{C}_X/\dot{P}$	1.11 (6.68)	2.04 (7.76)	10.00 (17.02)	1.19 (6.77)	1.78 (7.46)	1.34 (6.94)	1.95 (7.66)	1.00 (6.55)	1.64 (7.29)
$\dot{COST}/\dot{P}$	1.77 (64.4)	1.00 (52.2)	9.68 (189.2)	1.79 (64.6)	1.25 (56.1)	9.07 (179.5)	10.00 (194.2)	2.48 (75.6)	2.05 (68.7)
$\dot{U}/\dot{P}$	.69 (1.15)	.58 (.97)	.05 (.08)	.71 (1.19)	.62 (1.04)	.71 (1.19)	.62 (1.04)	.69 (1.15)	.58 (.97)
$\dot{W}/\dot{P}$	9.78 (9.88)	9.75 (9.85)	9.61 (9.71)	7.81 (7.89)	7.05 (7.12)	7.81 (7.89)	7.05 (7.12)	7.81 (7.89)	8.13 (8.21)
$\dot{R}/\dot{P}$	.29 (.0065)	.17 (.0039)	1.59 (.0357)	.20 (0044)	.15 (.0034)	.20 (.0044)	.15 (.0034)	.35 (.0078)	.17 (.0039)
$\dot{Q}/\dot{P}$	.53 (.0313)	.62 (.0335)	0 (0)	.60 (.0323)	.54 (.0293)	.60 (.0323)	.54 (.0293)	.71 (.0382)	.62 (.0335)

Note: The figure -of-merit values are followed by the basic dimensional data which are enclosed in parenthesis. These dimensional data were used in the derivation of the figure-of-merit values.

lift flaps. Table XXXV records the comparative data for the directional system. Table XXXVI shows the comparative data for the longitudinal elements installed in tee or low horizontal tail configuration.

I.6 Extension of Moment Producer Study to Other Than Baseline Airplanes

The potential user of the moment producer trade study data may wish to consider the effect of changing airplane geometry.

The relative performance data for the horizontal tail and vertical tail candidates are easily extrapolated to other airplanes with different geometric characteristics. The relative aerodynamic performance, for each candidate using a fixed area vertical or horizontal tail surface with different geometric characteristics, will be the same as it was for the baseline airplane. The absolute values of control power must recognize the effects of geometric variations.

The wing mounted lateral control elements are affected by other parameters that must be included in the evaluation of these systems. From the equation for the surface area influenced by the lateral control element developed in Appendix I, it is seen that the wing taper ratio, the element span length, and the location of the element along the wing span are very significant in the determination of the lateral control element control power. The following equation indicates the method of converting the section lift characteristics, of Tables XXI through XXV, to an incremental control coefficient.

$$\Delta C_{\ell_{2D}} = K_3 C_{L_{max_{2D}}} \quad \text{where } K_3 \text{ is shown on Figures 85 through 88.} \qquad (92)$$

The coefficient method of expressing roll power permits easy inclusion of changes in wing area, inertial properties, and dynamic pressure. The value of K_3 for this equation has been plotted on Figures 85 through 88 for various element spans and for various wing taper ratios. The $\Delta C_{\ell_{2D}}$ does not include the three-dimensional aerodynamic flow characteristics. Therefore, Figure 4.1.3.2-41 of reference 16 (DATCOM) must be used to compute the appropriate 3-D correction factor.

Wings with taper ratios less than four-tenths have a reduced effectiveness for control elements mounted near the tip of the wing. (See Figures 85-88.)

This method of extending the control data from this study to other airplanes is demonstrated in Figure 89 where lateral control power is computed for several Boeing airplanes using high lift flap systems. The $\Delta C_{\ell_{computed}}$ value was obtained using the $C_{L_{max}}$ data shown in Table XXII through XXIV. Vented spoiler lift characteristics were used to represent the panel spoiler characteristics when used with fowler flaps. The ΔC_{ℓ} test in this figure used data obtained from wind tunnel and early flight tests to represent the best estimate of actual capability of these airplanes. In general, the control power indicated by this computation process is higher than the control power measured from wind tunnels and actual flight data.

A least squares fit of the computed versus actual data indicates that the following equation best approximates the actual data.

$$\Delta C_{\ell}{}_{test} = -.0012 + .96\Delta C_{\ell}{}_{computed} \quad (93)$$

A significant discrepancy appeared in two data points. These points were for the 737 and the 747 spoilers with flaps extended. In Investigation of the flaps up versus flaps down ΔC_{ℓ} characteristics of these airplanes has indicated a departure from the factor assumed for this study. The ratios of the actual flaps down to the flaps up roll control power (points A and C) were plotted for these two airplanes in Figure 90 and is compared with the value used in this study (point B). When the actual K factor (point A or C) is used in lieu of that indicated by point B, the new $\Delta C_{\ell}{}_{computed}$ in Figure 89 are represented by points C and A for the 747 and 737 respectively. These are seen to be an improved estimate of control power.

Therefore, although this estimation technique proposed herein gives a reasonable approximation of roll control power, confidence in the spoiler/flap factors used in the computation of the lateral control power must be established from wind tunnel testing.

TABLE XXXV

BASIC MOMENT PRODUCER DATA - DIRECTIONAL ELEMENTS

TRADE STUDY PARAMETER	RUDDERS					VECTOR MODULATION		
	BLOWN		DOUBLE HINGED					
	ENGINE BLEED	APU BLEED	INCREASED SURFACE AREA	BASELINE	CONVEN-TIONAL	ROTATING CASCADE	THREE BEARING	DUAL SWIVEL
$\dot{R}$	1.00 (.158)	1.00 (.158)	2.43 (.145)	5.53 (.117)	10.00 (.076)	6.93 (.104)	7.04 (.103)	7.48 (.099)
$\dot{\Delta W}/R$	1.77 (129.7)	5.28 (207.2)	2.23 (140.0)	1.00 (113.0)	1.63 (127.1)	9.82 (307.1)	8.22 (271.8)	10.00 (311.1)
$\dot{C_X}/R$	5.32 (63.29)	6.38 (68.35)	1.00 (42.40)	2.48 (49.57)	6.10 (67.1)	9.12 (81.7)	9.10 (81.5)	10.00 (85.9)
$\dot{Cost}/R$	1.97 (290.6)	10.00 (1012.6)	2.80 (363.0)	2.57 (344.3)	2.43 (331.6)	2.50 (336.5)	7.37 (776.7)	1.00 (202.0)
$\ddot{U}/R$	.17 (1.24)	.17 (1.24)	.10 (.68)	.10 (.68)	.12 (.83)	4.14 (29.6)	4.14 (29.6)	4.14 (29.6)
$\ddot{W}/R$	0 (0)	0 (0)	0 (0)	0 (0)	0 (0)	.92 (4.2)	.99 (4.5)	1.14 (5.18)
$\ddot{P}/R$	1.40 (.608)	1.40 (.608)	1.71 (.745)	1.42 (.615)	1.36 (.592)	2.92 (1.27)	2.68 (1.17)	.66 (.286)
$\ddot{Q}/R$	.83 (.203)	.83 (.203)	.31 (.076)	.26 (.064)	.11 (.026)	.13 (.032)	.12 (.029)	.03 (.007)

Note:

The figure-of-merit values are followed by the basic dimensional data which are enclosed in parenthesis. These dimensional data were used in the derivation of the figure-of-merit values.

TABLE XXXVI

BASIC MOMENT PRODUCER DATA - LONGITUDINAL ELEMENTS

TRADE STUDY PARAMETER	TEE TAIL							LOW TAIL						
	ELEVATORS					FLYING TAIL		ELEVATORS					FLYING TAIL	
	BLOWN							BLOWN						
	DOUBLE SLOT	ENGINE BLEED	APU BLEED	DOUBLE HINGE	CONVEN-TIONAL	GEARED ELEVATOR	SLAB	DOUBLE SLOT	ENGINE BLEED	APU BLEED	DOUBLE HINGE	CONVEN-TIONAL	GEARED ELEVATOR	SLAB
$\dot{Q}$	3.06 (.581)	1.00 (.674)	1.00 (.674)	4.63 (.510)	8.85 (.320)	3.41 (.565)	7.04 (.401)	5.18 (.485)	3.45 (.563)	3.45 (.563)	6.48 (.426)	10.00 (.267)	5.41 (.472)	8.47 (.336)
$\Delta\dot{W}/\dot{Q}$	1.22 (4225)	1.00 (4162)	6.78 (5900)	1.37 (4270)	4.42 (5187)	6.02 (5669)	4.32 (5158)	3.98 (5062)	3.12 (4795)	10.00 (6868)	4.17 (5114)	7.82 (6212)	9.73 (6788)	7.70 (6177)
$C_{\dot{x}}/\dot{Q}$	1.33 (11.19)	6.23 (15.43)	7.08 (16.17)	2.03 (11.76)	7.18 (16.25)	1.00 (10.9)	4.45 (13.9)	2.70 (12.38)	8.70 (17.58)	9.73 (18.47)	4.13 (13.62)	10.00 (18.71)	1.63 (11.44)	5.33 (14.64)
$Cost/\dot{Q}$	1.33 (103.6)	2.03 (121.5)	8.29 (282.8)	1.20 (99.9)	1.00 (94.7)	4.93 (196.5)	3.53 (160.4)	1.77 (114.1)	2.63 (136.7)	10.00 (328.2)	1.60 (110.0)	1.43 (106.1)	5.53 (212.1)	4.10 (175.0)
$\ddot{U}/\dot{Q}$	.08 (.24)	.20 (.62)	.20 (.62)	.11 (.34)	.14 (.41)	.10 (.30)	.06 (.18)	.09 (.28)	.25 (.76)	.25 (.76)	.14 (.41)	.17 (.50)	.11 (.32)	.07 (.22)
$\ddot{W}/\dot{Q}$	3.06 (5.66)	3.06 (5.65)	3.06 (5.65)	3.06 (5.66)	3.06 (5.65)	3.06 (5.64)	3.06 (5.65)	3.68 (6.82)	3.68 (6.85)	3.68 (6.85)	3.68 (6.85)	3.68 (6.85)	3.68 (6.84)	3.68 (6.84)

NOTE: Numbers enclosed in parenthesis ( ) are the raw data used to evaluate the normalized parameter.

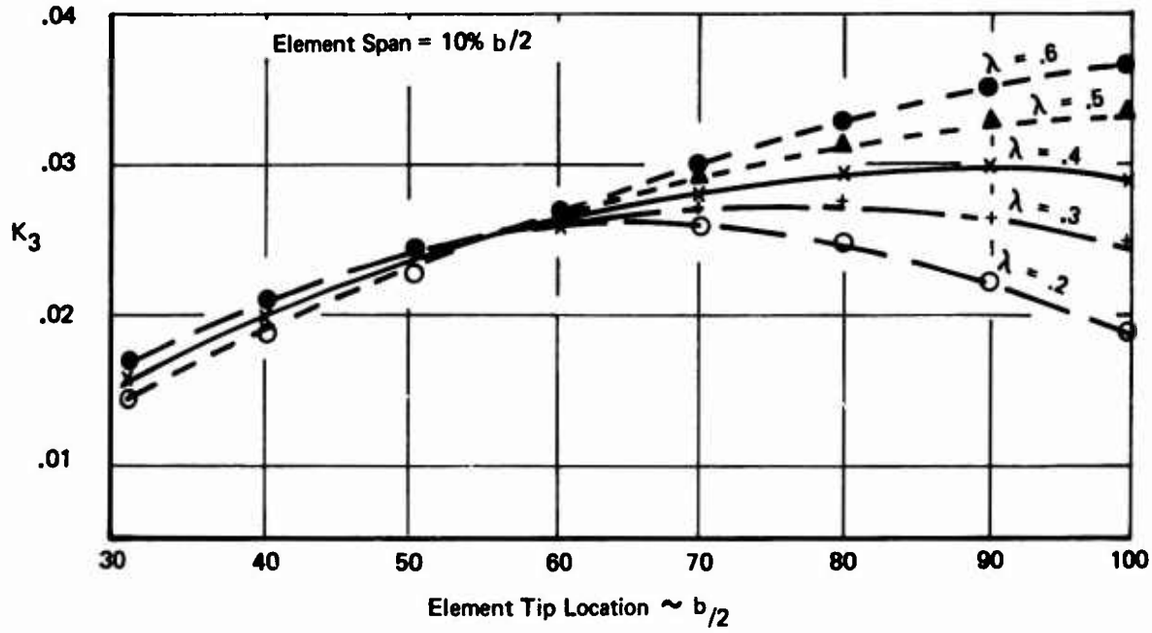

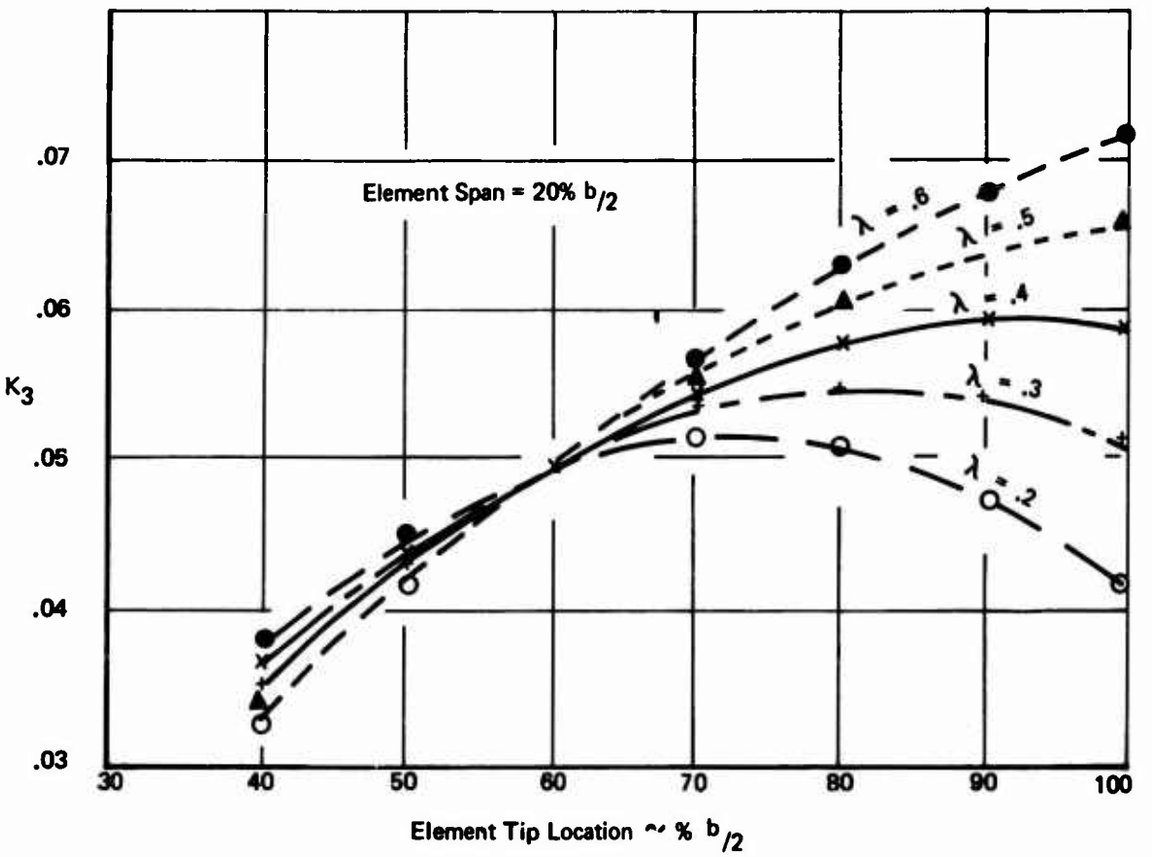

Figure 85: Roll Control Factor K_3 for 10% and 20% Element Semi-Span

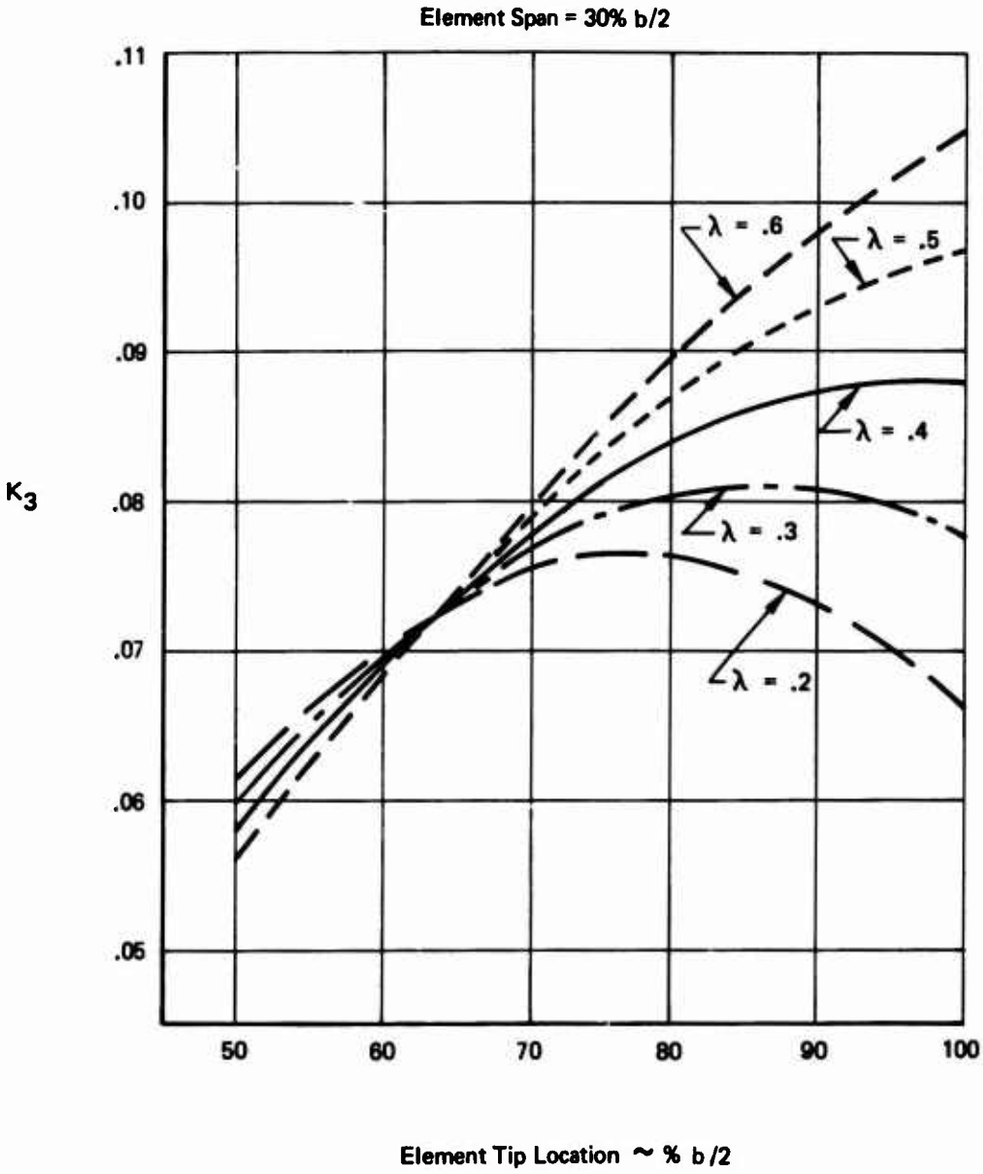

Figure 86: Roll Control Factor K_3 for 30% Element Semi-Span

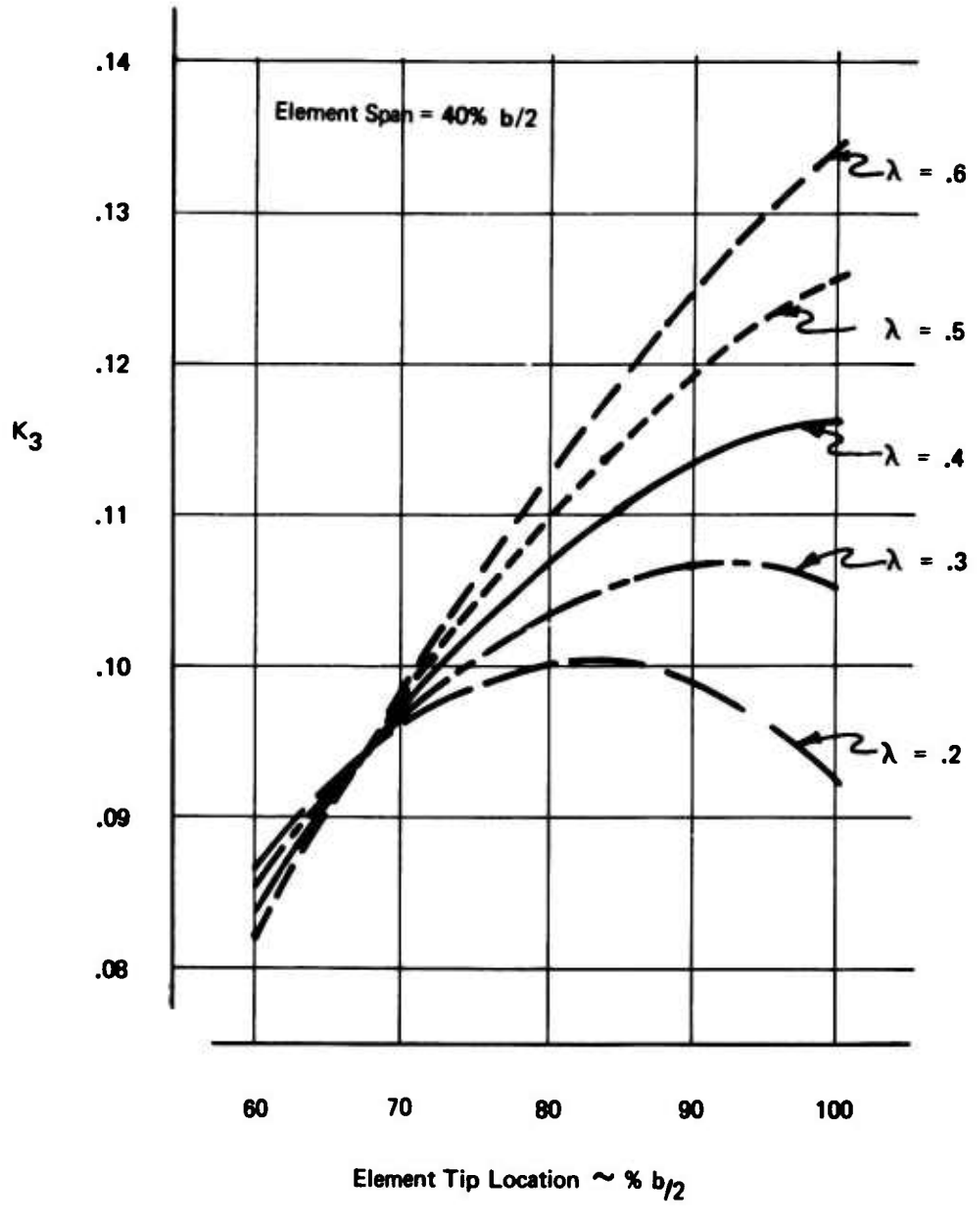

Figure 87: Roll Control Factor K_3 for 40% Element Semi-Span

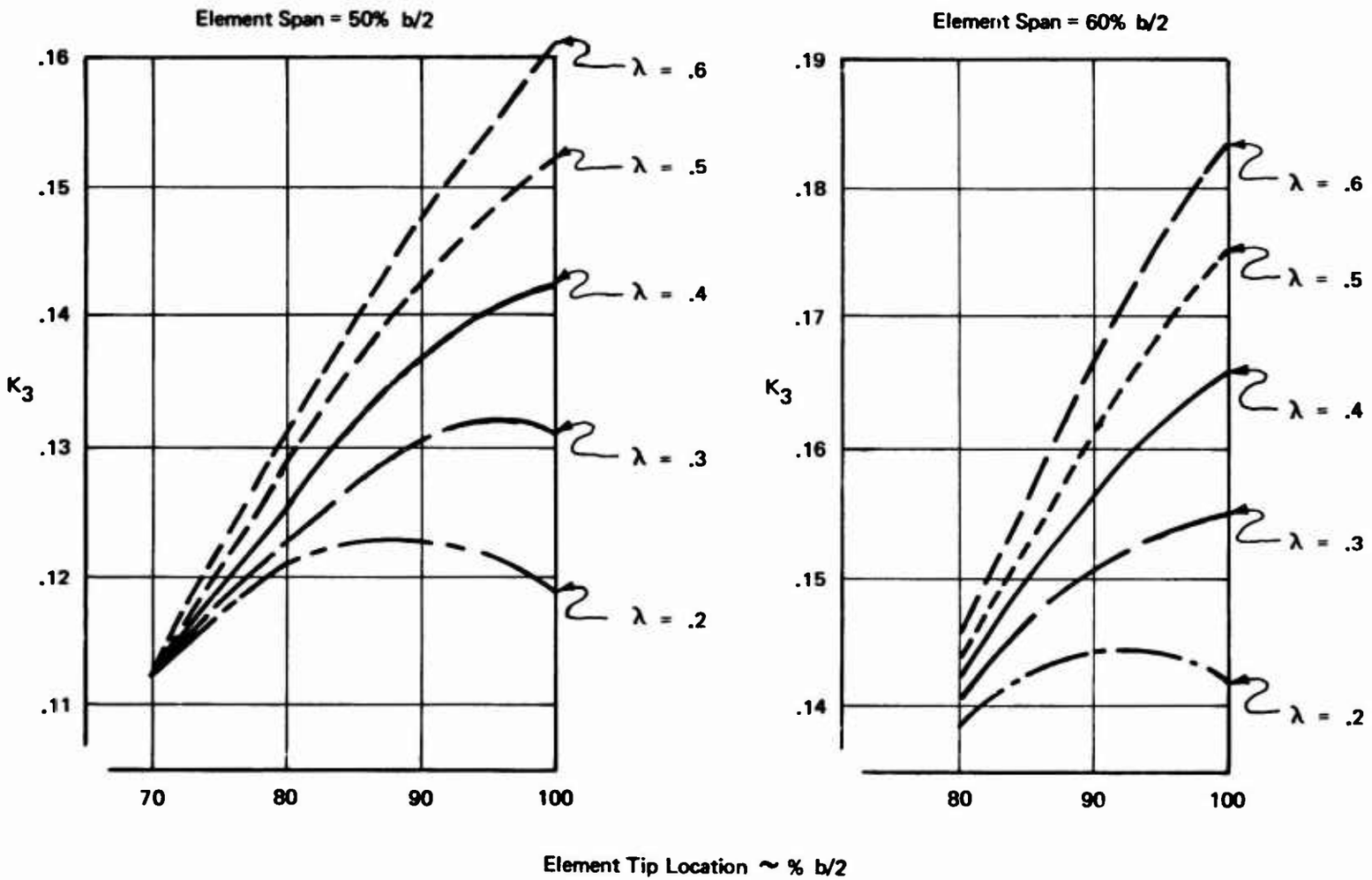

Figure 88: Roll Control Factor K_3 for 50% and 60% Element Semi-Span

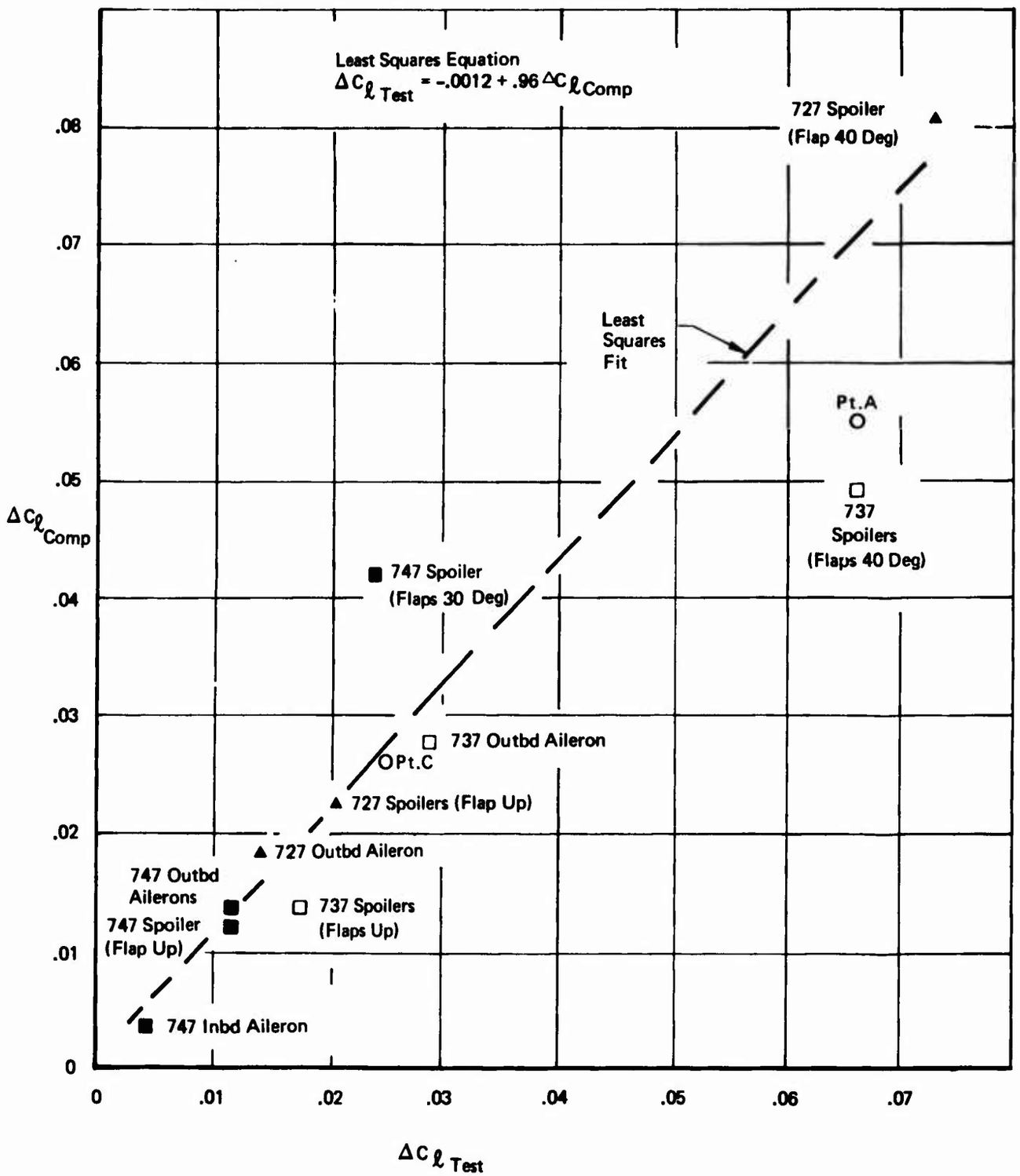

Figure 89: Comparison of Predicted and Actual Roll Control Capability

Notes: 1. Spoiler Characteristics at
$a_W = 0^o$

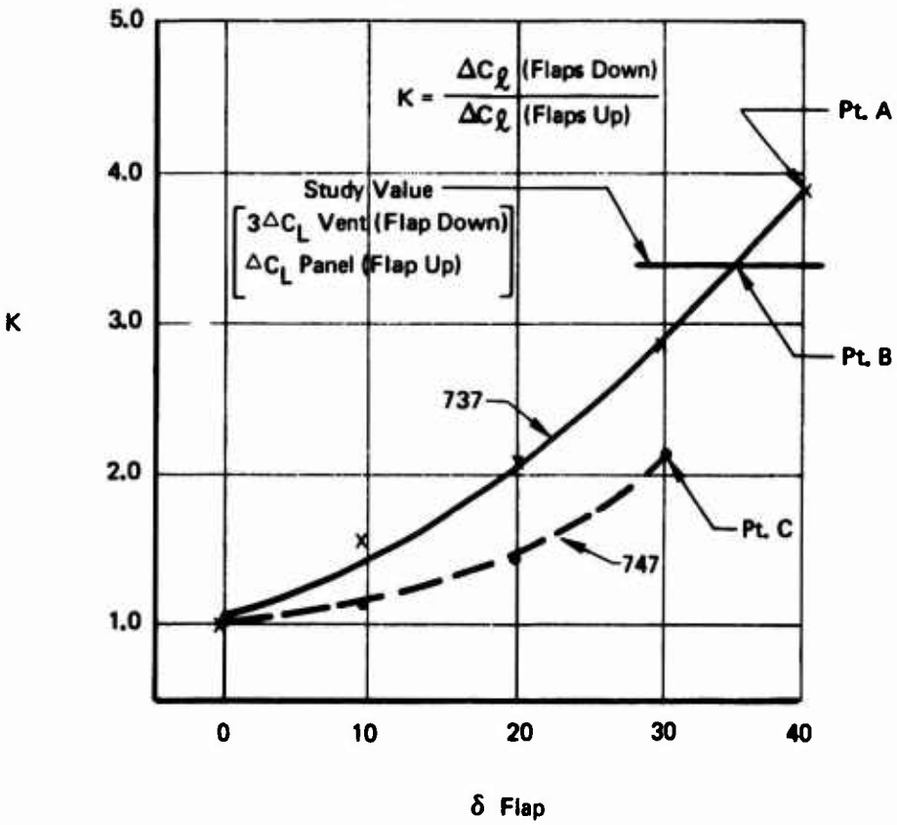

Figure 90: Roll Control Capability as a Function of Flap Position

APPENDIX II

LINEAR EQUATIONS OF MOTION AND AERODYNAMIC DATA

This appendix contains the equations of motion used in the synthesis of longitudinal and lateral/directional control systems. The equations of motion are shown in matrix form with Figure 91 representing the longitudinal equations and Figure 92 representing the lateral/directional equations.

The aerodynamic data, used in the initial phase of the control system analysis, is identified as data set #1 and was based upon early MST wind tunnel studies. Data set #2, used in the final control low analysis phase, included wind tunnel data obtained during the STAI study. In addition to the two landing approach data sets, data are shown for the high speed and transition flight phases of the STAI airplane.

$$
\begin{bmatrix}
S-X_u & 0 & -X_W & \frac{W_o S}{57.3} \\
0 & 1 & \frac{57.3}{U_o} & -1 \\
-Z_u & 0 & \frac{S(1-Z_{\dot{W}})}{-Z_W} & -S\left[\frac{U_o}{57.3} + Z_q\right] \\
-M_u & 0 & -M_{\dot{W}}S & \frac{S^2}{57.3} \\
 & & -M_W & -M_q S
\end{bmatrix}
\begin{bmatrix} u \\ \gamma \\ w \\ \theta \end{bmatrix}
=
\begin{bmatrix}
X_{\delta_c} & X_{\delta_\sigma} & X_u & X_W \\
0 & 0 & 0 & 0 \\
Z_{\delta_c} & Z_{\delta_\sigma} & Z_u & Z_W \\
M_{\delta_c} & M_{\delta_\sigma} & M_u & M_W
\end{bmatrix}
\begin{bmatrix} \delta_c \\ \delta_\sigma \\ u_g \\ w_g \end{bmatrix}
$$

NOTE

Equations are in body axes; for stability axes, $W_o = 0$.

FIGURE 91 LONGITUDINAL PERTURBATION EQUATIONS OF MOTION

$$
\begin{bmatrix}
C_{Y_\beta} & C_{Y_\phi} & \left(\frac{b}{2V}\right)C_{Y_r} & 0 \\
-\frac{mVs}{qS_w} & +\left(\frac{b}{2V}\right)C_{Y_p}s & \frac{-mV}{qS_w} & \\
\hline
 & \left(\frac{b}{2V}\right)C_{\ell_p}s & \left(\frac{b}{2V}\right)C_{\ell_r} & \\
C_{\ell_\beta} & -\frac{I_{xx}s^2}{qS_wb} & +\frac{I_{xz}}{qS_wb}s & 0 \\
\hline
 & \left(\frac{b}{2V}\right)C_{n_p}s & \left(\frac{b}{2V}\right)C_{n_r} & \\
C_{n_\beta} & +\frac{I_{xz}}{qS_wb}s^2 & -\frac{I_{zz}}{qS_wb}s & 0 \\
\hline
-\frac{V\,S}{57.3} & +\frac{g}{57.3} & -\frac{V}{57.3} & 1
\end{bmatrix}
\begin{bmatrix} \beta \\ \phi \\ r \\ A_y \end{bmatrix}
=
\begin{bmatrix}
-C_{Y_{\delta_w}} & -C_{Y_{\delta_R}} & -C_{Y_\beta} \\
\hline
-C_{\ell_{\delta_w}} & -C_{\ell_{\delta_R}} & -C_{\ell_\beta} \\
\hline
-C_{n_{\delta_w}} & -C_{n_{\delta_R}} & -C_{n_\beta} \\
\hline
0 & 0 & 0
\end{bmatrix}
\begin{bmatrix} \delta_w \\ \delta_R \\ \beta_G \\ 0 \end{bmatrix}
$$

Note

S_w = wing area

S = LaPlace Transform Variable

Equations are in stability axes

V ~ FPS

q ~ Lbs/Ft^2

FIGURE 92 LATERAL/DIRECTIONAL PERTURBATION EQUATIONS OF MOTION

TABLE XXXVII

MST
LONGITUDINAL DIMENSIONAL DERIVATIVES

DATA	ALT. FT	MACH	V Kn.	Xu SEC^{-1}	Zu SEC^{-1}	Mu $\frac{1}{FT.\ SEC}$	Xw SEC^{-1}	Zw SEC^{-1}	Mw $\frac{1}{FT.\ SEC}$	$Z\dot{w}$ -	$M\dot{w}$ FT^{-1}	Zq FT/SEC	Mq SEC^{-1}	$X\delta_e$ FT/SEC^2	$Z\delta_e$ FT/SEC^2	$M\delta_e$ $\frac{1}{SEC^2}$	$X\delta_{DLC}$ FT/SEC^2	$Z\delta_{DLC}$ FT/SEC^2	$M\delta_{DLC}$ $\frac{1}{SEC^2}$	$X\delta_\delta$ FT/SEC^2	$Z\delta_\delta$ FT/SEC^2	$M\delta_\delta$ $\frac{1}{SEC^2}$	AXIS SYSTEM
Data Set #1	0	.114	75	-.048	-.266	-.00099	.118	-.449	-.00239	.0303	-.001	-.0619	-.012	0	-.0655	-.0116	.0700	-.328	-.00307	-.209	-.0679	-.0003	Body (W_o = 20 FPS)
Data Set #2	0	.114	75	-.079	-.321	-.00123	.0749	-.415	-.00178	.0303	-.001	-.0619	-.012	0	-.0655	-.0116	.0700	-.328	-.00307	-.209	-.0679	-.0003	Body (W_o=20 FPS)
Flaps Down	0	.141	93	-.0763	-.412	0.	.100	-.512	-.0029	.0303	-.001	-.0765	-.015	0	-.100	-.0181	.0255	-.309	-.0029	---	---	---	Sta-bility
Flaps Up	0	.256	169	-.0270	-.332	0.	.166	-.720	-.0035	0.	0.	0.	-.031	0.	-.413	-.0826	---	---	---	---	---	---	Sta-bility
Flaps Up	0	.40	265	-.0126	-.144	0.	.072	-1.17	-.0051	0.	0.	0.	-.046	0.	-1.07	-.194	---	---	---	---	---	---	Sta-bility
Flaps Up	20,000	.78	470	-.0159	-.079	0.	.0092	-2.05	-.0090	.016	-.0005	-.210	-.066	---	---	---	---	---	---	---	---	---	Sta-bility
Flaps Up	40,000	.64	366	-.0079	-.106	0.	.0106	-.602	-.0027	.0075	-.0002	-.075	-.019	---	---	---	---	---	---	---	---	---	Sta-bility

Note

W = 133,000 lbs.
S_W = 1640 $ft.^2$
c = 15.7 ft.
Iy = 1.46×10^6 Slug-$Ft.^2$
g = 32.2 FPS^2

Velocities in Ft./Sec.
Angles in Degrees

TABLE XXXVIII

AMST LATERAL/DIRECTIONAL
NON-DIMENSIONAL DERIVATIVES

DATA	ALT. FT.	MACH	V Kn.	Cy_β	Cy_p	Cy_r	$Cy_{\delta R}$	$Cy_{\delta S}$	Cl_β	Cl_p	Cl_r	$Cl_{\delta R}$	$Cl_{\delta S}$	Cn_β	Cn_p	Cn_r	$Cn_{\delta R}$	$Cn_{\delta S}$
DATA SET #1	0	.114	75	-1.23	.49	.070	.515	0.	-.166	-.560	1.11	.0258	.452	.183	-.410	-.310	-.269	.040
DATA SET #2	0	.114	75	-1.09	.51	.030	.515	0.	-.206	-.590	1.15	.026	.190	.258	-.415	-.340	-.264	.024
FLAPS DOWN	0	.141	93	-1.09	.51	.030	.515	0.	-.206	-.590	1.15	.026	.190	.258	-.415	-.340	-.264	.024
FLAPS UP	0	.256	169	- .80	0.	.425	.560	0.	-.138	-.452	.220	.063	.061	.110	-.060	-.202	-.272	0.
FLAPS UP	20,000	.78	470	- .86	0.	.540	---	---	-.180	-.670	.132	---	---	.141	.030	-.255	---	---
FLAPS UP	40,000	.64	366	- .80	0.	.480	---	---	-.176	-.560	.094	---	---	.106	.019	-.230	---	---

Note

Cy_ϕ = W/q S_W
W = 133,000 lbs.
b = 114.5 ft.
g = 32.2 FPS^2
Ixx = 1.26 x 10^6 $Slug\text{-}Ft^2$
Izz = 2.62 x 10^6 $Slug\text{-}Ft^2$
Ixz = 0.142 x 10^6 $Slug\text{-}Ft^2$
S_w = 1640 $Ft.^2$
Angles in Radians

APPENDIX III

CONTROL MECHANIZATION BACKGROUND DATA

III.1 Purpose

This appendix contains the derived data used in the comparison of mechanized control systems. Also included in this appendix are additional details relative to specific parameter evaluations which provide further insight into the analytical process used in the study. Thus, this appendix supplements the analytical technique portion of sub-section 3.3 by providing computation examples.

III.2 Control System Performance Evaluation

In the discussion of sub-section 3.3.2, it was noted that the piloted simulation data was used to derive an overall performance rating where:

$$P_R = .25\ P_{H.Q} + .25\ P_F + .50\ P_T \qquad (94)$$

It is seen that the final performance rating is dependent approximately 25% on the normal state handling quality data ($P_{H.Q}$), 25% on the failure data state handling quality (P_F), and 50% on the IFR tracking performance data (P_T) if these values ($P_{H.Q}$, P_F and P_T) are approximately the same magnitude. Thus, the total performance rating has roughly 50% of the value obtained from the subjective pilot evaluation (Cooper-Harper rating) and 50% from the evaluation of observed system performance (e.g.: rms pilot activity and path errors). This satisfied the objective of having the system performance balanced between the subjective Cooper-Harper pilot rating and the quantitative data gathered during the pilot tracking task.

The raw data plus the cumulative factors $P_{H.Q.}$, P_F, P_T, and P_R are shown in Tables XXXIX and XL. The following discussion relates to the computation of these factors.

The handling quality portion of this rating factor uses the average of the individual overall handling quality evaluations for that particular control system. The best method of using pilot rating data is not obvious. Each pilot has provided a rating based upon his simulator experience and handling qualities expectations. This has resulted in a range of values for each mechanization model. Arguments can be made for using the extremes of the ratings, the median of the rating, or other methods of combining the ratings to best represent the composite pilot rating. For this study, where a single numerical value was needed to compare various control systems and where most control systems were only flown by two different pilots, it was decided that an average of these ratings best served this end. It is noted that the average is intended to provide a measure of comparative performance and does not represent the best guess at a "system pilot rating".

For the longitudinal systems, the handling qualities were evaluated using four specific tasks: (1) attitude control at constant speed, (2) flight path control while maintaining constant speed, (3) speed control while holding constant flight path, and (4) incremental changes in altitude while maintaining constant speed. Lateral/directional handling qualities evaluated the pilot's ability to make precise large and small heading changes in level flight. Also, decrab and "S" turn maneuvers were performed during the landing approach. Both the decrab and "S" turns began as a perturbation to the IFR tracking task when the airplane broke out of clouds at an altitude less than 200 feet. The perturbation consisted of an initial crosswind or a localizer offset of 100 feet.

The baseline pilot rating for failure states was accomplished by allowing the pilot to fly the IFR tracking task three times without failures. The IFR tracking task was then repeated several times with a single failure introduced during each flight. After having flown the airplane without failures and the airplane with failures, the pilot was asked to comment on how he would rate the airplane in light of the failures that he had encountered. The pilot was informed ahead of time that a satisfactory termination of the failure event was to continue to a landing or to set up a "go-around" or "wave-off" pattern.

All of the proposed mechanizations incorporate failure monitoring provisions for electrical element failure modes. This monitoring function was represented in the simulator by incorporating provisions to remove the transient (hardover) aspect of the failure after a pre-set time interval. The signal path gain was reduced simultaneously with the removal of the transient failure command. For electrical signal path failures a 2-second time interval was used during the evaluation of the control failures. Initially the surface actuation hardover failure modes, that could be traced to mechanical element failures, were corrected after a 3-second time period that simulated pilot initiated deactivation of the surface actuator. During the final validation using the Ames Moving Base Simulator, "mechanical" hardover failures were left in for the remaining portion of the flight. Since all such failures resulted in a satisfactory landing, it is considered unnecessary to remove these failures. The most difficult piloting task encountered during the failure analysis was associated with engine-out failures, and for most systems these could be easily controlled. The control systems most difficult to handle during failure studies were those using simple SAS or mechanical only control paths.

Time did not permit all systems to be tested for failure effects. Therefore, control systems that were characteristic of a specific mechanization technique were evaluated and the resultant pilot rating was judged typical for all control systems in that category. Special notes in Tables XXXIX and XL identify where this was done.

The IFR performance data consisted of pilot workload, pilot tracking error, and pilot touchdown performance data. To obtain a composite rating (P_T) from this data, the following procedure was used:

TABLE XXXIX
CONTROL SYSTEM PERFORMANCE DATA
LONGITUDINAL

System Designation	Pilot (N)	IFR TRACKING TASK δCOL ①	δCOL ②	δσP ①	δσP ②	εVT ①	εVT ②	εGS ①	εGS ②	ΔSX ①	ΔSX ②	P_T ⑦	Handling Qualities Pilot	H.Q. Rating	$P_{H.Q.}$	Failure Mode Pilot	H.Q. Rating	P_F	Rating P_R ⑧	
SP01	C(3)	.5497	7.81	.4224	8.54	7.70	5.96	.5716	9.0	70.60	2.16		C	2.0						
	A(3)	.4231	(.4864)	.3045	(.3635)	6.67	(7.185)	.565	(0.568)	41.60	(56.10)	6.19	A	3.5	2.75		④	5.00	5.03	
DP05A	C(4)	.43	5.85	.08	1.50	3.7	2.84	.23	1.00	144	4.06									
	---	---	(.43)	---	(.08)	---	(3.7)	---	(.23)	---	(144)	3.17	C	2.00	2.00		⑤	3.00	2.84	
DP05B	C(5)	.54	9.66	.09	1.75	4.8	3.83	.43	5.73	60	2.24									
	---	---	(.54)	---	(.09)	---	(4.8)	---	(.43)	---	(60)	5.00		③	2.00		⑤	3.00	3.75	
DP07	C(5)	.36	3.43	.06	1.00	4.4	3.47	.38	4.55	109	3.30									
	---	---	(.36)	---	(.06)	---	(4.4)	---	(.38)	---	(109)	3.78	C	3.0	3.00		⑤	3.00	3.39	
SP02A	A(3)	.4735	---	.2301	---	3.04	---	.3504	---	88.843	---					G	3.0			
(CP21)	C(3)	.4527	5.04	.2341	4.95	3.79	2.90	.3778	4.17	152.9	3.21		C	2.0		B	3.0	3.00	3.17	SP02A
	A(3)	.2934	(.4065)	.1929	(.2190)	4.46	(3.763)	.364	(.3641)	72.6	(104.78)	3.96	A	1.5	1.75	A	3.0			
																B	3.0	3.00	3.17	CP21
SP03	C(3)	.4779	6.13	.3027	6.39	5.32	3.24	.5171	7.58	418.82	7.44		C	2.0		B	6.0			
	A(3)	.3979	(.438)	.2508	(.277)	2.96	(4.14)	.498	(.508)	181.6	(300.71)	6.97	B	3.0	2.50	C	5.0			
																B	4.0	5.00	5.36	
SP04	C(3)	.4351	5.19	.2873	5.15	4.18	3.56	.6103	6.54	124.2	2.31		C	2.5						
	A(3)	.3864	(.411)	.1666	(.227)	4.82	(4.50)	.317	(.464)	2.6	(63.4)	4.58	A	1.5	2.00		⑤	3.00	3.58	
SP05	C(3)	.4001	3.54	.1601	4.00	2.48	1.38	.4098	5.87	51.9	2.39		C	2.0		G	7.0			
	A(3)	.3262	(.3632)	.2014	(.1808)	1.64	(2.06)	.462	(.4359)	82.3	(67.1)	3.84	A	1.5	1.75	B	4.0	5.5	3.55	
MP02	B(6)	.29	1.0	.248	5.67	11.7	10.00	.49	7.15	163	4.47					C	6.0			
	---	---	(.29)	---	(.248)	---	(11.7)	---	(.49)	---	(163)	5.42		⑥	4.75	A	5.5	5.75	5.34	

① This column shows the individual data entries. For IFR tracking tasks the data represents the sample statistical mean for all parameters except touchdown dispersion where the sample deviation is used. The sample size (N) is identified for each data set.

② This column contains the figure-of-merit value for the parameter followed by the average value of the parameter in parenthesis. The parameter range used for figure-of-merit program used the maximum and minimum values from ① column.

③ Same as DP05A by similarity in still air.

④ Similar to SP03.

⑤ Similar to SP02A.

⑥ The IFR task handling quality rating was used.

⑦ $P_T = .18\left[1.0(\delta col.) + .15(\delta\sigma_p) + .5(\epsilon_{VT}) + 2.0(\epsilon_{G.S.}) + 2.0(\Delta S_X)\right]$ where the values in parentheses are Column ② figure-of-merit values.

⑧ $P_R = .25\ P_{H.Q.} + .25\ P_F + .5\ P_T$

TABLE XL

CONTROL SYSTEM PERFORMANCE DATA LATERAL/DIRECTIONAL

SYSTEM DESIGNATION	IFR TRACKING TASK										HANDLING QUALITIES			FAILURE MODE			RATING	
	PILOT (N)	δ W P		δ PED		ϵ LOC		Δ SY		P_T ④	PILOT	H.Q. RATING	$P_{H.Q.}$	PILOT	H.Q. PATING	P_F	P_R ⑤	
		①	②	①	②	①	②	①	②									
SR20	A(3)	9.79	6.26	.1082	4.08	.298	3.89	23.55	8.14		A	5.5		C				
	C(3)	9.76	(9.78)	.1000	(.1041)	.230	(.264)	14.30	(18.93)	5.88	D	7.0	6.25	A	③	4.83	5.71	
SR21	D(3)	3.544	3.46	.1495	3.81	.3780	6.03	3.5416	7.61		A	2.5		B	6.0			
	A(3)	9.38	(6.462)	.0489	(.0992)	.2570	(.3175)	6.82	(5.1808)	4.05	D	6.0	4.25	C	4.5			
														A	4.0	4.83	4.30	
FR20	A(3)	7.470	2.60	.0747	5.09	.1920	6.67	6.0825	3.24					G	3.0			FR20
	. (3)	4.3117	---	.1772	---	.4165	---	1.1679	---		A	3.5		B	3.0	3.0	3.70	
(CR20)		4.5287	(5.4368)	.1143	(.1221)	.3919	(.3335)	12.9422	(6.7309)	4.40	D	2.5	3.0	B	2.5			CR20
														A	3.0	2.75	3.64	
FR21	A(3)	7.7300	4.04	.0769	4.20	.2027	3.99	8.7813	5.53					B	3.0			
	D(3)	4.8177	---	.1647	---	.3349	---	22.8058	---		A	2.0		A	2.5	2.75	3.81	CR21
(CR21)	A(3)	8.88	(7.1426)	.0766	(.1061)	.262	(.2665)	5.75	(12.4457)	4.50	D	5.0	3.5	B	3.0			
														G	3.0	3.00	3.88	FR21
MRO821	B(4)	14.21	10.00	.21	10.00	.33	6.53	14.8	6.48					C	8.0			
	---	---	(14.21)	---	(.21)	---	(.33)	---	(14.8)	7.13	A	8.0	8.0	A	7.0	7.50	7.44	

① This column shows the individual data entries. For IFR tracking tasks the data represents the sample statistical mean for all parameters except touchdown dispersion where the sample deviation is used. The sample size (N) is identified for each data set.

② This column contains the figure-of-merit value for the parameter followed by the average value of the parameter in parenthesis. The parameter range used for figure-of-merit program used the maximum and minimum values from ① column.

③ Same as SR21 by similarity.

④ $P_T = .19\left[1.0(\delta_{W_P}) + .15(\delta_{PED}) + 2.0\ (\epsilon_{LOC}) + 2.0\ (\Delta S_Y)\right]$ where the values in parentheses are Column ② figure-of-merit values.

⑤ $P_R = .25\ P_{H.Q.} + .25\ P_F + .5\ P_T$

(1) The glide slope or localizer tracking capability and the touchdown dispersion data was considered to be the most significant. These were assigned a weighting factor of 2.0.

(2) The pilot column and wheel activity were considered the most important pilot workload factors and were assigned a weighting factor of 1.0. The thrust vector incremental changes and the rudder pedal changes were rated lower since these controllers were only intermittently used by the pilots. A weighting factor of .15 was assigned to these variables.

(3) The speed error for the longitudinal task was considered of a lower priority than the glide slope tracking task and was assigned a weighting factor of 0.5.

To provide a common base for this weighting process, the figure-of-merit technique discussed in sub-section 3.1.2.5 was utilized to obtain a value of 1 to 10 for each parameter.

The composite performance rating (P_T) was obtained from the weighted figure-of-merit parameters using the following expressions

Longitudinal Systems

$$P_T = .18\ [1.0\ (\delta_{Col}) + .15\ (\delta\sigma_P) + .5\ (\varepsilon_{VT}) + 2.0\ (\varepsilon_{G.S}) + 2.0\ (\Delta_{SX})] \quad (95)$$

Lateral Systems

$$P_T = .19\ [1.0\ (\delta_W) + .15\ (\delta_{PED}) + 2.0\ (\varepsilon_{LOC}) + 2.0\ (\Delta_{SY})] \quad (96)$$

where the values in parentheses indicate in the figure-of-merit values for the specific parameter.

III.3 Safety Analysis

The safety analysis for the candidate control systems involved three major areas of concern.

(1) The loss of control capability defined as the inability to accomplish a safe CTOL landing.

(2) The probability of control system failures inducing aircraft structural damage.

(3) The probability of encountering excessive pilot workload, considered in this study to be Level 3, during the STOL landing approach.

Before the general failure modes can be identified for loss of system control, structural damage, or excessive pilot workload, the underlying analysis assumptions must be identified.

(1) Loss of System Control

(a) Three hydraulic systems are used throughout this analysis.

(b) Four electrical power systems are used with FBW systems; three electrical systems were used with all other control mechanizations.

(c) For those feel systems using two mechanical feel units (i.e., springs and cams only), dual feel system failures result in a jammed mechanical path.

(d) Loss of pitch control or loss of thrust control will result in the inability to control the airplane in the longitudinal degrees of freedom. The pitch control of the airplane would be inadequate for CTOL landing if three of the four elevator panels are inoperative. Likewise, the thrust control would be inadequate after the loss of thrust control for three engines.

[Note: Failures of the engine and engine controller are not included in this study and are considered as part of the special failure category assigned to engine failures.]

(e) Control of the thrust vector is not required for safe CTOL landing. If a thrust vector becomes inoperative at other than the cruise angle, reduction of the thrust level of that engine will allow a safe CTOL landing.

(f) Both the lateral and directional control paths must be maintained to assure adequate lateral/directional control.

(g) The plane can be landed safely, CTOL, if either the normal rudder path or the rudder trim path is available.

(h) The lateral/directional control is adequate if one-third of the directional or roll control capability is maintained.

(2) STOL Level 3 Faiure Modes

The determination of the failure modes that would result in Level 3 STOL operation were established by data obtained during the control law analysis and the fixed base piloted simulation.

(a) Longitudinal system response without feedback resulted in Level 3 operation due to the "aerodynamic/powered lift" coupled effects.

(b) Lateral/directional system operation without feedback resulted in Level 3 operation because of turn coordination and spiral divergence problems.

(c) Failures in fly-by-wire systems that reduce the forward path gain by a half result in Level 3 operation.

(d) Systems relying on mechanical feel units incorporating dynamic pressure compensation revert to Level 3 operation if the compensation portion of the feel system fails.

(e) Surface actuation failures causing Level 3 operation are:

- o two of the four elevator surfaces are lost, or
- o two of the three rudder surfaces are lost, or
- o two groups of spoilers on one wing are lost, or one group of spoilers plus one aileron are lost.

(3) Probability of Structural Damage

(a) The actuators are sized for torque saturation versus hinge moment variation with dynamic pressure such that:

- o The rudder can stand one hardover panel with full hydraulic pressure supplied to the actuator or three hardover panels with reduced hydraulic pressure supplied to all actuators.
- o The horizontal tail can stand two elevator panels hardover with full hydraulic pressure supplied to the actuators.
- o The lateral control can stand momentary full lateral demand at maximum speed without structural damage.

(b) The limited average force voting characteristic of the FBW actuators will limit the failed surface transient to approximately $\pm 5°$.

(c) The probability that the pilot will exert excessive forces and override the safety features of feel computers could not be determined and are not included in this study.

(d) The active signal path failures are determined to be:

- o Cable breakage causes a hardover command, due to the cable preload, for mechanical system with a single control cable.

- o The hardover failure mode probabilities of electrically computed signals and electro-hydraulic servo systems are a fixed percentage of the total probability of those elements.

- o Mechanical actuation systems had two hardover failure modes (i.e., loss of mechanical feedback or jamming of the actuator control valve).

(e) Failures of the thrust vectoring or thrust magnitude systems did not cause structural damage.

The probability of component failures were obtained from studies for the SST redundant control system, the failure analysis of the 747 auto-land, and other reliability data gathered from Boeing commercial airplane experience. This data is recorded in Tables XLI through XLII.

C.3.1 Computation of the Probability of Loss of Control

Based upon the assumptions detailed above and referring to Figure 57 for the relationship of the major control system elements, generalized failure modes can be identified for each mechanization category.

To simplify the computation of these failure probabilities for varying mechanizations, the common elements between the various mechanizations are identified. This technique is best shown by an example where the failure probabilities for longitudinal MCS, SAS, CAS, FBW, and FBW + Rev. systems are computed. Therefore, the following subsections will define the general failure modes and will include specific descriptions of the applicable longitudinal failure modes.

(1) (MCS) - Any failure that would disable the signal processing capability of block (M_1) or any failure in block (SA) that would reduce the control authority below that defined in assumption 1d above will cause system failure.

(2) (SAS or CAS) - Since stability augmentation is not required for safe CTOL flight, the failure modes of these systems are the same as the mechanical system.

(3) (FBW) - In this system it is assumed that only the feed forward signals through the block (G_2) and the computer block (C) are required to provide adequate CTOL operation. Therefore, those failures that would disable the (G_2) or (C) blocks, or any failures in the (SA) block that result in inadequate control power will cause system failure.

(4) (FBW + Rev.) - In this system, two success paths are available for the signal commands. Either the normal path, (G_2) and (C), or the reversion path, (M_1) including the reversion transfer element, will allow the proper signal transmission. Therefore, loss of control would

TABLE XLI

COMPONENT FAILURE PROBABILITY

AND COMPONENT COMPLEXITY

COMPONENT OR SUBSYSTEM FAILURE MODE	SYMBOL	FAILURE PROB. 8 HR. FLT. ($\times 10^{-6}$)	FAILURE PROB. SOURCE	COMPLEXITY	UNIT COST
Actuator Elements					
Jammed Actuator	$Q_{Act.}$	.57	(1)	- - -	- - -
Actuator Control Valve	$Q_{C.V.}$	1.1	(1)	- - -	- - -
Excessive Leakage	- - -	15.0	(1)	- - -	- - -
Loss Mechanical Feed Back	$Q_{Mech\ f.b.}$	.8	(2)	- - -	- - -
Total Actuator Failure	Q_{PCU}	17.5	- - -	1.0	- - -
Dual Hyd. Actuator Failure	Q_{DPCU}	1.7	- - -	2.0	- - -
Electro-Hyd. Servo Valve	- - -	64.0	(3)	- - -	- - -
Servo Amplifier	- - -	34.0	(4)	- - -	- - -
Actuator Jam + Leakage	- - -	15.6	(1)	- - -	- - -
Position Transducer + Signal	- - -	- - -	- - -	- - -	- - -
Path Electronics	- - -	7.0	(4)	- - -	- - -
Electro-Hyd. Actuator Failure	Q_{ECS}	121.0	- - -	1.2	- - -
Single Voted Actuator	Q_{VPCU}	- - -	(6)	2.2	- - -
Dual Voted Actuator	Q_{DVPCU}	- - -	(6)	4.4	- - -
Integrated Actuator Package (IAP)	- - -	880.0	(2)	- - -	- - -
Mechanical Elements					
Mechanical Detent	Q_{Detent}	8.0	(3)	.05	- - -
Mechanical Column	Q_{Col}	.8	(3)	.30	- - -
Quadrant	$Q_{Quad.}$	8.2	(3)	.10	- - -
Control Cable	Q_{Cable}	.24	(3)	.05	- - -
Control Pulley	Q_{Pulley}	.10	(3)	.05	- - -
Mech. Feel Unit	$Q_{Mech.\ Feel}$	32.0	(3)	.10	- - -
Computed Feel Unit	$Q_{Comp.\ Feel}$	320.0	(3)	2.00	- - -
Trim Jack Screw	- - -	73.0	(3)	- - -	- - -
Voting Link	$Q_{V.L.}$	9.0	(2)	.20	- - -
Mechanical Lock-Out	$Q_{Lock-Out}$	17.0	(2)	1.0	- - -
Hydraulic Source	$Q_{Hyd.}$	670.0	(3)	1.5	- - -
Pneumatic Sensor	Q_{Sensor}	640.0	(3)	- - -	- - -
Pneumatic Regulator	$Q_{Reg.}$	240.0	(3)	- - -	- - -
Surface Elements					
Single Hinged	$Q_{Surf.\ S.H.}$	.57	(1)	- - -	- - -
Double Hinged	$Q_{Surf.\ D.H.}$	11.4	(2)	- - -	- - -

(1) Reference (22)
(2) Estimated - Insufficient failure to compute
(3) Boeing reliability group
(4) 747 Auto-land study
(5) SST Data
(6) See Text for detailed failure mode equations.

TABLE XLII

COMPONENT FAILURE PROBABILITY

AND COMPONENT COMPLEXITY

COMPONENT OR SUBSYSTEM FAILURE MODE	SYMBOL	FAILURE PROB. 8 HR. FLT. ($\times 10^{-6}$)	FAILURE PROB. SOURCE	COMPLEXITY	UNIT COST
Electronic Elements					
Force Transducer*	Q_{Force}	40.0	①	.25	$ 1,200
Electronic Voter (Quad.)	$Q_{Elec.\ Vote}$	30.0	②	.20	3,600
Flight Control Computer	$Q_{Comp.}$	230.0	③	.50	6,000
Electronic Monitor	$Q_{Mon.}$	5.4	②	.20	- - -
Electrical Power	$Q_{Pwr.}$	58.0	②	.80	- - -
Air Data Computer	$Q_{Air\ Data}$	2600.0	④	.70	12,000
2 Axis Attitude Gyro	$Q_{Attit.}$	1100.0	①	2.00	3,990
Inertial Navigation Sys.	$Q_{Ins.}$	1200.0	①	4.00	35,000
Multiplier/Divider	- - -	52.0	③	.05	- - -
Rate Gyro	Q_{Rate}	460.0	①	.50	1,395
Accelerometer	$Q_{Accel.}$	150.0	①	.50	975
Solenoid Value	$Q_{Solenoid}$	10.0	④	.05	- - -
Trim Switch	- - -	16.0	④	.05	- - -
Electric Trim Motor Plus Control Relay	- - -	16.0	④	.20	- - -

* Includes signal path elements

① 747 auto-land study

② SST data

③ Estimated

④ Boeing reliability group

require the failure of both the normal path, (G_2) or (C), and the reversion mechanical path, (M_1) or the reversion transfer element. The surface actuation failure modes are the same as existed in fly-by-wire system.

For the longitudinal example, the specific failure modes and the resulting failure mode equations are detailed below. The definition of failure probability for each subscripted Q variable is shown in Tables XLI and XLII.

(1) MCS, SAS, or CAS - The following specific failure modes are identified for these systems:

(a) Signal path failures - loss of dual mechanical pitch signal path or loss of three engine control paths. These failures include column, throttle lever, cable, quadrant, cross-tie detent, feel system, and etc.

(b) Actuation failures - loss of two single unit elevator actuators plus a dual elevator actuator, or loss of two dual elevator actuators plus a single unit elevator actuator, or loss of three of four elevator surfaces, or loss of three hydraulic systems will reduce the actuation capability below an acceptable level.

In the "Q" notation these are expressed as:

$$Q_{LC} = Q_{\text{signal path elevator}_1} + Q_{\text{signal path throttle}_1} + Q_{\text{act. elevator}_1} \quad (98)$$

where subscript LC stands for loss of control

$$Q_{\text{signal path elevator}_1} = (Q_3)^2 + 2Q_3\,(Q_{\text{detent}}) + Q_{\text{feel pitch}} \quad (99)$$

$$Q_3 = (Q_{\text{col.}} + 2Q_{\text{quad.}} + Q_{\text{cable}} + 8Q_{\text{pulley}}) \quad (100)$$

$$Q_{\text{feel pitch}} = 2\,[\,(Q_{\text{comp. feel}} + Q_{\text{Hyd.}})(Q_{\text{Mech. feel}})\,]^2 \quad (101)$$

$$Q_{\text{signal path throttle}_1} = 3\,[Q_{\text{column}} + 2Q_{\text{quad.}} + Q_{\text{cable}} + 6Q_{\text{pulley}}]^3 \quad (102)$$

$$Q_{\text{act. elevator}_1} = 2(Q_{PCU})^2\,(Q_{DPCU}) + 2(Q_{DPCU})^2\,(Q_{PCU}) + 4\,(Q_{\text{surf. D.H.}})^3 \quad (104)$$

(2) FBW + Rev. - The following specific failure modes are identified for this system.

(a) Signal path failures - loss of both electrical and mechanical signal paths. The electrical signal path is lost when the force sensors or the computer paths are lost. The mechanical path is lost when the mechanical elements or reversion clutch are disabled.

(b) Actuation failures - all of the general actuation failure modes for the mechanical system apply to fly-by-wire voting actuators. In the computation of the actuator failure probabilities, the unique characteristics of the voting actuators must be considered. The voting links introduce an additional failure mode where the jamming of both elevator voting links disables complete elevator control.

In the "Q" notation, these are expressed as:

$$Q_{LC} = Q_{\text{signal path elevator}_2} + Q_{\text{signal path throttle}_1} + Q_{\text{act. elevator}_2} \quad (104)$$

where:

$$Q_{\text{signal path elevator}_2} = (Q_{\text{elev. elec.}})\ (Q_{\text{elev. mech.}}) \quad (105)$$

$$Q_{\text{elev. elec.}} = 2\ (Q_{\text{force}})^2 + 3\ [\ 2(Q_{\text{elec. vote}}) + Q_{\text{comp.}}\ ]^2 \quad (106)$$

$$Q_{\text{elev. mech.}} = (Q_{\text{col.}})^2 + 2Q_{\text{quad.}} + Q_{\text{cable}} + 8Q_{\text{pulley}} + Q_{\text{lock-out}} \quad (107)$$

$$Q_{\text{signal path throttle}_1} = \text{(same as mechanical system)} \quad (108)$$

$$Q_{\text{act. elevator}_2} = 2(Q_{\text{VPCU}})^2\ (Q_{\text{DVPCU}}) + 2(Q_{\text{DVPCU}})^2\ (Q_{\text{VPCU}}) + (Q_{\text{V.L.}} + Q_{\text{detent}})^2 + 4\ (Q_{\text{surf. D.H.}})^3 \quad (109)$$

$$Q_{\text{VPCU}} = Q_{\text{elec. vote}} + Q_{\text{C.V.}} + Q_{\text{act.}} + Q_{\text{hyd.}} + (Q_{\text{ECS}})\ (Q_{\text{ECS}} + Q_{\text{V.L.}}) \quad (110)$$

$$Q_{\text{DVPCU}} = Q_{\text{elec. vote}} + 2(Q_{\text{C.V.}} + Q_{\text{act.}}) + (Q_{\text{hyd.}})^2 + (Q_{\text{ECS}})\ (Q_{\text{ECS}} + Q_{\text{V.L.}}) \quad (111)$$

(3) FBW - The following specific failure modes are identified for the fly-by-wire mechanization.

(a) Signal path failures - loss of capability through the redundant voted longitudinal path or loss of three single thread throttle paths constitute a catastrophic signal path failure.

(b) Actuation failures - the actuation failure modes are identical with the FBW + Rev. actuation system.

The new equations for the signal path failures are:

$$Q_{\text{signal path elevator}_2} = (Q_{\text{command}}) + (Q_{\text{compute}}) \quad (112)$$

$$Q_{command} = 2(Q_{detent})\ (Q_{col.}) + 2\ (Q_{force})^2\ (Q_{col.}) + (Q_{force})^4 + (Q_{col.})^2 \quad (113)$$

$$Q_{compute} = 4\ [\ Q_{elec.\ vote} + Q_{compute} + Q_{pwr.}\ ]^3 \quad (114)$$

The computed values for the control system failure probabilities are shown in Tables XLIII through XLV.

C.3.2 Computation of the Probability of Excessive Pilot Workload

The probability of excessive pilot workload is equivalent to Level 3 operation for STOL flight tasks. The following general failure modes are identified for each control mechanization category.

(1) (MCS) - This system cannot provide better than Level 3 operation since stability augmenting feedbacks are not available.

(2) (SAS or CAS) - The Level 3 failure modes in these systems are loss of two of the three feedback paths incorporated in block (G_1). In addition, those failures, in the computation block (C) and the actuation block (SA) that preclude the transmittance of feedback signals or result in inadequate control power, will result in Level 3 operation.

(3) (FBW and FBW + Rev.) - The failure modes for the mechanization categories are the same as for SAS and CAS except different redundancy levels are used and the impact of the electronic voters must be evaluated.

The specific failure modes are shown below for the longitudinal example. For this discussion, the longitudinal systems are based upon a common control law. These systems are CP21, SP02R, and SP02A.

(1) MCS - It is mentioned above that the probability of Level 3 operation ($Q_{EW} = 1$).

(2) SAS or CAS - The failure modes are related to loss of feedback, loss of computed electrical signals, including the electric command servos (ECS) conversion to mechanical signals, and loss of surface actuation.

(a) Feel system failure - loss of both feel computers is assumed to result in Level 3.

(b) Feedback path failures - since the feedback paths are electrically voted, loss of two paths are required to cause loss of the feedback function.

(c) Electrical signal failures - three independent signal paths are available where two must be lost to cause Level 3

Table XLIII: Longitudinal Control Mechanization Data

CONTROL						COST K$	WEIGHT LBS.	COMPLEXITY	DESIGN RISK	VULNERABILITY	SAFETY						
											FAILURE PROBABILITY			RATING			
Control Axis	MODE	SYSTEM NUMBER	SURFACE	TYPE							Q_{LC} ($X10^{-10}$)	Q_{SD} ($X10^{-15}$)	Q_{BM} ($X10^{-5}$)	P_{LC}	P_{SD}	P_{BM}	WEIGHTED S_R
Longitudinal	Manual	MP02	Thrust	External Deflector		60	3191	43.25	5	2.1							
			Vector	TVTR		---	---	---	--	---							
			Stabiliser	TRIM		5	225	8.2	0	.8							
			Engine Thrust	Throttle		10	120	7.56	0	1.2							
					Sub-Total (1)	75	3536	59.41	5	4.1							
			Elevator	Double Hinge		100	1134	24.65	0	.8							
					Total	175	4670	84.06	5	4.9	8.86	1.02	1.0 $X10^{5}$	8.86	1.0	1X10^5	10.0 (2)
	SAS	SP03			Sub-Total (1)	75	3567	64.66	5	4.1							
			Elevator	Double Hinge		177	1138	25.85	0	.8							
			Elec-tronics			66.4	106	6.88	1	0							
					Total	318.4	4811	97.39	6	4.9	4.86	29	7.7	4.86	3.55	7.70	4.62
	CAS	CP21			Sub-Total (1)	75	3567	64.66	5	4.1							
			Elevator	Double Hinge		177	1138	25.85	0	.8							
			Elec-tronics			74.5	118	7.23	1	0							
					Total	326.5	4823	97.74	6	4.9	8.86	1.02	5.53	8.86	1.00	5.53	5.38
	FWB + Rev.	SP02R, SP04R, SP05R	Elevator	Double Hinge	Sub-Total (1)	75	3567	60.66	5	4.1							
						202	1035	21.96	1	.8							
			Elec-tronics			74.5	118	7.23	1	0							
					Total	351.5	4720	93.85	7	4.9	4.86	29	7.7	4.86	3.55	7.70	4.62
		DP05R, DP07R	Elevator	Double Hinge	Sub-Total (1)	75	3567	64.66	5	4.1							
						202	1035	21.56	1	.8							
			Elec-tronics			155.2	310	6.32	3	0							
					Total	432.2	4912	92.94	9	4.9	4.86	29	7.2	4.86	3.55	7.20	4.57
	FBW	SP02A, SP04, SP05	Elevator	Double Hinge	Sub-Total (1)	75	3567	64.66	5	4.1							
						183	955	18.75	1	.8							
			Elec-tronics			135.3	162	11.57	2	0							
					Total	393.3	4684	94.98	8	4.9	6.47	29	7.68	6.47	3.55	7.63	5.42
		DP05, DP07	Elevator	Double Hinge	Sub-Total (1)	75	3567	64.66	5	4.1							
						183	955	18.75	1	8							
			Elec-tronics			216	354	12.66	4	0							
					Total	474	4876	96.07	10	4.9	6.47	29	7.18	6.47	3.55	7.3	5.37

(1) Subtotal includes thrust vector, stabiliser trim, and engine throttle.

(2) Limited to 10.0

TABLE XLIV

LATERAL/DIRECTIONAL CONTROL MECHANIZATION DATA - (BLOWN AILERON)

CONTROL						SAFETY										
											FAILURE PROBABILITY			Rating			
Control Axis	Mode	System Number	Surface	Type		COST K$	WEIGHT lbs.	COMPLEX-ITY	DESIGN RISK	VULNER-ABILITY	Q_{LC} ($\times 10^{-10}$)	Q_{SD} ($\times 10^{-15}$)	Q_{EW} ($\times 10^{-5}$)	P_{LC}	P_{SD}	P_{EW}	WEIGHTED S_p
LATERAL/ DIRECTIONAL	Manual	MR0821-1	Aileron Spoiler Panel	Blown Double		65.5	1994	42.3	3	2.3							
			Rudder	Hinge		144	985	38.3	0	1.3							
					Total	209.5	2979	60.3	3	3.6	3.0	0.0	$1X10^5$	3.0	0.0	$1X10^5$	10.0 (1)
	SAS	SR20-1	Aileron Spoiler Panel	Blown Double		68.8	2009	42.3	3	2.3							
			Rudder	Hinge		260.0	987	22.6	0	1.3							
					Sub Total #1	328.8	2996	64.9	3	3.6							
			Elec-tronics			56.7	97	6.32	1	0							
					Total	385.5	3093	71.22	4	3.6	3.0	.8	6.8	3.0	.94	6.8	2.56
	SAS	SR21-1			Sub Total #1	328.8	2996	64.9	3	3.6							
			Elec-tronics			77	120	8.32	1	0							
					Total	405.8	3116	73.22	4	3.6	3.0	.8	6.8	3.0	.94	6.8	2.56
	CAS	CR20-1			Sub Total #1	328.8	2996	64.9	3	3.6							
			Elec-tronics			77	120	8.17	1	0							
					Total	405.8	3116	73.07	4	3.6	3.0	.8	6.8	3.0	.94	6.8	2.56
		CR21-1			Sub Total #1	328.8	2996	64.9	3	3.6							
			Elec-tronics			72.7	112	9.32	1	0							
					Total	401.5	3108	74.32	4	3.6	3.0	.8	7.16	3.0	.94	7.16	2.61
	FBW + Rev.	FR20R-1	Aileron Spoiler Panel	Blown Double		70.8	2038	42.0	4	1.8							
			Rudder	Hinge		296	930	22.5	1	1.2							
					Sub Total #3	366.8	2968	64.5	5	3.0							
			Elec-tronics			94.7	128	10.77	2	0							
					Total	461.5	3096	75.27	7	3.0	3.0	.39	6.72	3.0	.54	6.72	2.59
		FR21R-1			Sub Total #3	366.8	2968	64.5	5	3.0							
			Elec-tronics			90.6	119	11.22	2	0							
					Total	457.4	3087	75.72	7	3.0	3.0	.39	7.11	3.0	.54	7.11	2.59
	FBW	FR20-1	Aileron Spoiler Panel	Blown Double		60.6	1872	34.9	4	1.8							
			Rudder	Hinge		271	852	20.75	1	1.2							
					Sub Total #5	331.6	2724	55.65	5	3.0							
			Elec-tronics			118.5	162	12.01	2	0							
					Total	450.1	2886	67.66	7	3.0	7.63	.39	6.72	7.63	.54	6.7	4.86
		FR21-1		Sub-Electronics	Total #5	331.6	2724	55.65	5	3.0							
						114.3	153	13.16	2	0							
					Total	445.9	2877	68.81	7	3.0	7.63	.39	7.11	7.63	.54	7.11	4.90

(1) Limited to 10.0

Table XLV

LATERAL CONTROL MECHANIZATION DATA - (DOUBLE HINGE AILERON)

CONTROL AXIS	CONTROL MODE	CONTROL SYSTEM NUMBER	SURFACE	TYPE		COST K$	WEIGHT LBS.	DESIGN COMPLEXITY	DESIGN RISK	DESIGN VULNERABILITY	SAFETY FAILURE PROBABILITY Q_{LC} X10^{-10}	Q_{SD} X10^{-15}	Q_{EW} X10^{-5}	SAFETY RATING P_{LC}	P_{SD}	P_{EW}	WEIGHTED SR
Lateral/ Directional	Manual	MR0821	Aileron	Double Hinge													
			Spoiler	Panel		63.1	1871.9	36.9	0	2.1							
			Rudder	Double Hinge		144	785	18.3	0	1.3							
					Total	207.1	2857	55.2	0	3.4	3.0	0.0	1X10^{5}	3.0	0.0	1X10^{5}	10.0①
	SAS	SR20	Aileron	Double Hinge		66.5	1887	36.9	0	2.1							
			Spoiler	Panel													
			Rudder	Double Hinge		260	987	22.6	0	1.3							
					Subtotal #2	326.5	2874	59.5	0	3.4							
			Elec-tronics			56.7	97	6.22	1	0							
					Total	383.2	2971	6.72	1	3.4	3.0	.8	6.8	3.0	.94	6.8	2.57
		SR21			Subtotal #2	326.5	2874	59.5	0	3.4							
			Elec-tronics			77	120	8.32	1	0							
					Total	403.5	2994	67.82	1	3.4	3.0	.8	6.8	3.0	.94	6.8	2.56
	CAS	CR20			Subtotal #2	326.5	2874	59.5	0	3.4							
			Elec-tronics			77	120	8.17	1	0							
					Total	403.5	2994	67.67	1	3.4	3.0	.8	6.8	3.0	.94	6.8	2.57
		CR21			Subtotal #2	326.5	2874	59.5	0	3.4							
			Elec-tronics			72.7	112	9.32	1	0							
					Total	399.2	2986	68.82	1	3.4	3.0	.8	7.16	3.0	.94	7.16	2.61
	FBW	FR20	Aileron	Double Hinge													
			Spoiler	Panel		58.2	1750	29.5	1	1.6							
			Rudder	Double Hinge		271	852	20.75	1	1.2							
					Subtotal #6	329.2	2602	50.25	2	2.8							
			Elec-tronics			118.5	162	12.01	2	0							
					Total	447.7	2764	62.26	4	2.8	7.63	.39	6.72	7.63	.54	6.72	4.86
		FR21			Subtotal #6	329.2	2602	50.25	2	2.8							
			Elec-tronics			114.3	153	13.16	2	0							
					Total	443.5	2755	63.41	4	2.8	7.63	.39	7.11	7.63	.54	7.11	4.90
	FBW + Rev.	FR20R	Aileron	Double Hinge													
			Spoiler	Panel		68.4	1916	36.6	1	1.6							
			Rudder	Double Hinge		296	930	22.5	1	1.2							
					Subtotal #4	364.4	2846	59.1	2	2.8							
			Elec-tronics			94.7	128	10.77	2	0							
					Total	459.1	2974	69.87	4	2.8	3.0	.39	7.11	3.0	.54	7.11	2.59
		FR21R			Subtotal #4	364.4	2846	59.1	2	2.8							
			Elec-tronics			90.6	119	11.22	2	0							
					Total	455.0	2965	70.32	4	2.8	3.1	.39	7.11	3.1	.54	7.11	2.64

① Limited to 10.0

operation. Since ECS units are involved, the loss of two hydraulic sources will result in loss of this function.

(d) Actuation failures - the loss of any two surfaces will result in Level 3 operation.

The failure mode equations are therefore:

$$Q_{EW} = Q_{fb_3} + Q_{elec.\ path} + Q_{act_3} + (Q_{comp.\ feel} + Q_{hyd.})^2 \quad (115)$$

where:

$$Q_{fb_3} = 3\ [\ Q_{air\ data} + Q_{attit.} + Q_{rate} + Q_{pwr.}\ ]^2 \quad (116)$$

$$Q_{elec.\ path} = 2\ (Q_{force})^2 + 3\ [\ 2(Q_{elec.\ vote}) + Q_{comp.}\ ]^2 + 2(Q_{ECS})^2 \quad (117)$$

$$Q_{act_3} = (Q_{PCU})^2 + (Q_{DPCU})^2 + 2\ (Q_{PCU})\ (Q_{DPCU}) + (Q_{hyd.})^2 \quad (118)$$

(3) FBW + Rev. - The failure modes are similar to the CAS mechanization since similar redundancies are employed.

(a) Feedback path failures - identical to CAS system.

(b) Electrical signal failures - similar to CAS except ECS function is inherent in fly-by-wire actuators and is not part of the electrical signal path.

(c) Actuation failure - the loss of any two surface controls will result in Level 3 operation. In addition, the jamming of either servo voting link will result in Level 3 operation.

The Level 3 failure mode equations are:

$$Q_{EW} = Q_{fb_3} + Q_{elec._3} + Q_{act.\ vote_3} \quad (119)$$

where: Q_{fb_3} is same as CAS.

$$Q_{elec._3} = 2(Q_{force})^2 + 3\ [\ 2(Q_{elec.\ vote}) + Q_{comp.}\ ]^2 \quad (120)$$

$$Q_{act.\ vote_3} = (Q_{VPCU})^2 + (Q_{DVPCU})^2 + 2(Q_{VPCU})\ (Q_{DVPCU}) + 2(Q_{hyd.})^2 + 2(Q_{V.L.} + 2\ Q_{detent}) \quad (121)$$

(4) FBW - The feedback and actuation failure modes are identical to FBW + Rev. The increase in computation redundancy changes the signal path probability.

Electrical signal failures - the four channels of electronics will transmit a satisfactory signal until three channels are lost. Loss of three signal paths results in loss of control. Therefore there is no unique signal path failure causing Level 3 operation.

The Level 3 failure probability is then:

$$Q_{EW} = Q_{fb_3} + Q_{act.\ vote_3} \tag{122}$$

where Q_{fb_3} and $Q_{act.\ vote_3}$ are defined above.

III.3.3 Computation of Probability of Structural Damage

The proposed configurations have been designed considering projected failures and failure effects. Therefore, the failures that can cause structural damage are minimized. The general failure modes for each mechanization category are listed below followed by the equations for specific examples in each mechanization category.

(1) (MCS) - Loss of the pitch feel system, part of block (M_1), or failures to the surface actuation, block (SA), causing three concurrent elevator surface hardovers will result in structural damage. Three concurrent rudder hardovers plus the failure of a pressure regulation device on any rudder will result in structural damage.

(2) (SAS or CAS) - The same mechanical failures noted for the (MCS) mechanization apply to these systems. When a rudder pressure regulator fails concurrent with the failure of two electric rudder command signals or two electro-hydraulic servos plus their failure monitoring system, structural damage will result.

(3) (FBW or FBW + Rev.) - The actuation voting characteristics of these systems alter the failure modes. The following rudder failure modes, occurring together with the failure of a pressure regulating device on any rudder, will exceed structural limits.

(a) Hardover failure of three rudder servos, or

(b) Hardover failure of three voted commands, or

(c) Hardover failure of two voters plus a failure of their monitor system.

The elevator failure modes are the same as the rudder except that the simultaneous pressure regulator failure is not applicable. The "feel" is inherent in the command/response characteristic of these systems so loss (i.e., jamming) of the feel system will not cause structural problems.

Due to the limited number of failure modes causing structural damage, the following examples are not limited to the longitudinal axis but include all failure conditions.

The probability of "active" or "hardover" failures of electrical components is assumed to be nine-tenths the total failure probability of that component. The exception to this rule is for electronic voters where special design effort reduces this factor to five-tenths.

(1) MCS - Actuator hardovers are caused by mechanical element failures only.

$$Q_{SD} = Q_{\text{pitch feel}} + Q_{\text{act. rudder}} + Q_{\text{act elevator}} \tag{123}$$

where

$$Q_{\text{pitch feel}} = 2 \left[(Q_{\text{comp. feel}} + Q_{\text{hyd.}}) (Q_{\text{mech. feel}}) \right]^2 \tag{124}$$

$$Q_{\text{act. rudder}} = 3 \left[(Q_{\text{mech. f.b.}} + Q_{\text{C.V.}}) \right]^3 \left[Q_{\text{reg.}} + Q_{\text{solenoid}} + Q_{\text{sensor}} \right] \tag{125}$$

$$Q_{\text{act. elev.}} = 4 \left[(Q_{\text{mech. f.b.}} + Q_{\text{C.V.}}) \right]^3 \tag{126}$$

(2) SAS or CAS - The actuator failures for the rudder can be caused by mechanical failures on two simultaneous electrical command failures because of the authority of the rudder series servos.

$$Q_{SD} = Q_{\text{pitch feel}} + Q_{\text{act. elevator}} + Q_{\text{act. rudder + elec.}} \tag{127}$$

the first two terms are same as for the MCS system above.

$$Q_{\text{act. rudder + elec.}} = .9 \ (3) \ (Q_{\text{comp}})^2 \ (Q_{\text{mon}}) + 3 \left[.9 \ (Q_{ECS} - Q_{\text{act.}}) + Q_{\text{mech. f.b.}} + Q_{\text{C.V.}} \right]^3 \left[Q_{\text{reg}} + Q_{\text{solenoid}} + Q_{\text{sensor}} \right] \tag{128}$$

(3) FBW + Rev. - Because the fly-by-wire actuators incorporate a voting function, a majority of the commands must fail plus additional safety features such as the voter monitors or the rudder hydraulic pressure reducers before structural damage will result.

$$Q_{SD} = Q_{S.D.\ elec.} + Q_{act.\ vote\ elev.} + Q_{act.\ vote\ rudder} \quad (129)$$

$$Q_{S.D.\ elec} = [.3(3)\ (Q_{comp.})^2\ (Q_{mon.})] \quad (130)$$

$$Q_{act.\ vote\ elev.} = 4\ [.9\ Q_{ECS}]^3\ [Q\ mon.] \quad (131)$$

$$Q_{act.\ vote\ rudder} = 9\ [.9\ Q_{ECS}]^2\ [Q\ mon][Qreg. + Q\ solenoid + Q\ sensor] + [.9\ Q_{ECS}]^3\ [Q\ mon.] \quad (132)$$

(4) FBW - This system is the same as the FBW + Rev except for the additional redundancy in the electrical path.

$$Q_{SD} = Q_{S.D.\ elec._4} + Q_{act.\ vote\ elev.} + Q_{act\ vote\ rudder} \quad (133)$$

where $Q_{act\ vote\ elev.}$ and $Q_{act\ vote\ rudder}$ are defined above.

$$Q_{S.D.\ elec._4} = 4\ [.9\ (Q_{comp})^3\ (Q_{mon.})] + [.9\ (Q_{comp})^2\ (Q_{mon.})] \quad (134)$$

III.3.4 Tabulation of Safety Analysis Data

The individual failure probabilities plus the ranked and weighted safety data is recorded in Tables C-V through C-VII. Subsection 3.3.1 defines the ranking and weighting procedure used to compute the safety rating;

$$S_R = .5\ (P_{LC}) + .4\ (P_{SD}) + .1\ (P_{EW}) \quad (135)$$

The weighting factors were established as an indication of the severity of the safety parameter.

The individual failure probabilities Q_{LC}, Q_{SD}, and Q_{EW} are converted to a figure-of-merit value between 1 and 10 which are identified as P_{LC}, P_{SD}, and P_{EW} respectively.

III.4 Computation of Control System Complexity

The system complexity had to consider both mechanical and electrical elements in an unbiased manner. This was accomplished by comparing the complexity of the system components to a fixed reference (i.e., a single hydraulic surface actuator with mechanical control). The relative complexity of the components are recorded with the failure probability data in Tables XLI and XLII.

The system complexity is determined by taking the summation of the complexity of individual system components. These complexity summations are included as a part of the general mechanization data in Tables XLIII through XLV.

III.5 Weight and Cost Data

Both the weight and cost data rely upon statistical data obtained from previous aircraft programs. This is especially true of that data reflecting the mechanical elements (e.g., controllers, cables, quadrants, hydraulic installations, surface actuations, and surface attachments). The electronic systems were not always representative of systems that have been employed on existing aircraft, therefore the cost and weight of these systems were computed independently. The component costs for the major electrical system components are shown in Table XLII. The installed cost was computed as follows:

$$\text{Cost}_{\text{installed}} = 1.35 \sum_{i=1}^{n} \text{component cost} \qquad (136)$$

where the 35% factor represents installation costs.

The cost and weight of the "mechanical" and "electrical" sub-systems are shown along with total system cost and weight in Tables XLIII through XLV.

III.6 Design Risk

Sub-section 3.3.5 defined the separation of design risk evaluation into discrete values of zero to five. In this study the factors that had a non-zero design risk are shown in the following table.

TABLE XLVI

ELEMENT DESIGN RISK

Control System Element	Design Risk
Triple Channel Voted Electronics	1
Mechanical Reversion Lock-Out	1
Quad. Channel Voted Electronics	2
Blown Aerodynamic Control Surface	3
"Strap-Down" INS Plus Triple Electronics	3
"Strap-Down" INS Plus Quad. Electronics	4
Thrust Vector Control Combined with Integrated Thrust Reverser	5

The individual design risk assignments, as they apply to the candidate mechanizations, are shown for the "mechanical" and "electrical" sub-systems in Tables XLIII through XLV.

III.7 Vulnerability Assessment

The vulnerability assessment considered the number of points in the control system where a single 9 mm armor piercing round could cause loss of control, Level 3 performance, or Level 2 performance. As defined in sub-section 3.3.6, the vulnerability rating was computed using the following equation:

$$R_V = 1.0\ N_{LC} + .4\ N_{L_3} + N_{L_2} \quad \text{where the subscripted factors are for} \quad (137)$$

loss of control (LC), Level 3 (L_3), and Level 2 (L_2) respectively. The weighting factor indicates a level of severity. A single round did not result in loss of control for the mechanizations that were considered. Therefore the rating became.

$$R_V = .4\ N_{L_3} + .1\ N_{L_2} \quad (138)$$

The projected number of bellcranks, pulleys, cables, and quadrants for each system are defined in Table C-IX. From these factors, recognizing the hydraulic and component redundancy, the number of points resulting in Level 2 and Level 3 performance were identified, weighted, and recorded in Tables XLIII through XLV. Each hydraulic distribution system was considered as a single failure point in this evaluation.

TABLE XLVII

QUANTITY OF MECHANICAL CONTROL ELEMENTS

Sub-System	Mech. Type	Quadrants	Paired Pulleys & Idlers	Bell Cranks & Push Rods
Elevator	MCS, SAS, CAS	4	14	13
	FBW + Rev.	2	7	10
Rudder	MCS, SAS, CAS	4	14	18
	FBW + Rev.	2	7	11
Lateral	MCS, SAS, CAS	8	14	20
	FBW + Rev.	6	10	26
Thrust Vector	MCS, SAS, CAS, FBW + Rev.	4	14	38
Throttle	MCS, SAS, CAS, FBW + Rev.	8	10	36

(Page 240 Blank)

REFERENCES

1. Carroll, R. H., Jants, J. W., and Milns, P., Configuration Defination, Medium STOL Transport with Vectored Thrust/Mechanical Flaps, AFFDL TR-73-XX, Volume I.

2. Blakelock, J. H., Automatic Control of Aircraft and Missiles, John Wiley & Sons, Inc., 1965.

3. Ashkenas, I. L., and Stapleford, R. L., Analysis of Several Handling Quality Topics Pertinent to Advanced Manual Aircraft - (Section IV), AFFDL-TR-67-2, August 1967.

4. Neal, P. T., and Smith, R. E., An Inflight Investigation to Develop Control System Design Criteria for Fighter Airplanes, AFFDL-TR-70-74, December 1970.

5. Kriechbaum, G. K. L., et. al., An Investigation of Direct Sideforce Control for Improving Maneuver Capability of Attack Aircraft, Document D180-14004-1 - Final Report Navy Research Contract N00014-71-C-0200.

6. Foster, B. E. F., and Kriechbaum, G. K. L., Analytical and Experimental Studies of VTOL Handling Qualities, Boeing Document D6-15709, November 1967.

7. McRuer, D. T., Graham, D., et. al., Human Pilot Dynamics in Compensatory Systems, AFFDL-TR-65-15, July 1965.

8. Mitchell, K., Analytical Synthesis of a Decoupled Lateral - Directional Stability Augmentation System, Boeing Document D6A11132-1, December 1967.

9. Berg, R. A., Shirley, W. A., Teper, G.L., and Craig, S. J., A Flight Simulator Study of STOL Transport Directional Control Characteristics, FAA-RD-71-81, June 1971.

10. Hooker, D. S., Kisslinger, R. L., and Smyth, M. S., Survivable Flight Control System Program Simplex Actuator Package, AFFDL-TR-70-135, November 1970.

11. Flight Mechanics Panel of AGARD-NATO, V/STOL Handling Qualities Criteria, AGARD Report No. 577, December 1970.

12. Bisgood, P. L., A Review of Recent Research on Handling Qualities, and its Application to the Handling Problems of Large Aircraft Part III Longitudinal Handling, Royal Aerocraft Establishment (RAE) R. & M. No. 3606, January 1968.

13. Chalk, C. R. and Wilson, R. K., "Airplane Flying Qualities Specification Revision", page 232 of May - June 1969 Journal of Aircraft.

14. Anderson, S. B. and Quigley, Stability and Control Considerations for STOL Aircraft, AIAA Paper 65-715, June 1965.

15. Hooker, D. S., Kisslinger, R. L., Smith, G. R., and Smyth, M. S., Survivable Flight Control System Interim Report No. 1; Studies, Analysis and Approach, AFFDL-TR-71-20, May 1971.

16. Anon., USAF Stability and Control Handbook (DATCOM) Douglas Aircraft Company, 1960.

17. Eldridge, A. H., Grow, T. L., and Kirk, P. S., Approximate Calculation Procedures for Airplane Aerodynamic Characteristics, Boeing Document D6A12022-1, July 1970.

18. Owen, R. B., A Correlation of Blown Flap Test Data with Design Charts for Estimating Blown Flap Lift and C_μ Required, Boeing Document D6-8111, March 1962.

19. Rubbert, A., Theoretical Characteristics of Flapped Airfoils at Low Speeds, Boeing Document D6-7253, May 1961.

20. Anon., Collections of Test Data for Lateral Control with Full-Span Flaps, NASA Report TN1404, September 1947.

21. Anon., Aerodynamic Characteristics of a Spoiler-Slot-Deflector Control on a 45° Sweptback-Wing-Fuselage Model at High Subsonic Speeds, NASA Report TN D-2037.

22. Anon., "Study of Air Carrier Mechanical Reliability Reports on Flight Control Systems and Control Surfaces for the Years 1964 through 1966 - Preliminary Draft", Aerospace Industries Association of America, Inc. (AIA) May 1967.

23. Chalk, C. R., Neal, T. P., Harris, T. M., Pritchard, F. E., Background Information and User Guide for MIL-F-8785B(ASG), "Military Specification - Flying Qualities of Piloted Airplanes," AFFDL-TR-69-72, August 1969.

24. Flight Mechanics Panel of AGARD-NATO, V/STOL Handling-Qualities Criteria (I-Criteria and Discussion), AGARD-R-577-70, December 1970.